
High Throughput Confocal Screen of 1,727 Compounds to Identify Novel Regulators of Primary Cilia Structure

---

Megan Ruth Mc Fie

A thesis presented in partial fulfilment for the degree of

Doctor of Philosophy

May 2021

Supervisors:

Prof. Martin Knight

Dr Cleo L. Bishop

School of Engineering and Materials Science

Queen Mary University of London

Statement of Originality

I, Megan Ruth Mc Fie, confirm that the research included within this thesis is my own work or that where it has been carried out in collaboration with, or supported by others, that this is duly acknowledged below and my contribution indicated.

I attest that I have exercised reasonable care to ensure that the work is original, and does not to the best of my knowledge break any UK law, infringe any third party's copyright or other Intellectual Property Right, or contain any confidential material.

I accept that the College has the right to use plagiarism detection software to check the electronic version of the thesis.

I confirm that this thesis has not been previously submitted for the award of a degree by this or any other university.

Signature: Megan Ruth Mc Fie

Date: 26th May 2021

Statement of Confidentiality

Due to IP reasons and continuing QMUL funded Proof of Concept project work, the names of compounds used and identified within this thesis have not been disclosed and are not yet available for discussion.

Abstract

The primary cilium is a singular microtubule-based cell organelle present on most quiescent eukaryotic cell types and is required for numerous signalling pathways. Primary cilia length and incidence have been reported to be altered by many mechanical and chemical stimuli. Furthermore, a group of diseases termed ciliopathies are associated with genetic disruption to primary cilia. Alterations in primary cilia structure have been associated with modified cell signalling events, of which the hedgehog signalling pathway is the most well established as having a ciliary link.

The aim of this thesis project was to identify compounds that regulate primary cilia expression in healthy chondrocytes, and in turn to investigate the effect of altered cilia structure on cilia function. It is envisaged that this will support future work to use cilia modifying compounds as potential 'ciliotherapies' for the treatment of established ciliopathies and diseases with a ciliary component.

A high throughput screen was optimised and executed to enable the unbiased investigation of the effect of 1,727 compounds on cilia expression and structure. Primary bovine articular chondrocytes were utilised; an ideal cell model for the interrogation of primary cilia structure due to their high expression of flat lying cilia *in vitro* 2D culture. Compound treatment of a confluent monolayer culture was uniformly performed using liquid handling robotics, followed by cellular fixation and immunofluorescent labelling. Nuclei, F-actin and the cilia axoneme components acetylated-α-tubulin and polyglutamylated tubulin were labelled and imaged with automated 3D confocal microscopy. High content image analysis of the 552,960 images generated in first pass screen collected data on over 60 cellular parameters.

The data was stored in a database of compound effect with accompanying z-score matrix.

From the full library, 233 (13.5%) compounds were identified as altering either cilia length and/or incidence. Using hierarchical clustering, six phenotypic clusters were found amongst these compounds. A cluster of 68 compounds causing an increase in cilia length with a predominantly ciliary specific effect were validated in cells isolated from two additional animals. The 22 validated compounds were carried forward for investigation in a human chondrocyte cell line.

The viability of the 22 candidate compounds was tested in a human chondrocyte cell line, of which 16 compounds were found to maintain cell number. Of the viable compounds, 15 increased primary cilia length in the human cells, replicating the effects seen in bovine. The impact of this cilia elongation on subsequent cilia function, specifically on hedgehog signalling was examined by RT-PCR, with ligand induction of the pathway. Although effects were inconsistent, across all compounds there was a trend towards an inhibition to Gli1 induction with the addition of Ihh ligand.

These studies identified a robust group of candidate compounds that induced primary cilia elongation in multiple biological replicates using chondrocytes from both bovine and human sources. Although cilia elongation in healthy cells did not cause a consistent effect on ligand-induced hedgehog signalling, these compounds may have future potential as novel 'ciliotherapies' to correct cilia dysfunction.

Acknowledgements

This project was funded by a QMUL Principal's Scholarship, QMI Innovation Award and the continued work is funded by a QMI Proof of Concept Award.

"It is a marathon not a sprint"

First and foremost, I would like to thank my supervisors Prof Martin Knight and Dr Cleo Bishop for their advice, guidance and constant support of both my work and my wellbeing throughout my PhD. Your ability to adapt and continue to provide this support throughout a global pandemic was incredible and greatly appreciated. We eventually managed to call checkmate on this thesis!

A special thank you to Dr Luke Gammon for his invaluable advice and support in the Blizard screening facility. Thank you also to Dr Clare Thompson and members of the Knight group for discussion and advice regarding all things primary cilia and sometimes just cili-ness.

Thank you to the members of the Bishop group, both past and present and to all those at the Blizard Institute who welcomed me and created such a supportive working environment. In particular to Deb, Stef, Ryan, Hannah, Emily and my bay bud Beth for making my rapid senescing over the last 3 years an incredibly enjoyable and supported experience. To Elly (and Mike) for all of the guidance and advice regarding screening and in helping me landscape and cultivate the final stages of my PhD. To Jordan for being the twin and brotherly support I never knew I would be lucky enough to find.

Finally I want to thank my mum and dad, Ingrid and George, and my sister Amy for being there to help pick up the pieces when things went wrong and for always helping me remember to celebrate the highs. Thank you so much to my family, and to all the friends who became family along the way, I hope you know who you are. I could never have completed the annual physical and mental marathons, let alone the marathon of a PhD experience without all of your support. Thank you!

Table of Contents

List of Figures

List of Table

List of Abbreviations

Abbreviation	Full name
ACIII	Adenylyl cyclase type III
Ac-α-tub	Acetylated-α-tubulin
ADPKD	Autosomal dominant polycystic kidney disease
AF	Alexa Fluor
Arl13b	ADP ribosylation factor like GTPase 13B
2βME	2-Mercaptoethanol
BBS	Bardet-Biedl syndrome
BCA	Bicinchoninic acid
cAMP	Cyclic adenosine monophosphate
cDNA	Complementary deoxyribonucleic acid
CB	Cytoskeletal buffer
Col2a	Collagen type II a
Cre	Carbapenem-resistant Enterobacterales
CT	Cycle threshold
CV	Ciliary vesicle
DAPI	4’,6-diamidino-2-phenylindole
DMEM	Dulbecco’s modified eagle medium
DMSO	Dimethyl sulfoxide
DNA	Deoxyribonucleic acid

ECM	Extracellular matrix
EDTA	Ethylenediaminetetraacetic acid
EGTA	Ethylene glycol tetraacetic acid
FDA	Food and Drug Administration
FCS	Foetal calf serum
FLA	Flagellar assembly
GAPDH	Glyceraldehyde 3-phosphate dehydrogenase
GPCR	G-protein-coupled receptor
GTP	Guanosine-5'-triphosphate
HDAC	Histone deacetylase
Hh	Hedgehog
Hr	Hour
IFT	Intraflagellar Transport
Ihh	Indian hedgehog
IR	Infrared
KIF	Kinesin-like protein
LiCl	Lithium chloride
Min	Minute
MSC	Mesenchymal stem cells
MTOC	Microtubule organising centre
OA	Osteoarthritis
ORPK	Oak Ridge Polycystic Kidney

PBS	Phosphate buffered saline
PC	Polycystin
PCR	Polymerase chain reaction
PFA	Paraformaldehyde
PKD	Polycystic kidney disease
PTCH	Patched
r-Ihh	Recombinant Indian hedgehog
RNA	Ribonucleic acid
RT	Room temperature
RT-qPCR	Real time quantitative PCR
Shh	Sonic Hedgehog
SMO	Smoothened
TGF	Transforming growth factor
TBST	Tris-buffered saline with Tween
U	Units
Wnt	Wingless/integrated
WT	Wild type

1. Introduction

1.1. Primary cilia structure

Once thought to be a vestigial cell organelle, the primary cilium has been highly preserved throughout evolution and is a microtubule based structure, ubiquitously expressed by most quiescent eukaryotic cells. It is membrane-bound and represents a distinct compartment, extending out into the extracellular environment. Unlike its motile counterparts, the primary cilium lacks accessory components, such as dynein arms and radial spokes that facilitate force generation, rendering it immotile. Except for sperm flagellum, motile cilia predominantly occur in large numbers on individual cells, while primary cilia typically occur as a solitary organelle (Berbari, et al. 2009).

Figure 1.1 shows a schematic illustration of the structure of the primary cilium alongside confocal (Thompson, et al. 2016) and TEM (Muhammad, et al. 2012) images of cilia in chondrocytes, the cell type used throughout this thesis. The ciliary membrane is continuous with that of the cells phospholipid bilayer, although distinct in that it contains a unique localisation and collection of membrane receptors and ion channels. Enclosing the ciliary compartment from the cytosol and thought to regulate entry and exit of proteins in the cilium are transition fibres and the transition zone; comprised of y-shaped linkers and the membranous ciliary necklace (Gilula and Satir 1972).

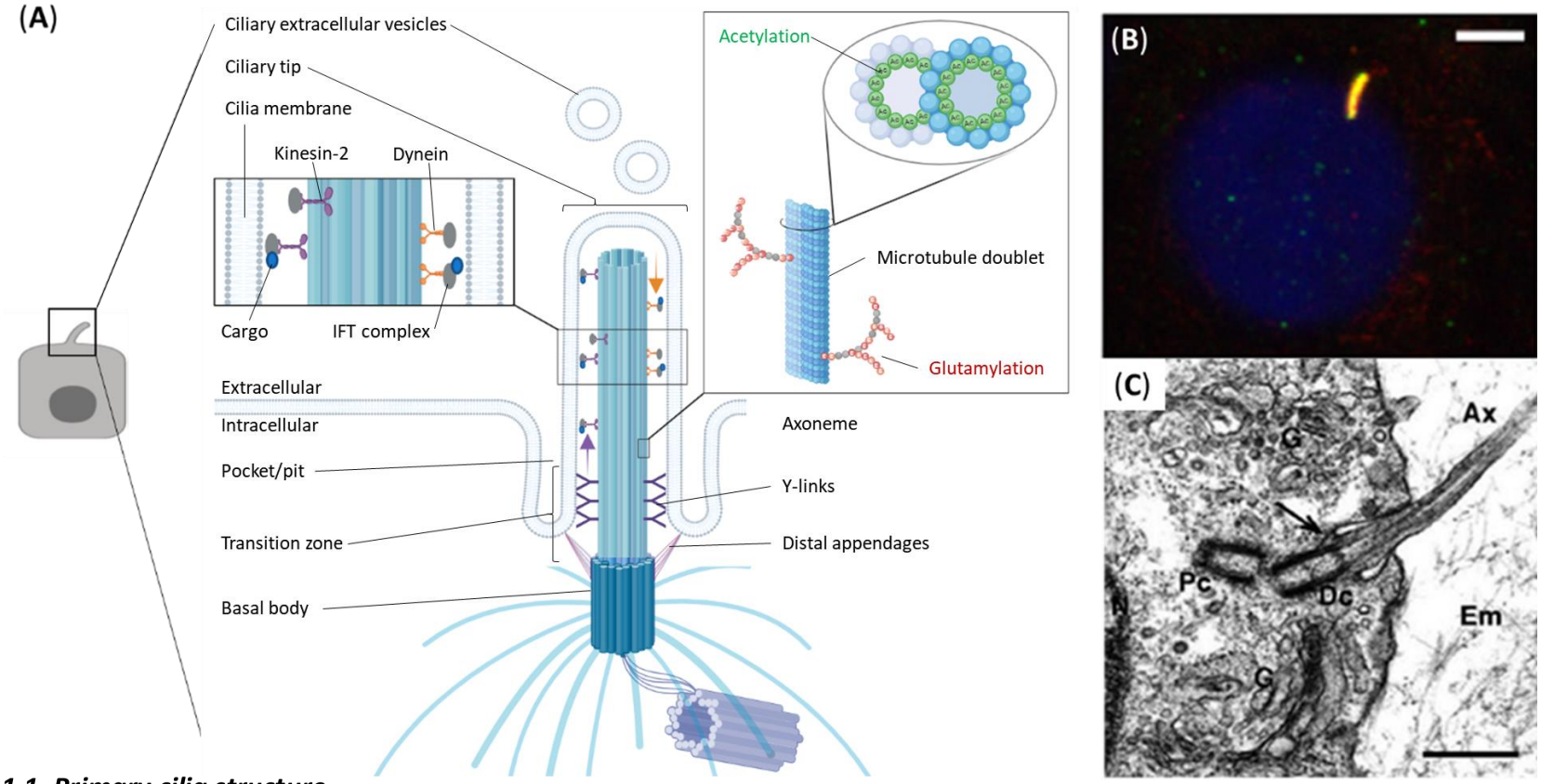

Figure 1.1. Primary cilia structure

(A) Primary cilia structure. Chondrocyte primary cilia visualised by (B) immuno-fluorescent confocal microscopy (Thompson, et al. 2016) and (C) transmission electron microscopy image (Muhammad, et al. 2012). In the confocal image the cilium is labelled with ac-α-tub (red) and Arl13b (green) and the nucleus counterstained with DAPI (blue), scale bar = 5µm. The TEM image shows the axoneme (Ax) projecting out into the extracellular matrix (Em), with proximal (Pc) and distal (Dc) centriole in close proximity to the Golgi (G). Scale bar = 500nm.

The predominant structure of the cilium is a cylindrical, slender feature called the axoneme, composed of nine microtubule doublets. In contrast to the 9+2 structure of the motile cilia axoneme, the primary cilium is denoted as 9+0, which refers to the peripherally located microtubule doublets, lacking the central pair found in motile cilia. Anchoring the axoneme to the cell is the basal body, a modified and matured centriole. The basal body is composed of nine microtubule triplets, two of which contribute to the formation of the axoneme during cilium formation, a process termed ciliogenesis. The basal body and the associated transition zone proteins regulate protein entry and exit into the cilia (Marshall 2008; Pazour and Bloodgood 2008; Berbari, et al. 2009). Proteins common to all cilia include tubulins, microtubule motors, intraflagellar transport (IFT) complexes, Bardet-Biedl syndrome (BBS)-related protein complex and vesicular trafficking-related small GTPases, with few differences observed in additional proteins between cell types, hypothesised to convey specialisation of function (Avasthi, et al. 2017).

Ciliogenesis and the stages of the cell cycle are intrinsically linked, as the ciliary axoneme is derived from the centriole that also coordinates the centrioles of the mitotic spindle (Rieder, et al. 1979). The synchronisation of cilia expression and the phases of the cell cycle are described in the scheme below, Figure 1.2. Upon cell cycle exit, the centrosome of the microtubule organising centre (MTOC) matures into the basal body, from which the axonemal tubulin emerges. Two pathways of early cilia generation are described, the intracellular and the extracellular pathways (Figure 1.2A). During the intracellular pathway, the extension of the ciliary axoneme begins in the cytoplasm upon association of the basal body with the ciliary vesicle (CV); a vesicle formed through the action of EHD1 protein, causing the fusion of

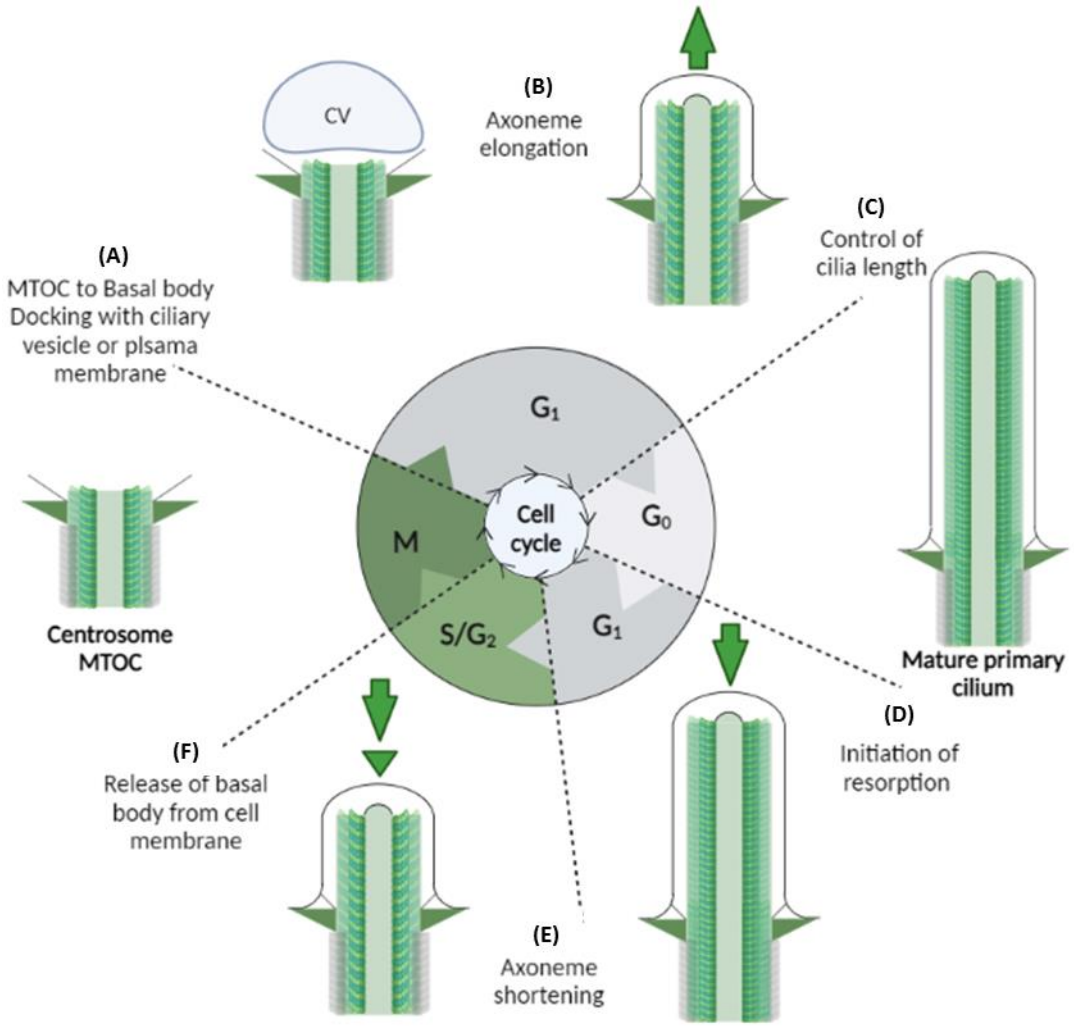

Figure 1.2. Cell and ciliogenesis cycles

*Schematic depiction of the alignment of the ciliogenesis cycle and its multiple steps (**A-F**) with various stages of the cell cycle. Adapted from (Izawa, et al. 2015).*

Rab-8a positive vesicles associated with the distal appendages of the mother centriole (Lu, et al. 2015). In the extracellular pathway the basal body docks directly with the plasma membrane of the cell prior to axonemal microtubule formation (Sorokin 1962).

Once docked, the kinase TTBK2 facilitates the uncapping of CEP110 from the distal end of the mother centriole, thereby allowing microtubule growth and primary cilia axonemal lengthening (Goetz, et al. 2012). This cilia elongation and length

control (Figure 1.2B and C) occur during G1 and G0 (Wheatley, et al. 1996), and are dependent on motor-driven intraflagellar transport (IFT), discussed in more detail in section 1.4. Mature primary cilia are present during G0 and remain until the formation of the mitotic spindle and cell cycle re-entry (Rieder, et al. 1979; Pazour and Witman 2003). The lumen of microtubules that form the doublets of the mature primary cilia axoneme undergo post translational modifications, with acetylation of lysine 40 of the α-tubulin subunit occurring. This modification of the axonemal microtubules is thought to stabilise the structure and allows for more effective binding of IFT motor proteins (Reed, et al. 2006). This reversible modification is catalysed by α-tubulin acetyltransferase (ATAT1), while histone deacetylases (HDACs), predominantly HDAC6, mediate deacetylation of the α-tubulin, triggering ciliary disassembly (Ran, et al. 2015).

The exact point of ciliary resorption during the cell cycle (Figure 1.2D) is dependent on cell type, with some cells initiating cilia resorption during S-phase, and other in the G2 to M transition (Rieder, et al. 1979; Jensen, et al. 1987). The release of ciliary extracellular vesicles has been suggested as a possible trigger for ciliary resorption and a molecular link between the life cycle of the cilium and cellular division cycle (Phua, et al. 2019). Axonemal shortening (Figure 1.2E), occurs as the rate of ciliary disassembly exceeds the rate of ciliary assembly. Finally, the basal body is released from the cilium, freeing up the centrioles (centrosome) to undergo the stages of centriole duplication. Formation of the procentrioles occurs during S-phase, with the oldest of the daughter centrioles acquiring distal and subdistal appendages and finally separation of the two new centrioles occurs prior to initiation of mitosis (Kobayashi and Dynlacht 2011).

1.2. Articular cartilage

Throughout this thesis, studies have used a single cell type, namely the articular chondrocyte. These cells are derived from articular cartilage and *in vitro* can be cultured to a quiescent state where they have a high prevalence of primary cilia expressed on the basal surface in a 2D monolayer. This makes chondrocytes an ideal cell type for analysis of primary cilia length control as discussed in subsequent sections (see section 3.3.5). Chondrocyte cilia are also known to regulate a wide variety of signalling pathways influencing cartilage development, health and disease such as osteoarthritis (OA).

Articular cartilage is fundamentally a mechanoresponsive tissue that is exposed to complex, dynamic mechanical loading during everyday activity. The physical response of the tissue to this loading is critical to its biomechanical function, while the mechanobiological response of the cells ensures maintenance of this tissue. Disruption of either the mechanical environment (e.g. abnormally high or low levels of loading) or the cellular mechanosignalling behaviour leads to cartilage degradation and loss of functionality, associated with musculoskeletal joint disease. Cartilage is an aneural, avascular connective tissue composed predominantly of extracellular matrix (ECM). Articular cartilage, covering the surface of bones in diarthrodial joints, such as the knee, provides a smooth, low-friction surface and functions to distribute the compressive forces experienced by normal articulating joints, thereby protecting the underlying bone from high stress. Articular cartilage has a limited capacity for repair, with the chronic degenerative disease, osteoarthritis, developing as a result of tissue damage.

During normal physiologic movement, articular cartilage is subjected to dynamic mechanical loading, which promotes cartilage matrix production, joint health, and joint maintenance. The articular cartilage ECM composition is regulated by the singular cartilage cell type, the chondrocyte, which makes up only 10% w/v of the tissue's total volume. In particular, chondrocytes are responsible for both the synthesis and degradation of the ECM. These processes are influenced by biochemical and biomechanical stimuli by interacting with the ECM via integrins and other receptors and ion channels expressed at the cell surface (Poole 1997). During joint loading, the extracellular environment of chondrocytes is altered such that the cells are subjected to shear, tensile, and compressive strain; fluid flow; and changes in pH, hydrostatic pressure, and osmolality. Chondrocytes are specially adapted to sense and respond to these physicochemical stimuli and regulate their metabolic profile according to the frequency and amplitude of the load applied (Wilsman and Fletcher 1978; Urban 1994; Kim, et al. 2008).

The mechanisms by which chondrocytes convert mechanical signals into intracellular responses that modulate cell behaviour are not well understood. Given the variety of mechanical stimuli the chondrocyte experiences (Urban 1994), it is unlikely that any one mechanism will prove to be wholly responsible for the multitude of responses that have been observed upon loading. Numerous pathways involving the cellular cytoskeleton, integrins, and mechanosensitive ions have been identified in the process of chondrocyte mechanotransduction. Indeed many excellent reviews of chondrocyte mechanosignalling have been published (Urban 1994). More recently, primary cilia have been suggested as providing a nexus for mechanosignalling in a variety of different cell types including chondrocytes.

1.3. Chondrocyte primary cilia expression

The majority of articular chondrocytes elaborate a primary cilium (Wilsman and Fletcher 1978; Meier-Vismara, et al. 1979; Poole, et al. 1985; Poole, et al. 2001; McGlashan, et al. 2007; McGlashan, et al. 2008; McGlashan, et al. 2010; Wann and Knight 2012). The prevalence, length, orientation, and positioning of chondrocyte primary cilia *in situ* varies with cartilage depth. In bovine patellae, less than 40% of cells in the superficial zone exhibit a primary cilium with a mean length of 1.1 µm. This increases to 65% in the deep zone where the mean ciliary length is 1.5 µm (McGlashan, et al. 2008). Primary cilia in the middle and deep zones are frequently found on the medial or lateral surface of the cell, with respect to the articular surface (McGlashan, et al. 2008; Farnum and Wilsman 2011). While in the superficial zone, where cells experience the greatest levels of compressive strain, ciliary length is at its lowest and the cilia are almost exclusively found pointing away from the articular surface (Guilak, et al. 1995; McGlashan, et al. 2008; Farnum and Wilsman 2011). Chondrocyte primary cilia are significantly longer when cells are isolated from their ECM and cultured in a two-dimensional monolayer, where cilia have a mean length of 2-3 µm and prevalence is up to 90%. These findings suggest a relationship between the mechanical environment and cilium expression.

1.4. Intraflagellar transport (IFT) and cilia length control

As primary cilia lack independent protein synthesis machinery, the assembly, maintenance and function of the primary cilium is reliant on protein transport into and out of the ciliary compartment. Discovered in the green alga, *Chlamydomonas*, intraflagellar transport (IFT) is the mechanism that facilitates protein movement along the ciliary axoneme and is crucial for cilia assembly (Kozminski, et al. 1995; Marshall and Rosenbaum 2001). IFT refers to the transport of protein complexes between the base of the cilium through the transition zone to the distal tip. The transport of proteins can either be anterograde, toward the tip of the cilium, or retrograde, toward the base. Complex A and B are the individual polypeptide subcomplexes that control the bidirectional transport. The polypeptide Complex B is responsible for anterograde transport and relies on proteins belonging to the kinesin 2 family (KIF3A and KIF3B). Complex A controls retrograde transport and is composed of proteins belonging to the dynein 2 protein family (DYNC2 proteins) (Scholey 2003; Pedersen and Rosenbaum 2008).

Controlling cilium length is a dynamic process with continuous turnover of tubulin at the ciliary tip. The initial cilium growth is rapid, occurring within a few hours until a steady-state length is achieved, whereby the rate of assembly and disassembly is equal (Rosenbaum and Child 1967; Marshall and Rosenbaum 2001). IFT is therefore essential for the maintenance of cilia length. Huang *et al.* (1977), demonstrated this by arresting ciliary anterograde transport using a flagellar assembly (FLA) mutant gene *FLA10,* in *Chlamydomonas reinhardtii* which subsequently impaired flagellar regeneration (Huang, et al. 1977). How exactly flagella and cilia set length are determined is still debated with numerous models hypothesised. The cargo loading

model suggest that the amount of cargo loaded onto IFT particles regulates cilia length, such that an increase of cargo loaded onto IFT results in growing or longer cilia, while shorter and resorbing cilia are seen to have reduced cargo (Wren, et al. 2013). The balance point model suggests the ciliary set length is maintained when the assembly rate reaches equilibrium to the set rate of continuous disassembly; it is now suggested that rather than frequency, the size of IFT trains scales inversely as a function of cilia length, where the total cellular quantity of IFT protein remains constant (Engel, et al. 2009). The grow and lock model suggests that a cilium elongates until and locking event occurs, thereby fixing the ciliary length (Bertiaux, et al. 2018), however the molecular mechanism of this process is unclear. Regulation of cilia extracellular vesicle release could also possibly be a mechanism of length control (Phua, et al. 2017). Irrespective of the mechanism, typical cilium length ranges between 1-10µm depending on cell type and environmental conditions (Poole, et al. 2001). Genetic and sensory cues affect the cilium length, with subsequent impact on function.

Cilia diameter is regulated by the axoneme structure and therefore has a standard diameter of 0.2µm. However, super resolution microscopy of bovine primary chondrocytes labelled with acetylated-α-tubulin (Ac-α-tub) and arl13b has shown that the axoneme diameter typically reduces from base to tip (Thompson, et al. 2016; Thompson, et al. 2017). Electron tomography studies of both chondrocytes and epithelial cells have suggested that this tapering is due to not all 9 microtubule doublets extending to the ciliary tip (Jensen, et al. 2004; Sun, et al. 2019). In addition, the presence of cilia with bulbous tips has been reported upon exposure to lithium

chloride (LiCl) and in the genetic disease alkaptonuria and attributed to alterations in IFT trafficking (Thompson, et al. 2016; Thorpe, et al. 2017).

1.5. Primary cilia function

The primary cilium has evolved to have multiple diverse functions, owing to the distinct cellular compartment and unique lipid and receptor composition of this organelle. These include chemosensation, mechanosensation, and signalling pathway regulation, all of which are dynamic and dependent on the differentiation state and the microenvironment of the cell (Anvarian, et al. 2019). Primary cilia are thought to coordinate several signalling pathways that are critical for development, physiology, and regeneration including the hedgehog, transforming growth factor (TGF) β, G-protein-coupled receptor (GPCR), and wingless/integrated (Wnt) pathways (Labour, et al. 2016; Bangs and Anderson 2017; Liu, et al. 2018; Anvarian, et al. 2019). The most well-characterised cilia signalling pathway is hedgehog signalling as shown schematically in Figure 1.3. Movement of hedgehog signalling proteins such as Ptch1 and Smoothened on and off the ciliary axoneme regulates downstream hedgehog gene transcription targets important in development, health and disease (Rohatgi and Scott 2007).

With a heterogeneous mixture of receptors, ion channels, and proteins distinctly localised to or concentrated at the primary cilium, this specialised and dynamic cellular compartment has a wide variety of denoted functions. As previously discussed, cilia expression and the cell cycle are intrinsically linked, where docking of the basal body and cilia expression sequesters the centrosome, thereby acting to supress cell cycle progression.

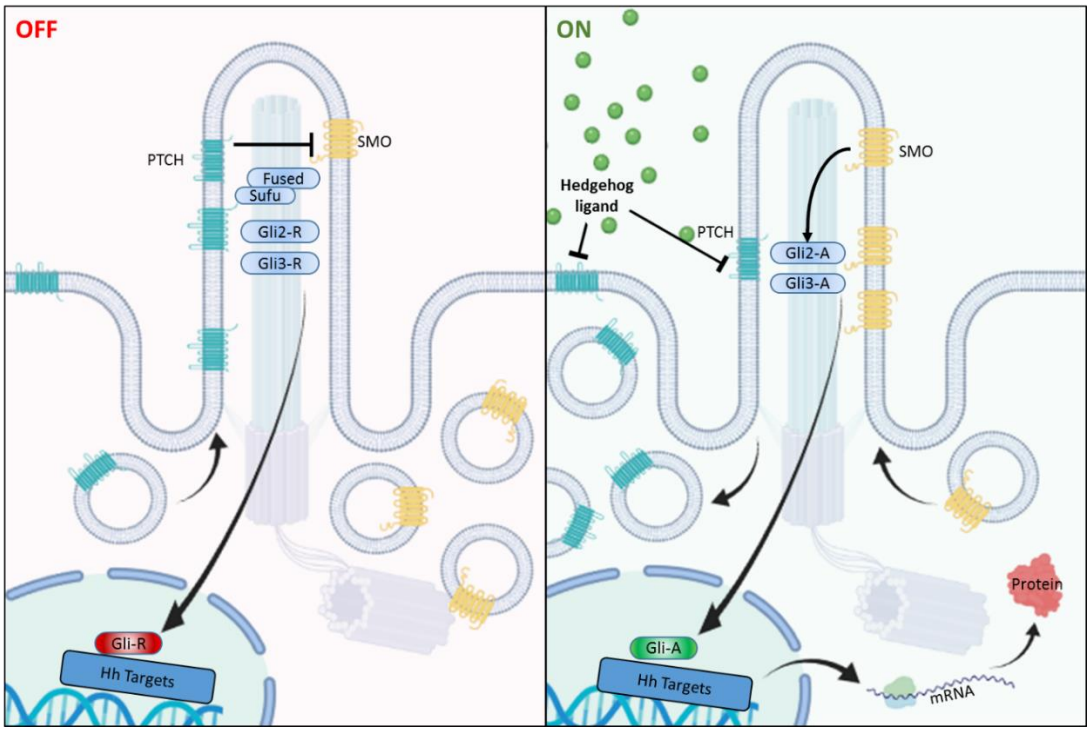

Figure 1.3. Primary cilia in hedgehog signalling

In the absence of Hh ligand (left panel), Ptch1 acts to inhibit Smo and its ciliary localisation. This allows ciliary Gli processing into its repressor form (Gli-R) which is then translocated to the nucleus of the cell where it acts to inhibit hedgehog genes. In the presence of Hh ligand (right panel), binding to Ptch1 results in its degradation, releasing its inhibition on Smo. Smo then accumulates in the cilium preventing Gli cleavage and releasing the activator form. Gli-A is translocated to the nucleus where it induces transcription of Hh genes. Adapted from Satir, P (2010).

One of the earliest known sensory roles for the cilium was in photoreception and olfaction (Berbari, et al. 2009). For light detection, photoreceptors use a modified cilium connected to an outer segment composed of discs derived from the plasma membrane. The maintenance of this outer segment relies on IFT, as demonstrated in *Kif3a* and Oak Ridge Polycystic Kidney (ORPK) mutant mice, in which absence of IFT resulted in blindness (Pazour, et al. 2002). Furthermore, IFT is an established method of protein transport from the outer segment to the inner cell, via the cilium. In olfaction, the dendritic endings of sensory neurons may have non-

motile cilia, which provide sensory transduction through an adenylyl cyclase type III (ACIII)-mediated cyclic AMP (cAMP) process, with signal amplification via Ca^{2+}-activated chloride channels (McEwen, et al. 2008).

The role of the cilia as a mechanosensor was first reported in kidney epithelium, whereby deflection of the cilia in response to fluid movement triggered an intracellular calcium signal (Praetorius and Spring 2001). The role of the cilia as a mechanosensor has subsequently been reported in multiple organ types and tissues such as the kidneys (Praetorius and Spring 2001; Praetorius and Spring 2003), and endothelium developmental processes. However, it has been suggested that whilst the cilium may be required for mechanotransduction, in cells, such as the chondrocyte, it is not necessarily the initial mechanoreceptor. Rather, primary cilia have been shown to be required for downstream ATP reception, as cells lacking a primary cilium have been reported to not elicit the same Ca^{2+} response to exogenous ATP as wild type cells that express a functional primary cilium (Wann, et al. 2012).

1.6. Ciliopathies

A seminal discovery highlighting the link between ciliary dysfunction and human pathology was through work performed in the ORPK mouse/Ift88^{orpk}, which presents with autosomal dominant polycystic kidney disease (ADPKD) (Pazour, et al. 2000). IFT88 is a component of anterograde IFT and is required for ciliogenesis (Lehman, et al. 2008), and thus ORPK mice have few cilia and those present are abnormally short (Pazour, et al. 2002), linking primary cilia and ADPKD. Given the diverse expression and function of primary cilia in human physiology is it not surprising that genetic defects in this organelle can lead to numerous pathological conditions commonly termed ciliopathies. Summarised below in Table 1.1 (adapted from (Ware, et al. 2011)), these ciliopathies are associated with genetic mutations to numerous different genes. Many of the ciliopathies such as Sensenbrenner syndrome and Jeune Asphyxiating thoracic dystrophy have musculoskeletal phenotypes. However, several tissues and organs are reported as being affected in the clinical features of these diseases, as is seen in Table 1.1. Further to the genetic ciliopathies, in more recent years aberrant primary cilia have also been reported in other diseases such as atherosclerosis and osteoarthritis. Human diseases associated with ciliary dysfunction have been extensively characterised, see reviews for further details (Hildebrandt, et al. 2011; Novarino, et al. 2011; Waters and Beales 2011).

Table 1.1. Summary of ciliopathies, their associated genes and clinical features, adapted from Ware, et al. 2011

Ciliopathy	Gene(s)	Clinical features
Sensenbrenner syndrome	IFT122, WDR35	Cranioectodermal dysplasia, narrow thorax, dental anomalies, hepatic and renal involvement
Jeune Asphyxiating thoracic dystrophy	IFT80	Skeletal dysplasia, thoracic deformities; polydactyly; renal cysts; retinitis pigmentosa
Ellis van Creveld syndrome	EVC1, EVC2	Skeletal dysplasia; congenital heart defects; polydactyly; ectodermal dysplasia
Short rib polydactyly	NEK1, DYNC2H1	Lethal skeletal dysplasia, polydactyly, multiple congenital anomalies
Bardet-Biedl syndrome	BBS1, 2, ARL6, BBS4,5, MKKS, BBS7, TTC8, BBS9, 10, TRIM32, BBS12, MKS1, CEP290, C2ORF86, MKS1, MKS3, CCD28B	Polydactyly, obesity, retinitis pigmentosa, anosmia, congenital heart defects
McKusick-Kaufman syndrome	MKKS (BBS6)	Postaxial polydactyly, urogenital anomalies including hydrometrocolpos, congenital heart defects
Oral-facial-digital syndrome type 1	OFD1	Oral cavity, face, and digit anomalies, CNS abnormalities, cycstic kidney disease; X-linked with male lethality
Carpenter syndrome	P4HB	Bone fragility, craniosynostosis, ocular proptosis, hydrocephalus
Primary cilia dyskinesia	DNAI1, DNAH5, DNAH11, DNAI2, KTU, TXNDC3, RPGR, RSPH4A, RSPH9, LRRC50, CCDC40, CCDC39	Bronchiectasis, sinusitis, otitis media, infertility, situs defects
Polycystic kidney disease	PKHD1, PKD1, PKD2	Renal cysts, hepatic fibrosis, autosomal dominant and recessive forms
Nephronophthisis	NPHP1-4, IQCB1, CEP290, GLIS2, RPGRIP1L, NEK8, SDCCAG8, TMEM67, TTC21B	Renal cysts with or without extra-renal symptoms
Meckel-Gruber syndrome	MKS1, TMEM216, TMEM67, CEP290, RPGRIP1L, CC2D2A	Renal cysts, CNS anomalies, polydactyly, congenital heart defects
Senior-Loken syndrome	NPHP1-6, SDCCAG8	Juvenile nephronophthisis, Leber amaurosis
Leber congenital amaurosis	GUCY2D, RPE65, LCA3-14, CEP290	Visual impairment in first year of life; pigmentary retinopathy
Joubert and related syndromes	JBTS1, TMEM216, AHI1, NPHP1, CEP290, TMEM67, RPGRIP1L, ARL13B, CC2D2A	Hypoplasia of the cerebellar vermis, dysregulated breathing pattern, retinal dystrophy, renal anomalies
Alstrom syndrome	ALMS1	Dilated cardiomyopathy, obesity, sensorineural hearing loss, retinitis pigmentosa, endocrine abnormalities

1.7. Chondrocyte primary cilia signalling

A variety of *in vivo* and *in vitro* models have been used to investigate the role of the primary cilium in chondrocyte signalling. *In vivo* genetic mutation models have suggested a role for the primary cilium in the development and maintenance of articular cartilage. In particular, the ever important $Tg737^{ORPK}$ mouse, introduced earlier, has increased articular cartilage cellularity and the tissue exhibits altered expression and distribution of collagen II (McGlashan, et al. 2007). Furthermore, mice with a cartilage-specific deletion of primary cilia (Col2a-Cre; $Ift88^{loxP/loxP}$) have been reported to have thicker, more cellular articular cartilage with increased collagen II and aggrecan in the pericellular region (Chang, et al. 2012). It is important to note that although IFT88 is a ciliary associated protein, it has also been demonstrated to have other functions in the cell, such as to specify the inflammatory response by tuning NFκB signalling independently of the primary cilium (Mc Fie, et al. 2020). This highlights the potential for non-ciliary functions of cilia proteins within the cell. Other studies have investigated cartilage in BBS, a human ciliopathy presenting with a musculoskeletal polydactyly phenotype (Chang, et al. 2012). In mice harbouring mutations in several of the BBS proteins, the proteoglycan content of the cartilage matrix was reported to be lower and the tissue exhibited a reduced thickness relative to WT mice (Kaushik, et al. 2009).

Owing to the complexity of the mechanical environment within the articular cartilage *in situ*, numerous *in vitro* studies have used isolated chondrocyte models to investigate mechanotransduction and the role of the primary cilium in this process. In these experimental systems the influence of different mechanical stimuli can be

examined in isolation from the physicochemical changes associated with compression of the charged ECM. These models include either isolated chondrocytes in a monolayer subjected to tensile strain (Millward-Sadler, et al. 2000; Huang, et al. 2007; Nishida, et al. 2008) or fluid flow (Yellowley, et al. 1997; Degala, et al. 2012), or chondrocytes seeded within 3D constructs (e.g., agarose) and subjected to compressive strain (Tanaka, et al. 2005; Pingguan-Murphy, et al. 2006; McGlashan, et al. 2010) or hydrostatic pressure (Browning, et al. 2004; Mizuno 2005). Wann *et al.* (2012) provided the first direct evidence supporting a role for the primary cilium in chondrocyte mechanotransduction using a mutant cell line generated from the $Tg737^{ORPK}$ mouse (Wann, et al. 2012). In WT cells, cyclic mechanical compression triggered ATP release and activated a Ca^{2+} signalling cascade, culminating in the upregulation of aggrecan gene expression and proteoglycan synthesis. In the mutant (ORPK) chondrocytes, no significant changes in aggrecan expression were observed and proteoglycan production was not altered in response to mechanical loading. Although the mechanosensitive release of ATP was observed in both WT and ORPK chondrocytes, the Ca^{2+} signalling downstream of this event was disrupted in ORPK hypomorphic IFT88 cells. This study indicated that the chondrocyte primary cilium and/or IFT88 is an essential component of the mechanotransduction response but intriguingly is not involved in initial mechanosensing.

Cleavage of the polycystin (PC) 1 C-terminal tail was increased in $IFT88^{ORPK}$ chondrocytes lacking cilia, suggesting PC1 may have a novel function in this mechanosignalling response (Wann, et al. 2012). Using the chondrogenic mouse cell line ATDC5, a model for growth plate chondrocytes, Rais *et al.* (2015) demonstrated

the importance of KIF3A, a fundamental ciliary motor protein, in chondrocyte mechanotransduction. KIF3A expression was knocked down in ATDC5 cells, mechanical stretch was applied, and a panel of mechanosensitive genes was examined. While some mechanosensitive genes were either completely or partially independent of KIF3A, others, such as aggrecan and collagen type X (major ECM components), had their responsivity abolished with KIF3A knockdown. Additionally, regulation of the primary-cilium-related genes PKD1, PKD2, IFT88, and IFT172, in response to mechanical load, is also KIF3A-dependent, such that when KIF3A expression is disrupted, these genes are also downregulated (Rais, et al. 2015).

Although the mechanistic pathway has begun to be elucidated, the exact mechanism and components behind the role of the primary cilium in chondrocyte mechanotransduction remain unclear. By contrast, the role of primary cilia in hedgehog signalling in all cell types, including chondrocytes, has been well characterised. As discussed in section 1.5, hedgehog signalling components are shuttled through the ciliary compartment. The effect of mechanical loading primary cilia structural alterations on hedgehog signalling are discussed further in section 1.9.

1.8. Mechanical and biochemical regulation of cilia expression

Increasingly, studies are reporting that the physicochemical environment to which cells are exposed can regulate their primary ciliary expression, with changes observed in prevalence, length, orientation, and position.

Primary cilia are known to disassemble and shorten in response to mechanical loading, in the form of compression (McGlashan, et al. 2010), tensile strain (Thompson, et al. 2014; Rowson, et al. 2018), fluid shear (Luo, et al. 2014), or hydrostatic pressure (Luo, et al. 2014). Studies have also reported modulation of ciliary length in response to other physicochemical stimuli including osmotic challenge (Rich and Clark 2012), changes in substrate stiffness, or changes in surface topography (Zhang, et al. 2017).

Mechanosensitive cilia disassembly appears to be conserved in multiple cell types including chondrocytes (McGlashan, et al. 2010; Thompson, et al. 2014), tenocytes (Rowson, et al. 2018), epithelial cells (Luo, et al. 2014), endothelial cells (Iomini, et al. 2004), and MSCs (Delaine-Smith, et al. 2014). However, some cell types appear to be more sensitive to mechanically-induced ciliary disassembly. For example, isolated tenocytes show almost complete loss of cilia in response to 5% cyclic tensile strain (Rowson, et al. 2018), whereas chondrocytes exhibit much more modest reduction in ciliary length in response to 20% strain (Thompson, et al. 2014). These differences may be due to the *in vivo* mechanical environment to which different cell types are exposed during normal physiologic activity. Tenocytes are unlikely to routinely experience strains above 2-3%, whereas chondrocytes routinely experience 10-20% compressive strain during normal activity. In endothelial cells,

alterations in fluid flow regulate cilium expression *in vivo* such that increased prevalence of elongated cilia is observed in areas of disturbed flow including bifurcation points (Van der Heiden, et al. 2008; Dinsmore and Reiter 2016). This mechanism of mechanically induced ciliary disassembly appears to involve activation of the tubulin deacetylase, HDAC6, which causes deacetylation of the axoneme and increased disassembly, leading to shorter cilia (Nguyen, et al. 2015). It is unclear whether this reflects a snapshot of a process leading to complete disassembly or a new stable shorter cilium set length.

Numerous studies have identified actin tension as being a key regulator of ciliogenesis and set length. Thus, changes in cilium expression may be initiated by changes in actin organisation, which are well known to occur in response to mechanical loading. The upstream mechanism associated with this alteration in actin may include mechanosensitive activation of calcium signalling, leading to conformational changes in actin-associated proteins. Other studies have described the importance of the Yap/Taz pathway in modulating actin organisation and cilium expression (Kim, et al. 2015; Nagai and Mizuno 2017).

1.9. Effect of cilia length on cilia signalling

The primary cilium is now an established signalling organelle capable of transducing a number of biophysical extracellular signals. Numerous studies have suggested a link between cilia structure and function. In particular, studies have reported correlations between cilia axoneme length and various signalling pathways including mechanosignalling, hedgehog signalling and growth factor signalling.

It is well established that genetic disruption of both motile and primary cilium structure is associated with loss of function in the so-called ciliopathies (for review see (Badano, et al. 2006; Hildebrandt, et al. 2011). However, more recent evidence suggests that mechanical, physicochemical, or pharmaceutical changes in primary cilium length are also associated with alterations in cilium-mediated signalling. For example, a slight ciliary disassembly induced by mechanical loading of bovine chondrocytes (0-20% cyclic tensile strain), inhibits hedgehog signalling at the level of Gli1 and Ptch1 expression levels (Thompson, et al. 2014). Inhibition to the disassembly of microtubules using tubacin, an HDAC6 inhibitor, prevented mechanically induced ciliary disassembly and restored normal levels of hedgehog signalling. However, despite the evidence that changes in ciliary expression and length are associated with alterations in ciliary function, the mechanisms for this environmental regulation of ciliary signalling remain unclear. In the case of mechanosignalling in response to fluid flow, as occurs in epithelial cells, osteocytes, and MSCs (Delaine-Smith, et al. 2014; Luo, et al. 2014), increases in the length of apical cilia are likely to result in greater levels of ciliary deflection (Spasic and Jacobs 2017; Corrigan, et al. 2019). This may increase activation of mechanosensitive ion channels, such as the PC1-PC2 calcium channel complex or TRPV4, located at the base

of the cilium where bending strains will be highest (Schwartz, et al. 1997; AbouAlaiwi, et al. 2009; Gambassi, et al. 2017). In other cell types, such as chondrocytes, it is less clear how changes in ciliary length may impact mechanosignalling since this does not appear to involve ciliary deflection.

For other cilium or IFT-dependent pathways, such as hedgehog signalling, Wnt signalling, growth factor signalling, and inflammatory signalling, the mechanism through which changes in length regulate signalling is unknown. However, previous studies have identified changes in ciliary length associated with alterations in hedgehog signalling induced by pharmaceutical antagonists (Rydholm, et al. 2010) and by high levels of mechanical strain (Thompson, et al. 2014). Similarly, cilium elongation has been associated with the modulation of IFT-dependent proinflammatory signalling by various chemical and physicochemical stimuli (Wann, et al. 2012). One possible mechanism suggests a relationship between the length of the ciliary axoneme and the rate of IFT protein delivered. According to the balance-point model and other related models of ciliary assembly, as the cilium lengthens, the rate of insertion of IFT cargoes is reduced(Marshall and Rosenbaum 2001; Engel, et al. 2009). When these IFT cargoes are carrying tubulin for assembly into the axoneme at the tip, this causes the rate of ciliogenesis to slow and eventually stop at a stable set length where the rate of anterograde delivery of tubulin is matched by the constant rate of disassembly and retrograde transport. It is therefore possible that the same mechanism controlling IFT cargo injection and tubulin delivery may also regulate the delivery on and off the axoneme and associated accumulation of signalling proteins necessary for ciliary function.

Alternatively, changes in ciliary length may be indicative of alterations in IFT, which may be the real driver for the modulation of signalling activity. In this scenario, the alterations in ciliary length are purely a readout of changes in ciliary function and are not the direct cause. Whatever the mechanism, there is clearly increasing evidence of a correlation between ciliary length and ciliary function.

In addition to axoneme length, other changes in ciliary expression and morphology may also influence the associated signalling. For example, it is unclear what drives cilia to be expressed on the apical or basal cell surfaces (Van der Heiden, et al. 2008) and yet a switch from one to the other could have profound consequences on ciliary deflection and mechanosignalling in response to fluid flow and potentially other signalling pathways. Similarly, alterations in the mechanical properties of the axoneme, possibly through posttranslational modifications of the tubulin or structural changes in its doublet structure, may lead to changes in IFT or mechanical deflection and the ability to respond to fluid shear (Nguyen, et al. 2015; Gambassi, et al. 2017). Other studies have measured the projection of the cilium from the ciliary pocket (for review see (Benmerah 2013)). In cells where the axoneme is largely invaginated within the pocket, it may be hypothesised that the responsiveness to external mechanical and chemical stimuli is attenuated or differs from those with primary cilia expressed in the extracellular environment. Furthermore, a cilia length increase may result in an increased ciliary membrane surface area and an increased ciliary compartment volume. This larger surface area and volume could allow for the increased accumulation of signalling receptors to the cilium, thereby increasing signal responsiveness. Alternatively, the increase in

surface area and volume could dilute or increase the separation of receptors and signalling molecules, thereby attenuating the signal strength and responsiveness.

Understanding the relationship between cilia function and cilia length and other structural parameters remains a key challenge important in the understanding of cilia biology, disease and the development of potential ciliotherapies.

1.10. High-throughput screening of cilia length control

Although primary cilia have been at the centre of a few screening and high content analytical studies, using gene targeting and proteomic analysis methodologies, most outputs report genes crucial for the assembly of the cilium and collections of protein specific to primary cilia expression. On a large screening scale, little work has been published identifying regulators of cilia set length and how alteration to this structure might regulate cell signalling events. There are at least two unpublished imaging screens of cilia length regulation using compound libraries. One screen from Chris Jacobs' group at Columbia University, USA and one from Colin Johnson's and John Sawyer's groups at University of Leeds and University of Newcastle, respectively. The fact that both screens remain unpublished is perhaps an indication of the complexity of establishing a reliable and fully validated screen.

The screen conducted in Chris Jacobs' group by Milos Spasic aimed to identify pharmacological regulators of primary cilia length and resulted in a patent (Jacobs and Spasic 2019). Conducted on a MLO-Y4 osteocyte cell line originating from mice, cells were cultured for a total of 72 hours in 384 well format and triplicate compound treated at a concentration of 10μM for 16hrs prior to cell fixation. The 6,931 compounds used were an accumulation of small molecules sourced from five different commercial suppliers with some overlap between libraries (i.e. certain molecules could appear up to 5 times in the library). There were 8 DMSO vehicle control wells on each of the screening plates. Once fixed, osteocytes were dual labelled with ac-α-tubulin and Hoechst, prior to wide field 2D imaging at 40x magnification on the GE INCell2000, where 4 fields of view were captured. A custom

MATLAB analysis protocol was developed that generated 3 outputs, namely the number of nuclei, number of cilia and average cilia length in each image. From these primary outputs cilia incidence could be derived. Hits were classified as having a normalised triplicate mean that was at least 1.5 standard deviations away from the population mean and a viability of at least 40%. From this, 105 individual compounds were identified as hits for either an increase in cilia length and/or incidence.

Although there are some similarities to the primary aim of this thesis project, there are several significant shortcomings to the methodology of the aforementioned screen. As previously mentioned, the screen was conducted on a murine derived osteocyte cell line rather than primary cells. *In vivo* osteocytes have very short cilia and although they claim this cell type was selected due to their consistent cilia length and incidence, they fail to report which surface the primary cilium is elaborated from on the cell in 2D culture. It is extremely challenging to accurately measure the length of apical cilia where these project parallel to the axis of the microscope. The orientation of the cilium in relation to the culture surface and the microscope will therefore significantly impact the accuracy by which ciliary projected length might be measured. This is especially true considering their choice to perform 2D wide field imaging rather than confocal 3D imaging. Additionally, wide field imaging would capture a single in focus region of the cultured cells, which could omit a proportion of the cilia present, depending on where they are expressed and hence prevalence measures will also be inaccurate.

Furthermore, the analysis parameters of this previous screen were highly focused, reporting only nuclear number, cilia incidence and average cilia length.

Screening hits were also reported in a unidirectional manner, looking only to identify those compounds that increase cilia length and incidence, limiting the scope of the potential screening outputs. Although, the screens dual staining methodology allowed for cilia length and incidence to be assessed, it limited the assessment of how ciliary specific the observed compound effects were. For example, although there is an enrichment in the ciliary axoneme of ac-α-tubulin, acetylation of cytoplasmic tubulin cytoskeleton may still occur, and this may have a profound effect on cell signalling. The limited analysis parameters included in this screen fail to capture what a compounds effect might be on the general cell acetylation profile. In addition, hyper-acetylation of cytoplasmic tubulin may reduce the reliability of automated cilia detection. Furthermore, compounds may alter the cells actin network which is a known regulator of ciliation, an effect that could not be assessed due the screens limited labelling panel. Therefore, cilia length may increase in response to a certain compound, but it would remain unknown if this was due to other cytoplasmic changes which may have a profound effect on cell signalling.

Finally, the 105 hits identified in this screen were classified with a low threshold of deviation from the population mean and with a viability threshold of 40%. A compound could be toxic to the point of reducing the number of cells imaged in the 4 fields of view by more than 50%, and still be classified as a hit. Furthermore, these 105 compounds are not validated with any further screening repeats, or in different cell lines, sources or cell types.

Therefore, due to the limitations to the minimal previous work done in this area, herein we aimed to conduct a rigorous primary cilia screen, in the hopes to better enable the understanding between cilia structure and function.

1.11. Project aims and objectives

The overall aim of this project was to design and run a high throughput screen that would enable the detection of primary cilia incidence and structural alteration in response to compound treatment. Identification of novel structure regulators would provide tools enabling investigation into the structure-function relationship of the primary cilium. Initially, this would be performed through further interrogation of the effect of cilia structural alterations on the hedgehog signalling pathway.

Therefore, the projects objectives were to:

- Optimise the culture conditions for high-throughput confocal screening in bovine chondrocytes.
- Select an appropriate compound library and format, and identify an incubation time allowing detection of cilia structural alteration.
- Develop a robotic liquid handling protocol for compound treatment and immunofluorescent labelling.
- Select a cell labelling regime to detect cilia structure alterations.
- Develop and validate a high-throughput imaging and image analysis pipeline.
- Utilise cluster analysis to identify hit compounds and validate in multiple animals.
- Validate hit compound in a human chondrocyte cell line.
- Develop RT-qPCR methodology to quantify hedgehog signalling in human chondrocytes.
- Investigating the effect of cilia structural alteration induced by hit compounds on ciliary hedgehog signalling.

2. General Materials and Methods

2.1. Cell culture preparation

2.1.1. Cell culture media preparation

Bovine chondrocyte cell culture medium consisted of low-glucose Dulbecco's modified eagle medium (DMEM, D5921, Sigma-Aldrich) supplemented with 10% (v/v) foetal calf serum (FCS, F7524, Sigma-Aldrich), 1.73mM L-glutamine (G7513, Sigma-Aldrich), 86.5 units(U)/ml penicillin, 86.5µg/ml streptomycin (P4333, Sigma-Aldrich) and 17.3mM HEPES (H0887, Sigma-Aldrich). Serum free culture media was made up without the addition of FCS.

Human chondrocyte C28 cell line culture medium consisted of a 1:1 ratio of Lonza BioWhittaker Ham's F-12 medium (BW12-615F, Thermo Fisher Scientific) and DMEM with 4.5g/L glucose, with L-glutamine (BW12-604F, Thermo Fisher Scientific), supplemented with 10% (v/v) FCS (F7524, Sigma-Aldrich), 86.5U/ml penicillin, 86.5µg/ml streptomycin (P4333, Sigma-Aldrich).

2.1.2. Isolation of primary bovine chondrocytes

This study utilised a well-characterised source of isolated primary articular chondrocytes (Chowdhury, et al. 2001; Chowdhury, et al. 2006; Thompson, et al. 2014; Thompson, et al. 2016). Bovine chondrocytes were isolated from full depth slices of articular cartilage, dissected under sterile conditions from the proximal surface of bovine metacarpophalangeal joints (steer age: between 3 and 8 months obtained from a local abattoir on the day of slaughter). Cartilage slices were finely diced, washed, and incubated on rollers at 37℃ for 1 hour (hr) with protease (P5157, Sigma-Aldrich). The concentration of protease was optimised at 20 U/ml as described in section 3.2. This was followed by a further overnight (12-16hr) incubation on

rollers at 37℃ in collagenase (100U/ml in culture media; C7657, Sigma Aldrich). The collagenase digestion mix was passed through a 70µm cell strainer and centrifuged at 733×*g* for 5 minutes (min). The resultant cell pellet was re-suspended in 20ml culture medium. Cell viability and concentration were determined using the Trypan Blue dye exclusion assay and haemocytometer.

2.1.3. 2D primary bovine cell culture

Cells cultured in 6-well culture plates (Corning Costar), were seeded at a density of 8×10^4 cells/cm^2 in 2ml/well of culture medium. For cells cultured on glass, sterile glass coverslips (1.5µm thick; 631-0150, VWR), were placed into 24-well culture plates (3526, Corning Costar) and media coated overnight at 37℃. Cells were then seeded onto the prepared coverslips at a density of 8×10^4 cells/cm^2, in 1ml/well of culture medium. Cells cultured in tissue culture treated 384-well cyclic olefin foil culture plates (Perkin Elmer, CellCarrier-Ultra tissue culture treated plates), were seeded at a lower optimised cell density of 6×10^4 cells/cm^2 in 50µl/well of culture medium. For all culture conditions cells were maintained at 37℃ in a humidified 5% CO_2 incubator, with media changes every 2-3 days, until confluence was reached (~day 6-7 of culture).

2.1.4. 2D cell culture of C28 human chondrocyte cell line

The C28/I2 cell line was kindly acquired from Karen Luis research group at UCL. Monolayer cell cultures were maintained in T75 centimetre squared (cm^2) vented flasks (Corning, UK) at 37°C in 5% carbon dioxide (CO2) and 95% humidity. Cells were passaged by removing culture medium, washing the cells in 10ml PBS before detaching the cells from the culture surface for ∼10min at 37°C in 7ml of

0.05% trypsin-ethylene diamine tetracetic acid (EDTA) with phenol red (25300054, Life Technologies). The trypsin-EDTA was neutralised by adding 7ml of culture medium (see 2.1.1. Cell culture media preparation) before the cell suspension was centrifuged at 700×*g* for 3min. The supernatant was carefully removed, without disruption to the cell pellet. The cell pellet was thoroughly re-suspended in 10ml of fresh cell culture medium. Cells were then counted and seeded into a new T75 flask at a cell density of 1 x 10^6 cells per flask or used at 1 x 10^4 cells/cm^2 , the desired cell density for the relevant experiments. Cell culture media was changed every 2-3 days.

2.2. Immunofluorescent labelling and microscopy

2.2.1. Fixation buffers and methods

All fixation incubations were either 10min or 30min in 4% paraformaldehyde (PFA) at room temperature (RT), for cells cultured of glass in 24-well culture plates or in 384-well screening plates, respectively. Appendix A describes optimisation of fixation techniques for cilia labelling. Cytoskeletal buffer (CB) (Hua and Ferland 2017) base consisted of 100mM NaCl (S9888, Honeywell), 300mM Sucrose (S0389, Sigma-Aldrich), 3mM $MgCl_2$ (M2670, Sigma-Aldrich) and 10mM PIPES (P1851, Sigma Aldrich). For CB solution the base constituents were made up in ddH_2O, filtered, aliquoted and stored at -20℃ until needed. CB-PFA was made by diluting 16% PFA (28908, Thermo Fisher Scientific) to 4% in ddH_2O, to which the various CB base components were added. Just prior to use, the CB base solution and/or the CB-PFA was thawed and 0.5% (v/v) TritonX-100 (T8787, Sigma-Aldrich) and 0.5%(v/v) of ethylene glycol tetraacetic acid (EGTA, 1M stock) were added. In house 4% PFA was made by adding 20g of PFA powder (ThermoFisher) to 450ml of ddH_2O, covered and maintained at 60℃ until dissolved. Five drops of 2 molar NaOH were added along with 50ml of 10xPBS, and the final solution adjusted to pH 7.2. Aliquots were stored at -20℃ and defrosted just before use.

2.2.2. Immunofluorescent labelling

After fixation, cells were permeabilised for subsequent immunofluorescent (IF) labelling. Cells cultured on glass coverslips were permeabilised by incubating for 5min at RT in 0.5% TritonX-100 made up in 0.1% bovine serum albumin (BSA)/phosphate buffered saline (PBS). Cells cultured in 384 screening plates were

permeabilised for 30min at RT in 0.1% TritonX100/0.1%BSA/PBS. Once permeabilised, cell preparations were then blocked for 1hr at RT in 5% donkey serum (D9663, Sigma-Aldrich)/0.1%BSA/PBS and incubated at 4℃ overnight with primary antibodies in 0.1%BSA/PBS (mouse anti-glu-tub 1:1,000). Cells were then washed in 0.1%BSA/PBS. Cells cultured on glass coverslips were sequentially stained, first incubated for 1hr at RT with or without phalloidin (1:1,000) made up in 0.1%BSA/PBS, followed by a 5min RT incubation with 4',6-diamidino-2-phenylindole (DAPI, 200ng/ml) in PBS. Cells cultured in 384-well screening plates were incubated in tandem for 1hr at RT with the appropriate Alexa Fluor conjugated secondary antibodies (goat anti-mouse 647 1:1,000), with or without phalloidin Alexa Fluor (AF) 555 (1:1,000), with DAPI (200ng/ml). Following washes in 0.1%BSA/PBS, cells were then incubated for 3hr at RT with AF 488 conjugated primary mouse anti-ac-α-tubulin (1:1,000), if required. All cell preparations were finally washed in PBS. Glass coverslips were mounted and sealed onto glass slides in ProLong Diamond Antifade (S36967; Life Technologies), whilst 384-well screening plate preparations were stored in PBS and wrapped in parafilm. Both slides and plates were stored long-term at 4℃ in the dark.

2.2.3. Microscopy

Epifluorescent: The Leica DMI4000B epifluorescent microscope with an oil immersion x63 objective was used to acquire manual wide field fluorescent images. When comparing staining protocols, laser intensities, exposure time, brightness and contrast settings were kept constant.

Zeiss LSM Confocal: A Zeiss LSM710 Confocal microscope with a x60/1.4NA oil objective was used to acquire manual full cell depth z-stack images (0.44µm step size). Pixel size of 0.22µm x 0.22µm (Nyquist criteria optimal pixel size = 0.11µm for this objective).

In Cell 2200: The In Cell 2200 microscope with a x4 air objective was used to acquire automated images of full well surface area to assess total cell numbers from 384-well cell culture plates. Intensities and exposure times were kept consistent for all images acquired in an experiment.

In Cell 6000: The In Cell 6000 confocal microscope with a x60/0.95NA air objective was used to acquire automated z-series images (0.5µm step size) from 384-well cell culture plates. Laser intensities and exposure times were kept consistent for all images acquired in an experiment. The fixed pixel size of 0.11 µm x 0.11 µm was used for this microscope (Nyquist criteria optimal pixel size = 0.16µm for this objective)

2.3. Polymerase chain reaction (PCR) assays

2.3.1. RNA isolation

Total RNA was isolated using a RNeasy Mini Kit (Qiagen), using RNase-free reagents, taking care to limit the introduction of RNA degradation contaminants, according to the manufacturer's instructions. Cells cultured in 24-well plates were lysed in 350uL of buffer RLT and stored at -80°C. Prior to RNA isolation, cell lysates were thawed and homogenised using a 200µl pipette tip. Homogenised cell lysates were then mixed with 350µl of 70% ethanol and transferred to a RNeasy Mini spin column. Lysates were centrifuged to bind the RNA to the column and the flow through discarded. Total RNA was washed once with 350µl buffer RW1 prior to 15min on column DNase digestion. After a second wash in 350µl buffer RW1, RNA was then washed twice with 500µl buffer RPE by centrifugation at 10,000*g* for 15s. Following a final dry centrifugation for 2min to remove excess buffer, the RNA was eluted from the column in 30µl RNase free water. RNA concentration, quality and purity were assessed by a Nanodrop ND-1000 spectrophotometer (LabTech) recording A_{260}/A_{280} and A_{260}/A_{230} ratios. A_{260}/A_{230} ratios between 2.0 – 2.2 and A_{260}/A_{280} of approximately 2.0 are considered acceptable for pure RNA, where these criteria were not met RNA precipitation was performed before further use.

2.3.2. Ethanol precipitation

To improve RNA purity, 30µl volume of RNA was precipitated with the addition of 75µl of 100% (v/v) ethanol (EtOH), 1µl GlycoBlue (Life Technologies) and 3µl 3M NaOAc at pH 5.2 and incubated overnight at -20°C. RNA was then pelleted by centrifuging at 13,000rpm for 20mins at 4°C. The supernatant was carefully removed,

and the pellet was washed with 500µl 80% EtOH (v/v). The pellet was re-centrifuged at 13,000rpm for 10mins at 4°C and the supernatant was removed. The pellet was washed for a second time in 500µl 80% EtOH (v/v), centrifuged and the supernatant removed. The pellet was then centrifuged at 13,000rpm for 1min and any excess EtOH was removed. The pellet was then left to air dry for 10mins at RT and re-suspended in 20µl RNase-free H2O. RNA purity and concentration were then detected using a Nanodrop, as described in Section 2.3.1.

2.3.3. Synthesis of complementary DNA (cDNA)

Isolated mRNA was converted to cDNA by reverse transcription, where 1µg of RNA was added to 1µl of 50µM oligoT^{18} (Millipore, UK) and 1µl of 10mM deoxynucleotides (ThermoScientific, USA). The appropriate volume of RNase free H_2O was added to ensure a total reaction volume of 13µL. The reaction was mixed well and incubated for 5min at 65°C followed by a 5min incubation on ice. This was followed by the addition of 4µl 5x first strand buffer (Invitrogen, UK), 1µl of 0.1M dithiothreitol (Invitrogen, UK), 1µL of 40u/µl RNase inhibitor (Invitrogen, UK) and 1µl of 200u/µl Superscript III Reverse Transcriptase (Invitrogen, UK) giving a final reaction volume of 20µl. The sample was then incubated for 45min at 50°C followed by 15min at 70°C to perform the cDNA conversion. The resulting cDNA was stored at -20°C for future use.

2.3.4. Quantitative PCR

To perform the real-time quantitative polymerase chain reactions (RT-qPCR) a master mix was made up to accommodate the number of reactions for each primer pair to be included in a run. This master mix consisted of 12.5µl 2x SYBR Green PCR

Mastermix (Applied Biosystems, UK), 0.2µl of 20µM 5'primer, 0.2µl of 20µM 3'primer, 10.1µl dH_2O and 2µl of converted cDNA per reaction. The final reaction volume was 25µl, run in duplicate for each gene of interest. Primers were sourced from Eurofins Genomics, UK and their sequences are listed in Table 2.1. The StepOnePlus™ Real-Time PCR System (Applied Biosystems) was utilised to facilitate the cycling conditions as listed in Table 2.2. CT values were automatically calculated using StepOne™ Software (Applied Biosystems) and the efficiency of each primer pair was calculated from a standard curve of cDNA dilutions (1 in 2, 4, 8, 16 and 32 cDNA stock dilutions). CT values were normalised to housekeeper genes (GAPDH and 18s) to calculate relative mRNA expression levels.

Table 2.1. Human primers for RT-qPCR

Gene		Sequence	Amplification	Melt curve	Standard curve (dilution, E, R^2)
GAPDH		F - GGCTGCTTTTAACTCTGG R - GGAGGGATCTCGCTCC	✓	✓	1:2, 1.98, 0.994
18s		F - CGGCTACCACATCCAAGGAA R - AGCTGGAATTACCGCGGC	✓	✓	1:10, 1.98, 0.997
Gli1	1	F - GCGTTGTAGAGAGGTTAACCC R - TGATGAAAGCTACGAGGGAG	✓	**X**	N/A
	2	F - AACGCTATACAGATCCTAGCTCG R - GTGCCGTTTGGTCACATGG	✓	✓	1:2, 2.07, 0.998
	3	F - GGGTGCCGGAAGTCATACTC R - GCTAGGATCTGTATAGCGTTTGG	✓	**X**	N/A
Ptch1	1	F - GGGTGGCACAGTCAAGAACAG R - TACCCCTTGAAGTGCTCGTACA	✓	**X**	N/A
	2	F - ACTTCAAGGGGTACGAGTATGT R - TGCGACACTCTGATGAACCAC	✓	✓	1:2, 2.07, 1.00
	3	F - CCAGAAAGTATATGCACTGGCA R - GTGCTCGTACATTTGCTTGGG	**X**	**X**	N/A

Table 2.2. Reaction conditions for RT-qPCR

Cycle Stage	Time	Temperature	No. Cycles
Denaturation	10min	95	1
Annealing/Extension	15sec 1min	95 60	40
Hold	5min	72	1
Melt Curve	15s 1min 15s 15s	95 60 96 60	1 1 1 1

2.4. Protein assays

2.4.1. Cell lysate collection

Cells were cultured to confluence in 6-well culture plates as described in section 2.1.3. Cell culture plates were placed onto ice and the media was removed and discarded before the cells were washed quickly in 1ml ice cold PBS with a protease inhibitor tablet (1 tablet/10ml, Roche). Cells were then lysed in RIPA buffer (R0278, Sigma) with protease inhibitor tablet (1/10ml) for 5min before cells were detached from the plate using a plastic cell scraper. Cells were left for a further 5min then homogenised and centrifuged for 10min in 1.5ml Eppendorf tubes. Without disrupting the resulting pellet, cell lysates were transferred to fresh 1.5ml tubes and stored at -20℃ for later use.

2.4.2. BCA protein assay

The Pierce BCA protein assay kit (ThermoFisher) was used to determine the concentration of total protein in cell lysates, following the manufacturer's microplate procedure.

2.4.3. Western blotting

Cell lysate protein concentrations were normalised and diluted 3:1 with four x Laemmli sample buffer (161-0747, Bio Rad)/10% 2 beta mercaptoethanol (2βME). Samples were heat denatured for 10min at 70℃ before 10.65µg/well of protein was loaded into a 4-15% Mini Protean TGX gel (Bio Rad, 456-1085). Samples were run with a pre-stained molecular weight marker (928-40000 64197860, LI-COR), at 200v for ~35min. Samples were transferred to nitrocellulose membrane using a Trans-Blot Turbo semi-dry transfer cell (Bio Rad), with a tris/glycine transfer buffer, using the

high molecular weight protocol (10min run time). Following transfer, membranes were blocked for 1hr at RT in tris-buffered saline (TBS, Odyssey), on a roller. After blocking, membranes were incubated in primary antibodies diluted in TBS/0.1% (v/v) tween-20 (TBST), overnight at 4℃ on a roller. Membranes were washed 3x10min in TBST before 1hr RT incubation with the appropriate species specific fluorescently conjugated infrared (IR) secondary antibodies (1:15,000, LI-COR), diluted in TBST. This was followed by a further 3x10min wash in TBST, with a final wash in TBS before membranes were imaged using the Li-Cor Odyssey infrared scanner.

2.5. Maximum intensity imaging macros

To enable single pass imaging and 2D analysis of variable depths of the fields captured by confocal microscopy during high throughput screening, Fiji macros were generated. These macros processed individual z-step tiff files into z-stacks which could then have various regions maximum intensity projected into 2D images, compatible with high throughput Developer toolbox analysis protocols (see Figure 2.1). For each well imaged, with 12 fields of view captured in 4 different channels, the macros automate 144 manual steps, generating both full depth and basal region maximum intensity projections.

<table>
<tr><td>IN Cell Output = Individual tiff files</td><td rowspan="5"> 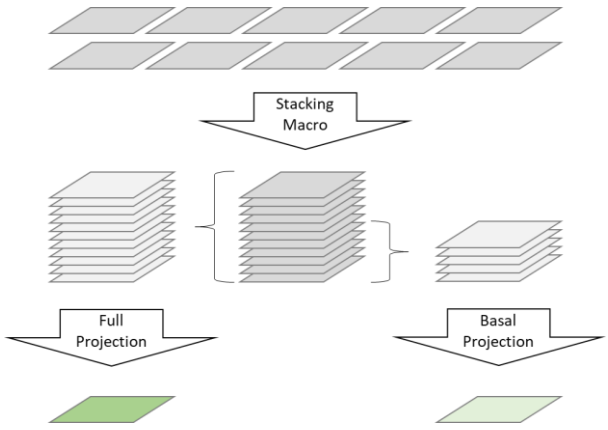
</td></tr>
<tr><td>Run stacking macro</td></tr>
<tr><td>Output = Z-stacks</td></tr>
<tr><td>Run Projection Macros</td></tr>
<tr><td>Output = Full + Basal projections</td></tr>
<tr><td colspan="2">Projections are then analysed using the Developer ToolBox image analysis protocols</td></tr>
</table>

Figure 2.1 Macro image processing workflow.

The In Cell output files are processed in a three-step macro protocol. The first phase of processing compiles the z-stacks, made up of ten individual z-steps. The stacks are then max projected in two separate ways during the second phase. All ten steps are maximum intensity projected to generate the full depth projections, while the first five are projected to generate the basal projections. The resulting max projections are the final image files that are analysed.

2.6. Data handling and analysis

2.6.1. Statistics and graphical representation

Graphical representation and statistical analysis were carried out either in R or using GraphPad Prism 8. Specifics of the data being analysed, n values and the statistical tests used are specified in the respective figure legends. All statistical tests were two sided and parametric tests assumed normal distribution, having confirmed the distribution using the D'Agostino-Pearson omnibus normality test. If the data was not normally distributed, non-parametric tests were employed. A p value less than 0.05 was considered to be statistically significant. Z-scores for a particular parameter were calculated as the difference between compound effect and the average of the DMSO control wells, divided by the standard deviation of the DMSO control wells.

2.6.2. High throughput screening data handling

Large data sets generated through the high throughput screening were imported into a MySQL database using a Python script. The database was interrogated using MySQL queries, generating z-score tables. From these tables, hierarchical clustering with graphical representations were performed using R for cluster identification, first pass hit identification and phenotypic discovery (see Figure 2.2).

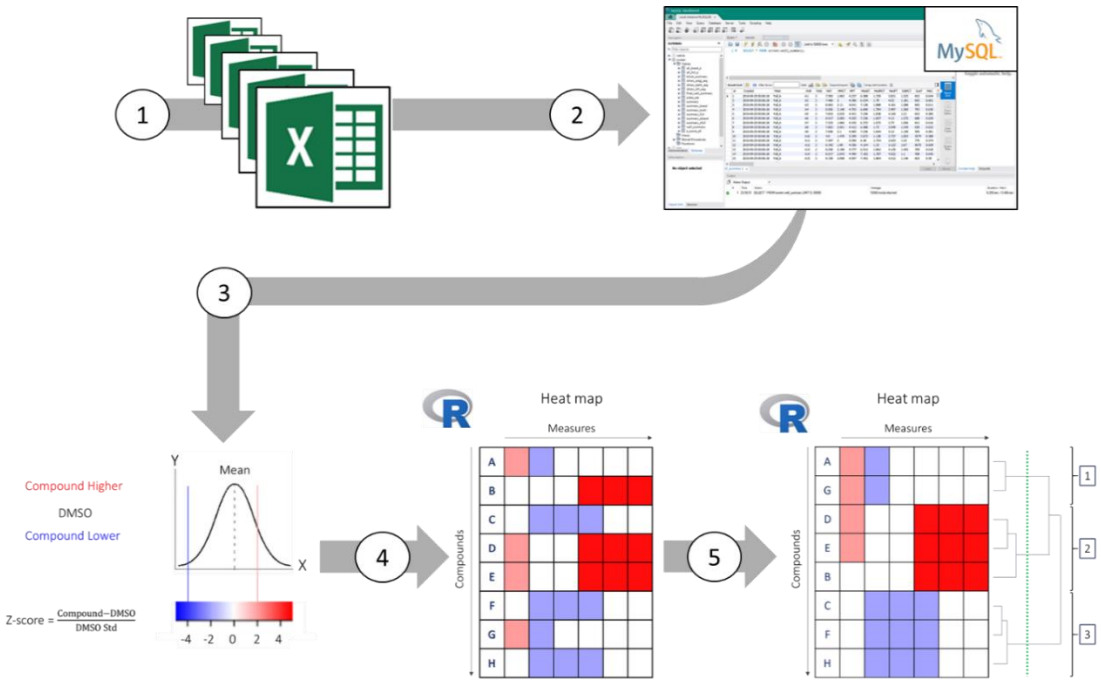

Figure 2.2. Workflow of screening data storage plan and handling.

1 *Well summary data is exported from the Developer toolbox analysis protocol as CSV files.* ***2*** *Raw measurement data were imported into a MySQL database, used to query the data, and generate z-score matrices for all the measures.* ***3-4*** *In R, z-scores were assigned a colour and plotted into heat maps.* ***5*** *Still in R, the heat maps were then organised into compound groups that have different phenotypic effects, by hierarchical clustering.*

2.7. Screening workflow

The compound screen and follow up validation experiments were run using the following workflow, described in Figure 2.3. Screening was made up of two phases, the wet work: starting at retrieval (see 2.1.2) and culturing (see 2.1.3) of the primary bovine chondrocytes, carrying through to the prepared fluorescently labelled cells in 384-well culture plates (see section 2.2), and the second phase consisting of data collection and management (see 2.5 and 2.6). This general workflow was utilised for first pass screening compound validation in both bovine and human chondrocytes.

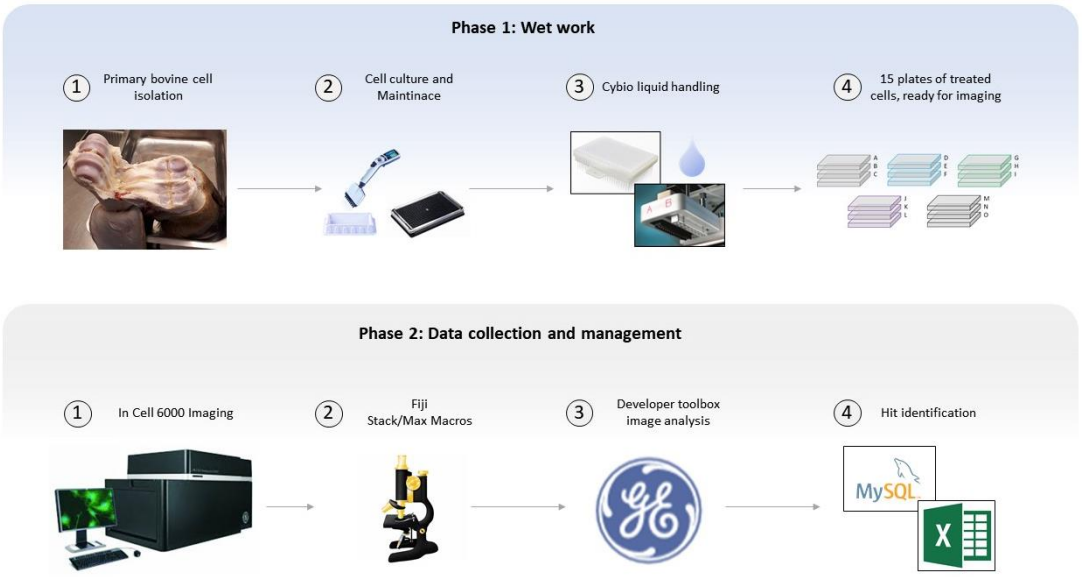

Figure 2.3. Compound screen workflow

The compound screen consisted of two phases. ***Phase 1****; wet work.* ***1.*** *Primary bovine chondrocyte isolation,* ***2****. Cell culture and maintenance to confluence,* ***3.*** *Cybio Liquid handling for compound splitting, dilution, and addition as well as IF labelling, and* ***4****. All plates of treated cells, labelled in four colours ready for imaging.* ***Phase 2****; data collection and management.* ***1.*** *In Cell 6000 image acquisition,* ***2.*** *Fiji macro processing of z-stacks into stacks and maximum intensity projections,* ***3.*** *Developer Toolbox automated image analysis, and* ***4.*** *Data management and hit identification.*

3. Development of the Compound Screen

3.1. Introduction

As discussed in chapter 1, the primary cilium is essential for the development and homeostasis of tissues and is involved in aging, health and disease. The structure of the primary cilium is known to be altered by both mechanical and chemical stimuli and altered cilia structure is also observed in numerous disease states. Furthermore, there are many associations made between altered cilia structure and changes in cell signalling. Nevertheless, the relationship between primary cilia structure and function remains poorly understood.

High content screens have been conducted to uncover genes and proteins that are required for correct primary cilia structural assembly, although large scale investigation of cilia structural regulators remains scarce, with little follow up on cell signalling implications. The initial objective of this project was to identify multiple compounds that alter cilia structure and incidence in primary bovine chondrocytes, with the future aim of running follow up studies to elucidate the effect of candidate molecules on cilia dependent signalling cascades. This chapter addresses the optimisation, validation and experimental design considerations required to perform the compound screen.

The chapter covers the following optimisation and validation steps

1. Identification of a suitable compound library and design of the library layout.
2. Optimisation of primary chondrocyte cell isolation to maximise cell yield.
3. Optimisation of cell culture conditions and investigation of animal variability.
4. Assessment of the basal or apical location of chondrocyte cilia in 2D culture.

5. Identification of a suitable positive control and compound incubation period that would enable detection of cilia structural alteration.
6. Design, optimisation and validation of a high throughput screening workflow to enable triplicate compound treatment of a full compound library and appropriate image acquisition for detection of primary cilia length and incidence.
7. Development and validation of a high content image analysis protocol and data management plan.

3.2. The screening plan and compound library

3.2.1. Library selection

There were a number of different compound libraries available, although not all of them were suitable for the compound screen. Ideally, all compounds used in the screen should have known bioactivity, usage and associated pathways and/or targets. This supports elucidating how structural alterations may be linked to pathways and/or targets and ultimately ciliary function. The compounds being FDA-approved, increases the potential for them to be repurposed for therapeutic application. Additionally, all compounds should be supplied at the same concentration and dissolved in the same diluent (e.g. DMSO), to reduce the complexity of the required vehicle controls on each screening plate. As the screen was to be run in 384-well culture plates, it was necessary that the compounds be provided in a 384-well format, to avoid complications of in-house library re-formatting. This eliminated libraries such as the Sigma LOPAC, Spectrum Collection, and Tocriscreen Plus libraries, all of which were supplied in a 96-well plate format. This left the Prestwick Chemical and SelleckChem libraries, both of which were supplied in fully customisable 384-well formats. Collaborators have identified several compounds in the SelleckChem library that increase both cilia length and prevalence in an osteocyte cell line [Personal communication Milso Spasic and Chris Jacobs]. Therefore, the SelleckChem FDA-approved drug library was selected for the screen.

3.2.2. Library layout

From the SeleckChem FDA-approved drug library, only those compounds that were supplied in DMSO at a concentration of 10mM and had a company provided

Indication, Pathway or Target were selected for inclusion in the compound screen. This totalled 1,727 compounds supplied across five master 384-well plates. Using the company supplied target information, the 384-well plate format was customised to have an equal number of compounds per plate, with compound target types distributed evenly across the five plates, so that no plate had an over representation of any particular target type. Columns 23 and 24 of all master plates were left blank for controls, with additional scattered blanks across the plates, for plate consistency checks. A list of compound hits were kindly provided from the osteocyte screen, of which 94 compounds overlapped with the 1,727 compounds included in our screen. Of these 94 compounds, 58 increased cilia incidence, 22 increased cilia length and 14 were identified as increasing both incidence and cilia length. Therefore, those compounds in our library that came up as hits in the osteocyte screen were also distributed across our five compound master plates. See Appendix C for the layout of control wells and Appendix D compound Indication, Target and Pathway distributions across the five master plates.

3.2.3. Screening plan and experimental considerations

Using our compound library, running the experiment for a single time point and dose, with triplicate technical replicates for each compound and with the addition of the appropriate controls, required 15 x 384-well culture plates (5,760 individual cell culture wells). Due to the large number of compounds and tissue culture plates involved, the screen was run at the Blizard Institute (QMUL) using Cybio liquid handling robotics for the addition of compounds, fixation and fluorescent labelling of the treated cells. The In Cell Analyser 6,000 with capabilities

for four colour z-series confocal imaging, was used to acquire images of the fluorescently labelled cell cultures (see section 2.2.3). The acquired 3D z-series images were then Fiji macro processed to generate 2D maximum intensity images, suitable for high throughput analysis (see section 2.5) . Developer ToolBox (GE, now Cytiva) was used to set up and apply analysis protocols to all the images. The automated image analysis generated CSV files, containing data for a variety of analysis parameters including cilia length and prevalence. The resulting data was imported into a database (MySQL) for investigation.

Each of the practical steps requiring optimisation have been summarised in Chapter 2, Section 2.7, Figure 2.3. The data from these studies is presented in the following sections. Initial experiments were conducted to assess the suitability of primary bovine chondrocytes cultured in monolayer for use in the compound screen.

3.3. Optimisation and validation of chondrocyte cilia expression

Primary bovine chondrocytes were utilised during the compound screen, isolated from the joints of steers and cultured in 2D monolayer (see section 2.1.2 and 2.1.3). These cells were isolated and manually seeded into 384-well cell culture plates and maintained to confluence as shown schematically in the workflow in Figure 3.1. Validation and optimisation was required to ensure that complete cartilage digestion and maximal cell yield was achieved upon primary cell retrieval. Animal variability was also assessed. The variability of primary cilia expression between animals was determined, and the consistency of cell seeding and cilia expression across a culture plate required validation.

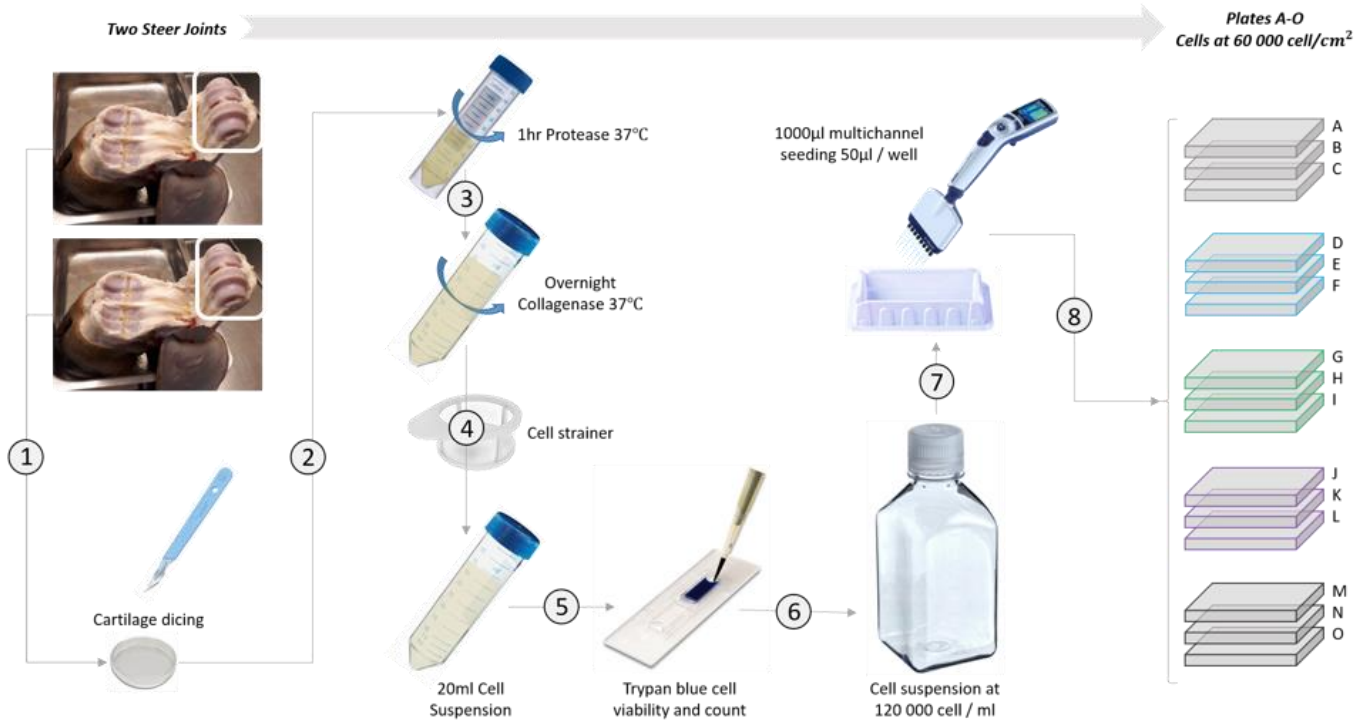

Figure 3.1. Optimised workflow for digestion of cartilage and manual cell seeding prior to compound screening.

*(**1**) Full depth cartilage dissection from the joints. (**2**) Diced cartilage incubation in protease for an hour. (**3**) Cartilage incubation in collagenase overnight. (**4**) Digestion mix passed through a cell strainer to remove any debris, before the cells were centrifuged and the cell pellet was re-suspended in cell culture media. (**5**) Cell yield and viability was assessed using the trypan blue exclusion assay before the (**6**) cells were made up to the final screen seeding concentration. (**7-8**) Cells were then manually seeded into 15 x 384-well tissue culture plates, with 50µl of cell suspension added to each well.*

3.3.1. Optimisation of cartilage digestion and cell yield

Primary bovine chondrocytes were isolated from bovine joints (see section 2.1.2). The protease incubation was important for initial cartilage degradation, allowing the collagenase to better infiltrate the cartilage to degrade the collagen, thereby freeing the cells from their extracellular environment. It was essential that complete cartilage digestion was achieved, not only to gain maximal cell yield but also to ensure that the cells were representative of the entire cell population *in situ*. Complete digestion was necessary to prevent, preferential isolation of cells in the superficial or middle zones since there are known depth-dependent differences in cilia prevalence, length and orientation as well as differences in cell morphology, metabolism and signalling behaviour (Aydelotte and Kuettner 1988; McGlashan, et al. 2008; Farnum and Wilsman 2011).

Initially, the 1hr protease incubation was performed using a concentration of 7U/ml. Incomplete cartilage digestion occurred at this enzyme concentration, as was evident by the large amount of visible cartilage in the digestion solution following the collagenase incubation and the low cell yield (Table 3.1). Therefore, the protease concentration was increased to 20U/ml for future isolations, resulting in near complete cartilage digestion with very little visible cartilage remaining after the collagenase incubation, and much greater cell yield (Table 3.1).

Table 3.1. Number of cells released following cartilage digestion with two different protease concentrations.

	Cell yield per joint (x 10^6 cells)	
	7U/ml	**20U/ml**
	4.7	20.1
	4.4	34.3
	7.8	23.7
		33.8
		28.1
		21.4
		35.2
		47.2
		36.3
Mean±Std	**5.6±1.9**	**31.1±8.6**

With the optimised chondrocyte isolation protocol using 20U/ml of protease, 31.3±8.6 million cells per joint could be isolated with >97% cell viability as determined by the Trypan Blue exclusion assay. Although the full proximal surface of a joint is dissected for digestion, this surface area can vary from joint to joint based on joint size and exclusion of minimally but noticeable damaged cartilage regions. Therefore, it is likely that the variability in cell yield is largely due to the viability in joint size and associated thickness and hence the amount of viable tissue per joint.

3.3.2. Animal variability and validation of chondrocyte cilia length and prevalence

Initial studies were conducted to characterise the effects of animal variability on cilia prevalence and length in isolated primary bovine chondrocytes in 2D culture. Cells were isolated from four different joints, seeded onto glass coverslips (section 2.1.3), and cultured to confluence. Cells were fixed with 4% PFA, labelled for ac-α-tub and arl13b (1:2,000), counterstained with DAPI and imaged using confocal

microscopy (section 2.2.3). Z-series were maximum-intensity projected for analysis of both cilia length and prevalence using Fiji (ImageJ).

The true length of cilia that are not flat within the confocal x-y plane may be underestimated using this method of analysis. However, the high throughput image analysis available at the time of the screen only permitted 2D image analysis. Additionally, 3D cilia length analysis introduces errors and a loss of precision due to the drop-in resolution in the z-axis apparent in most confocal imaging systems. Furthermore, corrected cilia length equations for assessment of length in 3D (Rowson, et al. 2016), often assume that cilia are straight, which may not always be true, as seen in Figure 3.2A.

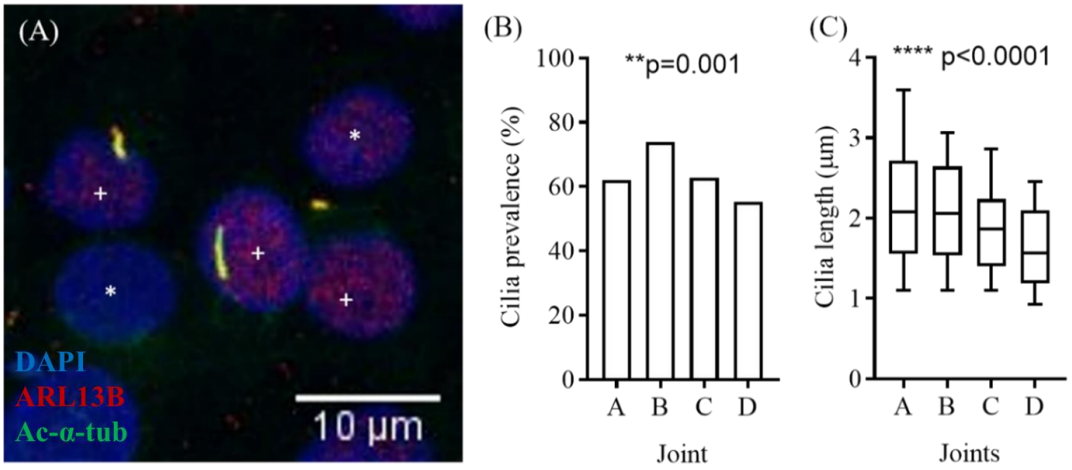

Figure 3.2. Animal variability in baseline cilia prevalence and length.

*(**A**) Representative maximum intensity projection showing primary cilia in isolated primary bovine chondrocytes cultured to confluence in monolayer. Nuclei labelled with DAPI (blue) and cilia are labelled for ac-α-tub (green) and alr13b (red). Cilia prevalence was determined by counting the number of cells with (+) and without (*) cilia. (**B**) Cilia prevalence is significantly different between animals, as determined by the Chi-square test (n > 220 cells per animal, **p=0.001). Percentage ciliated cells; A=61.9%, B=73.9%, C=62.8%, D=55.2%. (**C**) Baseline primary cilia length was significantly different between the four different animals. Data is presented as box and whisker plots, representing the median, interquartile range and range of the data. Median cilia length per animal; A=2.1µm, B=2.1µm, C=1.9µm, D=1.6µm. Data was analysed using the Kruskal-Wallis test followed by the Dunn's multiple comparison test (n > 125 cilia per joint, ****p<0.0001).*

These results broadly agree with previous studies using the same isolated primary articular chondrocytes from bovine metacarpal phalangeal joints, also cultured on glass, in which cilia set length was reported as 2.09±0.70µm and prevalence as ~75% (Thompson, et al. 2016). When comparing the four animals in this study, both baseline cilia prevalence (Figure 3.2B) and length (Figure 3.2C) were found to be significantly different between animals. Cilia set length and prevalence of animal D (1.6µm, 55.2% ciliated cells) was notably different from the previously

reported findings, while animals A-C had marginally lower cilia prevalence. When working with primary cells it may be unsurprising to find biological variation between animals. There is reported variability in cilia length and prevelance dependent on the zone in which a chondrocytes resides within the cartilage (McGlashan, et al. 2008). Therefore, differences in cilia length and prevelance with zone and possibly the position in the joint may lead to variations in 2D culture baselines, through variations in the cartilage tissue during the primary cell extraction process.

3.3.3. The Effect of LiCl on cilia elongation

Previously, lithium chloride (LiCl, 50mM) has been demonstrated to cause an increase in chondrocyte cilia length, over a 24hr time course (Thompson, et al. 2016). To identify a suitable screening compound incubation time during which a new cilia set length could be reached, time course experiments were conducted using LiCl. Experiments were also run to assess the variability between animals in their responsiveness to LiCl.

Initially, the effects on cilia length following a 1hr, 6hr, and 24hr exposure to 50mM LiCl was tested on cells isolated from a single joint of an animal. Cilia length was found to increase from a median length of 2.20µm to a median length of 2.98µm after a 1hr exposure time (35.5% length change, Figure 3.3A). The temporal dynamics of this length change appeared to plateau after 6hr (Figure 3.3B), increasing from a median length of 3.17µm after 6hr to a median length of 3.32µm after 24hr (less than 5% length change). As the greatest change in cilia length occurred during the first hour of this initial time course experiment, an additional time course (0.25, 0.50, 0.75, 1.00, 2.00, 4.00, and 24.00hr) was conducted on cells isolated from a single joint

of a different animal (Figure 3.3C). The temporal dynamics of this length change appeared to be very similar, plateauing after 4hr (Figure 3.3D), going from a median length of 2.95µm after 4hr to a median length of 2.96µm after 24hr (less than 0.34% length change between 4hr and 24hr). Again, the greatest change in cilia length occurred within the first hour (Figure 3.3E). Therefore, an incubation period of between 6 and 24hrs (~16hr), will be utilised for identification of candidate molecules during the compound screen.

To assess the variability between animals in their responsiveness to LiCl, the effects of a 45min exposure to 50mM LiCl was compared between cells isolated from the joints of four different animals. When comparing the cilia length reached after the single 45min incubation, there was no significant difference between the four animals (Figure 3.3F), with all animal's median cilia length increasing between 0 and 45min (Figure 3.3G), confirming that all animals were responsive to LiCl.

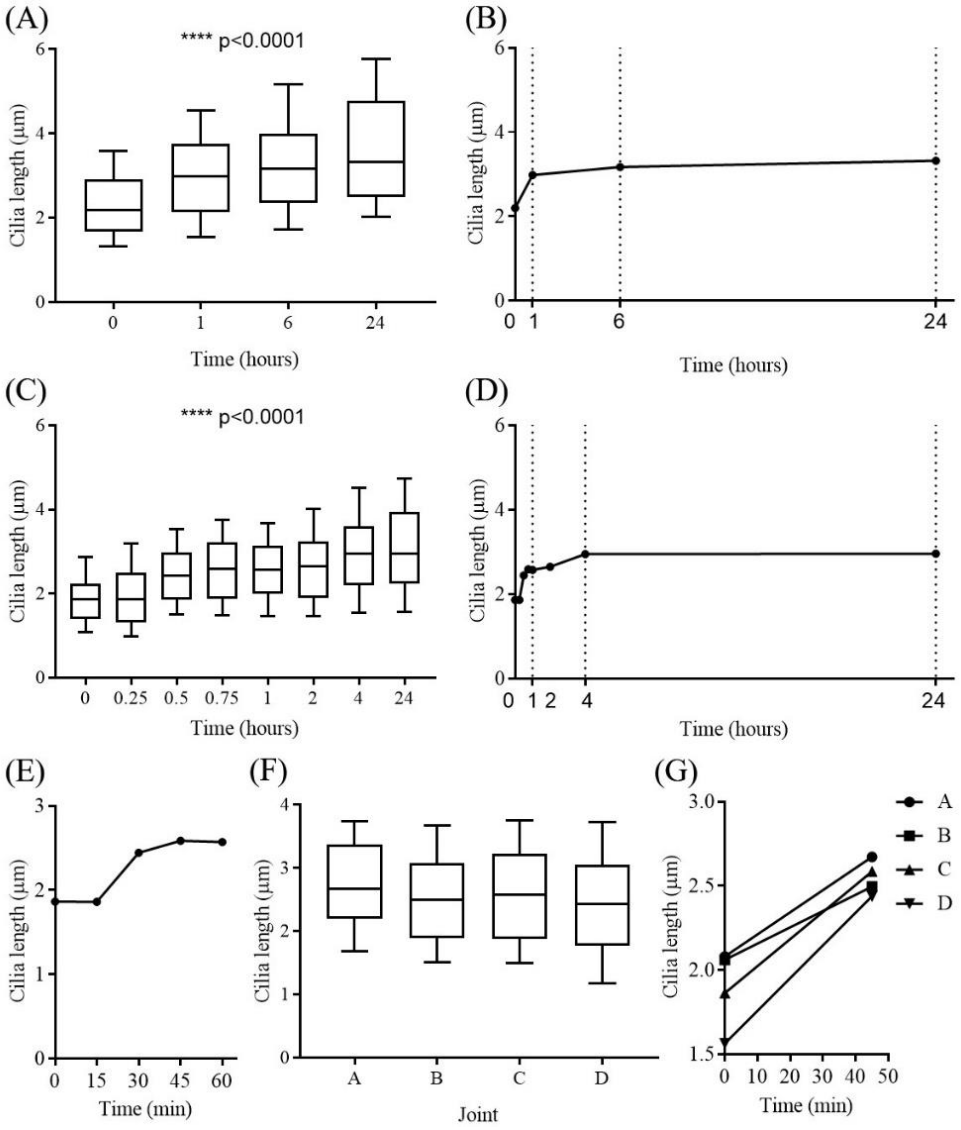

Figure 3.3. Cilia length and time course elongation with 50mM LiCl.

*(**A**) Response of primary cilia form a single joint after 1hr, 6hr and 24hr exposures to LiCl (50mM) and (**B**) the temporal dynamics of the induced length increase (data points are the median values for each time point). (**C**) Response of primary cilia form a single joint after 15min, 30min, 45min, 1hr, 4hr and 24hr exposures to LiCl (50mM) and the temporal dynamics of the induced length increase over the full 24hr (**D**) and the first 60min (**E**) of exposures (data points are the median values for each time point). (**F**) Primary cilia length of four different animals after 45min exposure to LiCl and the delta change in cilia length from their control set length (**G**), where data points are the median values for each joint. Data was analysed using the Kruskal-Wallis test followed by the Dunn's multiple comparison test (n > 90 cilia per condition).*

3.3.4. The effect of serum starvation

Serum starvation inhibits cell cycle re-entry, thereby promoting ciliation, maximising cilia expression and is a technique frequently employed by the field when studying primary cilia and analysis of set length *in vitro* (Wheatley, et al. 1996). During the compound screen, percentage ciliation would need to be sufficiently high so as to ensure reliable cilia length population sampling. However, if cilia expression was at its maximal level this would limit the ability of the screen to identify compounds that increase cilia prevalence. To test the effects of serum starvation on cilia length and prevalence in our hands, primary bovine chondrocytes were isolated and cultured to confluence on glass coverslips (see section 2.1.3). This was followed by a further 24hr in either complete serum containing media or in serum free culture media (section 2.1.1 for media composition). For these experiments, cilia length and prevalence were analysed in cells isolated from two different animals. Cells were fixed in 4% PFA (section 2.2.1) and cilia dual labelled (section 2.2.2) for acetylated-α-tubulin (ac-α-tub) and ARL13B. Image acquisition was performed using Zeiss LSM confocal microscopy (section 2.2.3). Cilia prevalence and length were manually quantified from combined channel maximum projections, using Fiji (ImageJ).

Serum starvation resulted in a significant increase in cilia prevalence (****$p<0.0001$), increasing from 71.8% in serum containing cultures to 88.9% of cells expressing cilia after serum starvation Figure 3.4 A). Cilia were also significantly longer (****$p<0.0001$ and ***$p<0.001$) after serum starvation, going from a median set length of ~1.55µm to a median length of ~1.86µm (Figure 3.4 B).

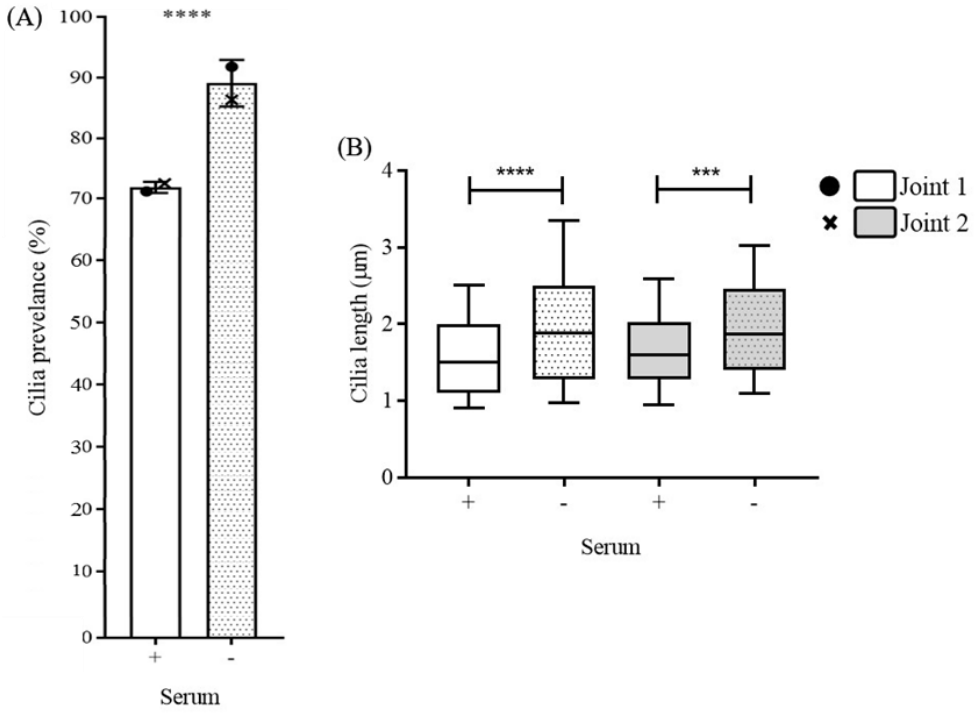

Figure 3.4. The effect of serum starvation on cilia length and prevalence.

*(**A**) Cilia prevalence with and without serum, for two joints. Prevalence was determined by counting the number of cells with cilia as a percentage of the total population of cells imaged with (n= 434 and n=433) and without (n=379 and n=426) serum for 24hr prior to fixation. Cilia prevalence with and without serum starvation (Chi squared test, ****p<0.0001). (**B**) Cilia length represented as median and interquartile range, with serum starvation (serum + n=309 and n=313 cilia, serum – n=348 and n= 310 cilia for each joint, respectively), statistical significance determined by Kruskal Wallis with the Dunn's Multiple comparison test (****p<0.0001, ***p<0.001).*

Considering the advantages and disadvantages of serum starvation, as outlined in Table 3.2, for the purposes of the screen, serum starvation will not be employed. Chondrocytes cultured to confluence become quiescent, thereby promoting ciliation, and a cilia expression of ~ 72% is adequate for the quantification

of cilia length, while still providing the potential to identify compounds that increase cilia prevalence.

Table 3.2. The advantages and disadvantages of using serum starvation in the cilia screen.

Advantages	Disadvantages
1. If compounds induce growth arrest or senescence, serum starvation would prevent these from arising as false positives. 2. Serum is highly variable from batch to batch, so the effects seen from a compound when culturing with a particular batch, may be variable from that effect seen with a different batch. 3. Provides a better estimate of stable cilia set length, as cells are not proliferating.	1. If compounds cause an increase in cilia prevalence, the maximum magnitude that could be quantified after serum starvation would be from 89% to 100% ciliation, while cultures not subjected to serum starvation would allow for a potential increase of 72% to 100%. A larger 'potential increase', better enables compounds to be distinguished based on the magnitude of their effect. 2. Serum starvation may reduce cell viability over long culture times, making follow up metabolic studies and time change analysis harder to conduct with a prior 24hr serum starvation protocol.

3.3.5. Characterisation of ciliary basal/apical expression

As described in section 3.3.2. Animal variability and validation of chondrocyte cilia length and prevalence, primary cilia length was quantified here from maximum intensity projections of full cell depth confocal z-series. Cilia that lie parallel to the culture surface will have their length most accurately quantified, while those that are positioned perpendicular to the culture surface will have their length underestimated, negatively skewing the population average length. It is hypothesised that cilia expressed on the basal surface, typically under the nucleus, will be flatter and therefore appear longer in maximum intensity images.

The following experiments were conducted to investigate whether cilia positioning on either the basal or apical surface, affects projected cilia length measurements. Cells were cultured on glass coverslips and cilia stained and imaged using Zeiss LSM confocal microscopy as described in sections 2.1.3, 2.2.2, and 2.2.3. Z-series were captured such that the first image in a series was the closest to the glass culture surface, with sequential slices moving further away. Cilia that appeared before the nucleus were defined as basal, while those appearing after the nucleus were apical and the number of z-sections the cilium appeared in was noted. Cilia length was quantified as previously described and the corresponding cilia position was noted as either basal or apical.

Figure 3.5A shows representative examples of basal and apical cilia visualised from z series in the x-y plane and x-z plane. More cilia were positioned on the basal surface at 61.6±4.3% of all cilia, compared to the 38.4±4.3% of apical cilia (Figure 3.5B). The projected cilia length of basal cilia was also longer (*mean±SD,* 2.09±0.26μm) than apical cilia (1.63±0.18μm), the difference being statistically significant (*p=0.026). This is likely to be due to basal cilia being aligned more parallel to the glass than those that are apically expressed, as hypothesised.

If a compound were to cause a switch between basal and apical cilia expression, that compound may come up as a false positive regulator of cilia length due to the reliance on projected length measurements for the screen. Therefore, for the purposes of the compound screen and unless otherwise stated, cilia length refers to the measurements determined from the projected cilia length of basal cilia (cilia appearing in the first 5 z-planes of the confocal stack), ensuring more accurate length

quantification and reducing the likelihood of false positive hits for length regulation. Although this approach may not accommodate the identification of compounds that predominantly regulate the length of apically expressed cilia, which would require 3D high throughput analysis, it allows for the most reliable identification of length regulators within the experimental parameters available at the time of this screen. In addition, the screen will measure the prevalence separately for basal cilia and all cilia and hence will determine any shift between basal and apical expression as well as total prevalence. As such, z-series imaging coupled with differential zone maximum intensity projection is required (see section 2.5).

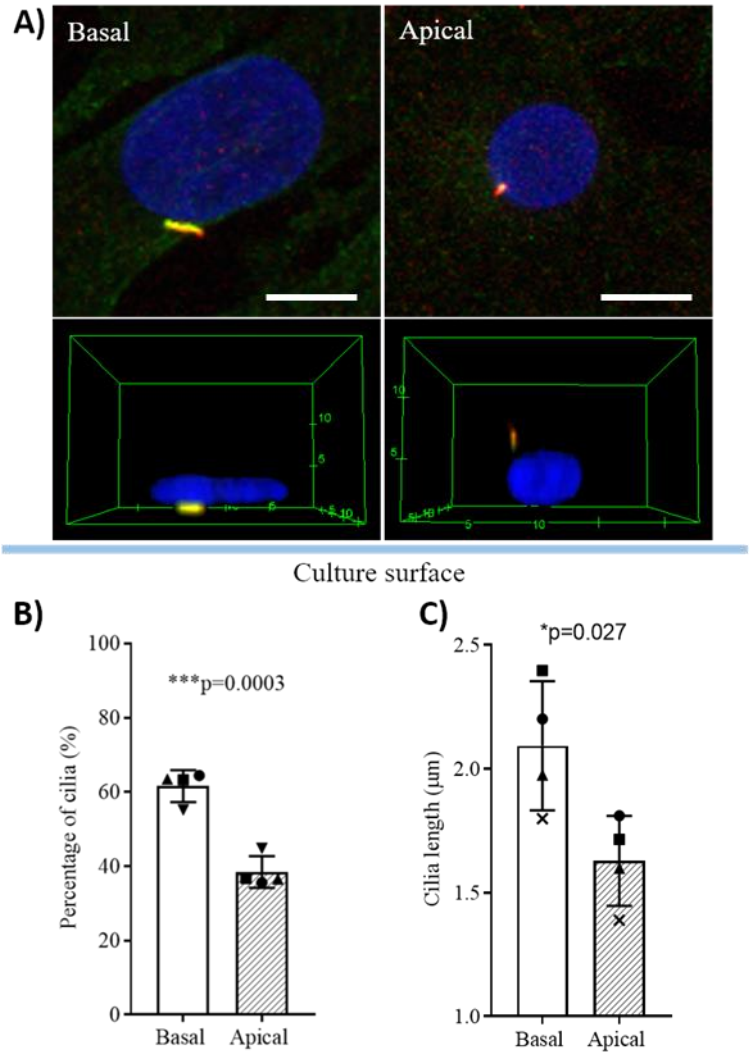

Figure 3.5. Basal vs apical cilia expression in glass monolayer cultures.

*(**A**) Representative images of maximum intensity projections (XY) and 3D reconstructions (XZ). Nuclear DAPI staining (blue), cilia labelled with ac-a-tub (green) and arl13b (red). Basal/apical cilia expression was quantified from primary cells isolated from 4 animals. Scale bar = 5µm. (**B**) Percentage of cilia that are expressed on the basal or apical surface of cells (n=4 joints, ***p=0.0003, statistical significance determined with Mann-Whitney test). (**C**) Projected cilia length measured from maximum intensity projections. Values represent median values for chondrocytes isolated from a single joint (n=4 joints,*p=0.027, >125 cilia assessed per joint). Bars represent mean±SD for all graphs.*

3.3.6. Consistency across PerkinElmer 384-well tissue culture screening plates

The compound screen would be run in 384-well tissue culture plates. Plate consistency and baseline conditions had to be assessed prior to formatting of the compound library and running the screen, to rule out the possibility of any inconsistencies across a plate or possible edge effects. Inconsistencies may arise due to consistent error in the manual cell seeding protocol or due to the outer wells of a plate being more susceptible to evaporation during culture in the incubator. If this affected cell number or cilia set length in a predictable way across a plate, the affected wells could be excluded during formatting of the screen. To address this, both the consistency in cell seeding and baseline cilia length were assessed, as detailed below.

Isolated primary bovine chondrocytes (see section 2.1.2) were seeded at a cell density of 1,000 cells/well in a 50µl volume, into PerkinElmer 384-well tissue culture plates. Seeding was carried out using a multi-dispense multichannel pipette, employing a consistent four-quadrant pattern for every plate seeded (see Figure 3.6A). Cells were cultured to confluence, before being fixed and labelled with DAPI. The IN Cell 2200 at x4 objective lens (see section 2.2.3) captured full surface area images of each well (Figure 3.6B) and cell number was quantified using automated analysis. No apparent edge effect was seen on quantification of cell number when looking across a plate by row (Figure 3.6B and C) or by column (Figure 3.6D).

As cilia length is one of the screens analysis parameters of primary interest, it was crucial to validate that there was no edge effect on cilia set length across a plate. As the cells were grown to confluence prior to fixation, the measured length is

presumed to be a stable set cilia length as the cells would have reached a quiescent state. Although there was some slight variability in set length from well to well, there was no apparent edge effect on measured cilia set length looking across a plate by row (Figure 3.6E) or by column (Figure 3.6F). As no plate inconsistencies or edge effects were found, the full 384-wells would be utilised for compound plate formatting and screening purposes.

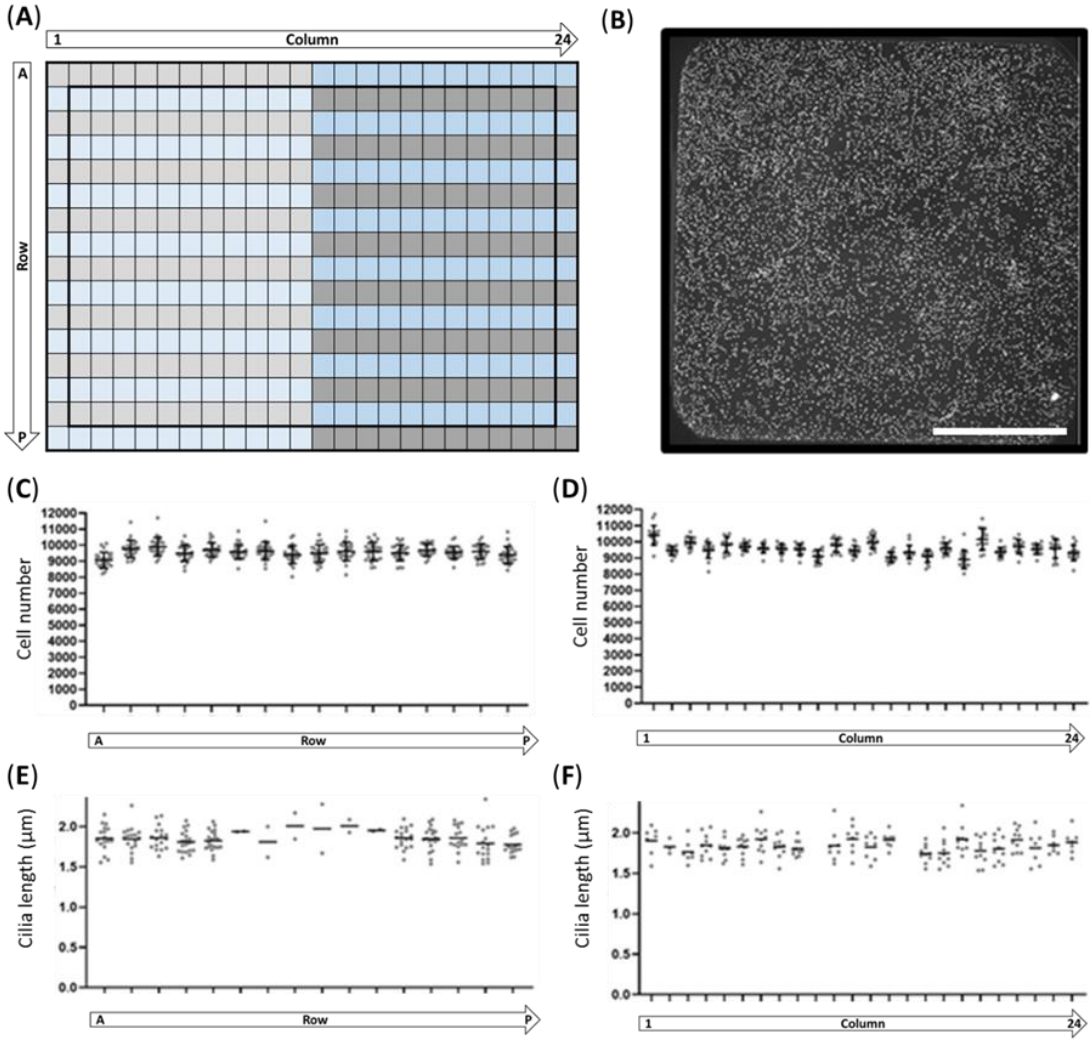

Figure 3.6. Consistency or cell number and cilia length across a 384-well culture plate.

*(**A**) Schematic of 384-well plate layout, with four colour representing the multichannel seeding quadrants. Columns run across the plate from 1-24 and rows run down the plate from A-P. Outer well highlighted by thick border. (**B**) x4 image of full well, cells labelled with DAPI (scale bar = 1mm). (**C**) Cell number per well by row. (**D**) Cell number by column. Mean cilia length per well across a plate by row (**G**) and by column (**H**). For all graphs each data point is an individual cell culture well and the line is the mean value.*

3.3.7. Four colour immunofluorescent target selection

The central axonemal structure of the primary cilium is microtubule based and surrounded by a specialised ciliary membrane, as discussed in Chapter 1 (see section 1.1). Ciliary tubulin, much like the tubulin of the entire cell cytoskeleton is subject to post translational modifications, proposed to contribute the specificity of tubulin function. Another cytoskeletal component, although largely excluded from the ciliary compartment, is actin which has been demonstrated to be a regulator of ciliary expression as discussed in section 1.8. As the primary aim of the project was to identify regulators of primary cilia length and incidence, immunofluorescent labelling would need to facilitate the identification of cell number, primary cilia and their structure. Ideally, the labelling panel would also facilitate the assessment of compound effect on other major known regulators of cilia expression, such as actin.

During the screen, cells could be labelled with up to four different targets. Various cell fixation methods and antibodies were tested (see Appendix A and Appendix B) to inform correct and reliable fixation and labelling of cellular and ciliary components. For the purposes of the screen the four channels were occupied as follows in order of wavelength (Figure 3.7A);

- DAPI (AF405nm); an intercalating dye labelling the nucleus would facilitate identification of cells.
- Ac-α-tub (conjugated primary AF488nm); there is a particular enrichment of the post translational modification acetylation running the length of the ciliary axoneme. This is a commonly used ciliary marker.

- Phalloidin (AF 555nm); used to label the F-actin network, an indicator of cell contractility, a known regulator of cilia expression.
- Glu-tub (secondary antibody AF 647nm); Polyglutamylation, a post translational modification found to be particularly enriched in the basal portion of the ciliary axoneme (Kukic, et al. 2016). Preliminary studies using y-tubulin to label the basal body, confirmed that Glu-tub is enriched in the basal portion of the primary cilium in chondrocytes (Figure 3.7B).

Both ac-α-tub and glu-tub labelled coinciding portions of the ciliary axoneme, with both available primary antibodies raised in mouse (see details of sequential antibody labelling in section 3.4.4). Therefore to avoid channel bleed through, the two fluorophore-conjugated secondary antibodies were chosen to have excitation and immersion wavelengths as far apart from one another as possible (See Figure 3.7A).

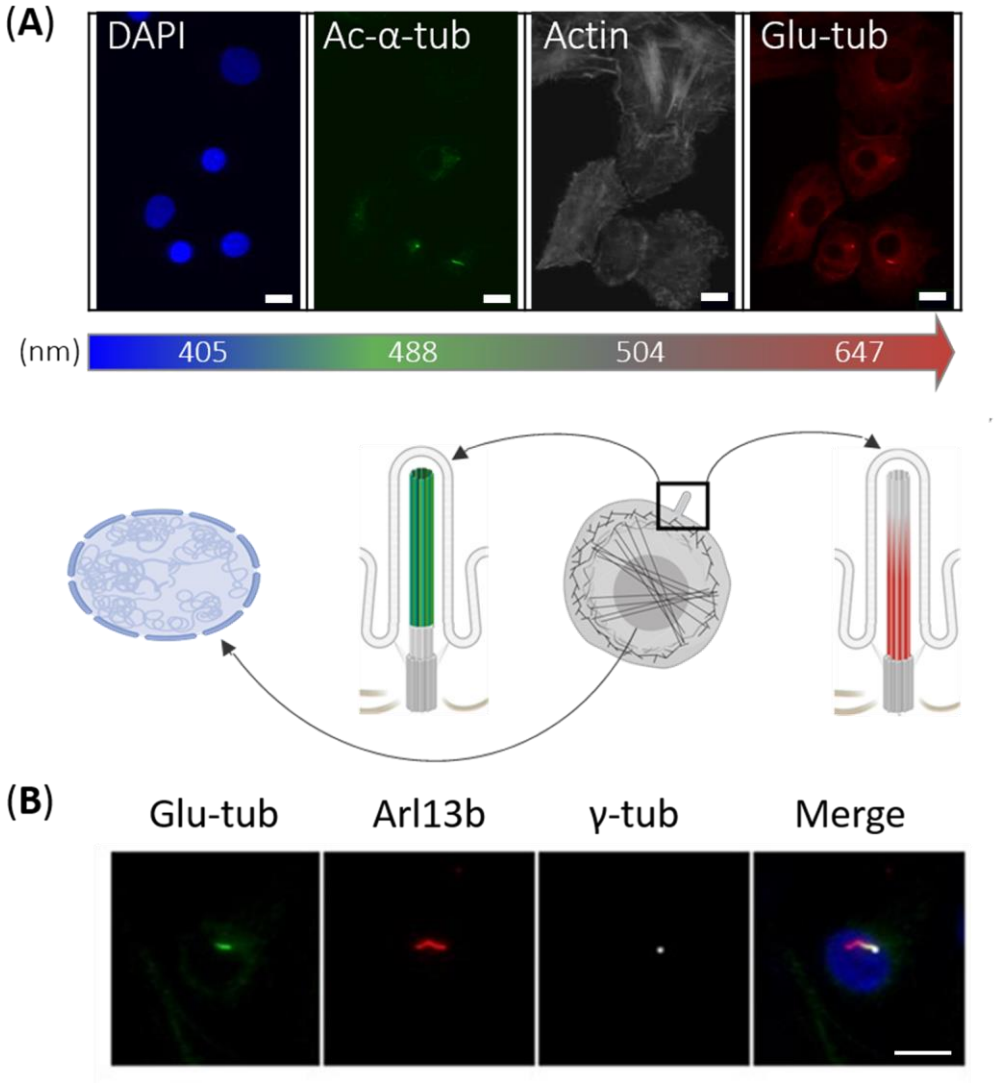

Figure 3.7. Four channel colour target selection and fluorophore allocation.

*(**A**) Four channel screen allocation with a representative schematic of the associated cellular component. DAPI (Blue) labels the cell nucleus, ac-α-tub (green) labels the ciliary axoneme while glu-tub (red) is particularly enriched in the basal portion of the ciliary axoneme. Actin is labelled by phalloidin (greyscale). (**B**) Shows a single representative cilium where glu-tub (green) labels the portion of the axoneme closest to the basal body. The axoneme is labelled with arl13b (red) and the basal body by γ-tub (greyscale). The cell nucleus is labelled with DAPI (blue). All scale bars = 10µm.*

3.4. Liquid handling robotics; optimisation and compound reformatting

Liquid handling robotics was employed during the compound screen to manage the handling of the large number of compounds and tissue culture plates involved. The liquid handling steps are summarised in Figure 3.8, 3.9 and 3.10 with details of each optimisation and validation step involved outlined in the following subsections.

3.4.1. Compound library master plate split

The compound master plates were provided at a 10mM concentration with a total volume of 100µl per well, in a 384-well plate format (compound layout details given in section 3.2.2. Library layout and Appendix D). To avoid multiple freeze-thaw events during the use of the compound library, the master compound plates were split into separate 384-well v-shaped plates using the Cybio 384 tip system. Initial plate compatibility with the liquid handling robot was tested and validated, with plate height to tip ejector distance set to ensure no mechanical errors occurred during operation. The compound plates were thawed and centrifuged for 1min. Each of the master plates was then stamped out into 384-well v-shaped plates. This resulted in four long term storage plates (Step 1 Figure 3.8, 20µl per well), 10 x screening plates (Step 2 Figure 3.8, 0.5µl per well) and one plate containing the remaining 15µl of 10mM compound in the original master plates, as described in section A of Figure 3.8. Prior to the split, mixing steps were included to ensure that the compounds were fully reconstituted and homogenous in solution. All plates were sealed under sterile conditions with opaque adhesive foils and stored at -80℃ for later use.

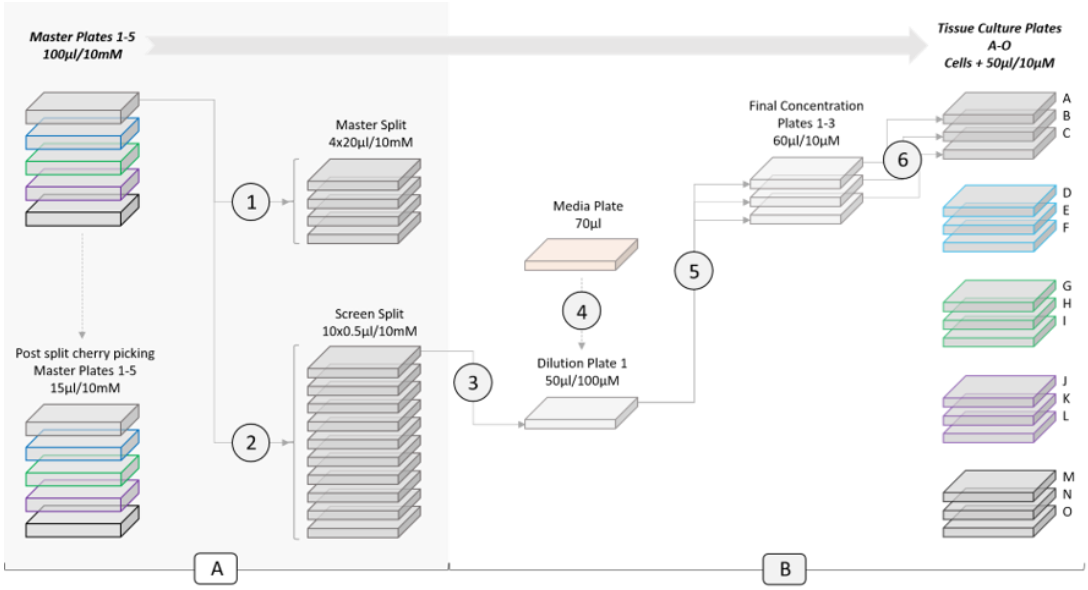

Figure 3.8. Optimised workflow for (A) Compound reformatting, and (B) dilution and addition to cell culture plates.

*(**1**) Each of the five compound **master plates**, containing a total volume of 100µl/well of each compound at a concentration of 10mM, were split into four x 20µl/well long term **storage plates**. (**2**) The remaining 20µl/well of compound was further split into 10 x 0.5µl/well **screening plates**. All plates were stored at -80℃ until needed. (**3**) During the compound screen a 0.5µl/well screening plate from each of the five original master plates was thawed. (**4**) An addition of 49.5µl/well of cell culture media was added, to each of the plates, diluting the compound down to a concentration on 100µM. (**5**) From the 100µM concentration plate, 3x 6µl/well was taken and placed into 3x v-shaped plates containing 54µl of cell culture media. This resulted in three x v-shaped plates with 60µl/well of compound at a final screening concentration of 10µM. (**6**) Cell culture media was completely removed from the cell culture plates before 50µl/well of 10µM compound was added.*

3.4.2. Compound dilution and addition to TC plates

The initial compound screen was run using a commonly used initial screen dose of 10µM and was selected to minimise false negatives although it does increase the likelihood of detecting false positives. However, false positives can be screened

out subsequently with dose response curves and further follow-up assays. The time point of 16hr post compound addition was used, which was a time point during the LiCl-induced primary cilium length elongation plateau phase (see section 3.3.3 and Figure 3.3B/D).

As the compound was supplied at 1,000x the initial screening concentration, dilution was required, utilising a robotic liquid handling protocol. This was performed prior to compound addition to the cell culture plates to minimise excessive mixing steps in the culture wells, as fluid flow has been shown to cause alterations in cilia length (Rydholm, et al. 2010). Five screen split plates (100mM, 0.5µl/well, see step 3 Figure 3.8), each originating from one of the five original master compound plates was thawed. The plates were centrifuged before 49.5µl/well was added to each of the plates (Step 4 Figure 3.8), leaving the compounds at a concentration of 100µM. From the freshly diluted 100µM concentration plate, 6µl was added to a v-shaped plate containing 54µl of cell culture media, leaving a final compound screening plate of 10µM with 60µl/well. This was repeated to generate triplicate plates for each of the master compound plates (Step 5 Figure 3.8). Finally, a full cell culture media removal (three x 25µl/well off) was performed before the diluted compound was added (two x 25µl/well on) to the cells for the compound incubation of 16hr (Step 6 Figure 3.8). All steps were performed using the Cybio 384-tip trough method, with the slowest reliable ejector speed of 60RPM used when adding compound to the plate, to reduce flow disruption.

3.4.3. Cell fixation

Initial testing showed that disruption to the confluent cell monolayer was more likely when handling liquids manually with a multichannel pipette (Figure 3.9A).

Therefore Cybio high throughput liquid handling robotics was utilised during the compound screen to avoid inconsistencies and possible disruption to cell monolayers. The liquid handling robotics has two methods by which liquid can be added to a culture plate. There is the 'comb ejector system' designed for dispensing liquid multiple times with no liquid uptake step required. However, this system can only eject liquid at high rates such as 200RPM and resulted in a fast liquid ejection speed that produced holes in the monolayer during 4% PFA addition for cell fixation (Figure 3.9B). The second option was the '384-tip trough system', which involved liquid uptake from a trough before it was dispensed into the culture plate at a lower rate of 60RPM and slower resulting liquid ejection speed. This second system left the monolayer intact after the addition of 4% PFA (Figure 3.9C) and was therefore adopted for the cell fixation method during the compound screen described throughout this thesis. Once fixed the cells could be treated using the comb ejector system without disruption to the cells (data not shown).

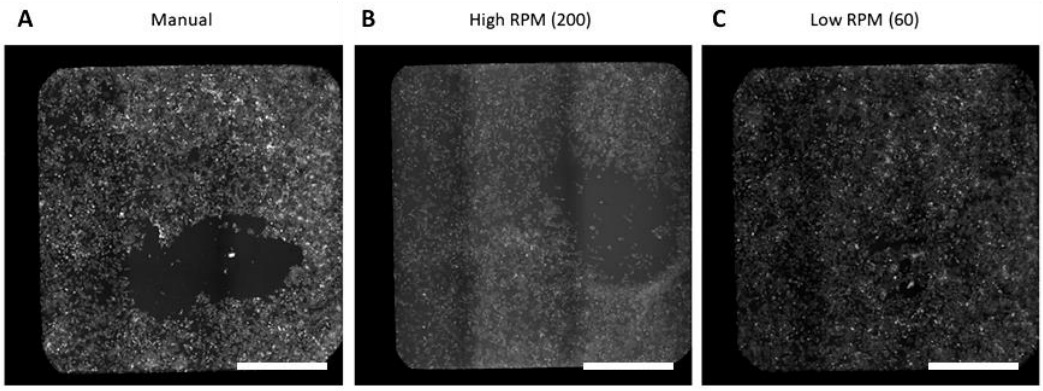

Figure 3.9. Effects of equipment on cell fixation.

*Disruption to the cell monolayer during fixation step when using (**A**) a manual multichannel pipette and (**B**) the Cybio comb ejector at 200RPM. (**C**) No disruption was evident when using the Cybio tip-trough at 60RPM. All images show full well (scale bare: 1mm) x4 fluorescence wide field images of phalloidin fluor* 555nm *labelled chondrocytes.*

3.4.4. Immunofluorescent labelling protocol

The full immunofluorescent labelling protocol, utilising CyBio liquid handing robotics is detailed in Figure 3.10. The protocol spanned two days and involved multiple liquid removal and addition steps. All IF solutions were made up in 0.1%BSA/PBS, and a pure 0.1%BSA/PBS solution was used during the wash steps. All liquid removal steps utilised the 384-tip trough system. Liquid addition was performed using either the 384-tip trough system or the comb ejector system, as indicated in Figure 3.10. All liquid incubation periods were 30mins unless otherwise stated. During the screen, compounds were removed after their 16hr incubation period, and the cells fixed in 4% PFA (see section 3.4.3. Cell fixation). This was followed by cell permeabilisation in 0.1% Triton-x 100, before a 1hr block in 5% donkey serum.

Primary antibody was added to the plates using the comb ejector system, dispensing 20µl/well at 200RPM. Following overnight incubation at 4°C in primary antibody and a subsequent wash step to ensure unbound antibody was removed from the wells, cells were co-incubated in 20µl/well secondary antibody, DAPI and fluorescently conjugated phalloidin for 1hr. After a second wash step, cells were incubated with conjugated primary antibody for 3hrs. Following the final wash step, cells were left covered in enough PBS to ensure they remained wet during imaging and for long term storage.

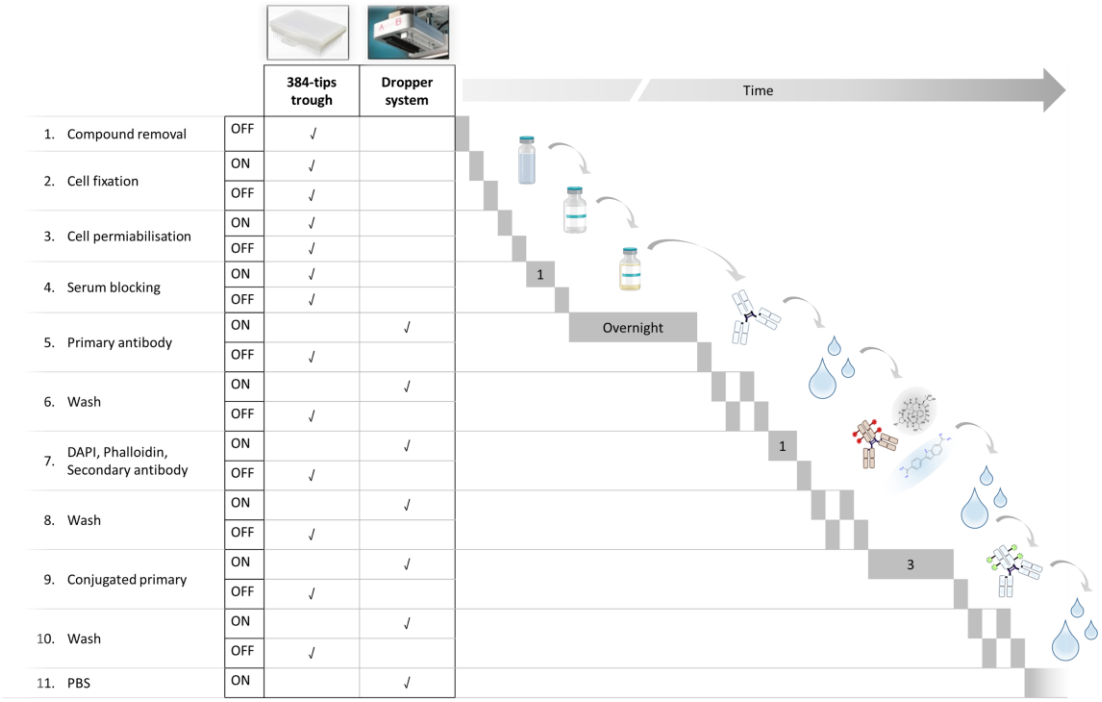

- ☑ Test timing to run 15 plates through a liquid change, 30 min
- ☑ 15 plate dry run, ensure tips don't crash into the plates at any point during the protocol
- ☑ Cell monolayer integrity check after all of the above liquid additions and removals
- ☑ First and last plate immunofluorescent intensity check

Figure 3.10. Workflow and Cybio steps involved during cell fixation and immunofluorescent labelling.

The cell fixation and immunofluorescent labelling protocol was carried out over two days. It involved numerous liquid handling steps (26/plate) as detailed in the above schematic.

Several checks had to be performed in setting up and during validation of the suitability of the liquid handling protocol, as outlined in Figure 3.10. Initially a full stack, 15 plate run through was performed to assess the time taken to get all the plates through a singular liquid removal and addition step. This was followed by a full

protocol 15 plate run through so as to minimise the risk of protocol failure on the day of the screen.

Studies checked that the numerous liquid removal and ejection steps and speed settings involved in the IF protocols, would not harm the integrity of the fixed cells. To do so we tested the effect of running all steps on a plate of manually fixed and DAPI stained cells. Once cells were manually fixed and stained, they were imaged on the IN Cell 2000 and cell number per well was assessed across the plate. The plate was then run through all liquid handling steps, re-imaged and cell number re-analysed. No difference in cell number was observed (data not shown), confirming that the liquid handling protocol was not disrupting the integrity of the fixed cell monolayer.

Finally, to ensure that the automated staining protocol and timings were consistently labelling the cells, a full stack 15 plate run through was conducted with first and last plates receiving antibody labelling incubations. These plates were then imaged and found to have been suitably labelled with no inconsistencies seen in the fluorescent intensities in the first and last plates of the stack (data not shown), providing the final check before carrying out the protocol during the screen.

3.5. Image acquisition optimisation

To ensure that the primary measures of interest, i.e. ciliary length changes and incidence, could be reliably captured and analysed in a high throughput manner, there were a few considerations to be made regarding a suitable image acquisition setup. The InCell6000 has a fixed image pixel size for each objective magnification. Initially the InCell6000 was equipped with a x40 magnification, 0.95 NA objective, image pixel size of 0.16µm. However, when attempting to image the small ($\approx 2.1\mu m$) primary cilia expressed by chondrocytes, it quickly became apparent that an objective of greater magnification would be more suitable due to the smaller pixel size. Although the number of cells/primary cilia per field of view would reduce with an objective of greater magnification, the number of pixels per cilium would increase. This would improve the detection of cilia length alterations. As such, for the purposes of the screen the InCell6000 with a x60 magnification, 0.95 NA objective with image pixel size of 0.11µm was utilised.

The x60 InCell objective setup enables two different approaches to image acquisition, an open aperture wide field imaging setup or a closed aperture confocal acquisition mode. As wide field imaging captures out of focus light, this results in cilia appearing fuzzy as seen in B, whereas the confocal approach captures only the light that is in focus for that particular z-section. Therefore the confocal imaging set up would be utilised. Due to minor cell culture plate tilt and biological variability in expression of cilia (basal/apical expression as described in section 3.2.3), not all cilia sit within the same z-section. Therefore a 3D confocal z-section image acquisition was opted for, to ensure that all cilia in a particular field of view were being captured.

3.6. Development of high-volume post-imaging macros

High throughput image analysis would be conducted using the Developer ToolBox (GE) software, which can only perform 2D image analysis. Either wide field images or maximum intensity projections from confocal z-series could be analysed. Therefore, primary cilia length measurements were quantified from projected cilia length. Due to the percentage of cilia that are apically expressed, many of which do not lie perpendicular to the objective plane, it is important for the screen that these be excluded from length measurements (see section 3.3.5). However, apical cilia should be included for prevalence quantifications. To achieve this, confocal imaging is required, such that only the z-slices capturing the basal cilia are maximum intensity projected for length analysis, while the entire cell depth is projected for prevalence quantification. In addition to this, confocal imaging would ensure that future 3D image analysis could be conducted if desired. The output of confocal imaging on the IN Cell 6000 are individual Tiff files for each z-slice taken in a channel (Figure 3.11).

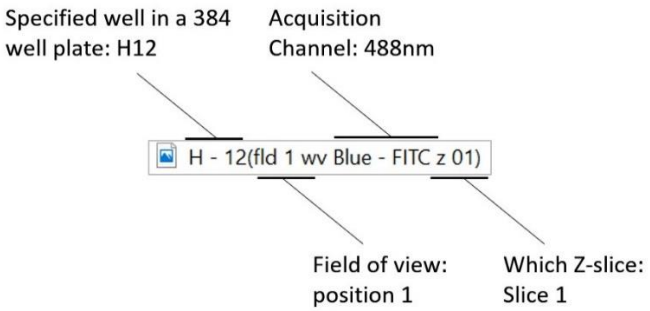

Figure 3.11. File naming convention using IN Cell 6000.

The well, field of view, acquisition channel and position within the Z-stack are all used to name a file acquired on the IN Cell analyser 6000.

After image acquisition, the z-series captured for each colour channel would need to be compiled into stacks. These stacks are then fully (all 10 z-slices) maximum

intensity projected for cilia prevalence analysis. Partial (first 5 z-slices) maximum intensity projection would be conducted to include only basal cilia for cilia length analysis. This processing would require 829,440 individual operations, as no high throughput software is currently available to perform this:

- 1,727 compounds in triplicate
- 15 x 384-well culture plates = 5,760 individual cell culture wells
- 12 fields of view per well
- Four colour channels acquired
- 10 z-sections per colour channel = 2,764,800 individual tiff files
- 276,480 stacking operations
- 276,480 full max operations
- 276,480 basal max operations

} = 829,440 individual operations

To conduct the high-volume post image acquisition processing, two operational macros were developed using Fiji (ImageJ). These are called on in batch files, to be run in command line, increasing processing speed. Macro image processing is run as described in section 2.5. These macros were used during screening, enabling the 55,296 processes required to prepare the images from a single plate for analysis to be set up and run in a single command.

3.7. Development and validation of automated analysis protocols

3.7.1. Manual validation of key measures

Cilia length and incidence were the primary screening outputs and the measures of particular interest in the first instance. As such, it was important that the automated measurements captured by the developer toolbox software be validated against measures captured manually. To do this 12 fields of view for 8 control wells were analysed, using DAPI and ac-α-tub channels. Manual measurements were obtained by performing visual inspection of the fields of view and counting the observable cilia, where objects touching the border of the field of view were excluded (see Table 3.3). Of the 8 control wells analysed, 7 were DMSO treated and 1 was LiCl treated. Individual cilia length data was collected by automated analysis, capturing length data from 12 FOV of a single DMSO well and a LiCl treated well. The length of the true positive cilia were then manually analysed using the Fiji segmented line tool, tracing a central line down the long axis of the cilium.

The automated and manual cilia lengths of true positive cilia determined by comparative visual investigation (~75% of cilia) were then plotted against one another (Figure 3.12B) to interrogate the relationship between manual and automated length measurement. A strong correlation was found between automated and manual measurements, with an r value of 0.8324. Incidence and ciliary length were both measured from basal maximum intensity projections.

Table 3.3. Identification of true positive, false positive and false negative cilia proportions from automated analysis of 8 control wells.

	Manual cilia count	Automated cilia count	Automated true positive		Automated false positive		Automated false negative	
	Raw	*Raw*	*Raw*	*%*	*Raw*	*%*	*Raw*	*%*
1	257	234	160	62.3	74	31.6	97	37.7
2	257	272	194	75.5	78	28.7	63	24.5
3	240	230	182	75.8	48	20.9	58	24.2
4	214	206	174	81.3	32	15.5	40	18.7
5	284	242	222	78.2	20	8.3	62	21.8
6	250	225	192	76.8	33	14.7	58	23.2
7	255	219	196	76.9	23	10.5	59	23.1
8	213	161	152	71.4	9	5.6	61	28.6
Average	**246.3**	**223.6**	**184.0**	**74.8**	**39.6**	**17.0**	**62.3**	**25.2**

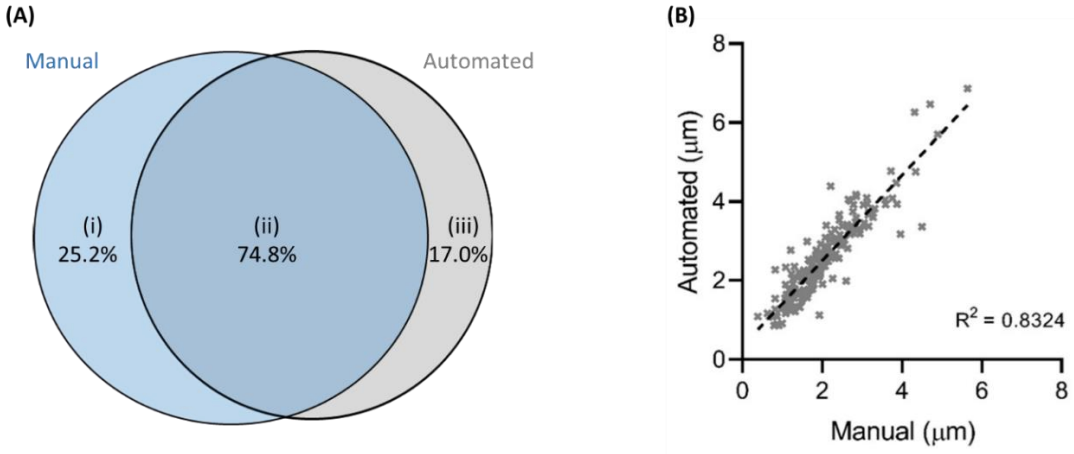

Figure 3.12. Manual verses automated cilia length identification and length comparison between automated and manual cilia length measures.

(A) *Ven diagram of summary data from Table 3.3, indicating (i) 25.2% of the cilia population appearing as false negatives in the automated analysis, (ii) 74.8% of the true cilia population appear as true positives, while (iii) 17.0% of the cilia identified by the automated analysis are false positives.* ***(B)*** *Correlation (line of best fit presented as a dashed line) of automated cilia length vs manual cilia length measures for cilia identified as true positives (Aii) in the automated analysis.* $R^2 = 0.8324$.

3.7.2. Full automated analysis protocol

Various image analysis approaches exist and can be utilised when it comes to image feature extraction, with numerous open access scripts available e.g. MATLAB Gabor feature extraction. In this study, an in house high content analysis approach was taken, utilising Developer Toolbox to set up an automated analysis protocol to capture data for greater than 60 measures in each field of view. An overview of the parameters analysed during the screen are detailed in Table 3.4, with further detail provided on the protocol set up in Appendix E. The key parameters, namely length and cilia incidence were validated against manual measures as described in section 3.7.1. Once this automated protocol was set up, it would be applied to both basal projections and full depth projections from all fields of view captured during the screen (69,120 fields of view maximum intensity projected in two different ways), enabling a consistent analysis approach. This analysis would generate a large volume of data, exported on a well summary basis, which would be managed and stored as described in section 2.6.

Table 3.4 Description of screen measures

Measure	Explanation of the measures	Exported
Nuclear count	Number of full nuclei in a field of view (FOV).	Sum
Nuclear area	Area of full nuclei in a FOV.	Mean, Median, Std
Nuclear perimeter	Perimeter of the nuclei in a FOV.	Mean, Median, Std
Nuclear form factor	Form factor (major/minor axis) of full nuclei, a measure of roundness.	Mean, Median, Std
Cilia count	Number of cilia in FOV. There are a few different cilia axoneme categorisations that are counted; a) All cilia (mask of Ac-α-tub and Glu-tub) b) All cilia in association with a nucleus** c) Ac-α-tub cilia d) Ac-α-tub cilia in association with a nucleus** e) Glu-tub cilia f) Glu-tub cilia in association with a nucleus** g) Minimum overlap of Ac-α-tub and Glu-tube h) Minimum overlap of Ac-α-tub and Glu-tube in association with a nucleus** **Nuclei are identified and their perimeters dilated. The overlap between the dilated nuclear field and cilia stains are assessed and paired such that a single cilium is paired with a single nucleus (one-to-one relationship)	Sum
Cilia Max Chord Curved	Maximum center line through the cilium, calculated for all types of cilia mentioned in 'Cilia count'.	Mean, Median, Std
Cilia curvature ratio	Curvature = Max Chord Curved/object length, (length = longest straight line through an object). Calculated for all categories of cilia mentioned in 'Cilia count' that are associated with a nucleus.	Mean
Cilia area	Area of all types of cilia mentioned in 'Cilia count'.	Mean, Median, Std
Cilia perimeter	Perimeter of all categories of cilia.	Mean, Median, Std
Cilia incidence	Incidence = 100 x ('Cilia count' / 'Nuclear count'), for all types of cilia mentioned in 'Cilia count'.	Well %
Cytoskeletal indicators	Area, density level and mass of either total Ac-α-tub, Glu-tub or actin structures in a FOV. Dividing these by the 'Nuclear Count' allows for an approximation of the cytoskeletal indicators on a cell by cell basis.	Mean

*** see Appendix E for further details on how these parameters were obtained using the developer software**

3.8. Discussion

Within this chapter, the optimisation, validation, and experimental design considerations required to perform the compound screen were addressed. The SelleckChem FDA-approved compound library was identified as a suitable for the screen. A selection of 1,727 compounds at a concentration of 10mM were ordered in a fully customised plate layout, enabling DMSO and positive controls to appear on every compound plate.

Primary bovine chondrocyte isolation was optimised to enable full digestion of all the layers of the dissected articular cartilage, maximising cell yield. Some variability in cilia set length and incidence is found between cells isolated from different bovine joints, which is unsurprising when working with primary cells. However, all cells responded to a 16hr LiCl treatment which caused cilia length increases in all cell cultures, irrespective of the joint origin. Therefore, LiCl was identified as a suitable positive control for this screening assay. Basal cilia (~60%) versus apical cilia (~40%) expression was found to be consistent across cultures, regardless of animal origin. The 2D projected cilia length consistently demonstrated that the length of apically expressed cilia was measured to be shorter than basal cilia, therefore justifying the 3D z-stack imaging approach taken in this screen, coupled to variable region maximum intensity projection.

Isolated primary chondrocytes were also found to culture evenly across the 384-PerkinElmer screening plates, with consistent cell number and cilia length across a plate. A high throughput liquid handling protocol was successfully designed to dilute and treat cells with the screening compounds, in triplicate. Liquid handling protocols

were also successfully established to fix and IF stain the culture plates without disrupting the cellular monolayer. This would enable consistent compound treatment and four colour IF labelling across all 5,760 culture wells in the screen, labelling with ac-α-tub, glu-tub, DAPI and phalloidin.

A 10 z-slice, x60 InCell 6000 imaging approach coupled with variable region maximum intensity projection was established to ensure reliable detection of primary cilia length and incidence. Finally, a high content image analysis protocol was developed and manually validated for key screening measures, and a database was established for management of the screening outputs.

The complete screening pipeline was established, enabling a reliable and robust screening approach.

4. High throughput confocal screen of 1,727 compounds to identify compounds that alter bovine chondrocyte primary cilia structure

4.1. Introduction

Various observations have been made in numerous cell types, reporting alterations to primary cilia length and incidence in response to a variety of stimuli (see section 1.8). Furthermore, structural changes to the primary cilium have been associated with altered cilia signalling in both healthy and diseased cells as well as being associated with genetic ciliopathies (see section 1.5). However, the mechanistic impact that alterations to primary cilia structure may hold, remains poorly understood. To date, the hedgehog pathway is the most well-established primary cilia-related signalling pathway. Previously, LiCl induced increase in primary cilia length has been reported to inhibit the induction of Gli1 and PTCH1 in response to r-Ihh ligand.

Here, we conducted a high throughput, confocal compound screen, utilising a library of bioactive FDA approved compounds with known targets, to identify novel regulators of primary cilia structure and expression, with a particular focus on cilia elongation effects.

4.1.1. Chapter aims

1. To perform a multi parameter screen of 1727 compounds in primary bovine chondrocytes and identify clusters of phenotypic effects.
2. To identify and interrogate a compound cluster with specific effect on primary cilia structure.
3. Validate the compound cluster of interest in additional animals, to identify reproducible candidate compounds that cause primary cilia elongation in bovine chondrocytes.

4.2. Screening methods and workflow for 1,727 compounds

The screening workflow (summarised in section 2.7 and in the schematic in Figure 4.1) was optimised prior to conducting the full screen, as described in chapter 3. The following sections describe the specifics of the final full compound library screen.

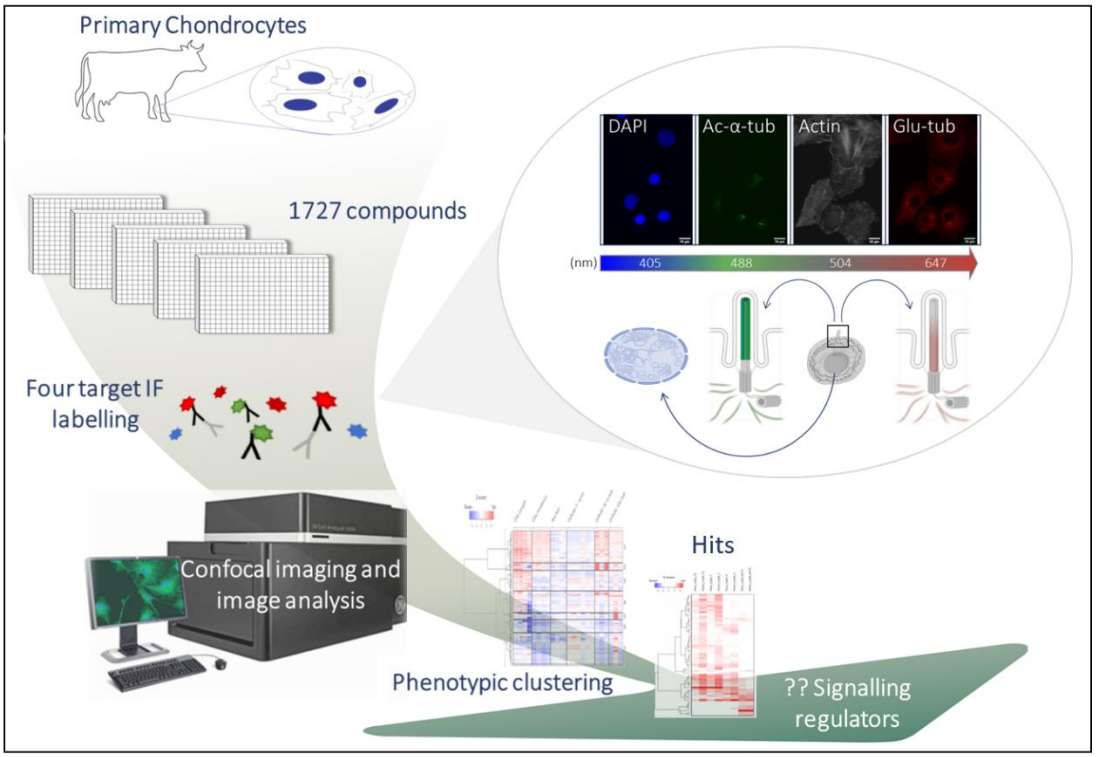

Figure 4.1. Schematic summary of the screening work flow.

Primary bovine chondrocytes in 2D culture were utilised for the purposes of this screen. A four colour immunofluorescent labelling approach, coupled with high throughput In Cell 6000 confocal imaging was used to interrogate the phenotypic effect of 1727 compounds on nuclear morphology (DAPI-Blue), cellular and ciliary acetylated alpha tubulin (Ac-α-tubulin – Green) and polyglutamylation profiles (Glu-tub – Red) as well as gross cellular actin (Grey) profiles. Phenotypic clustering paired with validation studies enabled compound hit identification, where candidates were to be carried forward as potential ciliary signalling regulators.

4.2.1. Cell isolation and batch seeding

Before conducting the compound screen, cell isolation (see sections 2.1.2 and 3.3.1) and culture (see sections 2.1.3 and 3.3) of primary bovine chondrocytes was optimised in a 2D PerkinElmer 384-well format. To ensure sufficient cell yield for the screen, full depth articular cartilage was dissected from the proximal surface of two metacarpal phalangeal joints taken from the same animal. After the overnight collagenase digestion (see section 2.1.2), a total of $65.5x10^6$ primary bovine chondrocytes were successfully isolated. The primary cells were then used to make up three batches of cell suspension at 120,000 cell/ml. The 15 PerkinElmer 384-well tissue culture plates were labelled A-O and manually seeded at 60,000 cells/cm^2 in a volume of 50µl/well, as described in section 2.1.3. The cells were seeded in three batches as described in Figure 4.2, and cultured to confluence over 7 days.

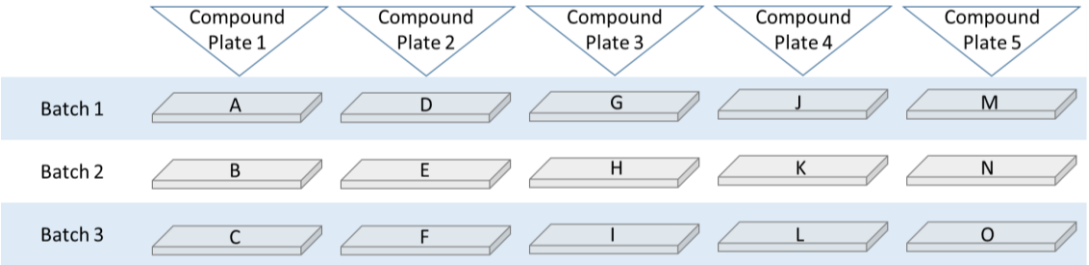

Figure 4.2. Schematic summary of cell seeding batches and compound treatment replicates.

Primary bovine chondrocytes were seeded in three batches of 5x384-well tissue culture plates. Batch 1 = ADEGJM, batch 2 = BEHKN, batch 3 = CFILO. One tissue culture (TC) plate from each seeding batch was used to make up the triplicate treatment batch for each of the five master compound plates. Master compound plate 1 = TC plates ABC, plate 2 = TC plates DEF, plate 3 = TC plates GHI, plate 4 = TC plates JKL, plate 5 = TC plates MNO.

4.2.2. Screening robotic liquid handling

Once confluent, the cells were ready for compound addition and incubation. For all robotic liquid handling steps, tissue culture plates were treated in alphabetical order, from A-O. To avoid excessive fluid disruption in the tissue culture plates, a single screening plate (0.5µl/well of compound at 10mM) originating from each of the five master compound plates, was thawed, diluted in cell culture media (see section 2.1.1) to a concentration of 10µM and mixed using robotic liquid handling into triplicate v-shaped 384-well treatment plates (see section 3.4.1. and part B of Figure 3.8). To these 15 compound treatment plates, 60µl/well LiCl (50mM) or DMSO (1:1000) controls were manually added to the last two columns of each plate (column 23 and 24, see Appendix C for control well layout). Complete media removal from the tissue culture plates was performed prior to a 50µl/well compound addition. This was run in batches of 3 tissue culture plates, such that each batch of culture plates received compounds from one of the original master compound plates (see Figure 4.2). Cells were incubated with compounds for 16hrs at 37°C in 5% carbon dioxide (CO_2) and 95% humidity.

Following the 16hrs incubation, cells were fixed in 4% PFA and run through the immunofluorescent liquid handling protocol as described in section 3.4.4. Immunofluorescent labelling protocol. This resulted in all 15 tissue culture plates being four colour labelled as described in section 3.3.7. Four colour immunofluorescent target selection , ready for automated imaging and quantification.

On visual inspection of the efficacy of the immunofluorecent labelling, tissue culture plates M-O were found to have aberrant IF labelling (Row 2 of Figure 4.3).

Although the DAPI staining qualitatively appeared to be similar to the well stained plates (Row 1 of Figure 4.3), the actin staining was less distinct and fainter. Of particular concern, the Ac-α-tub staining was very faint and did not clearly label cilia in the control wells. The Glu-tub staining was significantly less homogenous throughout the cell and appeared to have large punctate aggregates not obviously associated with a cilium. As such, screening for plates M-O was repeated, isolating cells from a new animal and re-running the screening and immunolabelling protocols for the compounds originating from master plate 5 (See Figure 4.3, Row 3). The data presented in subsequent sections utilises images generated from plates A-L from the first high throughput screen and plates M-O from this second screen.

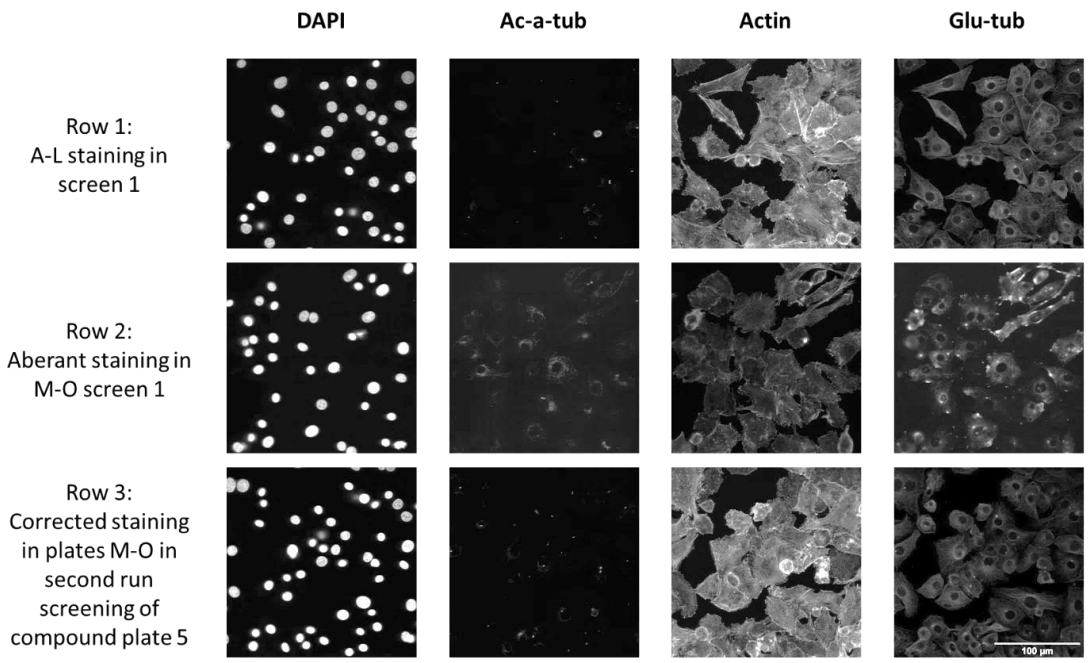

Figure 4.3. Representative images of successful vs anomalous IF staining from media control treated wells.

The following full fields of view images are taken from media treated wells and appear left to right as DAPI labelling the nuclei, Ac-α-tubulin that is usually enriched in the cilium, phalloidin labelling F-actin and polyglutamylation (Glu-tub) that is usually enriched in the cilium. ***Row 1*** *shows representative images from successfully labelled plates A-L in the first pass screen.* ***Row 2*** *shows representative images of aberrant staining in plates M-O of the first attempt screen.* ***Row 3*** *shows representative images from successfully labelled plates M-O in the second run of compound plate 5 screening. Scale bar bottom right = 100µm. Image brightness enhanced for clarity in this montage.*

4.2.3. In Cell imaging and maximum intensity projection processing

Once labelled, each of the 15 TC plates was first imaged on the In Cell 2200 (see section 2.2.3. Microscopy), to capture full well DAPI images enabling total cell counts per well. Each of the 15 TC plates were then imaged at x60 magnification on the In Cell 6000 (see section 2.2.3. Microscopy), capturing 10 z-slices (0.5µm step size) for 12 fields of view, in each of the four channels (see section 3.2.4). Imaging of a single plate took ∼11hr and generated 1.4TB of raw imaging data, with a total of ∼21TB of raw imaging data accrued for the full screen. To enable automated analysis of the images, the 3D z-slices were processed into stacks and then 2D maximum intensity projection images of two different regions were generated, as described in sections 2.6 and 3.6. These macro processing operations ran for a duration of ∼36hr for each of the 15 screening plates and generated an additional ∼1.69TB of imaging data per plate, equating to a total additional ∼25.35TB of imaging data for the full screen. Taken together, this amounted to a total of ∼170hr of imaging and ∼540hr of macro 2D image processing, resulting in a total ∼46.35TB of imaging data. This resulted in 552,960 2D maximum projection images ready for automated image analysis.

4.3. Screening analysis and exclusion criterion

4.3.1. Compound effect on cell number

To identify compounds that might drastically alter cell number, initial analysis was performed on the DAPI full well images captured on the In Cell 2200 (see representative image in Figure 4.4). Raw nuclear count was assessed using a Developer tool box analysis protocol and a cell number Z-score was calculated. As the screen was run with a triplicate dose for each compound, all primary analysis was performed on a Z-score average of the three triplicates. Using the average and standard deviation of the DMSO wells taken from all 15 screening plates, Z-score averages on cell number were calculated for each of the DMSO wells and for each compound.

Examination of the raw cell (nuclear) counts showed that 8 compounds were found to be toxic (marked by a black x on the graph in Figure 4.4A). Toxicity was defined as fewer than 6000 cells per well (i.e., which was the initial number of cells seeded into each well at day 1 of the experiment). The range of Z-scores for the DMSO full well cell number counts was found to be -4< Z-score <3. There were 22 compounds that were found to have at least 2 of their 3 triplicates and with a Z-score average less than -4), while there were 3 compounds that were greater than 3 Z-scores away from the DMSO average. Figure 4 shows representative images of cells treated with DMSO or compounds that were either toxic or induced an increase or decrease in cell number relative to DMSO (Figure 4.4 B-E respectively). This resulted in 33 compounds being excluded due to their effect on total cell number over the 16hr compound incubation. As a result, a total of 1694 compounds (98.1% of the original 1,727) emerged from this initial analysis.

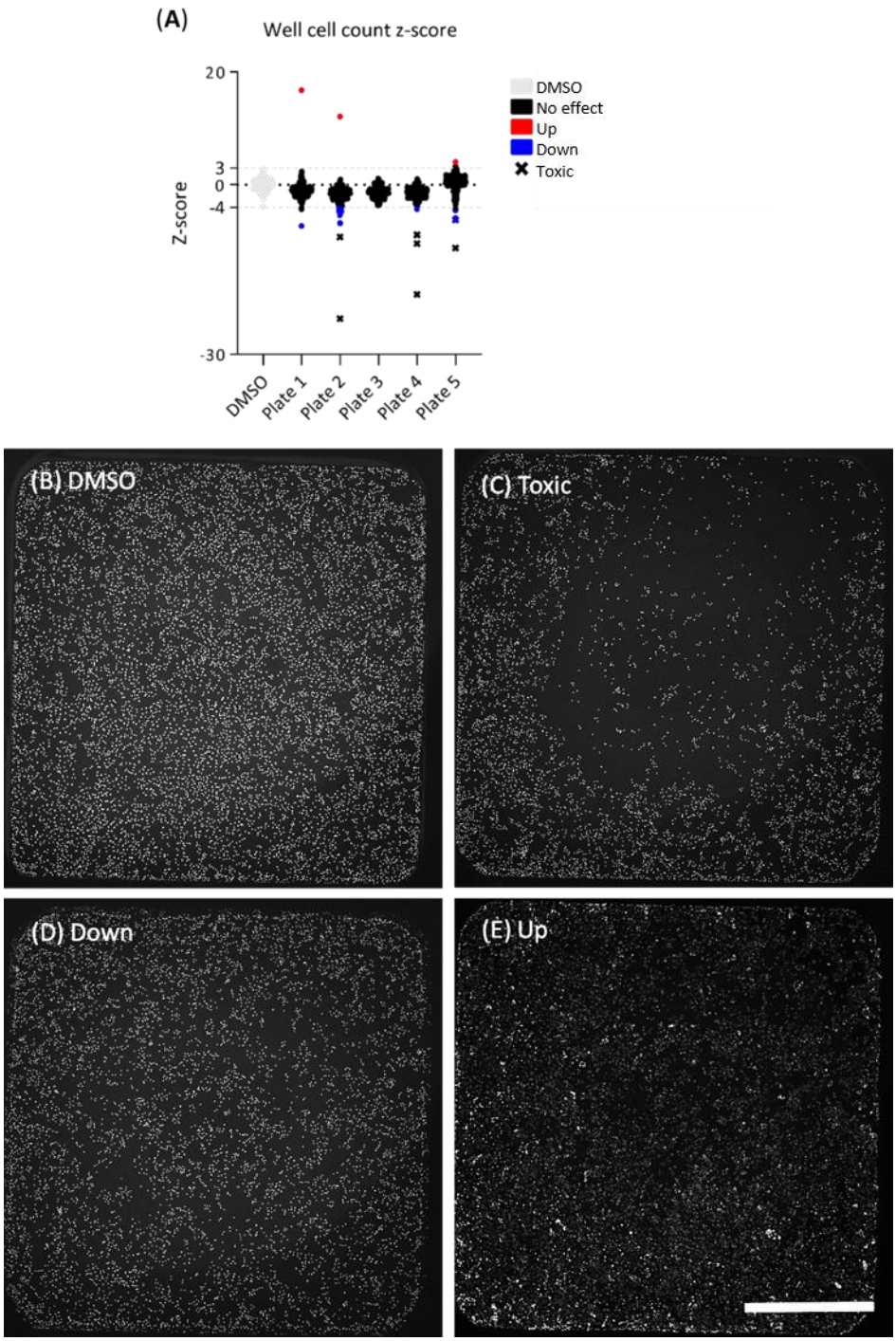

Figure 4.4. Compound exclusion based on total cell number.

*(**A**) Z-score average of total cell count per well for each compound plate, as compared to DMSO wells. (**B-E**) Representative full well images showing DAPI staining the nuclei of cells, scale bar = 1mm. (**B**) Is a representative of a DMSO control well, (**C**) a compound with toxic effects, (**D**) a compound resulting in a 4 Z-score reduction from the DMSO wells and (**E**) a compound resulting in a 3 Z-score increase from the DMSO control wells.*

4.3.2. LiCl positive control validation

Having established the effect of the compounds on total cell number, the In Cell 6000 high magnification images were then analysed using a Developer tool box, automated image analysis protocol, as described in section 3.7. The generated raw analysis data was imported into a MySQL database and converted into Z-score matrixes as described in section 2.7.2.

Z-score tables for LiCl positive control wells and media only wells were generated from the averages and standard deviations of DMSO wells. A ciliary length increase of ac-α-tub labelled cilia has previously been reported and was used as the positive control measure in this screening assay. The addition of DMSO as compared to media only wells was found to have had little effect on ciliary ac-α-tub length, while LiCl caused the predicted cilia length increase across all screening plates, indicated by the increase in Z-score (red) as seen in both the dot plot (Figure 4.5 A) and heat map (Figure 4.5 B). Dot plots for the additional ciliary length measures and their respective prevalence are also depicted. The absolute Z-score minimum and maximum ranges are provided in table F.1 in appendix F.

There are a few measures that can be taken into account when assessing the quality of a screening assay, such as the strictly standardised mean difference values (SSMD) or the Z' factor. In this instance the Z' factor was used to assess the quality of the screen where a factor of $0 < Z' < 0.5$ is acceptable, and a $Z'>0.5$ is optimal. The Z' factor for this assay was found to be $Z'=0.68$, showing that the assay was of high quality and reliable.

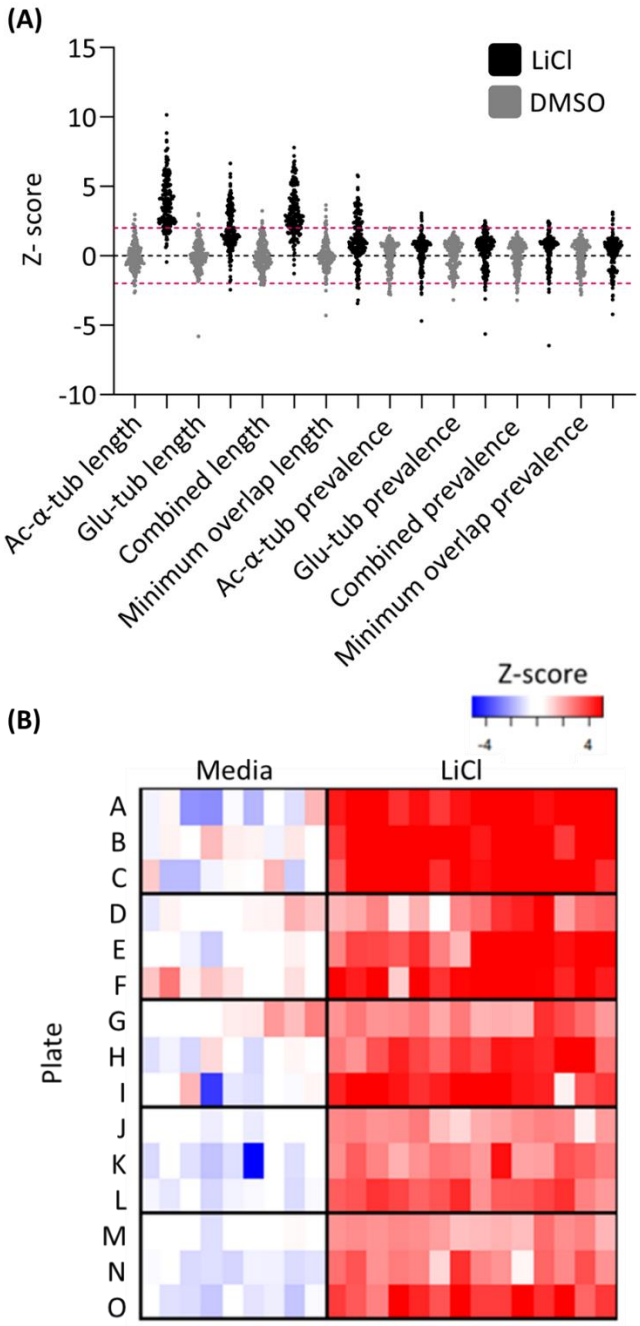

Figure 4.5. Effect of LiCl positive control across all 15 screening plates.

*(**A**) Dot plot of DMSO (grey) and LiCl (black), z-scores across all 15 screening plate for the primary measure of interest, Ac-α-tub cilia length, additional ciliary length measures and their respective prevalence measures. Dashed red lines indicate the -2 and 2 z-score range. (**B**) Heat map of Z-scores showing the effect of LiCl on Ac-α-tub cilia length measures for each control well across all 15 screening plates, where red indicates an increase in cilia length and blue indicates a decrease as compared to DMSO only wells.*

4.3.3. Identification of outliers

Having established that the positive LiCl control had the desired effect on all screening plates, the compound effects were then further interrogated. For investigation of compound phenotypic effect, Z-scores were calculated based on the DMSO averages and standard deviations of each of the seeding batches, such that averages were taken from plates ADGJ, BEHK, CFIL, and then the repeated plate 5 screen, MNO (see Figure 4.2). From the Z-score tables generated in the MySQL database, 506 compounds were found to have an average Z-score effect of less than -2 or greater than 2 (-2> Z-score >2), for at least one of the measured parameters in the screen. Hierarchical clustering was performed on all 506 compounds identified (see Figure 4.6 A). From this, a small cluster of 14 compound outliers were identified as generating an increased (red) Z-score of >40 for measures associated with overall cell cytoplasmic Ac-α-tub. These data suggest that the compounds may cause a hyper acetylation to the alpha tubulin in the entire cell tubulin network (see Figure 4.6 B and C). This effect would make automated identification of cilia length alterations unreliable, as such these compounds were excluded, leaving 492 compounds for further analysis.

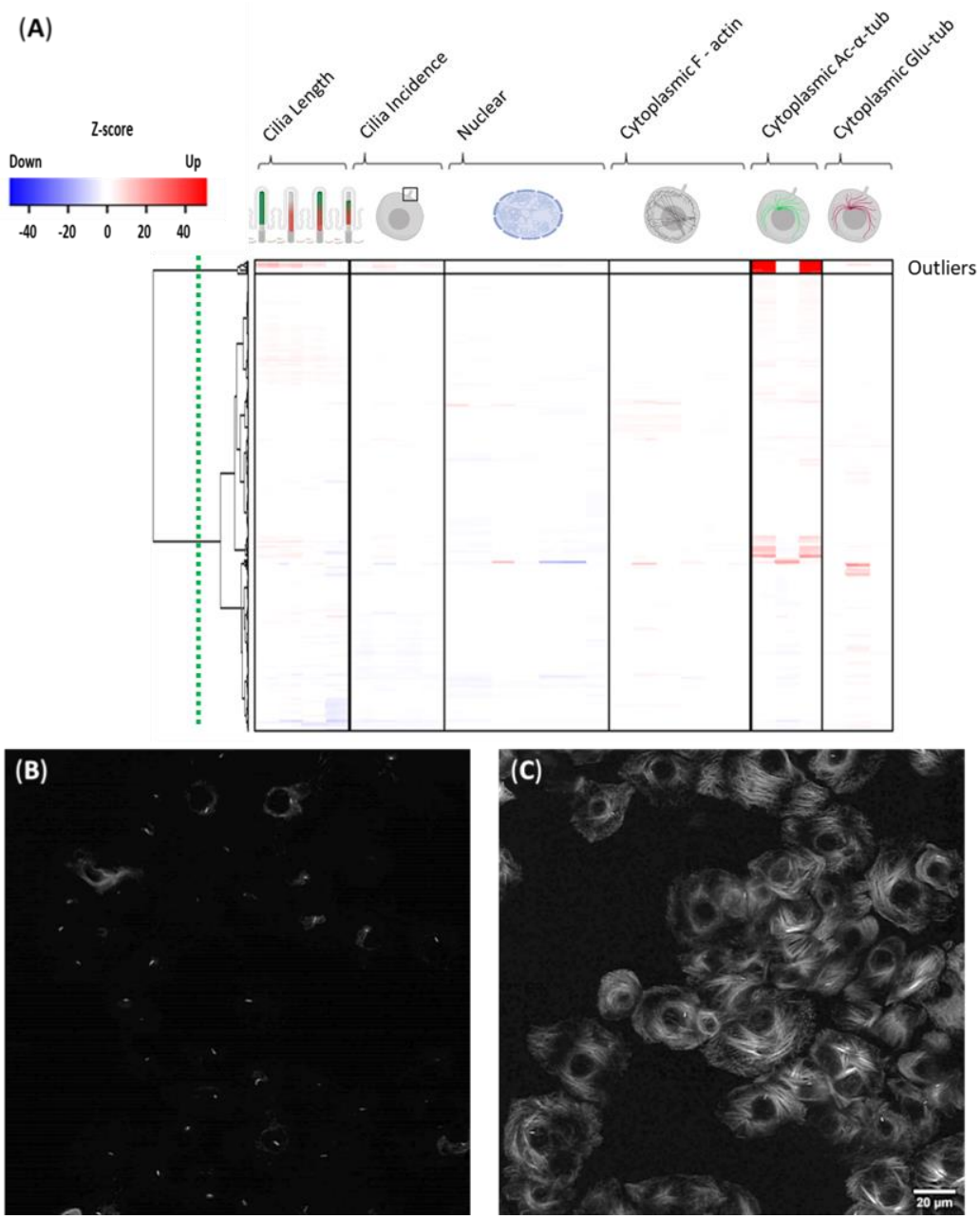

Figure 4.6. Hierarchical clustering of 506 compounds with an effect on at least one of the measured parameters and representative images of the identified outliers.

*(**A**) Heat map of 506 compounds, hierarchically clustered such that low Z-scores appear in blue and high Z-scores appear in red. Screen measures run horizontally, while compound Z-score averages run vertically. A distinct cluster of 14 compounds identified as having drastically increased cytoplasmic Ac-α-tub associated measures (Outliers). (**B**) Representative image of typical Ac-α-tub profiles in DMSO control well. (**C**) Representative image of Ac-α-tub profile identified in the outlier cluster. Scale bar = 20µm.*

4.4. Clustering on compound phenotypic effect

Having excluded compounds that drastically altered cilia number and the Ac-α-tub profiles of the cells, 492 compounds remained. Of the remaining compounds, 233 compounds were identified as having an average Z-score effect of at least 2 (-2 > Z-score >2) for one of the primary measures of interest included in the screen, namely cilia length and/or incidence. These 233 compounds were then hierarchically clustered to identify clusters of phenotypic effect (Figure 4.7 A). This was done using R scripts that performed Ward's hierarchical clustering method and Euclidian distance. Six clusters of phenotypic effect were revealed, represented such that those measures with a raised Z-score as compared to DMSO controls appear in red, and those with a reduced Z-score appear in blue. To ease the identification of the predominant measure that a compound cluster was influencing, the heat map had a threshold placed such that any effect that was greater than -2 and less than 2 Z-scores away from the DMSO control appeared white (-2< Z-score < 2) (Figure 4.7 B). The raw Z-scores for the measures of interest, cilia length and incidence are provided in Figure 4.8 and 4.9 A-D). Exploration of the compound targets or pathways annotated within the compound library found no particular clustering (data not shown).

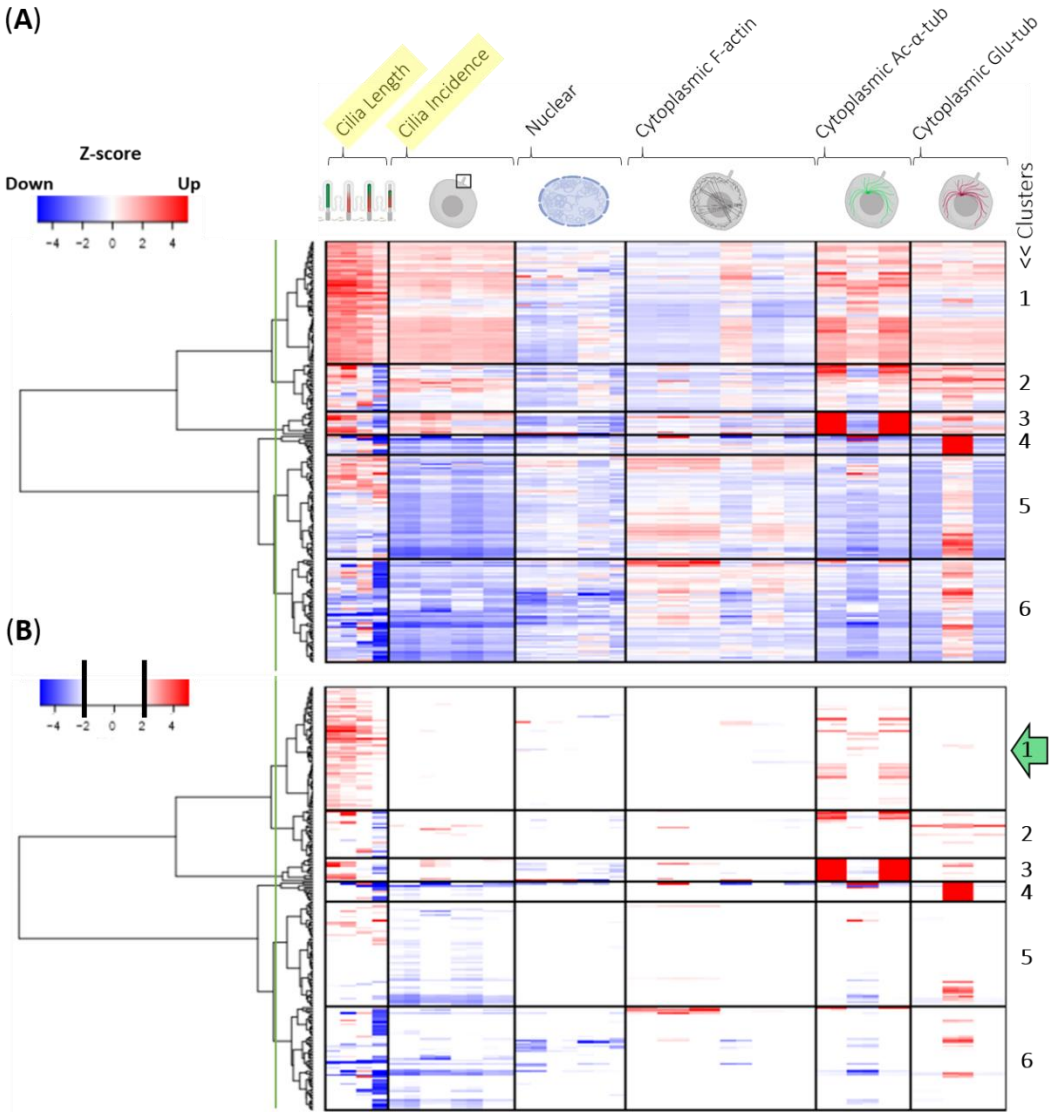

Figure 4.7. Hierarchical clustering of 233 compounds affecting any of the length or incidence associated measures.

*Measures are represented horizontally, and Z-score averages of triplicate compound treatments appear vertically. Heat maps of compounds effects, hierarchically clustered to reveal phenotypic effects and represented with either (**A**) continuous or (**B**) threshold cut off (absolute values of 2 or less appear white) colour scales. A decrease in Z-score average is represented in blue, while an increase in Z-score average for any particular measure is represented in red. Green line (left hand side) represents the dendrogram distance cut off for the identification of six clusters of phenotypic effect are identified.*

Although nuclear measures provided no distinction between the 6 identified clusters, a predominant distinction between clusters 1-3 and 4-6 was apparent in the effect on cilia incidence measures. Clusters 1-3 resulted in a subtle increase in cilia expression, while clusters 4-6 resulted in a reduction (see Figure 4.7 A and Figure 4.8 E-H). These effects on cilia incidence broadly appeared to positively correlate with effects on cytoplasmic Ac-α-tub and Glu-tub, while inversely correlating with the majority of actin associated measures. However, when a threshold of 2 Z-scores was applied (see Figure 4.7. B) the subtlety of these effects was highlighted.

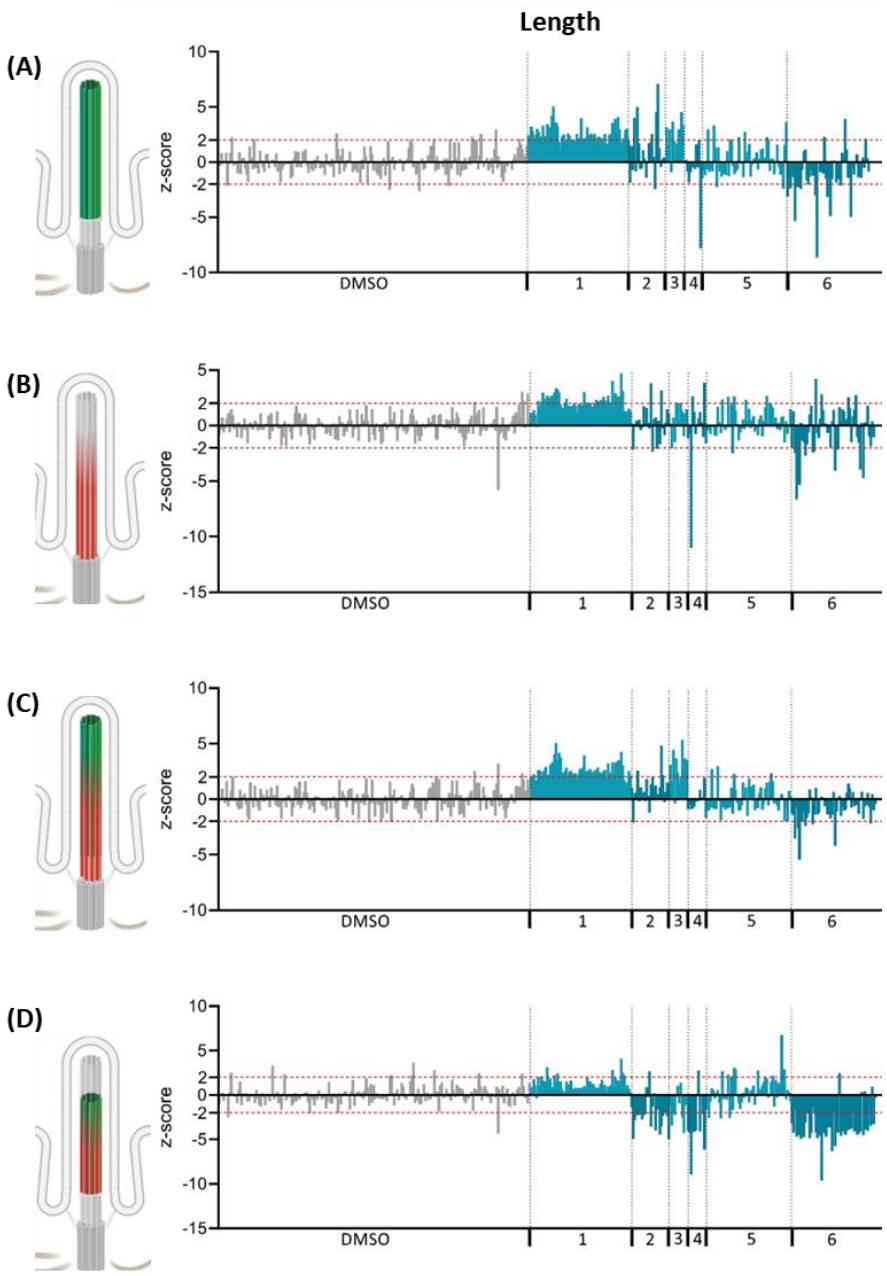

Figure 4.8. Raw z-scores for the various cilia length measures included in the screen.

*The z-scores for the four various cilia length measures (**A**) Ac-α-tub, (**B**) Glu-tub, (**C**) the combined length of Ac-α-tub and Glu tub and (**D**) the minimum overlap of Ac-α-tub and glu-tub. Z-scores are represented on the y-axis. DMSO (grey) and heat map compounds (blue) appear along the x-axis. Red dashed lines indicates values of z-score =2 and z-score =-2. Vertical dashed lines represent the separation of the 6 clusters.*

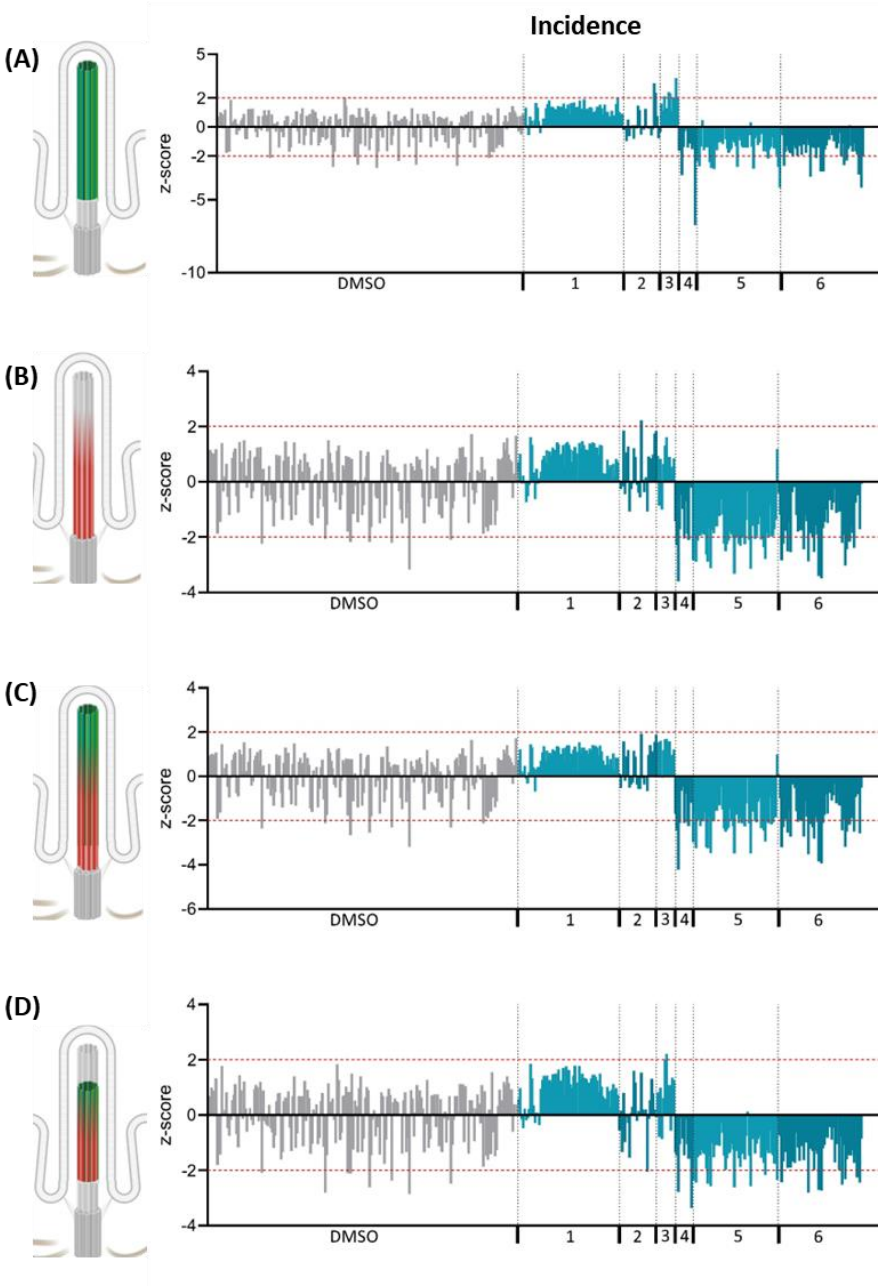

Figure 4.9. Raw z-scores for the various cilia incidence measures included in the screen.

*The z-scores for the four various cilia incidence measures (**A**) Ac-α-tub, (**B**) Glu-tub, (**C**) the combined length of Ac-α-tub and Glu tub and (**D**) the minimum overlap of Ac-α-tub and glu-tub. Z-scores are represented on the y-axis. DMSO (grey) and heat map compounds (blue) appear along the x-axis. Red dashed lines indicates values of z-score =2 and z-score =-2. Vertical dashed lines represent the separation of the 6 clusters.*

Cluster 1, comprised of 68 compounds, was identified as the cluster of interest as it held the majority of cilia elongation compounds that appear to have a largely cilia specific effect. These compounds increased cilia length, with few having a –2> Z-score >2 effect on any of the other screening measures. This is depicted in Figure 4.7. B where cilia length measures appear red in cluster 1, while other measures fall under threshold and appear white. Of these 68 compounds, 67 had an average Z-score>2 for at least one of the 4 cilia length measures. 63 were classed as cilia elongation screening hits, having both an average Z-score>2 and at least 2 of their 3 triplicates scoring a Z-score>2 for at least one of the 4 cilia length elongation measures. These 63 compounds (3.65% of the original library) were carried forward for further validation. Representative images for DMSO and cilia length elongation are provided in Appendices G.

4.5. Validation of cilia elongation compounds

Having identified 63 ciliary elongation hits in the first pass screen, the reproducibility of their effect was then validated in primary cells isolated from independent animals. The 63 hit compounds were manually reformatted into a new master compound plate prior to being stamped out as described in section 3.4.2. Cells were isolated from three addition animals, seeded and screened as described in section 4.2. Once fixed and labelled, DAPI channel full well images were captured on the In Cell 2200 to determine the average cell number in the DMSO wells for each animal (see Figure 4.10 A). All three validation animals had fewer cells per well at the end of screening than the original screening animal. This variability between biological samples might be expected due to factors, such as animal size, age, activity levels, cell adhesion properties and cell division rates. Animal V1 had almost half the cell density of the original screen with a mean cell density of 226.0 as compared to 489.8 of the first pass screen (Figure 4.10 A). As such, the cells in V1 were not sufficiently confluent, a key factor for cilia expression. Therefore, only animals V2 and V3 were considered for the validation of compound effect on cilia length.

Cells treated with compound were imaged on the In Cell 6000 and analysed as described in the first pass screen. Although four cilia length measures were captured (see schematic in Figure 4.10 B), ac-α-tubulin is one of the most well established and widely used markers of cilia length. Therefore, the validation of the compound effect was performed using this as the measure of interest, where a Z-score greater than 2 was defined as a successfully validated hit. To be classified as a validated cilia elongater, compounds had to score positive in at least two out of the

three animals (S, V2 and V3). There were 8 compounds found to cause cilia elongation in all three animals (see Figure 4.10 B). An additional 14 compounds caused cilia elongation in at least two of the animals. It should be noted that 2 of these 14 compounds scored for V2 and V3 but not the first pass screen (S) for Ac-α-tubulin cilia length. Taken together, the large-scale compound screen combined with the validation screen identified 22 compounds which robustly caused cilia elongation. These 22 compounds of interest will be carried forward to the interrogation of cilia structure on cell signalling.

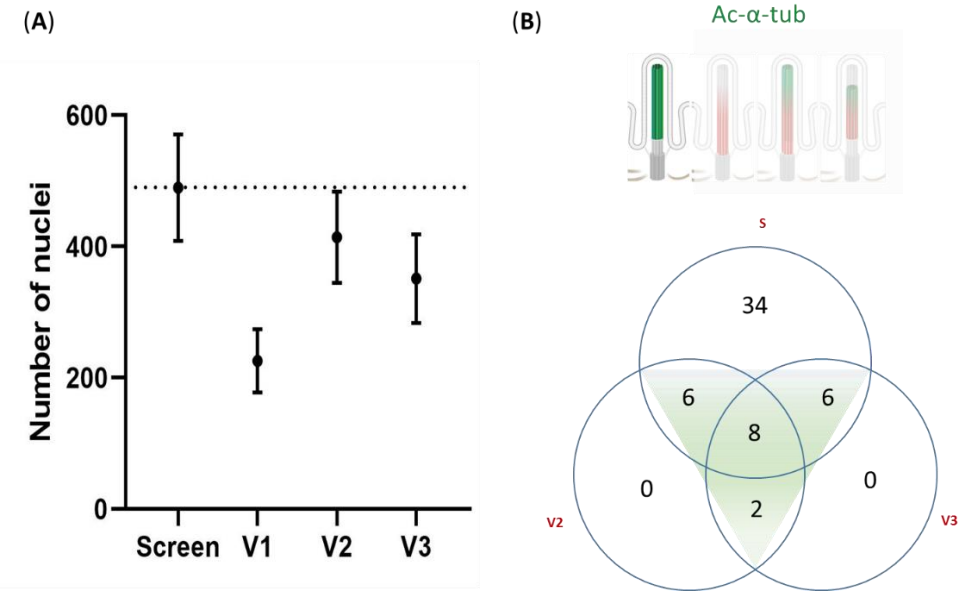

Figure 4.10. Validation of 63 cilia elongation compounds in additional animals.

*(**A**) The number of nuclei in 12 fields of view of DMSO control wells from the initial screen and 3 additional validation animals (V1-V3). Data presented as the mean and standard deviation with the screening animal at 489.8±81.0, V1 at 226.0±48.16, V2 at 414.1±69.5 and V3 at 351.3±67.6. (**B**) Venn diagram showing the number of compounds scoring a Z-score greater than 2 for primary cilia ac-α-tub length measures, looking at the intersect of those scoring in the original screen (S) animal and in two of the additional validation animals (V2 and V3), with 8 scoring in all three animals, and an additional 14 scoring in at least two of the three animals (region of interest highlighted in green).*

4.6. Discussion and future work

4.6.1. High throughput screening and the identification of 6 clusters of phenotypic effect

Within this chapter, a high throughput, confocal screen was successfully performed, enabling identification of novel compound regulators of cilia length and incidence in bovine chondrocytes. Having optimised a screening workflow, primary bovine chondrocytes were isolated, cultured to confluence and treated with the library of 1727 compounds. The phenotypic effects of the compounds were interrogated, and an inclusion criterion created, as summarised in Figure 4.11. Of the 1727 compounds screened, 1694 had no effect on total cell number after the 16 hour incubation. Of these, 506 compounds were found to have an effect of 2 Z-scores, for at least one of the measures included in the automated analysis protocol (see section 3.7.2). The effects of these 506 compounds was further interrogated by hierarchical clustering and represented in a heat map (Figure 4.6), where 14 outliers affecting automated primary cilia recognition were identified and excluded from further analysis. The remaining 492 compounds were found to include 233 that had an effect on at least one of the length or incidence measures, the primary interest of the first pass screen. Upon examination by hierarchical clustering and heat map representation, the screen identified 6 compound clusters of phenotypic effect, with no particular clustering of compound targets or pathways.

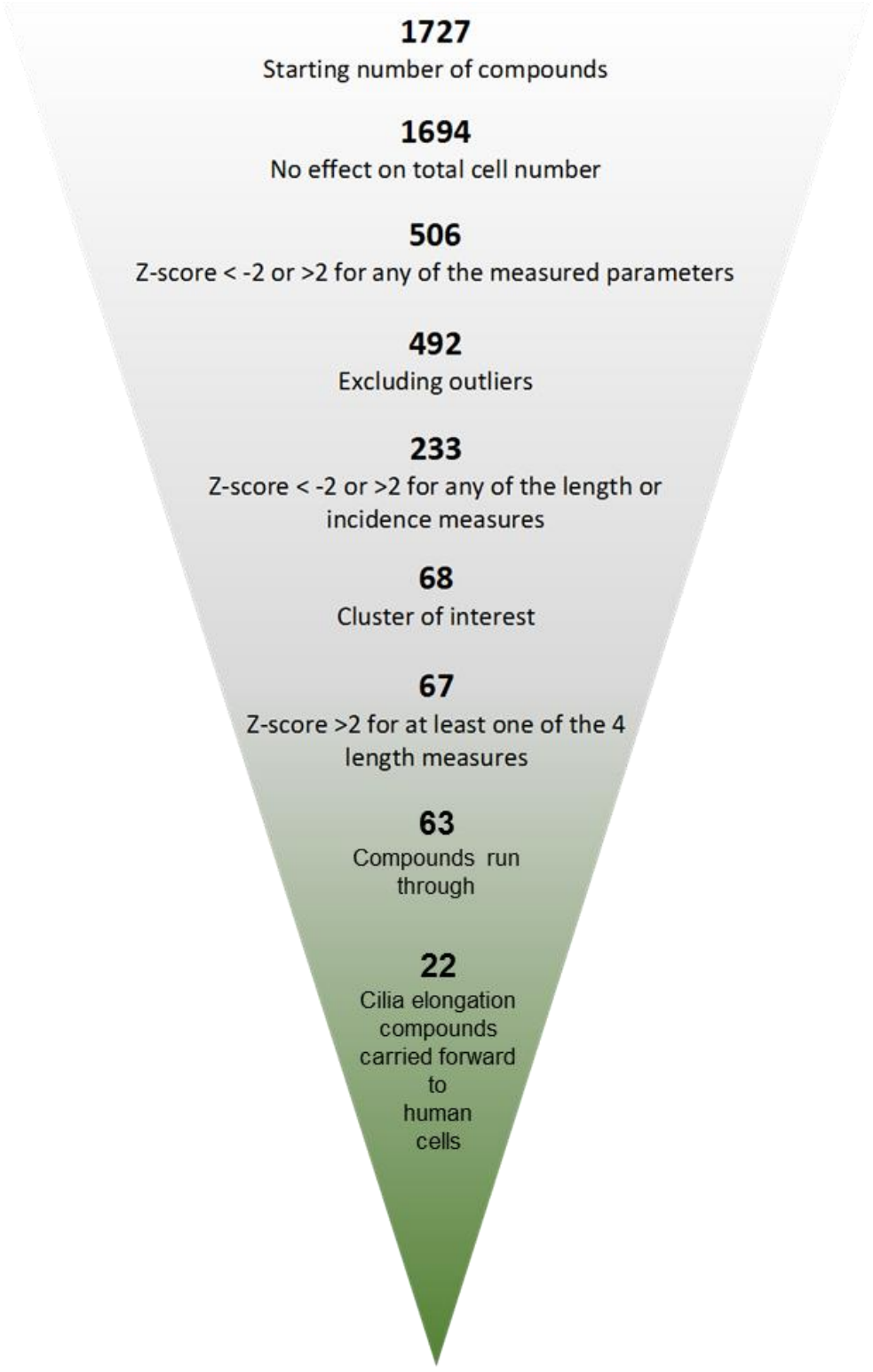

Figure 4.11. Summary of inclusion criteria for the 22 identified candidate compounds.

Schematic summary of the inclusion criterion followed to identify the 22 compounds which produce a robust primary cilia elongation in bovine articular chondrocytes.

4.6.2. Cluster of cilia elongation compounds

Although an association between cilia structural alterations and aberrant signalling have been reported numerous times in the literature, the link between structure and function still remains poorly understood. As discussed in section 1.4, the hedgehog signalling pathway is the most well connected to cilia structure, where previously cilia elongation has been reported to inhibit r-Ihh ligand induction of Gli1 and PTCH1. One of the primary aims of this project was to identify additional compounds that would enable further investigation of this structure-function relationship, initially through the hedgehog signalling pathway. As such, compound clusters causing cilia elongation were of primary interest, with cluster 1 identified to contain the most numerous of these.

Further to being the largest cluster of cilia elongation compounds, cluster 1 appeared to be the most ciliary specific in its effects. Of the 68 compounds falling into the group, 67 were found to have cilia length effects based off of triplicate average z-scoring. With a more stringent examination of individual technical replicates, 63 of these compounds were carried forward as first pass screening hits for cilia elongation (see Figure 4.11).

4.6.3. Validation and identification of 22 compounds of primary interest

The initial screen was conducted with cell isolated from a single animal, therefore the 63 hit compounds were validated in primary cells isolated from a further 2 animals. Of the four cilia length measures included in the screen, the length based off of Ac-α-tub is the most commonly used and well defined within the literature. As such, the 63 hit compounds were validated on this measure, where 8

compounds were found to cause the same effect in all three animals, with an additional 14 compounds causing cilia elongation in cells from at least two of the experimental animals. No one particular pathway or target appeared to be represented among the compound hits. Some unsurprising targets made the hit list, such as HDAC inhibitors, although of the 11 compounds targeting HDACs within the original compound library only 2 were classified within the 22 validated compound hits. Of the 94 included compounds identified in the osteocyte cilia screen only 1 compound reported to increase cilia incidence but not length in osteocytes appeared in the 22 cilia elongation compounds identified in this screen.

Although the initial focus of this project was to identify compounds causing cilia elongation and to interrogate their effects on cell signalling events, the conducted screen offers several avenues of future investigation. The ~46.35TB of imaging data alone provides a data resource for both further 2D automated and machine learning analysis, while the ongoing development of volumetric analysis tools provides potential for further spatial 3D analysis. In addition to the data generated in this screening analysis, the remaining 5 compound clusters all offer further potential insights with closer inspection of the compounds, their targets, pathways, and chemical families paired to their phenotypic effect. However, the successfully run and validated screen identified these 22 cilia elongation compounds, with various known targets and associated pathways, providing novel tools for further interrogation of how cilia elongation might impact associated signalling pathways. As such these compounds would be carried forward in future experiments as described in the following chapter.

Given that the links between hedgehog signalling and cilia elongation are perhaps some of the most well established, the 22 validated compounds which emerge would be investigated for their impact on hedgehog signalling. As the hedgehog signalling pathway is largely activated during development, the pathway is active during adolescence and down regulated into maturation. However, it has been seen to be upregulated in certain diseases such as OA, a potential environmental ciliopathy. In particular, Indian hedgehog (Ihh) expression has been reported to be increased in early cartilage legions and found to be at higher concentrations in the synovial fluid of OA patients (Zhang, et al. 2014). With the potential future avenue of utilising and repurposing the identified cilia elongation compounds as human ciliotherapies, it was ideal to validate the ciliary elongation and investigate the effect on hedgehog signalling in a human cell model, as described in the next chapter.

4.6.3. Critical evaluation of the screen

Although this screening pipeline was robustly designed, there are some shortcomings that could have been improved had data storage capacity and time not been limiting factors. The 1,727 compound library utilised in this screen is by no means the largest compound library to be employed in a screen of this nature, however it was sufficiently large to identify multiple robust and reproducible cilia length elongators. Due to limitation of space on the screening plates, DMSO and LiCl were the only controls included in the screen, where additional controls for known cilia length depletion and incidence regulation would have been ideal. However, the selected controls appeared on every screening plate and induced ac-α-tubulin labelled cilia elongation across all plates. This indicated the correct execution of liquid

handling protocols and demonstrated the responsiveness of the cells to elongation cues, while also demonstrating the capability of analysis protocol to identify length changes.

Primary chondrocytes, an ideal cell type for cilia length analysis were utilised, although due to the feasibility of scale, the initial screen was conducted on cells isolated from a single animal, where multiple animals would have been ideal. However, validation of the 63 cilia length regulators identified in the first pass screen was conducted in cells isolated from an additional two animals, although the reproductivity of effect was only assessed on the cilia length changes analysed from ac-α-tubulin labelled cilia rather than the full four characterisations of cilia in the initial screen. The reproducibility of the screening hit compounds was also less than 50%, however these were robust elongation compounds, with a stringent z-score cut off of 2. In this screen, the effect of compounds on basal cilia structure were reported, where the length effect on apical cilia remains unknown. However, this ensures that length alterations were reliably reported, where the effect on apical cilia could be interrogated in future with the development of better high content volumetric analysis approaches. Furthermore, detailed analysis of other screening outputs such as compound effect on F-actin remain underutilised in this screen.

In this screen, a single compound dose and time point were utilised. In future follow up work, dose responses and time courses should be investigated. Furthermore, dosing regimens could be investigated, enabling the examination of the stability of compound effect.

Although there are limitations to this screen, the parameters of the presented screening pipeline enabled the identification of robust and reproducible cilia elongation compounds, with largely ciliary specific effects.

5. Validation and Interrogation of the 22 Identified Bovine Cilia Elongation Compounds in a Juvenile Human Chondrocyte Cell Line

5.1. Introduction

The previous chapter described a high-throughput imaging screen to investigate the effect of a library of compounds on primary cilia expression. Having conducted the screen of 1,727 compounds and identified 22 compound of interest causing cilia elongation in primary bovine chondrocytes, this chapter validates the effects of these hits in human chondrocytes. The chapter then proceeds to investigate the cilia structure-function relationship. Altered cilia structure has been observed to accompany alterations and abnormalities in numerous different cilia signalling pathways, of which the best characterised is the hedgehog signalling pathway. For example, it has been demonstrated that LiCl induces robust cilia elongation, which is associated with an inhibition to the ligand induced induction of *GLI1* and *PTCH1* (Wann, et al. 2013). Therefore, this chapter describes the investigation of the effect of small molecule-induced cilia elongation on hedgehog signalling in human chondrocytes.

5.1.1. Chapter aims

1. Design an experimental approach to investigate hedgehog signalling.
2. Validate immortalised human chondrocyte cell culture and cilia expression quantification.
3. Assess cell viability and cilia response to the 22 bovine hit compounds in the human chondrocyte cell line.
4. Validate the quantity and quality of RNA isolated for the investigation of the hedgehog signalling pathway.
5. Identify suitable RT-PCR primers for the hedgehog targets Gli1 and Ptch1.

6. Assess the effects of the compounds on cilia elongation in the human chondrocytes.
7. Interrogate the effects of the compound treatment on baseline expression and ligand induced induction of *GLI1* and *PTCH1* as key markers of hedgehog pathway activation.

5.2. Experimental design for investigating the effect of compound on cilia signalling

5.2.1. The hedgehog signalling pathway

The coordinated trafficking of hedgehog signalling components within the cilium is required for pathway activation, as described in section 1.3 and Figure 1.2. Patched (Ptch1) is a hedgehog receptor that is trafficked onto the ciliary membrane in the absence of ligand, where it acts to inhibit the transmembrane protein Smoothened (Smo), which in turn regulates the activity of the downstream Gli (Gli2 and Gli3) transcription factors. In the absence of ligand, Gli is cleaved into its repressor form (Gli-R, predominantly Gli3) and is trafficked to the nucleus where it acts to inhibit pathway activation. Upon activation of the pathway with ligand, Ptch1 exits the ciliary membrane and is degraded as Smo is loaded onto the cilium. Smo, no longer inhibited by Ptch1, acts to prevent further Gli cleavage, thereby maintaining and releasing the activator form (Gli-A, predominantly Gli2) for translocation to the nucleus and subsequent activation of downstream targets such as Gli1. Expression of the transcription factor Gli1 up-regulates the expression of Ptch1. Increased levels of Ptch1 block Gli1 and Ptch1 transcription, thereby creating a negative feedback loop.

Several modes of investigating the effect of compound on hedgehog signalling were considered. Immunofluorescent (IF) labelling to monitor the switch between Gli-R and Gli-A in the nucleus of the cell in response to ligand, coupled with the high throughput screening and imaging system would offer an individual cell readout. Similarly, IF labelling of Smo to monitor its trafficking onto the cilium could

provide a cell and cilia specific readout. However, IF validated and Gli target specific antibody availability is currently limited and initial attempts to validate Gli antibodies were not successful (data not shown). Furthermore, these IF approaches would require precise temporal monitoring incompatible with the current screening pipeline and would not allow for the assessment of the compound's downstream functional influences on the hedgehog signalling pathway. Therefore, to begin to probe these downstream functional influences of compounds, levels of *GLI1* and *PTCH1* mRNA were measured; a commonly employed approach to assess hedgehog pathway activity (Thompson, et al. 2014; Thompson, et al. 2016; Thorpe, et al. 2017).

5.2.2. Experimental design and considerations

As described in section 4.6.3, with the potential future avenue of utilising and repurposing the identified cilia elongation compounds as human ciliotherapies, validating these compounds in a human cell model is ideal. As primary human chondrocytes are a precious resource with limited availability and potential issues of reproducibility, a human cell line was utilised. These were an SV40 immortalised chondrocyte cell line (C28/I2) originating from costal cartilage isolated from a 15-year-old female. This juvenile cell line was utilised to ensure detectable levels of hedgehog expression. Furthermore, with the future potential of ciliopathy treatments likely to be administered in infants, the efficacy of these compounds in juvenile cells is of interest. Due to the relevance of chondrocytes in the joint and cartilage, and the reported expression of Ihh in OA disease, r-Ihh ligand (1750-HH/CFBiotechne, R&D systems) was utilised for ligand-induced activation of the pathway. The ligand utilised in the experiments was an *E. coli*-derived Ihh protein.

In summary, to interrogate the impact of ciliary length on the hedgehog signalling pathway, juvenile human chondrocyte would be incubated for 16hr with compound to induce to a longer cilia length. Following this, cells would be stimulated with r-Ihh ligand in the presence of compound for a further 24hrs (total of 40hrs in compound), and RNA collected for later RT-PCR analysis of the downstream *GLI1* and *PTCH1* expression levels.

5.3. Human chondrocyte cell culture and compound viability validation

5.3.1. Human chondrocyte cell culture

A juvenile chondrocyte human cell line was maintained as described in section 2.1.4. To identify a suitable cell seeing density, cells were passaged and seeded at a range of densities from 1, 2, 3, 4, 5 and 6 x 10^4 cells/cm^2 in a 384 well cell culture plate. Human cells seeded at the same density as that used previously with primary bovine chondrocytes (6 x 10^4 cells/cm^2) were overcrowded (data not shown). However, those seeded at a concentration of 1 x 10^4 cells/cm^2 grew to a confluent monolayer over 6 to 7 days of culture, matching the time taken for a monolayer culture to be reached by primary bovine chondrocytes (data not shown). Therefore, a cell seeding density of 1 x 10^4 cells/cm^2 of the human cell line was used during all experimental conditions.

5.3.2. Cell viability with compound treatment.

The 22 hit compounds identified during the primary bovine chondrocyte screen were manually reformatted into new cilia elongation hit plates, ready for future validation and experimentation. With the aim to interrogate the effect of cilia length on hedgehog signalling, cells would first be treated with selected compounds for 16hrs to induce cilia elongation. Cells would then be incubated for an additional 24hrs with compound with the addition of hedgehog ligand to activate signalling. Therefore, it was necessary to validate the viability of the 22 hit compounds in the human chondrocyte cell line over a 40hr incubation period.

For cell viability assessment, cells were seeded into 384 well tissue culture plates at a concentration of 1 x 10^4 cells/cm^2 in a volume of 50µl cell culture media.

Cells were grown to confluence over 6 days with media changes every 2-3 days. Once confluent, a multichannel pipette was used to manually treat cells in triplicates with compound at a 10µM concentration. Additional LiCl and DMSO controls were employed and the cells cultured for 16hr or 40hr (16+24hr).

Following compound treatment, cells were fixed and stained as described in section 3.4.4 using a manual multichannel pipette rather than the liquid handling robotics. Cells that received the 16hr exposure to the compounds were stained for DAPI, ac-α-tubulin, phalloidin and glu-tubulin. Cells cultured for 40hr with compound were labelled only with DAPI enabling cell number to be used as an indicator of cell viability.

Once stained, both 16hr and 40hr exposure plates were imaged on the In Cell 2200 capturing full well DAPI images, as described in section 2.2.3. Having imaged the DAPI signal, the number of nuclei in the full well area was assessed. Compounds with at least 2 out of the 3 triplicates causing a reduction in cell number below the original seeding density of 1,000 cells per well, were classed as toxic. Compounds with a triplicate average cell number lower than the minimum range of the 16hr DMSO control were also excluded due to their effect on total cell number.

In line with the bovine chondrocyte screening timeline, after a 16hr exposure, none of the compounds were identified as toxic to the human cells (Figure 5.1 A). After a 40hr incubation with compounds, one compound was identified as toxic, and an additional five were identified as substantially reducing cell number. All of these compounds reduced cell number between 16hr and 40hr time points (Figure 5.1 B). These six compounds are coloured red in Figure 5.1 and were excluded from further

investigation. This left 16 compounds that were carried forward to further Hh signalling experiments.

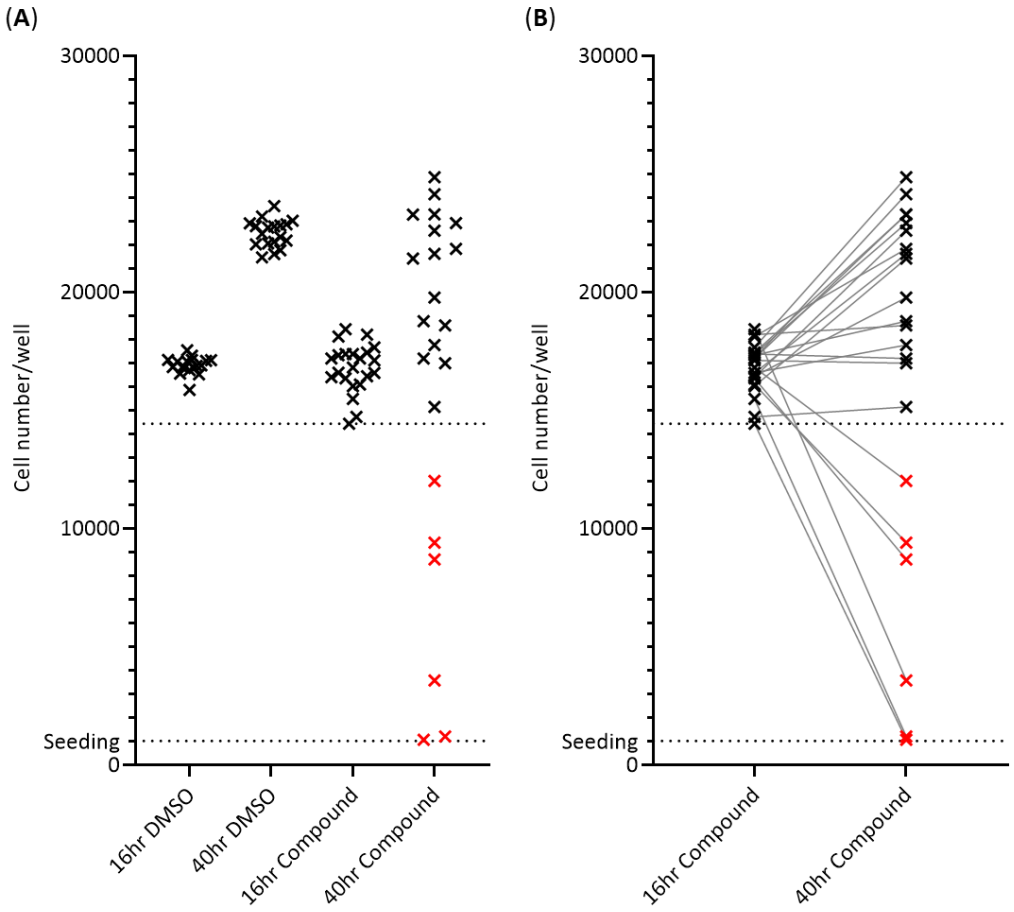

Figure 5.1. Compound viability in human cells

*(**A**) Graph showing the raw cell number distribution, representing cell number after 16hr and 40hr compound incubations with relative DMSO only controls. (**B**) Graph showing the compound specific cell number alterations between the 16hr and 40hr time points. Compounds represented in red were excluded from future experimentation. Dashed lines represent the initial cell seeding density and the minimum compound cell number at 16hr.*

5.3.3. Effect of viable compounds on cilia elongation

Having identified 16 viable compounds in the human cell line after a 40hr incubation time, the effect of these compounds on cilia length was assessed. The 16hr compound incubation plate described in section 5.3.2 was imaged on the In Cell

6000 as described in section 2.2.3 and with the same methodology as described in section 4.2.3 in the first pass bovine chondrocyte screen. Once the four-colour z-stacked images had been 2D processed, analysis was attempted using the automated developer analysis toolbox protocol described in section 3.7.2. However, the acetylated-α-tubulin profile of the human chondrocytes was quite distinct from that seen in the bovine, with a noticeable increase in the labelling of the cytoplasmic microtubule network (seen in Figure 5.2). In future work, techniques to minimise cytoplasmic acetylated tubulin staining in the human cell line may be considered; e.g. a 4℃ cell incubation 20min prior to fixation, however this may also have an effect on the cilia acetylation profile. The noticeable difference in cell number may be due to species variation but more likely is a result in variability of cell cycle rate between the primary bovine cells and the immortalised human cell line.

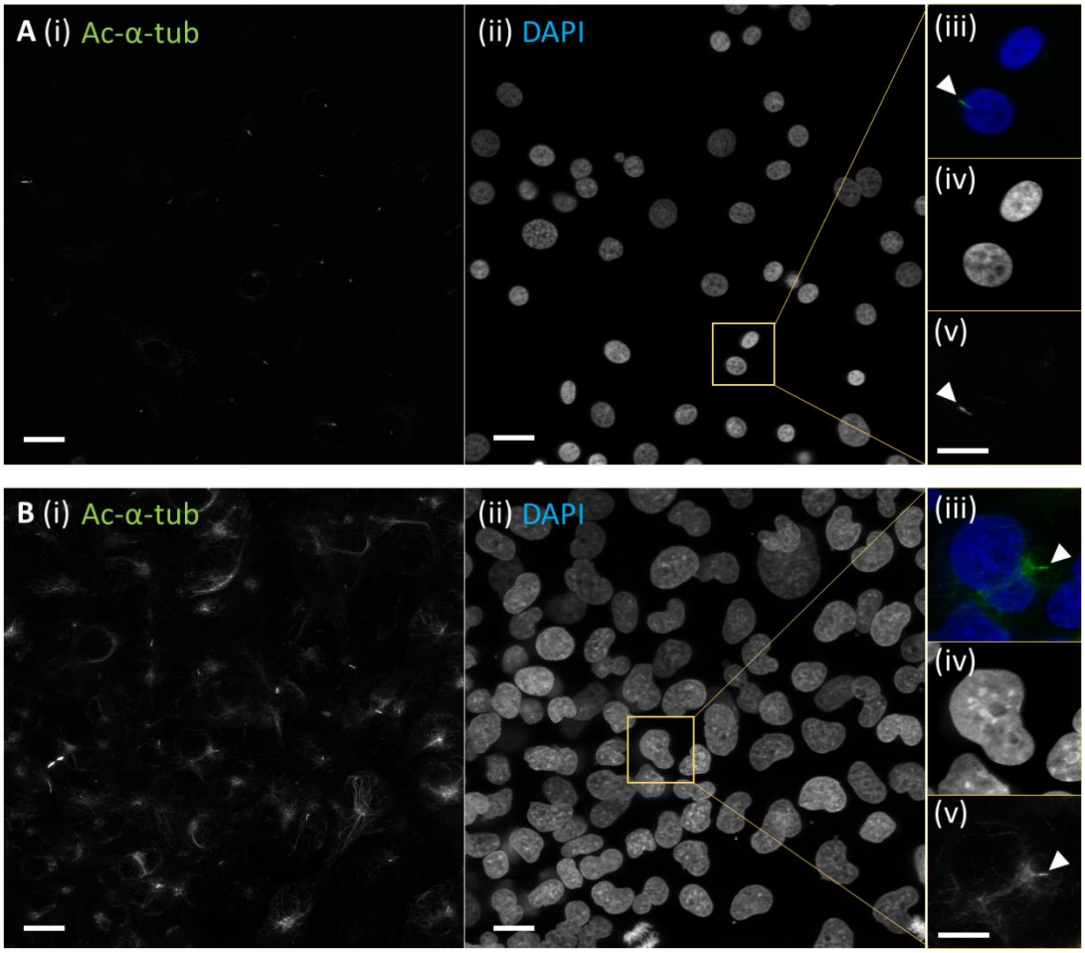

Figure 5.2. Qualitative comparison of the acetylated-α-tubulin profile between bovine and human chondrocytes.

*The figure panel is comprised of maximum intensity projections taken from DMSO treated (**A**) bovine and (**B**) human chondrocytes. (**i**) The acetylated-α-tubulin profile and respective (**ii**) nuclear DAPI staining. (**iii**) Zoomed in merge image and single channel representation of the (**iv**) nuclear DAPI in blue and (**v**) acetylated-α-tubulin in green. The white arrows indicate primary cilia. The scale bar in (i) and (ii) = 20µm, and the scale bar in (v) = 10µm.*

The increase in cytoplasmic acetylated-α-tubulin staining in the human cells meant that objects other than primary cilia were frequently detected by the automated analysis protocol. Therefore, the protocol would require further development, tailoring it to the human chondrocyte cell line and re-validation against manual cilia detection. As primary cilia could clearly be identified by eye, compound

effect on cilia length was manually analysed using Fiji. This manual analysis was performed by a final year undergraduate student, Beth Louise Cutting following careful training and observer validation.

Basal region maximum intensity projections of the acetylated-α-tubulin and DAPI channels were used. As these images were acquired from the first five z-slices, this analysis focuses solely on the basal cilia and thus no measurements pertaining to apical cilia were produced. Three fields of view from each of the three treatment triplicates were analysed, totalling nine fields of view per treatment group. Nuclear and cilia number were counted, excluding any nuclei touching the edge of the field of view. The lengths of counted cilia were measured by tracing a segmented line down the central axis of the ciliary axoneme. Additionally, the prevalence of any cilia with bulbous tips, breaks and double cilia were quantified.

The cilia length measures were pooled from the nine fields of view, and the mean cilia length calculated. Compounds were ranked based on mean cilia length, from shortest to longest (compounds A to P), as seen in Figure 5.3. Histograms are shown representing the relative cilia length distributions as a percentage of total cilia measured per treatment group, with a 0.5µm bin width. Of the 16 viable compounds, 15 were validated in the human chondrocyte cell line to cause significant increases in cilia length after a 16hr compound incubation, as assessed by students T-test.

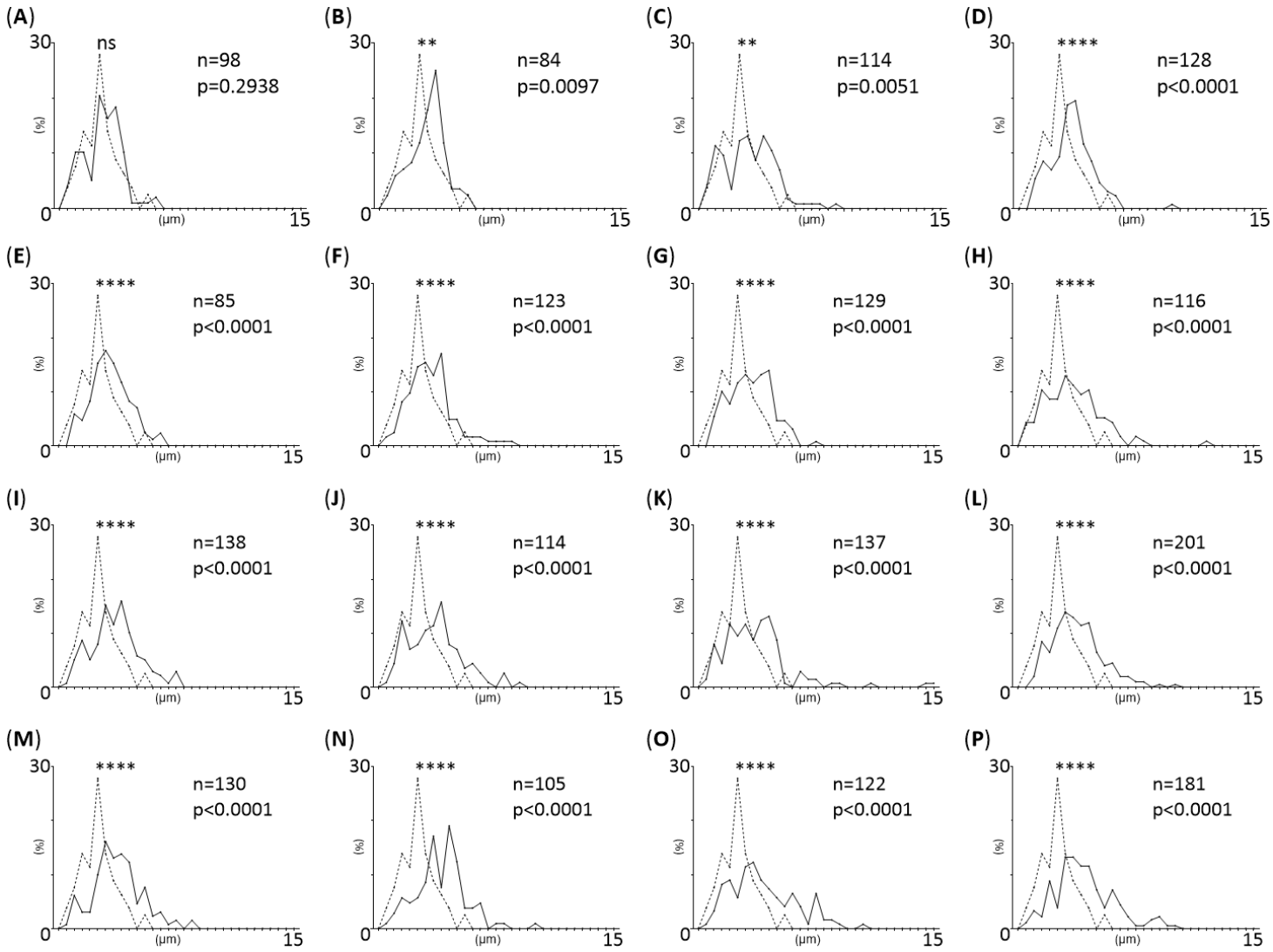

Figure 5.3. Manual analysis of human chondrocyte primary cilia length in response to compounds.

*Histograms presenting the relative frequency (percentage) of cilia length distribution for each compound. The 16 viable compounds appear in ascending order of mean cilia length (**A-P**). DMSO is represented as the dashed line and respective compounds by the solid line. For the DMSO control n=79 measured cilia. The number of measured cilia (n) and the significance of compound effect (p), determined by the T-test, appear on each compound graph.*

Upon inspection of the additional measures captured during manual cilia analysis, there were negligible occurrences of double cilia and cilia breaks. However, a small proportion of the cilia populations analysed were found to have bulbous tips (Figure 5.4. A), a potential measure of altered cilia IFT trafficking. In the DMSO treated cells, approximately 4% of cilia had bulbous tips (Figure 5.4. B). Compounds A and B, which had the smallest effect on cilia length, were found to double the percentage of cilia with bulbous tips compared to the DMSO control (Figure 5.4. C). However, none of the compounds produced a statistically significantly difference in the proportion of bulbous tipped cilia (assessed by Chi squared analysis), possibly due to the low prevalence levels and relatively small sample size (n≈100 cilia/compound).

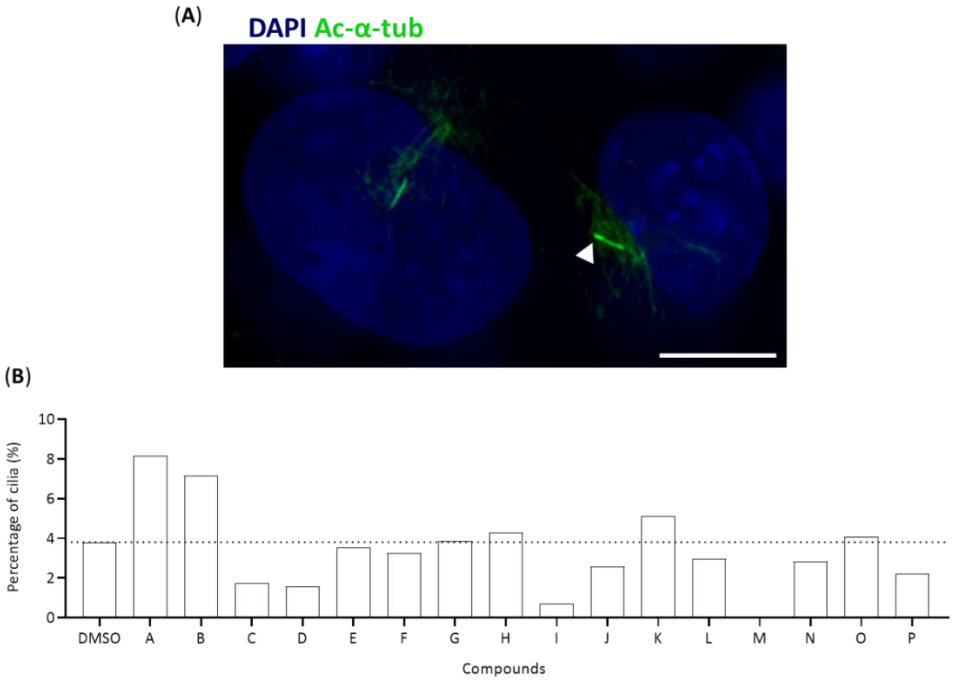

Figure 5.5. Effect of compounds on the prevalence of cilia with bulbous tips in human chondrocytes

*(**A**) Representative image of ciliary bulbous tip with nuclear DAPI staining in blue and Ac-α-tub in green. White arrow indicates bulbous tip and scale bar = 10µm. (**B**) Bar graph presenting the percentage of cilia with bulbous tips.*

5.4. Optimisation of RNA isolation and RT-qPCR hedgehog analysis

Having identified 16 viable compounds and validated their effects on cilia length in the human cell line, experiments were set up to interrogate the effect of these compounds on hedgehog signalling. As discussed in section 5.2.2, RT-qPCR analysis of the downstream *GLI1* and *PTCH1* expression levels would be utilised as a measure of pathway activity, with and without the presence of Indian hedgehog ligand, (to note, this experiment was conducted without a SMO agonist as a positive control). Initially RNA isolation yields were assessed and appropriate housekeeper genes, *GLI1* and *PTCH1* primer pairs were identified and validated. The optimisation and validation of the experimental pipeline are discussed in the following sections.

5.4.1. Cell culture and ligand treatment

Cells were seeded into 24-well tissue culture plates at a density of 1 x 10^4 cells/cm^2 in a volume of 1ml culture media and maintained to confluence with media changes every 2-3 days. Once confluent, six cell culture wells were treated with a DMSO vehicle control in a total volume of 300µl per well. After a 16hr incubation, r-Ihh ligand was spiked into three culture wells, to a final concentration on 1µg/ml and cultured for an additional 24hrs. At the end of the 24hr ligand incubation, cell culture media was removed, and any additional culture media was washed off with sterile PBS prior to cell lysis and RNA isolation.

5.4.2. Validation RNA isolation yields and cDNA conversion

RNA was isolated and the samples yield, and purity were quantified by nanodrop as described in section 2.3.1. RNA was purified through a process of ethanol precipitation as described in section 2.3.2. RNA concentration and purity were re-examined, and the data presented in Figure 5.5.

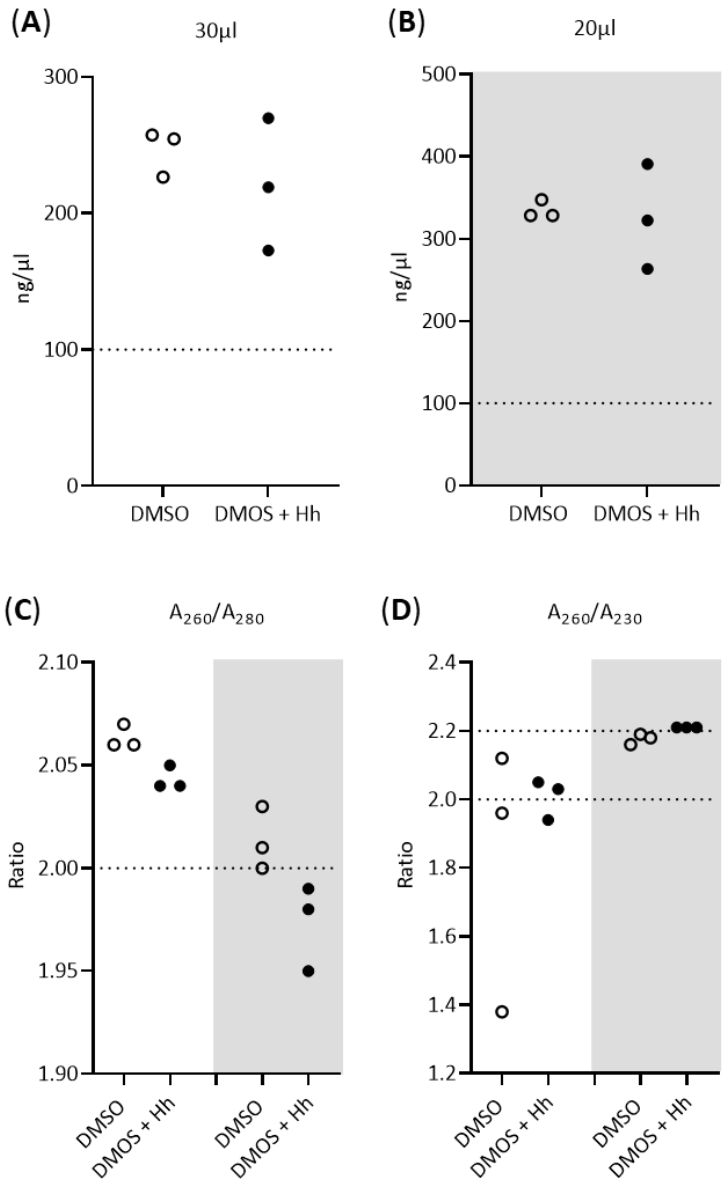

Figure 5.6. Yield and Purity of RNA isolated from 24-well tissue culture plates.

*(**A**) RNA concentration of freshly isolated samples eluted in a total volume of 30µl and (**B**) post ethanol precipitation eluted in a total volume of 20µl. Dashed line represents the minimum desirable RNA concentration of 100ng/µl. (**C**) The A_{260}/A_{280} ratios and (**D**) A_{260}/A_{230} ratios of the samples before (left hand side) and after (right hand side) ethanol precipitation. Dashed line represents the desirable measures for the respective ratios.*

Enough RNA was isolated from a single well of a 24-well plate to enable 1µg (100ng/µl in a 10µl volume) of RNA to be run per cDNA conversion reaction. Although

the pre-purification A_{260}/A_{280} ratios fell within the desired range the initial A_{260}/A_{230} ranges were variable between samples and required purifying through ethanol precipitation. After precipitation, A_{260}/A_{280} ratios were moderately reduced while A_{260}/A_{230} readings were improved. Following purification RNA was used at a concentration of 1µg per cDNA reaction as described in section 2.3.3.

5.4.3. RT-qPCR SYBR green primer validation

The fluorogenic dye SYBR-green which binds to dsDNA was the method employed to enable detection of the genes of interest as a measure of hedgehog pathway activity. The suitability of several primer pairs targeting the genes of interest were validated through the workflow described in Figure 5.6. These were tested using the samples described in section 5.4.2. Primers targeting *GLI1* and *PTCH1* were tested along with primers for the reference genes G*APDH* and *18s* with all primer sequences listed in Table 5.1. RT-PCR was run as described in section 2.3.4.

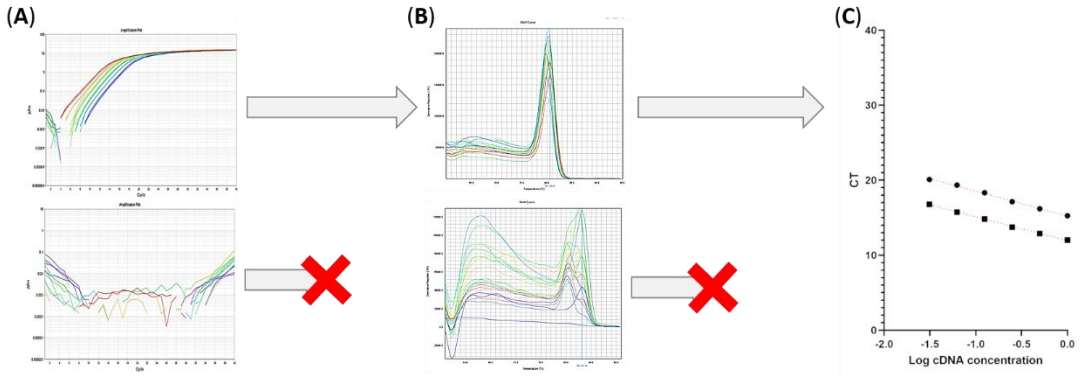

Figure 5.7. Schematic depiction of RT-PCR primer validation workflow.

(A) *A primer pair had to result in an amplification at a CT < 30 and generate a* ***(B)*** *melt curve with a single distinct peak prior to having a* ***(C)*** *standard curve being run to assess its reaction efficiency.*

Initially the reproducibility of amplification plots for replicate wells was assessed (Figure 5.6 A), and a duplicate well run and average CT method was employed for all future RT-PCR runs. If a primer pair had a suitable amplification plot and a melt curve with a distinct single peak (Figure 5.6 B), its reaction efficiency was interrogated using a standard curve (Figure 5.6 C). Standard curves were run at either a 1:2 or 1:10 dilution of cDNA, as stated in Table 2.1. (see section 2.3.4) Using a r-Ihh ligand treated sample, suitable primer pairs were identified for each of the genes of interest, all of which had an R^2 of greater than 0.99 for the linear range of their standard curves and a reaction efficiency (E) of 1.98-2.07 (98-107%). These validated primers were utilised in all future experimental RT-PCR experiments with the aim of utilising two housekeepers during normalisation.

5.5. Investigation of compound effect on baseline and ligand induced hedgehog signalling

5.5.1. Experimental cell culture, compound treatment and hedgehog ligand induction.

Once the experimental protocol and RT-PCR pipeline of analysis had been set up and validated, the effect of compound on hedgehog activity could be interrogated. Cells were cultured and treated as described in section 5.4.1, with the addition of a LiCl positive control treatment group at a concentration of 50mM, and treatment groups for each cilia elongation compound at a concentration of 10µM. This resulted in six replicates for each treatment condition. After a 16hr incubation, r-Ihh ligand was spiked in and gently mixed into three culture wells of each replicate group, to a final concentration on 1µg/ml and cultured in tandem with the compounds for an additional 24hrs. This resulted in triplicate wells for each treatment group $\pm$ r-Ihh ligand and a total of 108 individual samples. At the end of the 24hr ligand incubation, cell culture media was removed, and any additional culture media was washed off with sterile PBS prior to RNA isolation.

5.5.2. RNA isolation, quality control and cDNA conversion

RNA was isolated from the 108 samples and their yields, and purity quantified by nanodrop as described in section 2.3.1. RNA was purified through ethanol precipitation as described in section 2.3.2. RNA concentration and purity were re-examined, and the data presented in Figure 5.7.

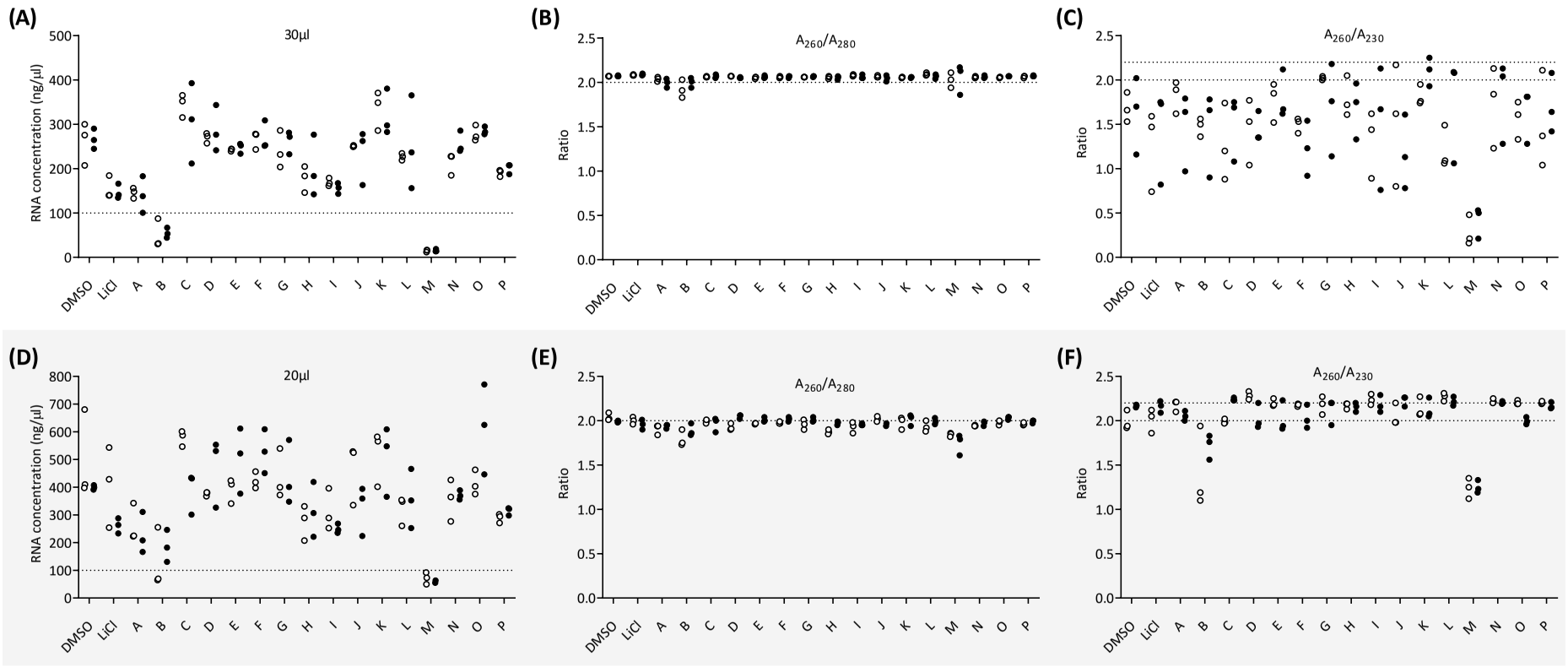

Figure 5.7. RNA concentrations and purity. *(**A and D**) Sample RNA concentrations, (**B and E**) A_{260}/A_{280} ratios and (**C and F**) A_{260}/A_{230} ratios directly after RNA isolation (**A-C**) and after ethanol precipitation (**D-E**). (**A and D**) dashed line represents minimum threshold of 100ng/µl RNA for cDNA conversion. Dashed lines on rest of the graphs represent the ideal values and ranges for the A_{260}/A_{280} and A_{260}/A_{230} ratios. Hollow and filled data points represent treatments with out and with hedgehog ligand, respectively.*

Samples isolated from most of the treatment groups provided greater than 100ng/µl yields and had desirable purity ratios (A_{260}/A_{230} =2.0-2.2, $A_{260}/A_{280}\approx2$) either prior to or after ethanol precipitation. Of the RNA samples analysed, two of the treatment groups were identified as not suitable for cDNA conversion and further RT-PCR analysis. These were the compound B and compound M treatment groups. Replicates in each of these groups had concentrations less than 100ng/µl of RNA (Figure 5.7 A and D), and after ethanol precipitation these samples still had poor A_{260}/A_{230} ratios (Figure 5.7 F). Therefore, these samples were excluded from further analysis. As summarised in Figure 5.8, from the initial 22 bovine primary cilia elongation compounds interrogated in the human cell line, 14 compounds were carried forward for hedgehog pathway activity analysis, with the addition of appropriate DMSO and LiCl controls.

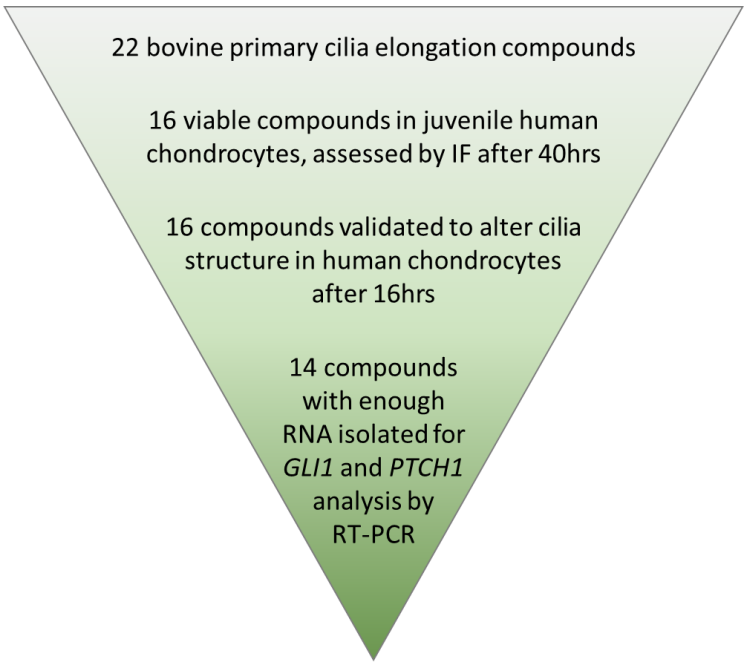

Figure 5.8. Summary of compound selection/exclusion prior to analysis of the effects on hedgehog signalling. *Schematic summary of the inclusion criterion followed to identify the final 14 compounds that were utilised during hedgehog pathway activity assessment by RT-PCR.*

5.5.3. RT-PCR set up and analysis for all experimental samples.

Once the primers were identified and validated, and the quality of the isolated RNA samples were assessed, samples were converted into cDNA as described in section 2.3.3. All samples were run in duplicate for each target, in a 96 well format. *GLI1, PTCH1* and *GAPDH* were run at a 1:2 cDNA dilution and 18s at 1:10 dilution. The three technical replicates $\pm$ r-Ihh ligand (6 samples in total) for a particular treatment group were run on a single RT-PCR plate, resulting in a total of 16 runs to analyse the 14 compound treatment groups with DMSO and LiCl controls. A DMSO only and a DMSO + r-Ihh sample were run on all 15 of the LiCl and 14 compound RT-PCR plates, serving as cross plate variability controls, at a 1:8 dilution for *GLI1, PTCH1* and *GAPDH* and 1:10 cDNA dilution for 18s. Using the standard curves for each gene, the respective CTs of undiluted cDNA were calculated for each sample.

GAPDH was found to be a robust reference gene across all 108 samples. However, upon inspection of 18s CT values on a per compound basis, it was concluded that, due to variability, 18s could not be used for data normalisation. Therefore, Gli1 and Ptch1 expression levels were normalised to relative GAPDH expression. The expression of Gli1 and Ptch1 for each treatment group were calculated as a fold change from the respective on plate DMSO only controls. The results for compound effect on both baseline and ligand induced expression levels of Gli1 and Ptch1 are presented in the following section.

5.5.4. Cell response to hedgehog ligand on pathway activity in the human cells.

Initially the effect of r-Ihh ligand treatment in the human cell line on hedgehog activity at the level of Gli1 and Ptch1 was interrogated. The 24hr r-Ihh ligand treatment resulted in a significant increase ($p=0.0260$) in mean fold change of Gli1 expression (Figure 5.9. A), but not of Ptch1 ($p=0.6382$) (Figure 5.9. B). Therefore, these cells appear to be ligand responsive at the level of Gli1 induction. Ptch1 is a downstream target of Gli1, therefore a 24hr ligand treatment may not be sufficiently long to observe an induction of Ptch1 in these cells.

Previously treatment with LiCl has been demonstrated to cause an increase in cilia length of primary bovine chondrocytes, accompanied by an inhibition to the ligand induction of Gli1 and Ptch1 (Thompson, et al. 2016). Therefore, the effect of the positive control LiCl and r-Ihh were next assessed. LiCl was confirmed to cause a significant increase in primary cilia length after a 16hr exposure in the human cells (Figure 5.9. C). LiCl did not have a significant impact on basal maximum intensity projection cilia incidence, however, it did cause a significant increase in the number cilia with bulbous tips (Figure 5.9. D). Here, LiCl resulted in a non-significant increase in mean Gli1 baseline expression and although r-Ihh ligand treatment still had a trend towards an increase in Gli1 expression, this was no longer a significant induction (Figure 5.9. E). Inversely, LiCl treatment resulted in a significant decrease in mean Ptch1 baseline expression in the human chondrocyte cell line with no observable induction in response to r-Ihh ligand (Figure 5.9. F).

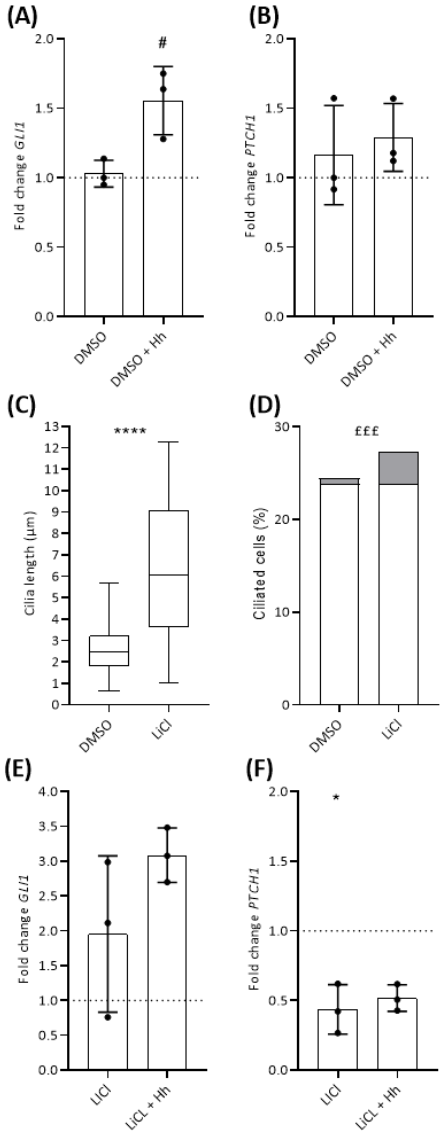

Figure 5.9. Hedgehog response in human chondrocytes and the effect of LiCl. (A) *Fold change in Gli1 and* ***(B)*** *Ptch1 expression levels, presented as mean and standard deviation where dashed line represents the DMSO only control.* ***(C)*** *Box and whisker plot of primary cilia length in response to 16hr LiCl treatment with whiskers presenting the 5-95 percentiles.* ***(D)*** *Stacked bar of cilia incidence in basal maximum intensity projections with the incidence of bulbous tips in grey after 16hr treatment. Chi squared tests used to assess the significance, where £££=p<0.001 difference in incidence of bulbous tips.* ***(E)*** *Fold change in Gli1 and* ***(F)*** *Ptch1 expression levels in LiCl treated samples. Students T-tests were used to assess significance of all other data. * = comparisons to DMSO controls, # = comparison to respective no ligand treatment. * or # = p<0.05 and ****=p<0.0001.*

Having established the effect of r-Ihh ligand on Gli1 and Ptch1 expression levels, and of LiCl, the effect of the 14 compounds were then interrogated. Data is presented for each compound treatment group in Figure 5.10, with mean trends summarised in the Figure 5.11. The effects of compounds on Gli1 and Ptch1 are subtle and variable. Compounds predominantly appear to result in a reduction in Gli1 baseline expression and r-Ihh-ligand induction. However, despite the shared effect of inducing cilia elongation, there does not appear to be any shared pattern on the impact of compounds on overall hedgehog activity.

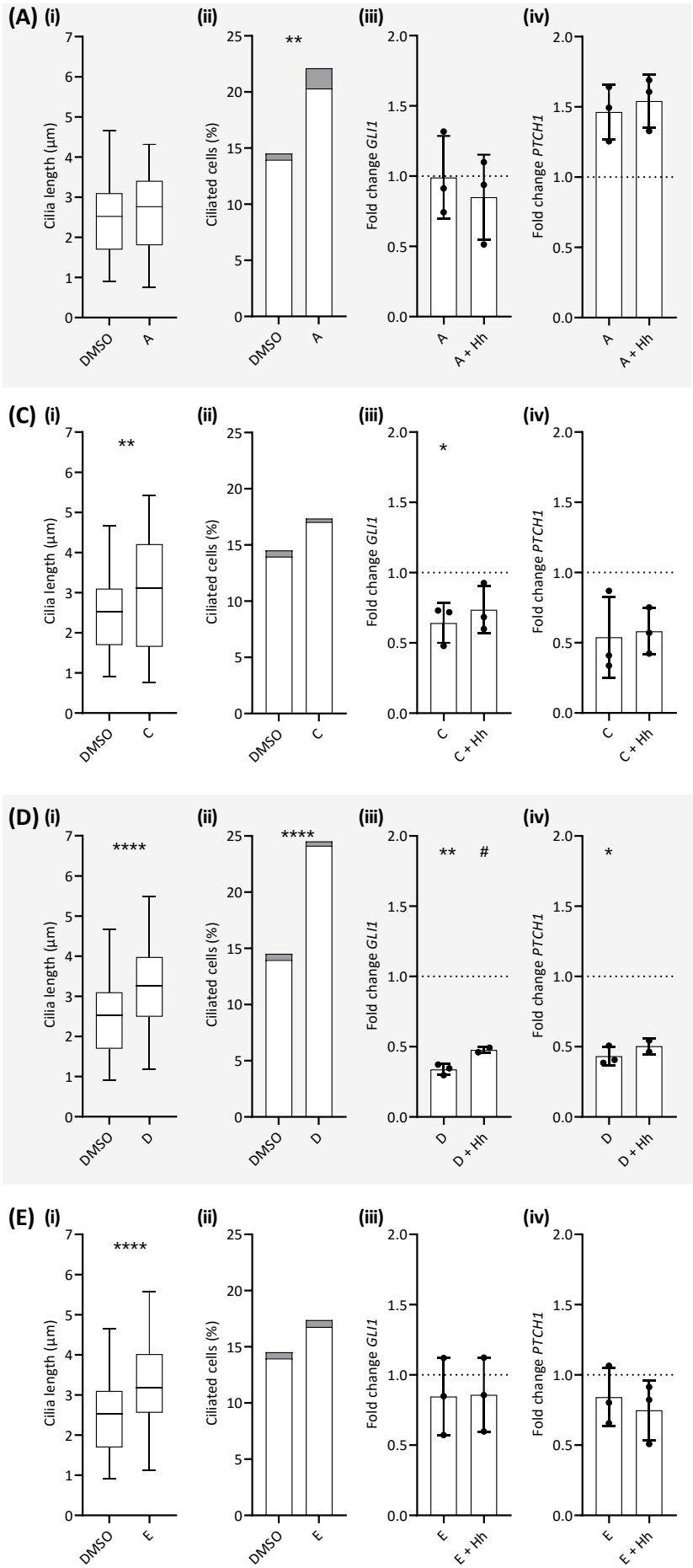
(A)
(i)
Cilia length (µm)
DMSO
A
(ii)
**
Ciliated cells (%)
DMSO
A
(iii)
Fold change GLI1
A
A + Hh
(iv)
Fold change PTCH1
A
A + Hh
(C)
(i)
**
Cilia length (µm)
DMSO
C
(ii)
Ciliated cells (%)
DMSO
C
(iii)
*
Fold change GLI1
C
C + Hh
(iv)
Fold change PTCH1
C
C + Hh
(D)
(i)
****
Cilia length (µm)
DMSO
D
(ii)
****
Ciliated cells (%)
DMSO
D
(iii)
**
#
Fold change GLI1
D
D + Hh
(iv)
*
Fold change PTCH1
D
D + Hh
(E)
(i)
****
Cilia length (µm)
DMSO
E
(ii)
Ciliated cells (%)
DMSO
E
(iii)
Fold change GLI1
E
E + Hh
(iv)
Fold change PTCH1
E
E + Hh

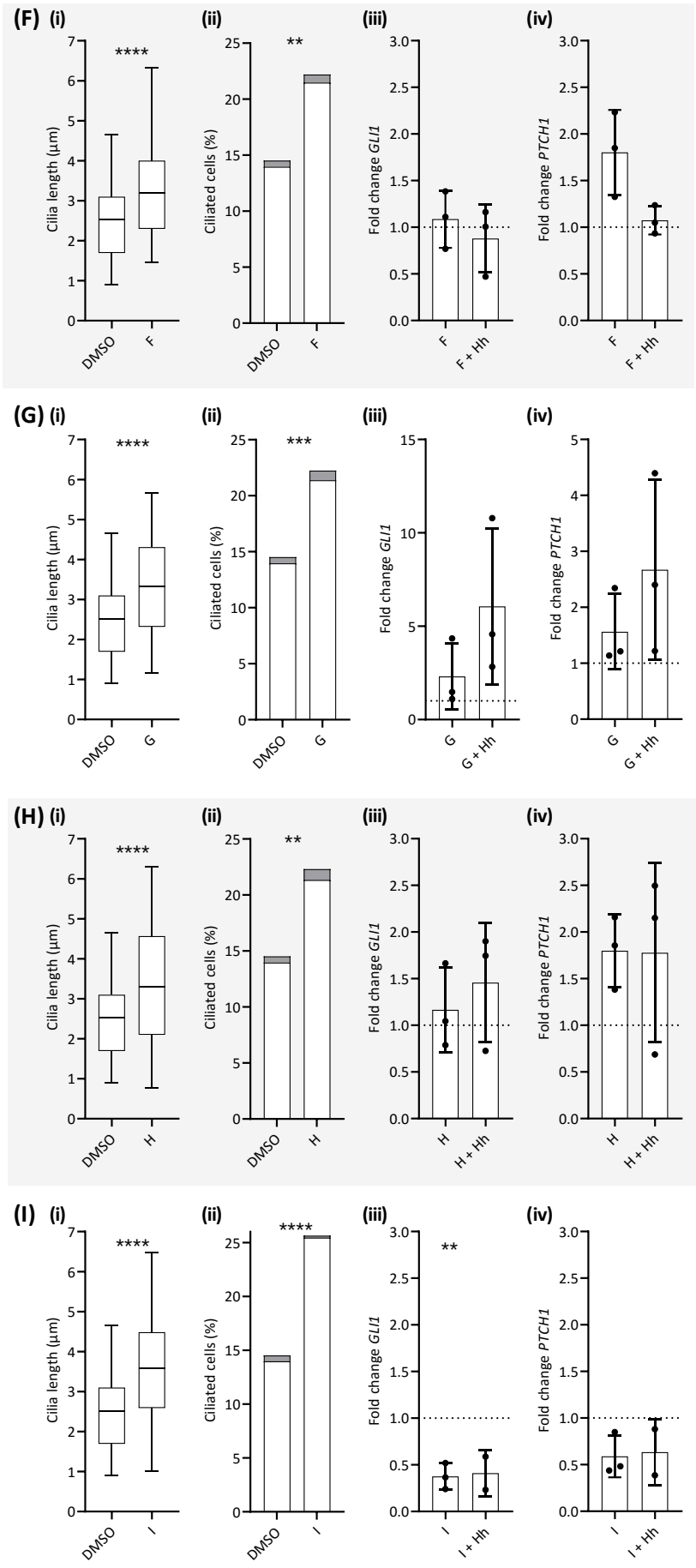
(F)
(i)
(ii)
(iii)
(iv)
Cilia length (µm)
Ciliated cells (%)
Fold change GLI1
Fold change PTCH1
****
**
DMSO
F
F + Hh
(G)
***
G
G + Hh
(H)
H
H + Hh
(I)
I
I + Hh

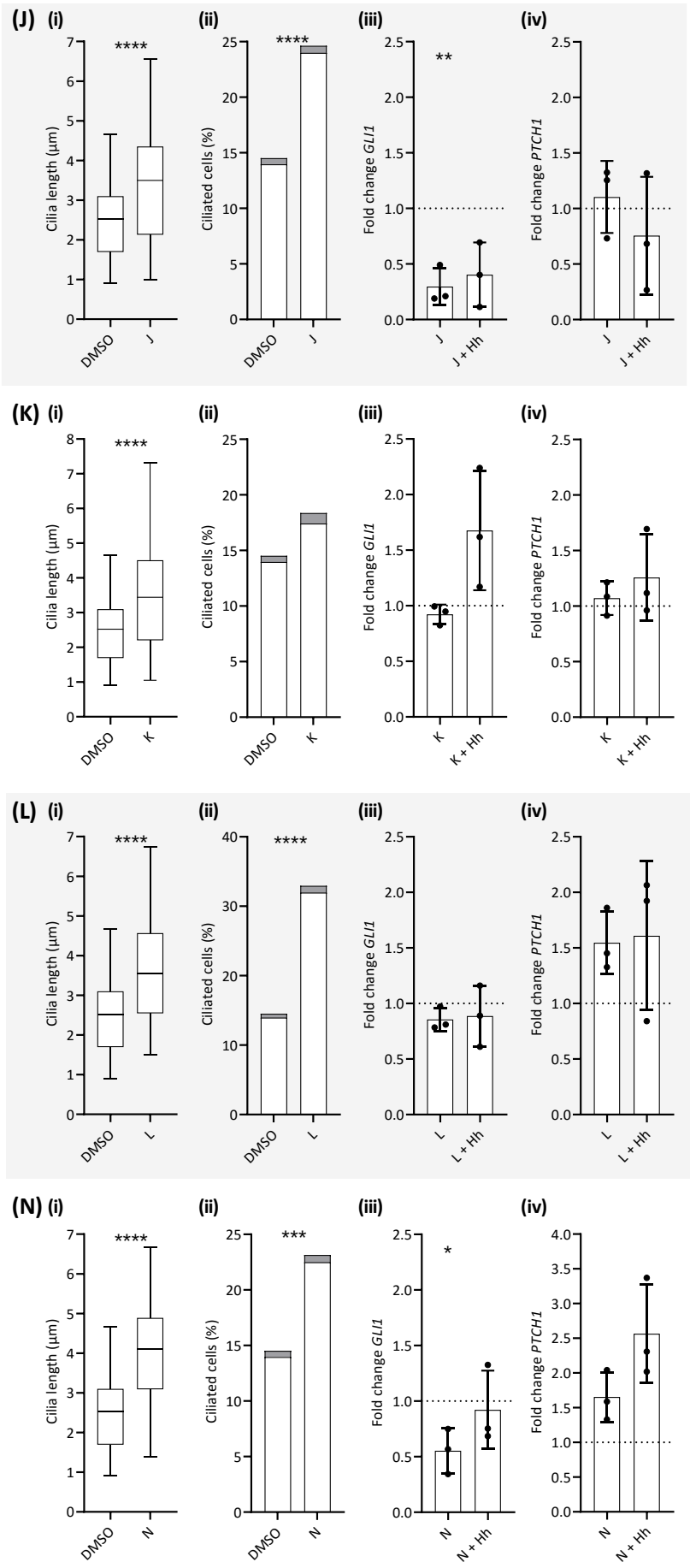
(J)
(i)
Cilia length (µm)
****
DMSO
J
(ii)
Ciliated cells (%)
****
DMSO
J
(iii)
Fold change GLI1
**
J
J + Hh
(iv)
Fold change PTCH1
J
J + Hh
(K)
(i)
Cilia length (µm)
****
DMSO
K
(ii)
Ciliated cells (%)
DMSO
K
(iii)
Fold change GLI1
K
K + Hh
(iv)
Fold change PTCH1
K
K + Hh
(L)
(i)
Cilia length (µm)
****
DMSO
L
(ii)
Ciliated cells (%)
****
DMSO
L
(iii)
Fold change GLI1
L
L + Hh
(iv)
Fold change PTCH1
L
L + Hh
(N)
(i)
Cilia length (µm)
****
DMSO
N
(ii)
Ciliated cells (%)
***
DMSO
N
(iii)
Fold change GLI1
*
N
N + Hh
(iv)
Fold change PTCH1
N
N + Hh

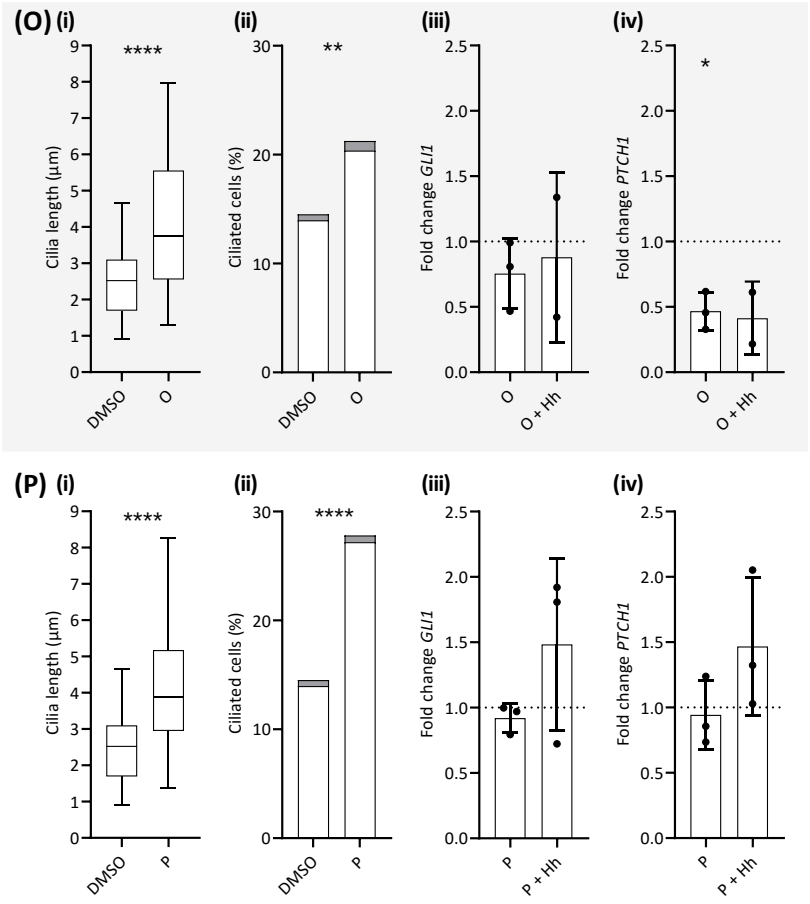

Figure 5.10. Effect of compounds on cilia structure and hedgehog activity. (A-P) *Compounds in ascending order of compound effect on mean cilia length, excluding compound B and compound M due to insufficient RNA. Each panel row presents data for a single compound.* ***(i)*** *Box and whisker plot of primary cilia length in response to 16hr compound treatment with whiskers presenting the 5-95 percentiles (Full frequency distributions are shown in Figure 5.3).* ***(ii)*** *Stacked bar of cilia incidence after 16hr compound treatment with the incidence of bulbous tips in grey. Chi squared tests used to assess significance where * represents significant difference is overall cilia incidence and no significant differences in incidence of bulbous tips were found with the compounds.* ***(iii)*** *Fold change in Gli1 and* ***(iv)*** *Ptch1 expression levels, presented as mean and standard deviation, where dashed line represents the DMSO-Hh control. Students T-tests were used to assess significance (i, iii and iv). * = comparisons to DMSO controls, # = comparison to respective no ligand treatment. */# = p<0.05, **/## = p<0.01, ***/### = p<0.001, ****/#### = p<0.0001.*

			Mean cilia length (µm)	Cilia incidence (%)	Mean Gli1 (fold change from DMSO)	Mean Gli1 + Hh (fold change from DMSO)	Mean Ptch1 (fold change from DMSO)	Mean Ptch1 + Hh (fold change from DMSO)
DMSO	Control		2.54	14.52	1.00	1.56	1.00	1.11
LiCl	Control		6.27	27.35	1.955	3.088	0.38	0.45
Compound	Disease indication	Pathway						
A	Cancer	Metabolism	2.72	22.12	0.991	0.851	1.26	1.33
C	Cancer	Protein Tyrosine Kinase	3.12	17.35	0.642	0.736	0.46	0.50
D	Cancer	DNA Damage	3.27	24.52	0.339	0.477	0.37	0.43
E	Cancer	Cell Cycle	3.30	17.38	0.847	0.859	0.72	0.64
F	Respiratory Disease	GPCR & G Protein	3.34	22.20	1.088	0.88	1.55	0.92
G	Respiratory Disease	GPCR & G Protein	3.36	22.24	2.31	6.061	1.34	2.30
H	Cancer	Protein Tyrosine Kinase	3.45	22.31	1.165	1.458	1.55	1.53
I	Cancer	DNA Damage	3.47	24.63	0.376	0.41	0.51	0.54
J	Cancer	JAK/STAT	3.61	25.65	0.297	0.403	0.95	0.65
K	Cancer	MAPK	3.67	18.36	0.922	1.677	0.92	1.08
L	Cancer	MAPK	3.74	32.95	0.856	0.887	1.33	1.38
N	Cancer	Metabolism	4.06	23.14	0.553	0.922	1.42	2.21
O	Viral infection	DNA Damage	4.11	21.25	0.755	0.88	0.40	0.36
P	Cancer	Protein Tyrosine Kinase	4.16	27.80	0.92	1.483	0.81	1.26

Figure 5.11 Summary of compound effect on cilia expression and hedgehog activity. *The disease indication and the target pathway are presented alongside a qualitative heat map of mean trends in cilia length, incidence, baseline and +Hh ligand treatment levels of Gli1 and Ptch1, all in relation to the relative DMSO control for each measure. Blue indicates a reduction and red indicates an increase in relation to DMSO. All Gli1 and Pitch1 data are presented in relation to the no ligand DMSO control. Red indicates an increase compared to DMSO control, and blue indicates a decrease compared to DMSO control.*

5.6. Discussion

Previously primary cilia structure and altered hedgehog signalling have been seen to be associated in various contexts, strongly supporting the idea that primary cilia structure is important for correct hedgehog signalling to occur. In the human genetic disorder endocrine-cerebro-osteodysplasia syndrome, a mutation in the intestinal cell kinase gene results in a longer primary cilium and reduced expression of Gli1 (Moon, et al. 2014). In the disease alkaptonuria, chondrocyte primary cilia length is reduced and an associated decrease in baseline Gli1 expression is reported, although diseased cells remain ligand responsive (Thorpe, et al. 2017). Chondrocytes undergoing cyclic tensile strain experience a loss in cilia length and an associated inhibition to the mechanical induction of hedgehog targets Gli1 and Ptch1. Treatment with tubacin to prevent the loss of primary cilia length was found to recover both cilia length and hedgehog responsiveness (Thompson, et al. 2014). Therefore, there is a well-established relationship between primary cilia structure and correct hedgehog signalling where intervention to correct cilia structure may be a potential therapeutic avenue for the treatment of ciliopathies.

In this chapter data is presented on the 22 compounds that cause primary cilia elongation in primary bovine chondrocytes where their viability and effect were validated in a juvenile human chondrocyte cell line. From these initial 22 compounds, 14 were identified as viable, with 13 causing significant increases in cilia length and 1 causing a doubling in the incidence of ciliary ac-α-tubulin bulbous tips. Having validated RNA isolation and purity, primers were identified and validated for the assessment of hedgehog activity at the level of Gli1 and Ptch1 expression. Despite

having a similar effect on primary cilia length, compounds had a diverse effect on the baseline and r-Ihh ligand induced levels of Gli1 and Ptch1. The predominant similarity between compound effects was to decrease the baseline expression levels of Gli1. Although there was no pattern in the induction or inhibition of the hedgehog pathway across the tested compounds, 13 of the 14 interrogated compounds abolished the significant induction from compound baseline expression of Gli1 with the addition of r-Ihh ligand. The hedgehog response is dynamic and involves negative feedback loops which should be considered when profiling Gli1 and Ptch1 expression levels post compound and ligand treatment. The kinetics of each compound may vary and therefore future work could include a time course of hedgehog activity following compound treatment to explore this in more detail.

There is no particular clustering as far as the pathways targeted by these candidate compounds. Two of the 14 compounds target pathways are involved in metabolism (8.3% of the original screening library), three work through the protein tyrosine kinase pathway (3.0% of the original library), three target DNA damage pathways (4.6% of the original library) and two work through GPCR and G proteins. Only one of the compounds act through cell cycle related pathways and one through Jak/Stat related signalling pathways, with less than 1% of the original compound library acting in this manner (0.98% and 0.93%, respectively). Finally, two compounds were found to act through the MAPK pathway, with as little as 0.81% of the original library acting in this way.

Interestingly of the 14 cilia elongation compounds presented in Figure 5.11, 78.6% of them are indicated to be used for use as cancer treatments, despite only

13% of all compound in the full library disclosed as being used in the treatment of cancer. This over representation of cancer compounds raises the question of whether the primary cilium is found to be longer as these compounds slow cell cycle progression allowing for a more established primary cilium to be formed, or if these compounds target cilia elongation which in turn slows cell cycle and therefore are useful cancer treatments. This could potentially be addressed in future studies.

Although few other similarities are seen between the compounds, the effect of these compound on other cellular parameters, such as glu-tubulin and actin, could be explored in more detail. For example, the development of an analysis protocol tailored to the human chondrocyte cell line may elucidate other subtle shared effects on cilia expression between groups of compounds which may in turn have similar effects on hedgehog signalling. A more detailed discussion of the interpretation of the data in this thesis and the possible implications for future work is presented in Chapter 6.

6. Discussion

6.1. Summary and key findings

The principle aim of this project was to identify novel compound regulators of primary cilia structure which would enable interrogation of the primary cilium's structure function relationship. Prior to conducting the screen, cilia expression in 2D culture of primary bovine chondrocytes was characterised. This demonstrated that ≈60% of cilia were present on the basal cell surface closest to the culture surface, with a consistency of expression seen between cells isolated from multiple animals (see section 3.3.5). This characteristic of chondrocytes makes these cells an ideal model for accurate analysis of cilia length, compared to other cell types with more apical expression. Initial studies quantified the temporal dynamics of cilia length change in response to the know cilia elongation compound LiCl (see section 3.3.3). This was used to identify a suitable compound incubation time for the compound library screen.

Having identified an appropriate compound library and treatment conditions, the high throughput screen was developed and successfully executed in bovine chondrocytes. This produced an unbiased identification of a cluster of 67 compounds that caused primary cilia elongation without modulation of actin organisation or nuclear morphology. These candidate compounds were further validated in independent animals, leading to the identification of 22 compounds that produced robust cilia elongation in bovine chondrocytes. The next step was to further validate the compounds in human cells using a juvenile human chondrocyte cell line. Six compounds from the original cluster of 22 were rejected as they caused notable reduction in cell number in the human cells over a 40hr incubation period. Of the remaining 16 compounds, 15 produced a significant effect on cilia elongation and

one resulted in a doubling in the occurrence of ciliary bulbous tips. From these 16 compounds, suitable yields of high-quality RNA were isolated from 14 compound treatment groups for the assessment of two key members of the hedgehog signalling pathway, Gli1 and PTCH1, by RT-PCR. The final step was to assess the effect of the 14 validated compounds on ciliary hedgehog signalling. The effect of the compounds on the mean expression levels of Gli1 and PTCH1 was variable, with the only significant effects seen in the inhibition to baseline expression levels, with 5 compounds producing a significant inhibition to Gli1 and 2 compounds inhibiting PTCH1.

This PhD project has therefore produced the following key outputs:

- Characterisation of cilia in bovine and human chondrocytes in 2D culture
- Development of a high throughput confocal imaging cilia screen methodology
- Validation of the screening methodology and automated analysis pipeline
- Curation of a database of measured effects of 1,727 compounds on multiple cilia and cellular parameters
- Identification of 6 compound clusters of phenotypic effect which predominantly regulate cilia structure
- Analysis and confirmation of reproducibility of effect of the identified compounds of interest in multiple animals and in human cells
- Analysis of the effect of cilia elongating compounds on hedgehog signalling, finding a variety of effects

Much of the discussion is included in the corresponding results chapter. However, the following sections provide additional general discussion, analysis of the limitations of the study and discussion of future work.

6.2. Cell type

Chondrocytes in 2D culture provide an ideal cell system for imaging-based investigation of primary cilia structure and have been utilised extensively for this purpose in previous research (McGlashan, et al. 2010; Wann, et al. 2013; Thompson, et al. 2014; Thompson, et al. 2016; Thompson, et al. 2017; Fu, et al. 2019). Chondrocytes express a high incidence of cilia, with the majority laying parallel to the culture surface, making them ideal for structural investigation in the projected imaging plane. This enables a more reliable identification of structural changes from projected maximum intensity images. Furthermore, the chondrocyte carries physiological relevance in both the genetic and environmental ciliopathies (see section 1.5). Chondrocyte primary cilia length is shown to be increased in the environmental ciliopathy osteoarthritis, although the implications of this remain poorly understood (McGlashan, et al. 2008). Moreover, numerous genetic ciliopathies present with musculoskeletal phenotypes and defects in the growth plate, where primary cilia are reported to be absent or stunted in the chondrocytes. Therefore, identification of cilia length regulators specifically in the chondrocyte bares disease relevance and offered a good model and starting point for investigation.

Further investigation into how these compounds might affect cilia structure in other cell types is of interest. The positive control LiCl, which was used in this study, has been shown to also induce cilia elongation in other cell types such as fibroblasts (Ou, et al. 2012), osteocytes (Spasic and Jacobs 2017), and neuronal cells (Miyoshi, et al. 2009). Interestingly, the screen described in this thesis found no overlap in the

compounds producing cilia elongation when compared to a previous unpublished screen using osteocytes (Personal communication Milos Spasic). However, there are important differences in the methodologies used as well as the difference in cell type (See section 1.10). Indeed, the methodology used here has been validated and shown to produce reproducible results. This gives confidence that some, if not all of the compounds found to elongate cilia length in chondrocytes hold the potential to regulate cilia in other cell types. Thus, further analysis in other cell types would be valuable following rigorous optimisation of the screening approach and analysis pipeline. However, differences in the prevalence of apical cilia in other cell types may preclude a 2D analysis methodology based on maximum intensity projection images.

6.3. Cell source

As discussed in sections 3.3.5 and 6.1, chondrocytes provided an ideal 2D cell culture system for the identification of regulators of primary cilia structure. There are both established chondrocyte cell lines and primary cells isolated from cartilage tissue, each of which have advantages and disadvantages. Although cell lines offer a highly reproducible culture system, primary cell sources provide a cell phenotype more closely mimicking that of the *in vivo* phenomenon. Moreover, identification of a phenotypic compound effect in cells from multiple biological replicates affords additional confidence of reproducibility. Therefore, the decision was made to work with primary cells isolated from tissue.

It is important that candidate compounds are eventually shown to be effective in human as the long-term aim of the current project was to identify compounds for use as ciliotherapies. Although human cartilage tissue can be sourced through surgical excision or cadaver dissection, these are precious and finite resources. Due to the numerous optimisation steps involved during our screening set up, the initial cell source was required to be readily available and plentiful. Although mouse tissue is commonly utilised in the field, many animals would be required to obtain a large enough tissue sample to ensure enough cells could be isolated. Bovine primary chondrocytes from the metacarpal phalangeal joint have been widely used in numerous studies. These isolated cells have the advantage of being derived from a large mammal with a biomechanical joint environment and associated structure closely resembling that in a human joint such as the knee (Calvert, et al. 2013). In addition, the large articular surface yields a large number of primary cells (20-36 x

10^6) from a single animal offering an abundant initial cell source. Furthermore, similarities have been reported in the responsiveness of human and bovine chondrocytes upon exposure to LiCl with regards to cilia length (Thompson, et al. 2016). For these reasons the screen was conducted using isolated primary chondrocytes from the bovine metacarpal phalangeal joint.

Follow up studies from the screen utilised a juvenile human chondrocyte cell line as a transition into human work. This increased the chances of detectable expression levels for the components of our initial signalling pathway of interest, hedgehog. Additionally, the practicalities for potential future work involving protein knockdown followed by compound cilia rescue experiments are more feasible when moving into human cells. Having identified compounds that increase both cilia length and regulate hedgehog signalling, future work could move into studies with primary human chondrocytes. Cells could be isolated from both healthy and osteoarthritic patients, as osteoarthritis is one of the aforementioned environmental ciliopathies where rescuing of healthy primary cilia structure may offer a potential therapeutic route. Validation of compound effect in human explant tissue could be conducted to investigate cilia recovery and cartilage regeneration potential prior to transition into clinical intervention strategies.

6.4. Data re-mining

During the screen 3D imaging data was captured for 4 different cellular components. As mentioned in section 3.3.7, fixed cells were labelled with DAPI, Ac-α-tub, phalloidin and Glu-tu, in ascending order of fluorescence excitation. Although these were analysed with a ciliary focus to address the primary aim of the project, the imaging data captured during both the first pass screen, validations and follow up studies, offer a large resource for image re-mining. This database of images could be interrogated with more refined and focused questions with regards to each of the individually labelled components, both independently and in relation to one another.

One example, worthy of future study involves analysis of actin cytoskeletal organisation. In the present study, the intensity of F-actin labelling with phalloidin was utilised as an indicator of actin contractility, known to regulate cilia expression (see section 1.8). More sophisticated analysis protocols could be developed to directly quantify organisation and hence identify regulators of actin tension which may be repurposed to modulate actin-dependent cell functions including endo- and exocytosis, apoptosis, regulation of nuclear morphology and protein trafficking, and cell ageing.

Further studies could also examine the posttranslational tubulin modifications of acetylation and polyglutamation which show particular enrichment on the axoneme of the primary cilium (Poole, et al. 1997; Kukic, et al. 2016). This enrichment of acetylated tubulin enabled ciliary detection in our screen where both cilia length and incidence were quantified. By using these markers in combination with nuclear and actin labelling, further structural and positional questions could be

asked. For example, the cytoskeletal cytoplasmic distribution which may indicate alterations to cellular trafficking events.

The effect of compound on cilia curvature, incidence of double cilia, ciliary breaks and bulbous tips might also be quantifiable form the images captured in the screen, some of which have been manually analysed and interrogated in this study. These phenomena could then be explored in more detail using higher resolution imaging methodology such as SIM and EM. The development of 3D analysis tools may enable the investigation of compound structural effect on apically expressed cilia and the potential shift of ciliary expression between the basal culture surface and the apical side of the cell. This induced shift may have physiological relevance for cilia, such as those of the luminal kidney epithelial cells, and even the positionality and direction of cellular division in other tissues. Beyond the ciliary focused analysis, the distribution and organisation of these posttranslational modifications throughout the cell's cytoskeleton could also be examined. These modifications may have implications for general protein trafficking throughout the cell and therefore the dynamics of cell signalling events and processes. All the aforementioned phenotypic changes may have cross correlations and interconnected mechanisms that could be assessed on a cell by cell basis, linking compound effect to cellular targets, signalling pathways and chemical families.

6.5. Further investigation of compound treatment regime

For the purposes of the compound screen, practicality, cost, cell yield and time were limiting factors that informed the screening workflow. Therefore, we conducted the initial screen with a single compound dose and for a single time point. With this approach we were able to identify various phenotypic changes. However, the temporal stability of these changes remains unknown. Going forward, the efficacy of the identified cilia elongation compounds could be further interrogated with a 10-point dose response over a time course. Additionally, the dosing effect of the compounds could be used to further interrogate the stability of the identified induced phenotypes. A dose and recover approach could be employed to examine the durability of effect or transience of cilia length changes. If a stably transfected immunofluorescent IFT or ARL13B cell line was utilised, this would enable a time course experiment and live cell imaging approach to increase the temporal resolution of the dynamics of cilia length alterations. Information provided by these studies could be utilised to help inform the selection of specific candidate compounds for more comprehensive interrogation as potential ciliotherapies.

6.6. 2D vs 3D culture and analysis environments

For the purposes of the high throughput screen the employed approach was a 2D monolayer cell culture of chondrocytes with primarily basal, flat lying cilia coupled with 2D image analysis of images captured in 3D z-step progression and maximum intensity projected. A caveat to the compounds identified solely by the basal projections is that an assumption was made that this same effect was occurring for the apical cilia. However, 3D image analysis would be required to test if this was indeed true. Furthermore, it remains unknown what relevance basal vs apical expression might have (see section 3.3.5). Other cell types that are amenable to the current screening pipeline would have to have primary cilia with basal projection, unlike the cilia found on kidney epithelial cells which are predominantly apical with *in vivo* luminal expression. Indeed, the use of cells with predominantly apical cilia is a major limitation of a previous screen conducted in osteocytes (see section 1.10). In summary, the effect of our compounds on apical cilia is yet to be elucidated.

Treatment of a 2D monolayer ensures all cells are exposed to compound. When moving into 3D culture systems there are benefits regarding physiological relevance and conserved phenotypic expression in cells, particularly for cartilage cells. However, perfusion of compounds into these systems may be limited and therefore not ideal for initial first pass screening. Furthermore, there are complications regarding practicality and financial feasibility of high throughput 3D imaging and associated the large-scale image analysis. Our identified phenotypic changes may be dependent on the 2D culture environment; however, they provide a practical starting point before moving into systems more relevant to *in vivo* environments.

6.7. Future work supported by the screen

The work presented here, and phenotypic effects identified within this screen have provided a resource of data that has already supported the development of several PhD studentship grants, a successfully awarded proof of concept project and a research grant proposal submitted to the British Heart Foundation.

- EPSRC DTP PhD studentship award: Use of organ-chip technology to test primary cilia manipulation of mechanobiology for treatment of Polycystic Kidney Disease (PKD).
- BBSRC (LIDo) PhD studentship: Role of primary cilia modulation in control of osteogenesis investigated using organ-on-a-chip technology.
- British Heart Foundation Project Grant (Application): The potential of ciliotherapy to regulate atherosclerosis.
- QMUL Proof of Concept Award: Novel ciliotherapy for treatment of Jeune syndrome (discussed in more detail in the following section).

6.8. Proof of concept project

Jeune syndrome is a disease, causing skeletal dysplasia in 1:100-150,000 births in the UK with approximately 600 people in the UK currently living with the syndrome. This is the focus disease of the successfully funded proof of concept grant. The work will build upon and be supported by the screening data reported in this thesis.

Jeune syndrome is an autosomal recessive disease that effects cilia associated genes, in particular *IFT80*. Mutations in *IFT80*, a key intraflagellar transport protein, disrupts ciliogenesis causing stunted cilia (Taschner, et al. 2018), and leads to dysregulated hedgehog signalling, with a reduction in hedgehog pathway activation at the level of *Ptch1* and *Gli1* expression (Rix, et al. 2011). This occurs particularly in the chondrocytes present in the growth plate. As a result, Jeune syndrome effects the development of the skeleton, most notably leading to a small chest and short ribs. This in turn restricts the growth and expansion of the lungs causing life-threatening breathing difficulties. They also have craniosynostosis (premature fusion of the skull at birth) which restricts brain growth and requires surgical intervention to be corrected.

There is no current cure for Jeune syndrome, other than managing the symptoms caused by skeletal dysplasia and the resulting breathing conditions. Severe cases require mechanical ventilation and surgical chest reconstruction. Surgery for craniosynostosis is also required. With improved surgical and mechanical ventilation techniques, many of these children are living into their teenage years and adulthood, albeit with ongoing skeletal deformity and breathing difficulties. Pharmaceutical treatment to reverse the stunting of primary cilia, and thereby

minimise the skeletal development abnormalities would be an ideal option for treating children born with this life-threatening syndrome. Although there are thought to be relatively few individuals living with this disease, due to its rarity, Jeune syndrome is severely under diagnosed, suggesting that the numbers effected may be significantly higher.

Two previous studies have shown the potential of cilia modifying drugs for use as ciliotherapies (Kathem, et al. 2014; Pala, et al. 2019). These studies demonstrate the efficacy of the cilia elongator, fenoldopam, in mouse models as a novel 'cilotherapy' intervention to treat vascular hypertension associated with the polycystic kidney disease which is one of the most prevalent genetic ciliopathies. We therefore look to explore the potential of our hit cilia elongation compounds for treatment of *IFT80* dysfunction in Jeune syndrome.

From the 1,727 FDA-approved compounds included, we unbiasedly identified 6 phenotypic clusters that alter primary cilia length or incidence, based on the high throughput confocal imaging screen. Within these clusters, there were compounds that increase both primary cilia length and incidence. We hypothesis that these compounds may be re-purposed as new and effective treatments for Jeune Syndrone by rescuing the expression of primary cilia. In particular, we have identified 22 validated compounds that increase bovine chondrocyte cilia length without disrupting other cytoskeletal organisation, viability or proliferation. Of these 22 compounds, 15 have been validated to cause cilia elongation in a human chondrocyte cell line associated with a variability of effect on hedgehog signalling.

An *Ift80* mouse model of Jeune syndrome with stunted cilia (see Figure 6.1 A), would be available to us through collaboration with Dr Jenkins at UCL Institute of

Child Health (data not yet published). The model has characteristic reduced femoral growth plate development (Rix, et al. 2011), a reduced ribcage with associated defects in costochondral cartilage, as well as polydactyly (see Figure 6.1 B) and craniofacial malformations (Figure 6.1 C and D). Using gene-editing techniques two novel exact mouse models have been generated. These carry either a missense (p.A701P) or a null frameshift (p.A554fsX) mutation, both of which are found in patients with the disease. This provides a series of genotypes with varying levels of disruption to IFT80, cilia elongation, hedgehog signalling and resulting bone density, thereby mirroring the spectrum of human phenotypes. Importantly for compound testing, all of the identified phenotypes are 100% penetrant in the p.A701P/p.A554fsX which in terms of statistical power, is essential for therapeutic investigations.

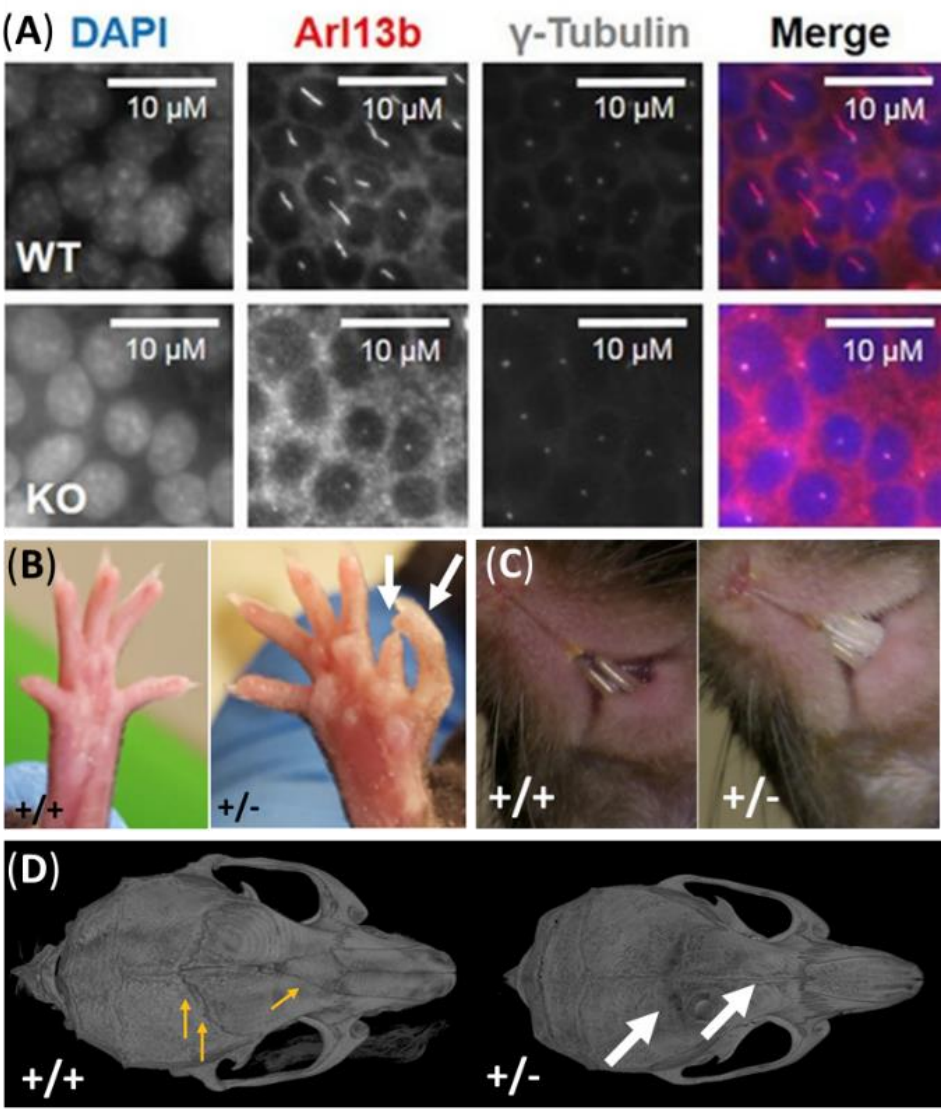

Figure 6.1. Jeune Syndrome mouse phenotype

Images adapted from Taschner, Lorentzen et al. (2018) and provided by collaborator Dr Dagan Jenkins. ***(A)*** *Ift80 KO from IMCD3 cells showing that 100% of cells exhibit reduced ciliary membrane formation (ARL13B staining) without disruption to the basal body (gamma tubulin staining.* ***(B) - (D)*** *Demonstrate the phenotypes present in the ift80 gene edited mouse model (+/-) as compared to the wild type (+/+).* ***(B)*** *Indicates the polydactyly,* ***(C)*** *Malocclussion band, and* ***(D)*** *indicates the craniosynostosis present in the Jeune syndrome mouse models.*

From these 22 compounds identified in the screen, we would look to progress these to 3 lead compounds for testing in the *in vivo* models of Jeune Syndrome. Cartilage cells isolated from mutant mice will be treated with hit compounds and the resulting changes in cilia length and hedgehog signalling quantified using the established confocal immunofluorescence and RT-PCR pipelines and assays. Studies will then confirm the response in human chondrocytes transfected to disrupt IFT80. Results from these initial studies will inform the selection of the 3 most promising compounds, which will be carried forward to *in vivo* studies that will examine potential to rescue the skeletal phenotype in adolescent *Ift80* mutant mice. Effects on phenotype severity will be assessed by histological and CT analysis of craniofacial, rib and femoral growth plate defects and associated bone mineral density changes. If this was found to be successful, this would open the door to ciliotherapy treatment of other ciliopathies and more widespread cilia-related pathologies such as the environmental disease osteoarthritis (8.5M people effected in UK alone)(Kelly 2006).

In summary, the proof of concept study would therefore aim to test the efficacy of 'ciliotherapy' for the treatment of cilia-related pathologies, either directly through drug re-purposing or by supporting the future development of related cilia modifying compounds.

7. Appendices

Appendix A: Optimisation of fixation and immunolabelling

Hua and Ferlands (Hua and Ferland 2017) comprehensively describe a variety of fixation methods available that may inequitably affect cilia immunolabelling. To enable multicomponent fluorescent labelling of primary bovine chondrocytes, a variety of these cellular fixation methods, antibodies, toxins and stains, were tested and compared. Cells were isolated and cultured (section 2.1.2) to confluence on glass coverslips (section 2.1.3) before fixation using either PFA with or without CB (section 2.2.1). Additionally, a variety of CB pre-fixation washes and methanol (MeOH) post-fixation antigen retrieval washes were tested. In total 6 protocols were tested as described in Table A 1.

Fixed, cells were then fluorescently labelled (section 2.2.2), using the primary and secondary antibodies and fluorescent conjugated dyes (Table A2, A3 and A4) as detailed below, and imaged using x63 wide field microscopy ensuring constant imaging parameters (section 2.2.3). Conclusions drawn were based on cell population observational assessment, with figures presenting representative images.

Table A 1: Fixation protocols

	Fixation protocol					
Key	**PFA**	**PFA > MeOH**	**CB-PFA**	**CB-PFA > MeOH**	**CB > CB-PFA**	**CB > CB-PFA >MeOH**
Pre-fixation wash PBS	√	√	√	√	√	√
Pre-fixation wash CB					√	√
10 min 4% PFA fixation	√	√				
10 min CB-PFA fixation			√	√	√	√
2 min ice cold post-fixation methanol wash		√		√		√

Table A 2: Primary antibodies and dilutions

Primary antibodies			
Antibody target	**Product code and company**	**Dilution**	**Antibody type**
Ac-α-tub	T7451, Sigma-Aldrich	1:2,000	Mouse monoclonal IgG2b
Ac-α-tub AF488	Sc-23950 AF488, Santa Cruz Biotechnology	1:1,000	Mouse monoclonal IgG2b conjugated Alexa Fluor 488
Arl13b	17711-1-AP, Proteintech	1:2,000	Rabbit polyclonal IgG
Caveolin-1	3238, Cell Signalling	1:200	Rabbit polyclonal
EHD-1	Ab75886, Abcam	1:200	Rabbit polyclonal IgG
IFT88	13967-1-AP, Proteintech	1:100	Rabbit polyclonal IgG
Glu-tub	AG-20B-0020-C100, AdipoGen Life Sciences	1:100 or 1:1,000	Mouse monoclonal IgG1k
CP110	1228-1-AP, Proteintech	1:100	Rabbit

These are the commonly used antibody dilutions, unless otherwise stated.

Table A 3: Secondary antibodies and dilutions

Secondary antibodies			
Antibody target	**Product code and company**	**Dilution**	**Antibody type**
Donkey anti-rabbit Alexa Fluor 555	A31572, Life Technologies	1:1,000	IgG (H+L)
Donkey anti-mouse Alexa Fluor 488	A21202, Life Technologies	1:1,000	IgG (H+L)
Goat anti-mouse Alexa Fluor 647	A21235, Life Technologies	1:1,100	IgG (H+L)

Table A 4: Dyes and dilutions

Dyes			
Target	**Product code and company**	**Dilution**	**Type**
Phalloidin Fluor 647	SC363797, Santa Cruz	1:1,000	Toxin
Phalloidin Fluor 555	SC363794, Santa Cruz	1:1,000	Toxin
DAPI Fluor 405	Sigma-Aldrich	200ng/ml	Intercalating dye

To determine cell number in any particular field of view, nuclear labelling is essential, achieved using DAPI staining, and was effective irrespective of the fixation method used (Figure A 1). For cilia prevalence and length to be quantified, it is necessary for the cilium to be labelled. Anti-ac-α-tub is frequently used to label the microtubule axoneme of the primary cilium, while anti-arl13b is used to label the ciliary membrane. Dual labelling of the primary cilium would be ideal for the quantification of ciliary prevalence and length. However, there was strong and unpredictable nuclear signal (see Figure A 1) given with the arl13b antibody, which would introduce cilia detection problems during automated analysis. Therefore a different ciliary marker needed to be investigated.

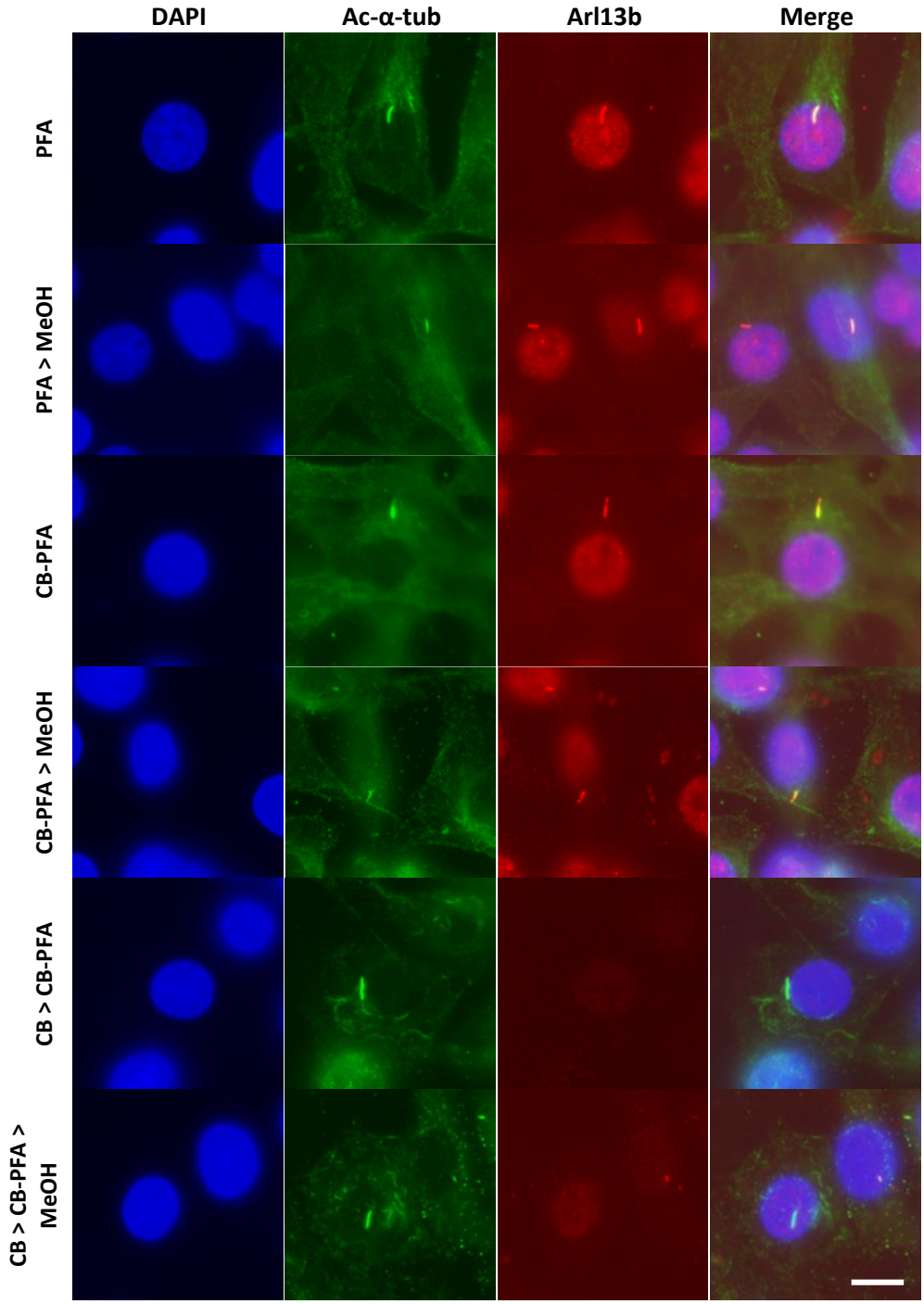

Figure A 1. Fixation techniques

The effects of fixation techniques on dual ciliary labelling with arl13b and ac-α-tub in primary bovine chondrocytes. Six different cellular fixation methods were tested, as described in Table A2. Images were acquired using epifluorescent wide field microscopy. DAPI staining (blue), ac-α-tub (green) and arl13b (red) Immuno-fluorescent labelling were compared for each of the fixation methods. Scale = 10µm.

The various fixation methods were also tested with additional ciliary markers. Although not all were intended for use in the compound screen these may be used to characterise the effect of candidate molecules in future work. Glu-tub, Caveolin-1, EHD-1 and CP110 were investigated as ciliary pocket and basal body markers whilst IFT88 was labelled as a marker of axonemal transport proteins. Representative images are shown in Figure A 2-6. Anti-caveolin-1 (Figure A 2), - EHD-1 (Figure A 3) and - CP110 (Figure A 4) antibodies did not work in any of the fixation methods. However, both anti - Glu-tub (Figure A 5) and anti - IFT88 (Figure A 6) antibodies successfully labelled their respective components of the cilium. However, IFT88 labelling was also present quite strongly in the cytoplasm of the cell, making it less ideal for cilia identification. Both of these, particularly the anti-Glu-tub antibody had worse target labelling in fixation methods that included a post-fixation methanol wash (PFA>MeOH and CB-PFA>MeOH).

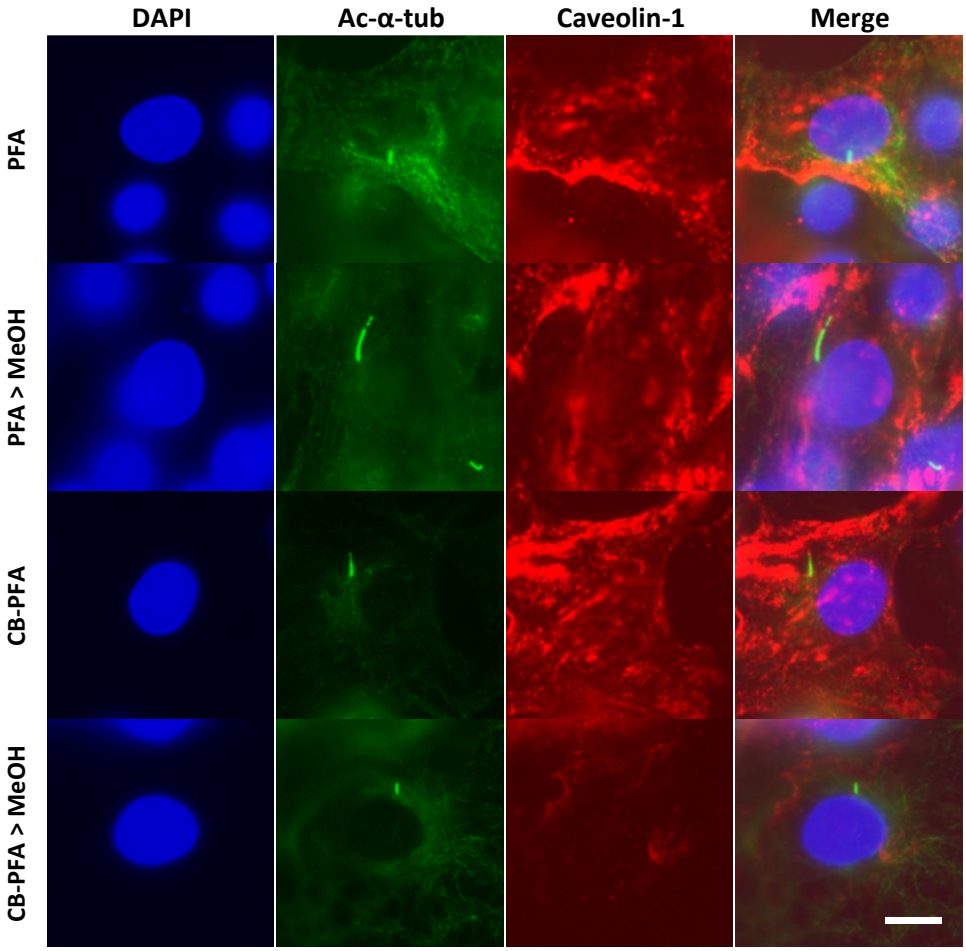

Figure A 2. Anti-caveolin 1 antibody

Testing anti-caveolin-1 antibody as a ciliary basal marker. Four different cellular fixation methods were tested, as described in Table A2 (protocols 1-4). DAPI staining (blue), ac-α-tub (green) and Caveolin-1 (red). Scale bar = 10µm.

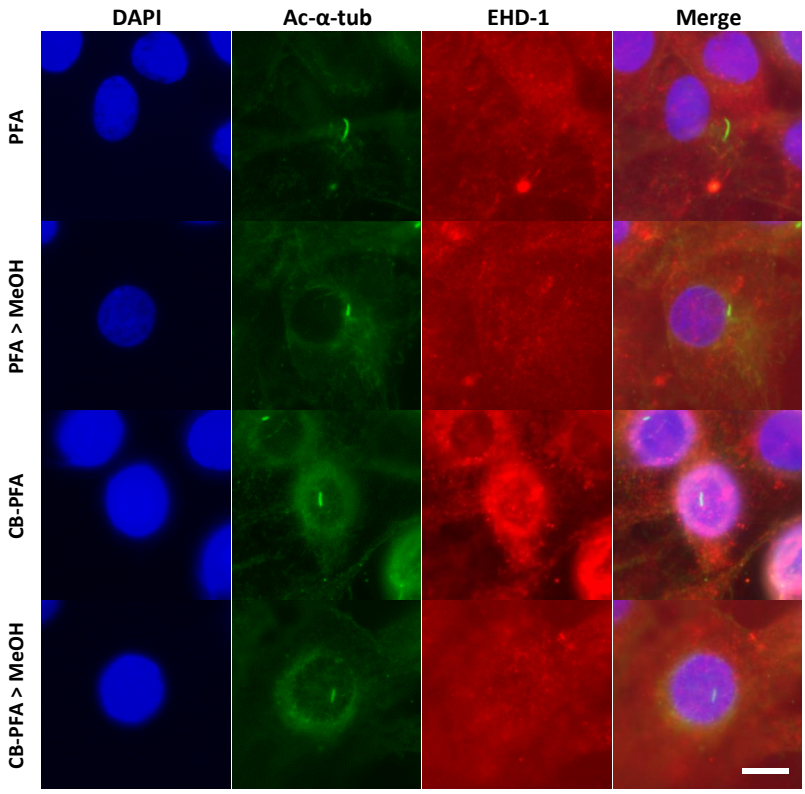

Figure A 3. Anti-EHD-1 antibody

Testing anti-EHD-1 antibody as a ciliary pocket/basal marker. Four different cellular fixation methods were tested, as described in Table A 2 (protocols 1-4). DAPI staining (blue), ac-α-tub (green) and EHD-1 (red) were applied. Scale bar = 10µm.

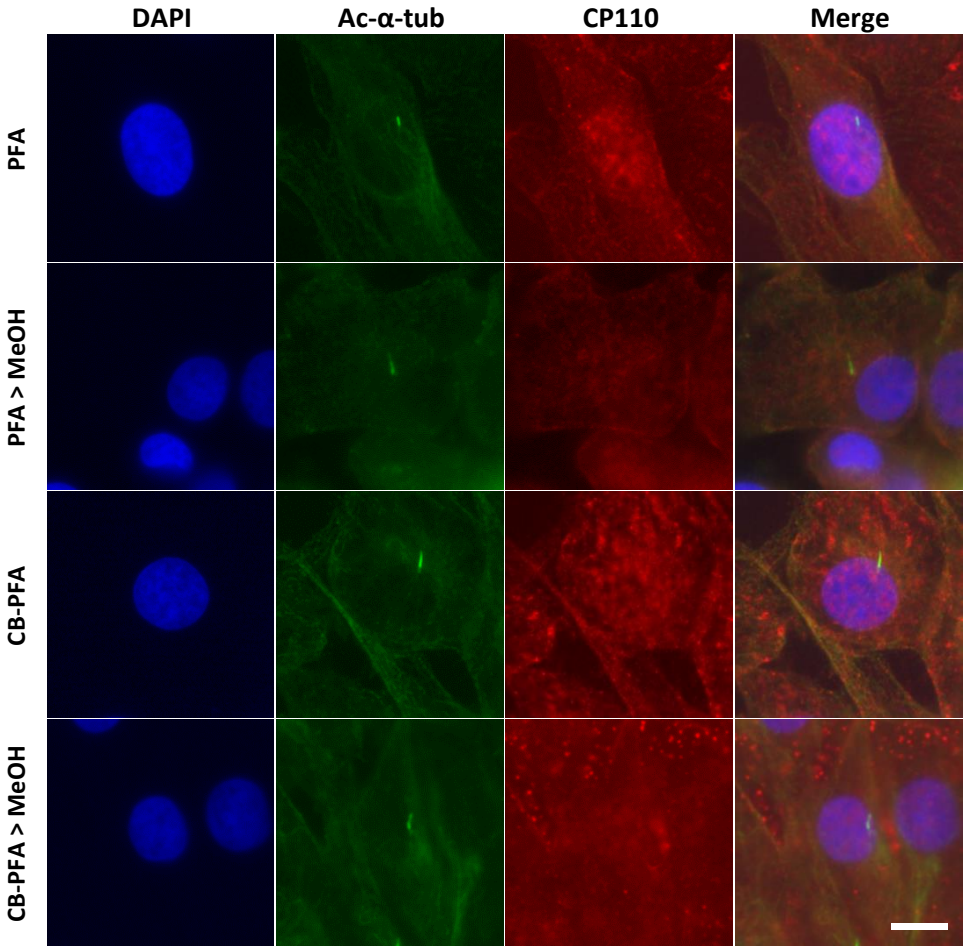

Figure A 4. Anti-CP110 antibody

Testing anti-CP110 antibody as a ciliary basal body marker. Four different cellular fixation methods were tested, as described in Table A 2 (protocols 1-4). DAPI staining (blue), ac-α-tub (green) and CP110 (red) were applied. Scale bar = 10µm.

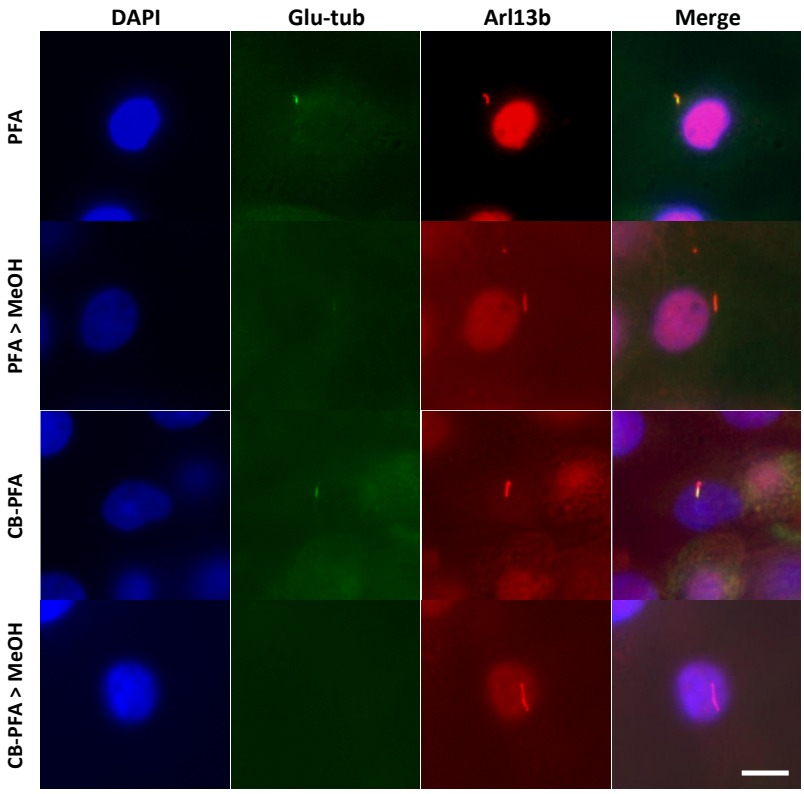

Figure A 5. Anti-Glu-tub antibody

Testing anti-Glu-tub antibody as a ciliary pocket/basal marker. Four different cellular fixation methods were tested, as described in Table A 2 (protocols 1-4). DAPI staining (blue), glu-tub (green) and alr13b (red) were applied. Scale bar = 10µm.

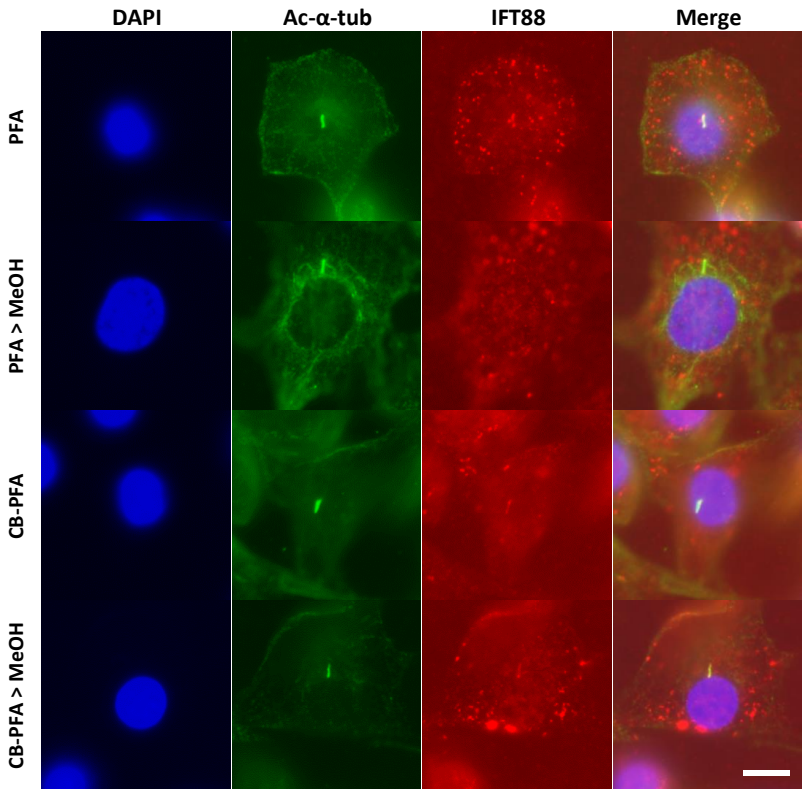

Figure A 6. Anti-IFT88 antibody

Testing anti-IFT88 antibody as a ciliary axonemal transporter marker. Four different cellular fixation methods were tested, as described in Table A 2 (protocols 1-4). DAPI staining (blue), ac-α-tub (green) and IFT88 (red) were applied. Scale bar = 10um.

The effects of fixation on actin staining are shown by representative images in Figure A 7. MeOH washing post fixation (PFA>MeOH and CB-PFA>MeOH), completely abolished actin staining by phalloidin. However, staining was successful in both PFA and CB-PFA fixation methods, with no notable differences between the two.

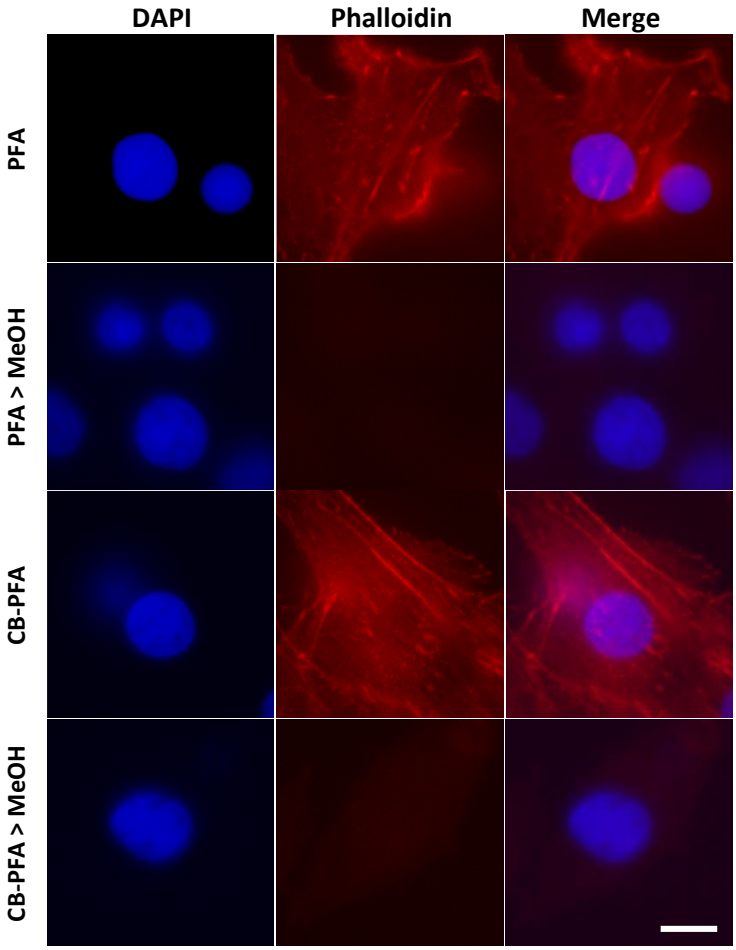

Figure A 7. Effect of fixation on Actin labelling

The effects of fixation techniques on actin staining by phalloidin. Four different cellular fixation methods were tested, as described in Table A 2. DAPI staining (blue) and actin phalloidin-fluor 647 staining (red). Scale bar = 10µm.

As the pre-fixation CB wash and post fixation MeOH wash negatively affected cell labelling, this left either the 4%PFA or CB-PFA fixation methods as options for the compound screen. Although ciliary labelling may be improved in IFT88 labelling with CB-PFA fixation, this method has no added benefit to actin or ciliary axoneme staining over 4%PFA. As the four colour labelling for the screen was to be occupied by DAPI, phalloidin, ac-α-tub and glu-tub, for the purposes of the screen the 4%PFA fixation method was be used.

Appendix B: ARL13b

As mentioned in Appendix A, the anti-arl13b antibody used to label the ciliary membrane also gave surprisingly strong nuclear labelling. Although the cilium was qualitatively distinct from the nuclear staining, adequate for manual ciliary identification, the intensity of the nuclear labelling may prove an issue for automated ciliary identification and analysis. A western blot was run (section 2.4.3) probing cell lysates taken from three repeat wells of primary bovine chondrocytes. Using the anti-arl13b antibody (1:1,000), revealed two distinct bands (Figure B 1), with the binding of the antibody appearing to be specific. One band was at the predicted 48kDa and the other at 100kDa, with the larger of the two likely to be detecting a post-translationally modified form of arl13b. However, to rule out the possibility that this larger 100kDa band is non-specific binding, further experiments would be needed.

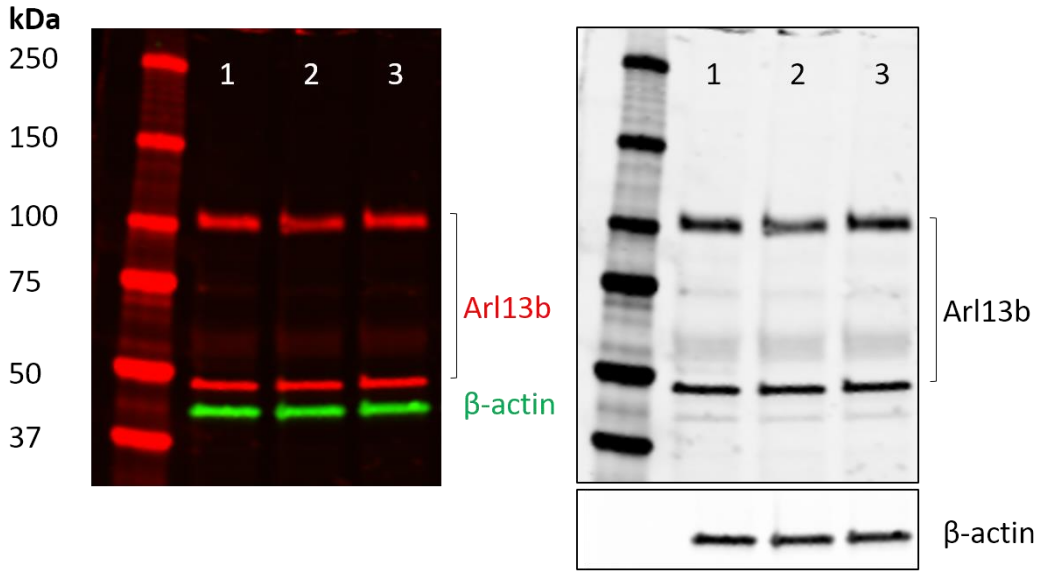

Figure B 1. Arl13b primary antibody validation.

Western blot showing expression of arl13b in full cell DIPA lysates from three different cell culture wells of confluent primary bovine chondrocyte monolayers. Two bands appear when probing for arl13b (red) at ~ 48kDa and ~100kDa. β*-actin was examined as a loading control (green), appearing as a single band at ~40kDa.*

With the aim of reducing nuclear labelling, chondrocytes were cultured to confluence on glass coverslips (section 2.1.3) and fixed for 10min using 4% PFA (28908, Thermo Fisher Scientific). Two different primary arl13b antibody concentrations (1:2,000 and 1:10,000) were tested, either alone or in tandem with ac-α-tub (used at 1:5,000, primary antibody details in Table A2). A variety of secondary antibodies were also tested, with anti-rabbit secondary antibodies used alone or in tandem with anti-mouse secondary antibodies, where ac-α-tub mouse primary was used (Table A2). Once labelled, coverslips were mounted and wide field epifluorescent microscopy was used for image acquisition (section 2.2.3).

Table B 1: Tested IF secondary antibodies

Secondary antibodies		
Antibody target	Alexa fluor	Product code and company
Donkey anti-rabbit	555	A31572, Life Technologies
Donkey anti-rabbit	488	A21206, Thermo Fisher
Goat anti-rabbit	488	A11008, Thermo Fisher
Donkey anti-mouse	488	A21202, Life Technologies
Donkey anti-mouse	555	A31570, Thermo Fisher

All tested combinations of primary and secondary antibodies gave nuclear labelling (Figure B 2), with both dilutions of the primary arl13b antibody providing distinct ciliary labelling. No apparent benefit was seen by incubating the antibody on its own or in tandem with other fluorescent labels, and no notable differences were observed between the three anti-rabbit secondary antibodies.

Primary bovine chondrocytes were seeded in 384-well culture plates and fixed for 15min in either the bought in (28908, Thero Fisher Scientific) or the in house 4%PFA. Cells were permeabilised for 30min using 0.1% Triton X-100/0.1% (BSA)/PBS. Arl13b and ac-α-tub antibodies were used in tandem at a 1:10,000. Donkey anti-rabbit and donkey anti-mouse secondary antibodies were used (Table B 1), before wide field epifluorescent microscopy was used to acquire images (section 2.2.3). No apparent difference was observed in the nuclear alr13b labelling between the two PFA fixations (Figure B 3). Cells cultured in 384-well plates have reduced arl13b nuclear intensity compared to glass coverslips (Figure B 2 and 3). As arl13b was unpredictable and often resulted in nuclear staining, it was dropped as a cilia marker

from the screen. However, arl13b could still be used during future work were manual cilia measurement would be acquired.

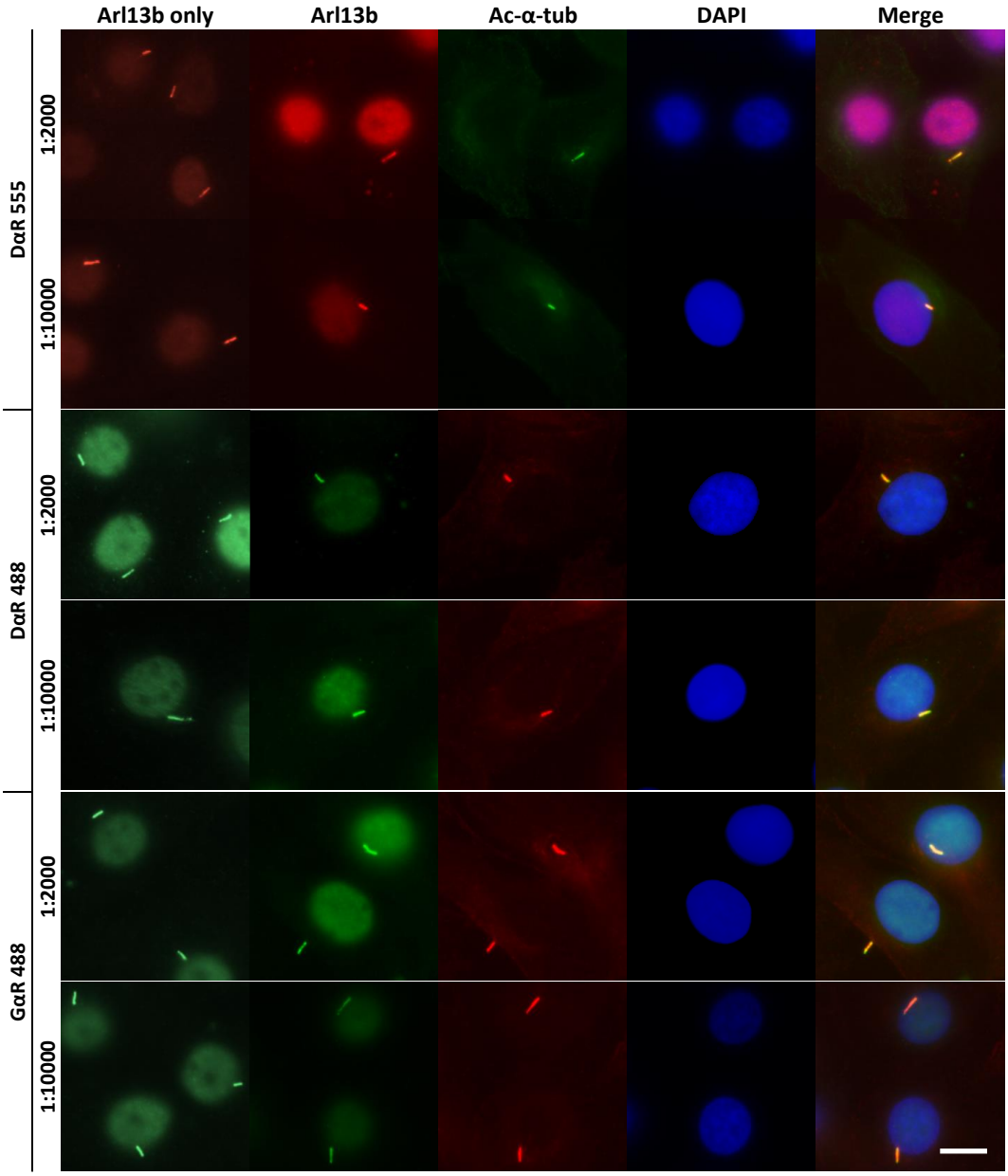

Figure B 2. Optimisation of ciliary ARL13B labelling

Two different ARL13B primary (rabbit) antibody concentrations (1:2000 or 1:10,000) were tested, either alone or with tandem nuclear DAPI staining (blue) and ciliary labelling of ac-α-tub. Three different anti-rabbit secondary antibodies were tested (Donkey anti-rabbit 555, Donkey anti-rabbit 488 and Goat anti-rabbit 488). Scale bar = 10µm. First two rows, Ac-α-tub in green, ARL13B in red. Last four row, ARL13B in green and ac-α-tub in red.

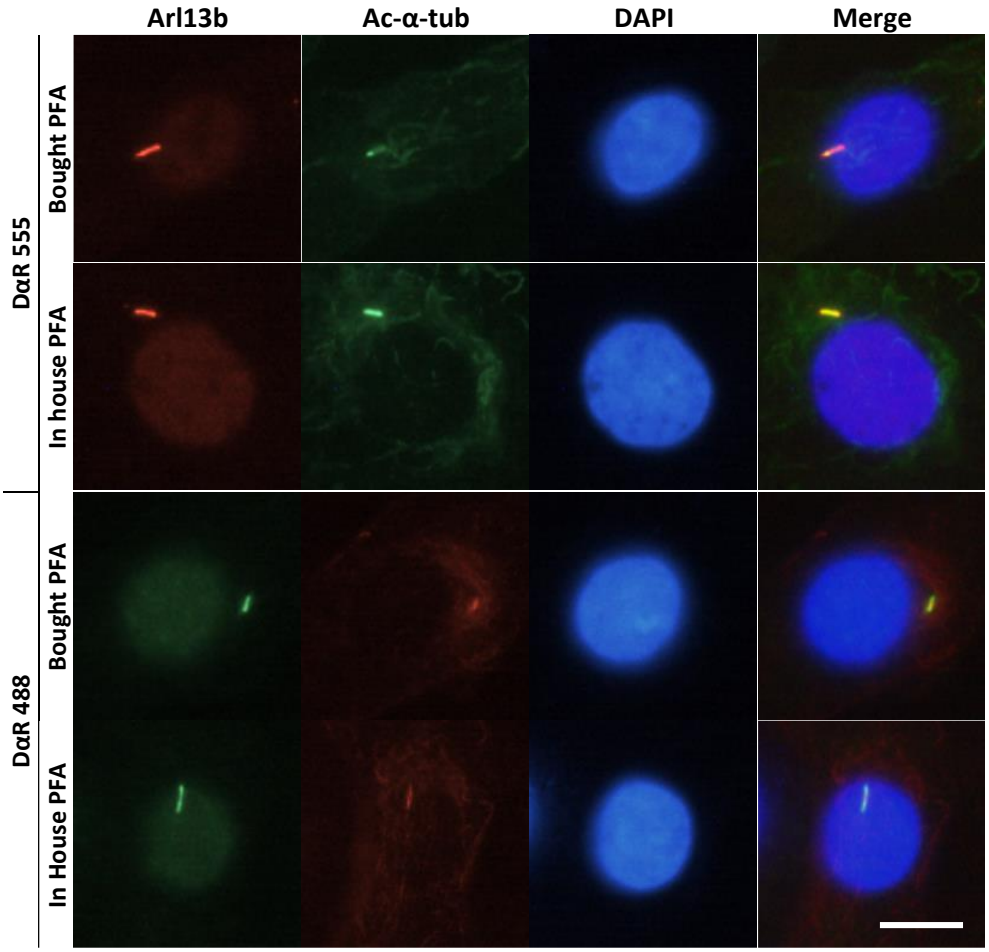

Figure B 3. Testing different PFA fixations for optimisation of ARL13B labelling.

An ARL13B primary (rabbit) antibody concentration of 1:10,000 and ac-α-tub, with nuclear DAPI staining (blue). Two different anti-rabbit secondary antibodies were tested (Donkey anti Rabbit 555, Donkey anti Rabbit). Scale bar = 10µm. First two rows, ac-α-tub in green ARL13B in red. Last two rows, ARL13B in green and ac-α-tub in red.

Appendix C: The compound plate control well layout

Media only in grey

LiCl in red

DMSO in blue

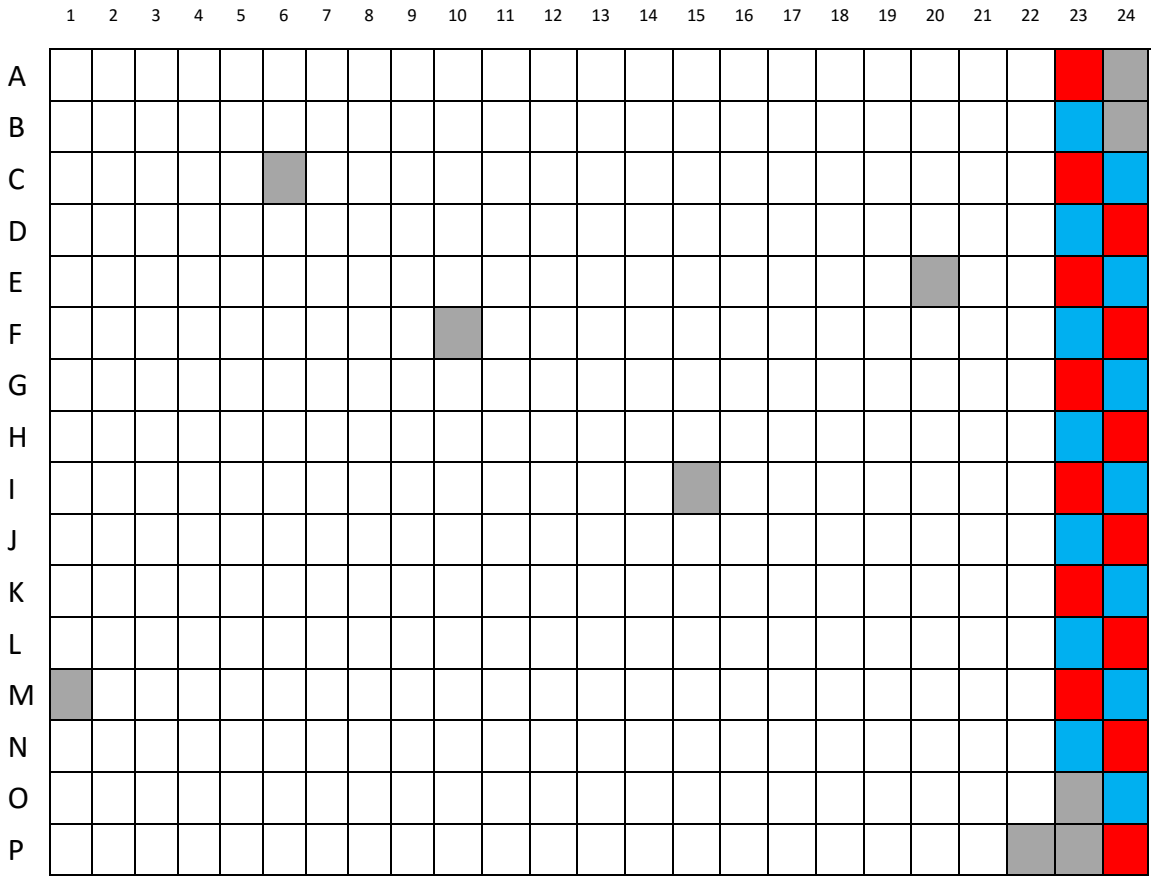

Appendix D: The compound library Indication, Target and Pathway distributions

Table D 1. Indication

Plate	**1**	**2**	**3**	**4**	**5**	**Grand Total**
Grand Total	**346**	**346**	**345**	**345**	**345**	**1727**
Infection	58	53	52	70	58	291
Neurological Disease	54	59	51	47	57	268
Cancer	58	50	38	35	44	225
Cardiovascular Disease	31	32	30	45	31	169
Others	24	20	27	15	25	111
Inflammation	19	15	21	26	22	103
Endocrinology	13	17	16	17	14	77
Metabolic Disease	10	14	13	11	17	65
Neuronal Signaling	12	6	11	11	12	52
Immunology	8	9	10	8	10	45
Respiratory disease	8	4	6	6	10	34
Metabolism	4	8	7	8	5	32
Microbiology	5	7	11	4	4	31
Gastroenterology	4	3	6	6	9	28
Neurological Diseases	1	6	9	2	2	20
Immunology & Inflammation	5	6	3	2		16
Proteases	3	2	4	3	2	14
Transmembrane Transporters	2	4	1	3	1	11
Cardiovascular Disease/Respiratory Disease		3		2	1	6
DNA Damage	3	1	1	1		6
Endocrinology & Hormones	1	2	3			6
Protein Tyrosine Kinase	1	1	2		1	5
Cancer/Immunology		2	1		1	4
Inflammation/Neurological Disease	1		1		2	4
Cancer/Endocrinology		1	1	1		3
GPCR & G Protein				2	1	3
Angiogenesis				2		2

Cardiovascular Disease/Metabolic Disease	1				1	2
Epigenetics		1	1			2
GPCR	1				1	2
Imflammation	1			1		2
Inflammation/Respiratory Disease		1			1	2
Ion-Channel	1		1			2
Kinase			2			2
Protease	1				1	2
Urology		1			1	2
enteric nervous system			1			1
10540-29-1				1		1
Aloprim			1			1
Alphacaine, Xylocaine, lignocaine			1			1
Alvocidib		1				1
Antipsychotic			1			1
Apoptosis	1					1
Avandia, BRL-49653		1				1
Batrafen, Loprox, Mycoster, Stieprox, HOE 296b			1			1
BAY 43-9006		1				1
BMS-232632-05, Reyataz				1		1
BMS-354825 Monohydrate				1		1
BMS-907351			1			1
Cancer,Inflammation			1			1
Cancer/Cardiovascular Disease/Immunology		1				1
Cancer/Diagnosis			1			1
Cancer/Infection	1					1
Cancer/Neurological Disease	1					1
Cancer/Respiratory Disease		1				1
Caner/Endocrinology					1	1
Cardiovascular Disease/Inflammation		1				1
Cardiovascular Disease/Neurological Disease	1					1

Celestone, Betadexamethasone, Flubenisolone, Sch-4831, NCS-39470	1					1
Cell Cycle				1		1
CHIR-258					1	1
CP-62993, XZ-450	1					1
Cytoskeletal Signaling				1		1
Daktarin IV, MJR 1762, Monistat IV, NSC 170986, R 18134, Zimybase					1	1
Decaprednil, Predonine		1				1
Di-Hydan, Dihycon, Dilabid, Diphedan, Diphenat, Diphenylan, Diphenylhydantoin, Hydantol, Lehydan, NS			1			1
Diprospan, Diprolene, Diprosone, Diprolene AF		1				1
Ditropan, Lyrinel XL, Oxytrol					1	1
Effient, Efient, Prasita					1	1
E-Mycin			1			1
F-ara-A, NSC 118218				1		1
Gabitril hydrochloride, NO050328 hydrochloride, NO328 hydrochloride, TGB hydrochloride	1					1
Gabitril, NO050328, NO328, TGB					1	1
Gastroenterology/Neurological Disease		1				1
Gastroenterology/Respiratory Disease			1			1
Gemzar		1				1
Glivec, CGP-57148B, STI-571	1					1
Immunology/Infection		1				1
Immunology/Inflammation				1		1
Immunology/Inflammation&Neurological Disease				1		1
Immunology/Metabolic Disease			1			1
Immunology/Neurological Disease		1				1
Infection Inflammation/Immunology				1		1
Infection/Inflammation				1		1
Inflammation/Immunology			1			1
Inflammmation				1		1

Isosorbide-5-mononitrate, Elantan, Monoket, Mononit, Imdur, Corangin					1	1
Istin	1					1
JAK/STAT	1					1
KT-611, BM-15275				1		1
Lamisil, Terbinex, Corbinal, Zabel					1	1
Levaquin, Tavanic			1			1
Lokren ,Kerlone				1		1
MAPK				1		1
Medroxyprogesterone 17-acetate, MPA		1				1
Metabolism system		1				1
Midamor, Colectril, Amipramizide, Guanamprazine hydrochloride	1					1
Mirapexin, Sifrol	1					1
MK-8931				1		1
MPV-1248, MPV1248, MPV 1248, Antisedan		1				1
N-(2-amino-4-[fluorobenzylamino]-phenyl) carbamic acid (2HCl), D-23129 2HCl			1			1
Nalfon					1	1
Nervous system		1				1
Neurological Disease/Immunology	1					1
Neurological Disease/Respiratory Disease				1		1
O-desmethylvenlafaxine	1					1
Ondemet, Emeset, Emetron		1				1
PF-05208749 HCl	1					1
Procaine, Novocaine, Vitamin H3, Duracaine, Spinocaine			1			1
Ranexa				1		1
SKF96022 sodium, BY-1023 sodium	1					1
SU-11248					1	1
Tacrine, Tetrahydroaminacrine, Tetrahydroaminoacridine					1	1
Viagra, Revatio			1			1
Voltaren, Solaraze, Ecofenac		1				1

Table D 2. Pathway

Plate	**1**	**2**	**3**	**4**	**5**	**Grand Total**
Grand Total	**346**	**346**	**345**	**345**	**345**	**1727**
Neuronal Signaling	70	65	70	72	72	349
Microbiology	53	55	50	60	48	266
Others	45	45	46	42	54	232
Metabolism	28	28	32	32	27	147
Transmembrane Transporters	24	27	25	24	21	121
Endocrinology & Hormones	23	23	21	18	21	106
DNA Damage	16	17	16	18	17	84
Immunology & Inflammation	13	12	11	13	14	63
Protein Tyrosine Kinase	14	13	12	8	9	56
Proteases	10	10	13	12	10	55
GPCR & G Protein	7	10	10	8	11	46
Angiogenesis	1	4	4	10	5	24
Cytoskeletal Signaling	6	4	3	3	5	21
Cell Cycle	3	2	2	5	5	17
Epigenetics	3	2	3	4	5	17
JAK/STAT	4	4	3	4	2	17
PI3K/Akt/mTOR	4	4	2	3	3	16
MAPK	4	2	3	4	1	14
Apoptosis	4	3	2		1	10
N/A	1	2	4		1	8
Neurological Disease	5		1		2	8
Infection	1	2	1		2	6
Autophagy	1	1	1		1	4
Cardiovascular Disease		1	1	1	1	4
Immunology		1	1	2		4
NF-κB		2	2			4
TGF-beta/Smad		3	1			4
GPCR	1				2	3
Metabolic Disease		1	1		1	3
Stem Cells & Wnt	1			1	1	3
Ion-Channel	1		1			2

Protease	1				1	2
enteric nervous system			1			1
Antipsychotic			1			1
Endocrinology					1	1
GPCG	1					1
Infection Inflammation/Immunology				1		1
Inflammation/Immunology			1			1
Kinase			1			1
Metabolism system		1				1
Nervous system		1				1
Neuronal Signaling		1				1
PKC	1					1
Ubiquitin					1	1

Table D 3. Target

Plate	**1**	**2**	**3**	**4**	**5**	**Grand Total**
Grand Total	**346**	**346**	**345**	**345**	**345**	**1727**
Anti-infection	41	41	41	41	41	205
Others	26	25	25	26	26	128
Adrenergic Receptor	19	19	19	18	20	95
5-HT Receptor	13	12	13	13	14	65
AChR	13	13	13	13	13	65
Bacterial	13	12	11	12	12	60
Histamine Receptor	10	10	10	10	10	50
Immunology & Inflammation related	10	9	10	10	11	50
COX	9	9	8	10	9	45
DNA/RNA Synthesis	9	8	9	9	10	45
Calcium Channel	8	8	8	7	9	40
Dopamine Receptor	8	8	8	8	8	40
Estrogen/progestogen Receptor	8	8	8	8	8	40
Sodium Channel	7	7	7	7	7	35
PDE	5	5	5	5	5	25
RAAS	5	5	5	5	5	25
Topoisomerase	5	5	5	5	5	25
Glucocorticoid Receptor	5	5	5		5	20
HCV Protease	4	4	4	4	4	20
P450 (e.g. CYP17)	4	4	3	4	5	20
Potassium Channel	4	4	4	4	4	20
Vitamin	4	4	5	3	2	18
Reverse Transcriptase	4	4	3	3	3	17
Dehydrogenase	3	3	3	3	3	15
DPP-4	3	3	3	3	3	15
JAK	3	3	3	3	3	15
Opioid Receptor	3	3	3	2	4	15
PPAR	3	3	3	3	3	15
HMG-CoA Reductase	3	2	3	3	3	14
Androgen Receptor	2	2	2	2	2	10
Aromatase	2	2	2	2	2	10

Carbonic Anhydrase	2	2	2	2	2	10
CDK	2	2	2	2	2	10
DNA alkylator	2	2	2	2	2	10
EGFR	2	2	2	2	2	10
GABA Receptor	2	2	2	2	2	10
HDAC	2	2	2	2	2	10
HIV Protease	2	2	2	2	2	10
MAO	2	2	2	2	2	10
Microtubule Associated	2	1	2	3	2	10
Proton Pump	3	2	2	1	2	10
Retinoid Receptor	2	2	2	2	2	10
SGLT	2	2	2	2	2	10
Thrombin	2	2	2	2	2	10
VEGFR	2	2	2	2	2	10
ROS	1	1	2	2	2	8
c-Kit,PDGFR,VEGFR	1	1	1	1	1	5
Glucocorticoid Recep				5		5
MEK	1	1	1	1	1	5
PI3K	1	1	1	1	1	5
S1P Receptor	1	1	1	1	1	5
Serine Protease	1	1	1	1	1	5
5-HT Receptor, Dopamine Receptor	1		1	1	1	4
Bcr-Abl		1	1	1	1	4
EGFR,HER2	1		1	1	1	4
Endothelin Receptor	1		1	1	1	4
metabolism		1	1	1	1	4
MMP		1	1	1	1	4
PDGFR	1	1	1	1		4
Proteasome		1	1	1	1	4
5-alpha Reductase		1	1	1		3
ALK		1	1	1		3
Aurora Kinase	1			1	1	3
Autophagy		1	1	1		3
CFTR	1	1	1			3
DHFR		1	1		1	3
Factor Xa		1	1	1		3

FXR			1	1	1	3
Hydroxylase			2	1		3
Integrase	1	1	1			3
Integrin	1				2	3
LTR				2	1	3
mTOR	1			1	1	3
mTOR,PI3K		1	1	1		3
NMDAR	1	1	1			3
PARP	1			1	1	3
PGFR			1	1	1	3
STAT	1	2				3
TRPV		1	1	1		3
Adenosine Receptor				1	1	2
AMPK				1	1	2
Angiotensin Receptor				1	1	2
ATPase	1	1				2
Autophagy,IL Receptor				1	1	2
Autophagy,Microtubule Associated	1	1				2
BTK				1	1	2
Caspase	1	1				2
c-Kit,FGFR,FLT3,PDGFR,VEGFR					2	2
c-Met	1	1				2
c-Met,VEGFR			1	1		2
CP450	1	1				2
Decarboxylase			1	1		2
factor Xa (fXa)	1				1	2
Glucocorticoid Receptor,Immunology & Inflammation related	1	1				2
GluR			1	1		2
HSP (e.g. HSP90)	1	1				2
mAChR	1				1	2
MT Receptor	1	1				2
MTP	1				1	2
NF-κB		1	1			2
p38 MAPK				2		2

P-gp	1	1				2
PKC		1	1			2
PLK				1	1	2
Src		1	1			2
Syk	1	1				2
TGF-beta/Smad		2				2
TNF-alpha		1	1			2
Tyrosinase	1				1	2
Vasopressin Receptor		1	1			2
11β-HSD	1					1
5-HT Receptor, Adrenergic Receptor		1				1
ABCB11		1				1
Abl/Src			1			1
acetylcholinesterase				1		1
Akt	1					1
ALK,c-Met					1	1
alpha1 adrenoreceptor	1					1
AMPA Receptor-kainate Receptor-NMDA Receptor		1				1
AmpC Beta-Lactamase			1			1
analgesic and antipyretic	1					1
Androgen Receptor,5-alpha Reductase	1					1
Androgen Receptor,Estrogen/progestogen Receptor		1				1
Androgen Receptor,P450 (e.g. CYP17)			1			1
anticholinergic		1				1
Anti-infection,DNA/RNA Synthesis					1	1
antithrombin III			1			1
ATPase,Anti-infection			1			1
Autophagy,Anti-infection					1	1
Autophagy,Calcium Channel	1					1
Autophagy,DNA/RNA Synthesis		1				1
Autophagy,HDAC			1			1
Autophagy,mTOR			1			1

Autophagy,Potassium Channel				1		1
Autophagy,ROCK					1	1
Bcl-2	1					1
Bcr-Abl,c-Kit,PDGFR	1					1
Bcr-Abl,c-Kit,Src		1				1
Bcr-Abl,FGFR,PDGFR,VEGFR			1			1
Beta Amyloid,Gamma-secretase				1		1
Cannabinoid Receptor					1	1
CaSR			1			1
CCR				1		1
Chloride Channel				1		1
c-Kit,FLT3,PDGFR	1					1
c-Kit,PDGFR		1				1
COMT					1	1
c-RET,VEGFR			1			1
CRM1				1		1
CSF-1R,c-Kit					1	1
CSF-1R,PDGFR,VEGFR	1					1
CXCR		1				1
CYP2D6.			1			1
Cysteine Protease				1		1
Cytochrome P450 Autophagy					1	1
DNA topoisomerase II			1			1
DNA/RNA Synthesis,STAT				1		1
EGFR,BTK	1					1
EGFR,HDAC,HER2		1				1
EGFR,Topoisomerase		1				1
ER-alpha		1				1
ERK			1			1
estrogen receptor				1		1
estrogen receptor					1	1
Estrogen Receptor/ERR					1	1
Estrogen/progestogen Receptor,Autophagy	1					1
Fatty Acid Synthase		1				1

FGFR,PDGFR,VEGFR			1			1
FLT3				1		1
FLT3,c-Kit,FGFR,PDGFR,VEGFR					1	1
FLT3,JAK	1					1
FLT3,TAM Receptor		1				1
GABA Receptor,HDAC,Autophagy	1					1
Gamma-secretase		1				1
ganglion-blocking			1			1
GC				1		1
GCS					1	1
Ghrelin receptor	1					1
GLI3		1				1
GluCl		1				1
GluR,Sodium Channel					1	1
GlyT			1			1
GSK-3		1				1
Hedgehog/Smoothened	1					1
HER2		1				1
HER2,EGFR			1			1
HIF				1		1
histamine					1	1
IAP	1					1
IDO		1				1
IGF-1R			1			1
IL Receptor				1		1
Integrase,HIV Protease				1		1
IκB/IKK		1				1
IκB/IKK,Immunology & Inflammation related			1			1
LDL	1					1
Lipase,Fatty Acid Synthase		1				1
Lipoxygenase			1			1
Melatonin Receptor	1					1
Microtubule Associated,AChR	1					1
MTH1			1			1
multidrug efflux pump		1				1

Muscarinic AChR			1			1
Na/Cl cotransporter				1		1
NAG/CPS 1					1	1
NF-kB	1					1
NF-κB,HDAC,Histone Acetyltransferase,Nrf2				1		1
NK1-receptor					1	1
NMDAR,Sodium Channel,AChR				1		1
Norepinephrine reuptake					1	1
NOS	1					1
NQO		1				1
Nrf2			1			1
ntestinal alpha-glucosidase				1		1
Nucleoprotein (Rift valley fever virus (STRAIN ZH-548 M12))					1	1
opioid antagonist		1				1
P2 Receptor			1			1
p38 MAPK,Tie-2	1					1
PDGFR,c-Kit,VEGFR					1	1
PDGFR,Raf,VEGFR	1					1
PGER		1				1
PGR			1			1
phosphatase				1		1
phosphatase,Immunology & Inflammation related					1	1
phosphodiesterase		1				1
PKA	1					1
Potassium Channel,Sodium Channel,Calcium Channel			1			1
Proton Pump,Anti-infection				1		1
Proton Pump,Autophagy					1	1
Raf	1					1
Renin		1				1
Rho			1			1
ROCK				1		1
RXRA					1	1

Sodium Channel,Calcium Channel	1					1
Src,c-Kit,Bcr-Abl				1		1
Substance P			1			1
sulfonamide and a carbonic anhydrase				1		1
Survivin		1				1
T3 receptor			1			1
TAM Receptor,VEGFR				1		1
TNF-alpha,PDE				1		1
TNF-alpha,ROS			1			1
TRP Channel	1					1
VDA,Hippo pathway				1		1
VDR					1	1
β-adrenergic receptor	1					1

Appendix E: Automated image analysis set up and measures

Table E 1. Analysis channels in Developer Toolbox

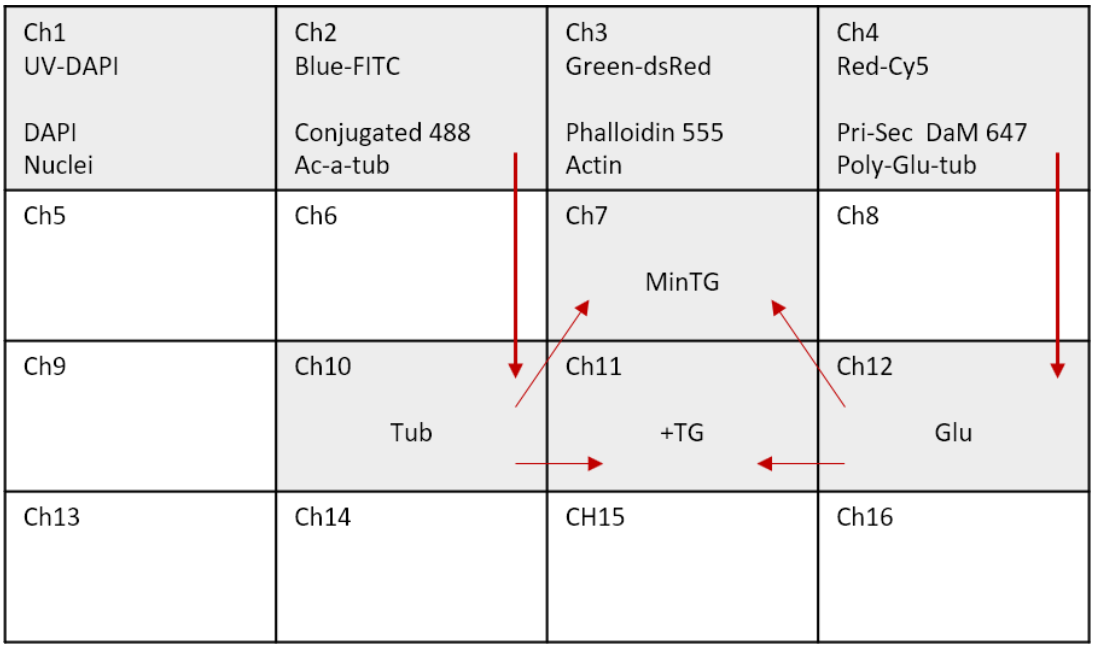

Ch1	DAPI nuclei
Ch2	All Ac-a-tub
Ch3	All actin
Ch4	All Poly-glu-tub
Ch7	Minimum overlap of ciliary Ac-a-tub and ciliary Poly-glu-tub
Ch10	Ciliary Ac-a-tub
Ch11	Full ciliary mask with merge signal of ciliary Ac-a-tub and Poly-glu-tub
Ch12	Ciliary Poly-glu-tub

Table E 2. Target Sets and how they are defined

The Target Set	Channel	Target set description	How it Is defined in developer toolbox
Field	1	Total area of a FOV	Segmentation Intensity Segmentation 0 to 65535
Tub Pos	2	All Tub positive structures in a FOV	Segmentation Intesntity Segmentation 200 to 65535 Postprocessing Sieve (Binary) area greater than 5 pixel
Act Pos	3	All actin positive structures in a FOV	Segmentation Intesntity Segmentation 300 to 65535 Postprocessing Sieve (Binary) area greater than 5 pixel
Glu Pos	4	All Glu positive structures in a FOV	Segmentation Intesntity Segmentation 500 to 65535 Postprocessing Sieve (Binary) area greater than 5 pixel
Nuclei Seed	1	Defines nuclei and helps to separate ones that are in close proximity by finding the seed/center of the nuclei.	Segmentation Nuclear Segmentation Minimum target area 4000 pixel Sensitivity 72 Low background Postprocessing Fill Holes Erosion (Binary) = Kernal Size 55 Sieve (Binary) = area greater than 300 pixel

Nuclei	1	Defines the nuclei and clump breaks them based on the Seed.	Segmentation Intensity Segmentation 450 to 65535 Postprocessing Fill Holes Clump breaking on Second Segmentation Nuclei Seed Sieve (Binary) = area greater than 2000 pixel
Nuclei D	1	Dilated nuclei, clump breaks based on the Nuclei	Segmentation Intensity Segmentation 65535 to 65535 Postprocessing Clump breaking on Second Segmentation Nuclei, including secondary target with radius of 15. Border Object Removal – touching borders, all borders
Tub	2 output to 10	Tub positive cilia	Acceptance criteria = [Dens – Levels]>300 Segmentation Object Kernel Size = 5, Sensitivity =10 Postprocessing Border Object Removal – touching borders, all borders Sieve (Binary) = area greater than 15 pixel Sieve (Binary) = area less than 500 pixel
Actin	3	Actin positive structures clump breaking on Nuclei	Acceptance criteria = [Dens – Levels]>150 Segmentation Object Kernel Size = 5, Sensitivity =85 Postprocessing Sieve (Binary) = area greater than 15 pixel

			Clump breaking on Second Segmentation Nuclei D
Glu	4 output to 12	Glu positive cilia	Acceptance criteria = [Dens – Levels]>300 Segmentation Object Kernel Size = 5, Sensitivity =20 Postprocessing Border Object Removal – touching borders, all borders Sieve (Binary) = area greater than 15 pixel Sieve (Binary) = area less than 200 pixel
+TG	11	All cilia (Tub and/or Glu positive)	Preprocessing Macro – Adds Ch10 and Ch12 Segmentation Intensity Segmentation 1 to 65535
MinTG	7	All overlapping portions of Tub and Glu cilia	Preprocessing Macro – Adds only the portions where Ch10 and Ch12 overlap Segmentation Intensity Segmentation 1 to 65535

Target Linking

- **ND**

  Primary – Nuclei

  Secondary – Nuclei D

  Criteria – Overlap (Any intersect, find any matched target)

- **Nuclei D_T**

  Primary – Nuclei D

  Secondary – Tub

  Criteria – Overlap (Any intersect, find the best matched secondary 'big target vs small target')

- **ND_T**

  Primary – ND

  Secondary – Nuclei D_T

  Criteria – Overlap (Any intersect, find any matched target)

- **Nuclei D_G**

  Primary – Nuclei D

  Secondary – Glu

  Criteria – Overlap (Any intersect, find the best matched secondary 'big target vs small target')

- **ND_G**

  Primary – ND

  Secondary – Nuclei D_G

  Criteria – Overlap (Any intersect, find any matched target)

- **Nuclei D_+TG**

  Primary – Nuclei D

  Secondary – +TG

  Criteria – Overlap (Any intersect, find the best matched secondary 'big target vs small target')

- **ND_+TG**

  Primary – ND

  Secondary – Nuclei D_+TG

  Criteria – Overlap (Any intersect, find any matched target)

- **Nuclei D_A**

  Primary – Nuclei D

  Secondary – Actin

  Criteria – Overlap (Any intersect, find any matched target)

- **ND_A**

Primary – ND

Secondary – Nuclei D_A

Criteria – Overlap (Any intersect, find any matched target)

- **Nuclei D_MinTG**

  Primary – Nuclei D

  Secondary – MinTG

  Criteria – Overlap (Any intersect, find the best matched secondary ‘big target vs small target’)

- **ND_MinTG**

  Primary – ND

  Secondary – Nuclei D_MinTG

  Criteria – Overlap (Any intersect, find any matched target)

- **Field_Tub**

  Primary – Filed

  Secondary – Tub Pos

  Criteria – Overlap (Any intersect, find any matched target)

- **Field_Glu**

  Primary – Filed

  Secondary – Glu Pos

  Criteria – Overlap (Any intersect, find any matched target)

- **Field_Act**

  Primary – Filed

  Secondary – Act Pos

  Criteria – Overlap (Any intersect, find any matched target)

Description of Measures

Target data;

Area	= Area of a target.
Perimeter	= Distance around a target.
Length	= Maximum distance across a target. Boundaries may be crossed.
Form Factor	= Estimate of circularity, expressed as a value between 0 and 1 (1 equals a perfect circle).
Mass	= The sum of all pixel values in the shape.
Max Chord-curved	= Maximum center line through target.
Dens – Levels	= Mean gray level value of the pixels contained within the target outline. Gray levels is an intensity scale, where black = 0.
Count	= number of objects in an outline (e.g. single cilium is a target, with count of 1).

Well and block summary data;

Sum	= addition of count target data
Mean	= average of target data
Median	= middle most of ranked target measures
Std	= standard deviation of the target data

Table E 3. The Raw Measures and their MySQL key

#	CSV file col name	MySQL table name (key: Stat-measure-Target)
1	Mean Area Tub	MAT
2	Mean Perim Tub	MPT
3	Median Area Tub	MedAT
4	Median Max Chord of Tub in um	MedMCT
5	Median Perim Tub	MedPT
6	Std Area Tub	StdAT
7	Std Max Chord of Tub in um	StdMCT
8	Mean Area Glu	MAG
9	Mean Max Chord of Glu in um	MMCG
10	Mean Perim Glu	MPG
11	Median Area Glu	MedAG
12	Median Max Chord of Glu in um	MedMCG
13	Median Perim Glu	MedPG
14	Std Area Glu	StdAG
15	Std Max Chord of Glu in um	StdMCG
16	Mean Max Chord +TG	MMCTG
17	Median Max Chord +TG	MedMCTG
18	Std Max Chord +TG	StdMCTG
19	Sum +TG	SumTG
20	Mean Max Chord MinTG	MMCMinTG
21	Median Max Chord MinTG	MedMCMinTG
22	Std Max Chord MinTG	StdMCMinTG
23	Sum MinTG	SumMinTG
24	Mean Area ND	MAND
25	Mean Perim ND	MPND
26	Mean FF ND	MFFND
27	Median Area ND	MedAND
28	Median Perim ND	MedPND
29	Median FF ND	MedFFND
30	Std Area ND	StdAND
31	Std Perim ND	StdPND

32	Std FF ND	StdFFND
33	Sum ND	SumND
34	Mean Area ND_T	MAND_T
35	Mean MCLen Ratio of ND_T	MMCLenRND_T
36	Mean Max Chord of ND_T in um	MMCND_T
37	Mean Perim ND_T	MPND_T
38	Median Area ND_T	MedAND_T
39	Median Max Chord of ND_T in um	MedMCND_T
40	Median Perim ND_T	MedPND_T
41	Std Max Chord of ND_T in um	StdMCND_T
42	Sum ND_T	SumND_T
43	Mean Area ND_G	MAND_G
44	Mean MCLen Ratio of ND_G	MMCLenRND_G
45	Mean Max Chord of ND_G in um	MMCND_G
46	Mean Perim ND_G	MPND_G
47	Median Area ND_G	MedAND_G
48	Median Max Chord of ND_G in um	MedMCND_G
49	Median Perim ND_G	MedPND_G
50	Std Max Chord of ND_G in um	StdMCND_G
51	Sum ND_G	SumND_G
52	Mean MCLen Ratio of ND_+TG	MMCLenRND_TG
53	Mean Max Chord of ND_+TG in um	MMCND_TG
54	Median Max Chord of ND_+TG in um	MedMCND_TG
55	Std Max Chord of ND_+TG in um	StdMCND_TG
56	Sum ND_+TG	SumND_TG
57	Mean MCLen Ratio of ND_MinTG	MMCLenRND_MinTG
58	Mean Max Chord ND_MinTG	MMCND_MinTG
59	Median Max Chord ND_MinTG	MedMCND_MinTG
60	Std Max Chord ND_MinTG	StdMCND_MinTG
61	Sum ND_MinTG	SumND_MinTG
62	Mean # Actin obj per ND_A	MActObND_A
63	Mean Average Area Actin per ND_A	MAvAActND_A
64	Mean Total Area Actin per ND_A	MTotAActND_A
65	Sum ND_A	SumND_A

66	Mean Area of Tub Pos in Field	MATPF
67	Mean DL of Tub Pos in Field	MDLTPF
68	Mean Mass of Tub Pos in Field	MMTPF
69	Mean Area of Glu Pos in Field	MAGPF
70	Mean DL of Glu Pos in Field	MDLGPF
71	Mean Mass of Glu Pos in Field	MMGPF
72	Mean Area of Act Pos in Field	MAAPF
73	Mean DL of Act Pos in Field	MDLAPF
74	Mean Mass of Act Pos in Field	MMAPF

Table E 4. Derived Measures and their MySQL key

#	MySQL table name (key: Stat-measure-Target)	What the measure is and where it is derived from	How it is calculated from the raw measures
1	MPrevT	Mean prevalence of Tub cilia	(SumT/SumND)*100
2	MPrevG	Mean prevalence of Glu cilia	(SumG/SumND)*100
3	MPrevND_T	Mean prevalence of ND_T cilia	(SumND_T/SumND)*100
4	MPrevND_G	Mean prevalence of ND_G cilia	(SumND_G/SumND)*100
5	MPrevND_TG	Mean prevalence of ND_TG cilia	(SumND_TG/SumND)*100
6	MPrevND_MinTG	Mean prevalence of ND_MinTG cilia	(SumND_MinTG/SumND)*100
7	MATPF_C	Mean Area of Tub Pos in Field	MATPF/SumND
8	MDLTPF_C	Mean DL of Tub Pos in Field	MDLTPF/SumND
9	MMTPF_C	Mean Mass of Tub Pos in Field	MMTPF/SumND
10	MAGPF_C	Mean Area of Glu Pos in Field	MAGPF/SumND
11	MDLGPF_C	Mean DL of Glu Pos in Field	MDLGPF/SumND
12	MMGPF_C	Mean Mass of Glu Pos in Field	MMGPF/SumND
13	MAAPF_C	Mean Area of Act Pos in Field	MAAPF/SumND
14	MDLAPF_C	Mean DL of Act Pos in Field	MDLAPF/SumND
15	MMAPF_C	Mean Mass of Act Pos in Field	MMAPF/SumND

Appendix F: Z-scores and ranges for screening measurements of interest

Table F 1. Minimum, maximum and Z-score values for control wells across all 15 primary screening plate

Condition	Z-score	Ac-α-tub length	Glu-tub length	Combined length	Minimum overlap length	Ac-α-tub prevalence	Glu-tub prevalence	Combined prevalence	Minimum overlap prevalence
DMSO	Min	-2.66	-5.81	-2.09	-2.52	-2.80	-3.17	-3.20	-2.85
	Max	2.97	3.03	3.24	3.66	1.99	1.72	1.72	1.83
	Mean	0.00	0.00	0.00	0.00	0.00	0.00	0.00	0.00
LiCl	Min	-0.44	-2.46	-1.28	-3.42	-4.70	-5.64	-6.46	-3.14
	Max	10.15	6.66	7.80	5.79	3.07	2.50	2.48	4.23
	Mean	3.85	1.93	3.07	1.15	0.339	0.363	0.444	0.173

Table F 2. Z-scores for length and incidence measures from full screen

#	Plate	Well	Length Z-scores				Incidence Z-scores				Heat map Cluster
			Ac-α-tub	Glu-tub	Combined	Min overlap	Ac-a-tub	Glu-tub	Combined	Min overlap	
1	1	B2	2.41	1.15	1.98	0.91	0.61	0.72	0.73	0.57	1
2	1	C10	2.19	0.81	2.00	0.37	1.35	1.01	1.22	0.97	1
3	1	G4	3.20	1.36	2.22	1.77	0.11	0.02	0.23	-0.17	1
4	1	G5	2.82	0.97	1.43	1.07	-0.56	0.22	0.12	-0.47	1
5	1	K12	2.48	2.21	2.62	2.05	0.45	-0.73	-0.12	-0.19	1
6	2	A14	1.61	2.96	2.48	1.67	1.67	1.61	1.45	1.85	1
7	3	A3	3.06	2.72	3.21	-0.08	0.10	0.13	0.41	-0.37	1
8	3	F6	5.06	3.36	5.06	1.48	1.83	0.94	1.36	1.42	1
9	3	G17	2.99	3.26	3.61	2.45	1.34	0.70	0.69	1.36	1
10	3	L13	2.53	2.42	2.84	1.50	1.33	1.06	1.07	1.40	1
11	3	N13	2.15	2.04	2.55	1.96	1.82	1.26	1.33	1.79	1
12	3	N16	2.48	1.62	2.45	0.46	1.90	1.39	1.54	1.78	1
13	3	P7	2.55	2.69	3.24	0.97	1.54	1.23	1.38	1.38	1
14	4	A6	2.44	4.01	3.30	2.82	1.54	1.34	1.38	1.50	1
15	4	A7	2.57	1.64	2.18	0.87	0.87	1.31	1.14	1.02	1
16	4	K21	3.55	2.90	3.34	1.92	1.05	0.31	0.72	0.68	1
17	4	O22	2.06	1.70	1.65	0.88	0.66	0.19	0.52	0.34	1
18	4	O3	3.95	2.63	3.53	1.64	0.76	0.30	0.50	0.60	1
19	4	P21	4.09	4.73	4.27	4.09	0.81	0.49	0.53	0.87	1
20	4	P8	2.98	3.09	3.05	2.51	0.58	0.60	0.78	0.29	1
21	5	G22	1.84	1.30	1.67	2.20	1.58	0.06	0.35	0.92	1
22	5	O12	2.94	1.54	2.54	0.73	0.80	0.83	0.85	0.97	1
23	1	M16	3.04	1.73	2.58	1.02	0.11	-0.54	-0.33	-0.11	1
24	1	N21	2.76	2.18	2.03	2.12	0.48	-0.12	0.20	0.22	1
25	2	A17	2.30	2.42	2.57	1.50	1.33	1.33	1.32	1.33	1

26	2	F17	3.31	1.67	2.89	1.37	0.39	0.33	0.39	0.35	1
27	2	F20	2.37	2.67	2.01	3.12	-0.41	-0.62	-0.68	-0.29	1
28	2	K1	2.01	2.54	2.20	1.71	-0.04	0.48	0.32	0.10	1
29	2	N20	3.44	2.27	3.06	1.92	0.58	0.01	0.42	0.07	1
30	3	F17	3.16	1.51	3.34	0.89	1.29	0.36	0.71	0.95	1
31	3	F18	4.19	2.97	4.06	2.23	1.58	0.79	1.08	1.28	1
32	3	G3	3.60	2.99	4.18	1.49	1.41	1.14	1.16	1.43	1
33	3	H14	3.24	1.87	3.76	1.55	1.33	0.62	0.79	1.23	1
34	3	I6	2.79	1.99	2.69	1.45	1.56	1.33	1.36	1.56	1
35	3	L11	2.34	2.00	2.55	0.38	1.43	1.23	1.22	1.48	1
36	3	L19	1.89	1.79	2.17	1.18	1.41	1.16	1.16	1.49	1
37	3	L4	2.04	1.68	2.49	0.54	1.33	1.42	1.37	1.32	1
38	3	L6	2.59	1.75	2.55	1.67	1.62	1.34	1.32	1.65	1
39	3	L7	2.42	1.20	2.10	0.66	1.26	0.95	1.02	1.25	1
40	3	M10	2.00	1.97	2.28	0.72	1.20	1.01	0.97	1.23	1
41	3	M11	1.97	1.78	2.32	0.79	1.56	1.32	1.26	1.69	1
42	3	M13	1.92	1.91	2.30	0.82	1.63	1.38	1.33	1.76	1
43	3	M14	2.57	1.98	2.71	0.76	1.41	1.44	1.40	1.49	1
44	3	M18	1.98	1.57	2.19	0.60	1.68	1.34	1.39	1.63	1
45	3	N1	2.18	1.86	2.83	0.85	0.97	1.18	1.04	1.11	1
46	3	N10	3.97	3.02	3.93	1.03	1.36	0.72	1.02	0.98	1
47	3	N11	2.13	1.82	2.42	0.65	1.41	1.11	1.19	1.43	1
48	3	N14	2.21	2.08	2.38	1.26	1.26	1.04	1.10	1.18	1
49	3	N15	3.17	1.97	2.71	1.54	0.38	-0.02	0.23	0.00	1
50	3	N5	2.22	1.72	1.83	1.24	1.13	1.20	1.07	1.30	1
51	3	N6	2.59	2.05	2.59	0.89	1.25	1.47	1.30	1.50	1
52	3	N7	2.30	2.30	2.68	0.84	1.27	1.33	1.30	1.35	1
53	3	N8	2.54	2.20	2.87	0.85	1.38	1.05	1.10	1.33	1
54	3	O11	1.78	1.79	2.45	0.73	1.32	1.16	1.17	1.29	1
55	3	O13	2.25	2.29	2.36	1.22	0.99	1.14	1.02	1.18	1
56	3	P17	1.83	2.58	2.56	1.12	1.13	1.34	1.17	1.33	1
57	3	P4	2.17	2.25	2.62	1.13	1.40	1.43	1.42	1.45	1
58	3	P5	1.55	2.18	1.97	0.38	1.20	1.39	1.18	1.47	1
59	3	P8	1.66	1.77	2.39	0.27	1.28	1.24	1.29	1.25	1
60	4	A12	1.38	2.09	1.84	1.12	0.89	0.96	0.93	0.85	1
61	4	P10	2.70	2.39	2.61	1.09	1.12	0.81	0.91	1.01	1
62	5	L3	2.16	1.14	1.57	1.13	1.04	0.17	0.27	0.88	1
63	5	P13	3.02	1.33	2.10	0.30	0.92	0.73	0.83	0.73	1
64	1	J18	2.13	0.07	1.68	-0.35	0.71	0.02	0.48	0.23	1
65	3	H3	1.82	1.58	2.39	0.65	1.23	1.10	1.06	1.26	1
66	3	M12	2.06	1.14	1.83	0.68	0.86	0.53	0.72	0.72	1
67	3	O4	2.32	2.07	2.09	1.73	1.06	1.39	1.26	1.17	1
68	5	H1	0.95	1.28	1.11	0.75	2.06	0.65	1.03	1.12	1
69	1	G7	2.06	0.13	1.03	-1.38	-0.20	-0.01	0.15	-0.55	2
70	1	M8	-1.88	-2.16	-2.10	-4.91	-0.20	-0.27	-0.53	0.17	2
71	2	A19	1.45	-0.05	0.59	-2.82	-0.97	-0.16	-0.02	-1.34	2
72	2	B12	-0.73	0.42	0.09	-0.85	0.52	1.86	1.59	0.79	2
73	2	O21	4.03	0.06	2.57	-2.27	-0.62	-0.46	-0.22	-0.99	2
74	2	P1	-0.83	0.52	0.03	-2.20	-0.08	1.06	0.91	0.01	2
75	3	B19	5.00	-0.42	1.07	-1.29	-0.03	1.28	1.19	-0.28	2
76	3	G11	1.70	-0.18	0.14	-2.76	-0.82	-1.07	-0.52	-1.54	2
77	3	G13	-0.63	1.74	0.64	-2.29	-0.04	-0.27	-0.37	0.07	2
78	3	G20	-0.59	0.25	-0.21	-2.14	-0.10	0.02	-0.28	0.29	2
79	3	I16	1.08	1.61	1.81	0.92	1.48	1.23	1.14	1.60	2
80	3	I19	0.31	0.26	0.31	-0.21	1.17	0.90	0.89	1.18	2
81	3	I2	-1.43	-0.25	-1.22	2.67	-0.50	-0.11	-0.38	-0.21	2
82	3	J16	-0.13	3.82	1.34	-3.57	-0.14	-0.39	-0.57	0.15	2
83	3	L17	1.72	-2.36	2.01	-1.31	-0.15	-0.57	-0.58	-0.03	2

84	3	L8	1.77	0.59	1.07	-0.05	1.25	2.22	1.93	1.54	2
85	3	M8	2.56	0.74	1.25	-3.96	0.10	0.07	-0.08	0.21	2
86	4	F20	0.46	-2.08	0.45	-1.63	0.04	-0.38	-0.36	0.07	2
87	4	L2	-2.43	0.43	-0.02	-1.55	0.07	0.17	0.06	0.21	2
88	5	J22	4.52	-1.70	1.10	-4.46	-0.58	-1.08	-0.67	-2.06	2
89	5	O1	7.08	3.15	4.85	-3.51	-0.16	0.91	0.96	-0.13	2
90	5	O15	1.25	-0.28	2.13	-2.33	3.01	0.85	1.41	0.54	2
91	5	O8	-0.44	-0.86	-0.29	-1.04	2.36	0.33	0.75	1.31	2
92	5	P15	0.22	0.30	0.66	-2.02	0.74	0.99	1.13	0.78	2
93	5	P2	0.41	1.50	1.52	-2.38	-0.76	1.75	1.57	0.20	2
94	5	P8	0.30	1.09	1.12	-4.94	-0.34	1.83	1.87	0.01	2
95	1	A10	3.18	0.21	3.11	-1.18	1.61	0.94	1.53	0.83	3
96	1	K15	1.55	-2.06	1.51	-3.42	1.11	-0.86	0.66	-0.80	3
97	2	A21	2.98	0.73	4.45	-2.04	2.11	0.83	1.61	0.99	3
98	2	G10	-0.90	-1.47	-0.39	-2.22	0.40	-1.00	0.03	-0.87	3
99	2	L1	3.67	2.07	3.70	0.05	1.30	0.64	1.19	0.61	3
100	3	D3	1.94	2.03	2.37	1.02	2.39	1.31	1.67	2.00	3
101	3	O10	0.36	0.37	1.34	-0.94	2.30	1.61	1.69	2.21	3
102	3	O19	1.70	2.03	1.97	1.39	1.09	0.27	0.58	0.61	3
103	4	P14	2.97	1.30	5.33	-2.53	2.06	0.89	1.57	1.09	3
104	4	P19	2.38	-0.97	1.56	-4.26	0.25	0.55	0.92	-0.57	3
105	5	B15	4.53	1.10	3.65	-0.60	3.37	0.23	0.96	1.36	3
106	5	O7	3.34	1.46	3.52	-1.09	2.00	0.85	1.21	1.26	3
107	2	J3	0.00	-1.14	-0.93	-4.02	-1.63	-1.43	-1.68	-1.36	4
108	2	J7	0.22	-0.67	-0.48	-4.27	-1.46	-2.29	-2.44	-1.47	4
109	2	L7	-0.85	-11.02	-0.90	-8.97	-3.32	-3.61	-4.22	-2.79	4
110	2	O15	-1.83	2.65	-0.83	-4.09	-1.38	-1.72	-2.11	-1.06	4
111	3	F22	-0.91	1.23	-0.67	-4.16	-0.30	-0.48	-0.64	-0.10	4
112	3	J9	-0.52	-0.78	-0.11	-3.96	-0.12	-0.98	-0.46	-0.84	4
113	3	K17	-0.44	0.12	-0.22	0.09	-1.41	-2.04	-2.10	-1.45	4
114	3	L22	-0.63	0.63	-0.15	2.76	-0.32	-0.70	-0.79	-0.15	4
115	4	H15	1.58	1.24	0.84	-4.08	-1.14	-1.88	-2.08	-1.06	4
116	4	K9	-0.47	0.30	-0.10	-0.28	-1.52	-2.11	-2.25	-1.58	4
117	5	F7	1.98	-1.02	-0.01	-2.10	-1.24	0.04	-0.19	-1.34	4
118	5	H18	-7.80	3.88	1.92	-6.13	-6.74	-0.20	-1.21	-3.36	4
119	1	E18	-1.50	-1.64	-1.71	-1.65	-2.34	-2.83	-2.98	-2.36	5
120	1	H21	-0.77	-0.47	-0.73	-0.25	-1.17	-1.93	-1.68	-1.50	5
121	1	K18	-1.19	-0.23	-1.07	-2.59	-2.70	-2.90	-3.26	-2.45	5
122	1	N13	-0.65	-0.77	-0.78	-0.74	-1.34	-2.12	-2.00	-1.52	5
123	1	N15	2.95	-0.09	2.70	0.75	0.47	-0.44	0.03	-0.04	5
124	2	D3	-0.87	-0.11	-0.84	0.55	-1.59	-1.96	-2.23	-1.44	5
125	2	E4	-0.51	-0.88	-0.59	-0.36	-1.31	-1.85	-2.03	-1.25	5
126	2	F3	-0.82	-0.90	-0.89	-0.02	-1.39	-1.90	-2.05	-1.38	5
127	2	G17	3.32	1.71	2.97	0.54	-0.92	-1.92	-1.63	-1.41	5
128	2	H3	1.34	0.30	-0.17	-0.91	-2.41	-2.63	-3.22	-1.94	5
129	2	J19	-2.26	-0.67	-1.88	-2.61	-2.82	-2.90	-3.26	-2.49	5
130	2	J9	1.35	2.36	0.09	2.67	-1.56	-1.67	-1.83	-1.46	5
131	2	L19	-0.83	0.05	-0.72	-0.46	-2.87	-3.13	-3.48	-2.57	5
132	2	N4	-1.34	-0.39	-0.95	-0.17	-1.13	-1.75	-2.01	-1.01	5
133	2	O3	-0.68	-0.17	-0.76	-0.50	-1.59	-1.85	-2.05	-1.51	5
134	3	D21	-1.10	2.59	-0.82	2.32	-1.05	-1.18	-1.29	-0.93	5
135	3	D9	-1.16	-0.14	-0.72	-2.56	-1.03	-1.61	-1.56	-1.09	5
136	3	M22	0.99	1.91	1.01	2.02	-0.62	-0.69	-0.63	-0.65	5
137	3	N22	-1.28	-2.49	-1.31	-1.71	-1.18	-1.25	-1.31	-1.12	5
138	3	O9	2.08	2.63	2.28	3.08	-0.08	-0.62	-0.43	-0.29	5
139	4	B16	1.90	1.38	0.82	2.86	-0.83	-1.17	-1.50	-0.65	5
140	4	C17	-0.40	-0.05	-0.32	-0.15	-1.48	-2.24	-2.37	-1.47	5

141	4	D19	-1.10	-1.33	-1.02	-0.91	-1.77	-2.51	-2.50	-1.98	5
142	4	D5	-0.86	-0.62	-1.03	-1.57	-1.59	-2.25	-2.42	-1.56	5
143	4	E10	-0.64	-0.27	-0.55	-0.82	-1.45	-2.13	-2.31	-1.39	5
144	4	E16	2.26	0.57	1.48	-0.01	-0.90	-1.78	-1.45	-1.36	5
145	4	E19	-0.11	-0.33	-0.04	-0.28	-1.05	-1.89	-2.02	-1.04	5
146	4	F15	0.05	2.31	1.09	0.82	-1.30	-2.04	-2.26	-1.24	5
147	4	G10	-1.36	0.39	-1.51	0.74	-2.73	-3.32	-3.50	-2.62	5
148	4	G13	2.75	1.51	1.87	-0.85	-0.61	-1.58	-1.67	-0.62	5
149	4	G18	0.43	-0.23	0.31	0.44	-0.92	-2.01	-1.73	-1.30	5
150	4	G22	0.93	0.50	1.14	0.57	-1.32	-2.24	-2.11	-1.57	5
151	4	H3	1.68	0.87	1.31	1.08	-1.40	-2.31	-1.90	-1.88	5
152	4	H6	-1.34	-0.55	-1.01	-1.10	-1.38	-2.02	-2.14	-1.39	5
153	4	H7	-0.22	-0.25	-0.80	0.10	-1.42	-1.94	-2.02	-1.41	5
154	4	I12	0.33	-0.89	-0.83	2.79	-1.43	-2.27	-2.27	-1.61	5
155	4	I15	0.19	0.58	0.58	0.14	-0.55	-1.38	-1.23	-0.76	5
156	4	I17	0.90	0.89	1.10	0.63	0.31	-0.33	-0.10	0.12	5
157	4	J12	-0.67	-0.98	-0.94	1.09	-1.35	-2.10	-2.13	-1.47	5
158	4	J19	0.32	0.43	-0.43	1.47	-2.85	-3.15	-3.49	-2.57	5
159	4	J9	1.15	1.65	0.97	2.02	-0.76	-1.59	-1.60	-0.88	5
160	4	K10	1.24	2.67	1.47	1.83	-0.59	-0.89	-0.86	-0.59	5
161	4	K12	0.21	0.17	-0.58	-0.28	-1.23	-2.07	-2.03	-1.40	5
162	4	K15	0.35	2.03	1.61	0.15	-1.04	-1.97	-2.08	-1.04	5
163	4	K16	2.25	1.85	2.35	1.47	-0.37	-1.54	-1.15	-0.87	5
164	4	K22	2.06	1.61	1.60	2.18	-0.47	-1.27	-0.98	-0.75	5
165	4	K3	-0.79	0.25	-0.41	-1.30	-1.67	-2.09	-2.34	-1.54	5
166	4	L12	0.31	0.72	0.10	1.72	-1.18	-1.98	-1.83	-1.42	5
167	4	L13	0.33	-0.31	-0.58	-0.26	-1.70	-2.37	-2.45	-1.72	5
168	4	L16	-1.10	0.22	-1.03	1.34	-2.17	-2.79	-2.95	-2.17	5
169	4	L19	0.11	-0.42	0.13	0.70	-1.53	-1.85	-2.04	-1.27	5
170	4	L7	1.60	0.76	0.45	6.77	-1.38	-2.00	-2.13	-1.38	5
171	4	M21	-0.44	0.83	-0.11	2.60	-0.71	-0.85	-0.92	-0.56	5
172	4	N10	-1.13	-1.54	-1.97	2.88	-1.47	-1.97	-2.18	-1.38	5
173	4	N14	-0.68	0.39	-0.75	-0.48	-1.50	-1.95	-2.10	-1.45	5
174	4	O8	-2.43	-0.72	-1.99	0.57	-1.91	-1.71	-1.87	-1.75	5
175	5	F16	1.55	-0.13	0.73	0.30	-2.73	-1.38	-1.84	-1.77	5
176	5	O6	3.62	1.47	0.27	-0.73	-4.17	1.19	0.98	-2.35	5
177	1	E13	-3.11	-1.95	-1.29	-3.19	-0.11	-0.40	-0.02	-0.70	6
178	1	F19	-1.45	1.29	-1.47	-4.23	-0.55	-1.17	-0.98	-0.75	6
179	1	J11	-2.39	-2.49	-3.52	-1.65	-2.68	-2.84	-3.20	-2.43	6
180	1	J19	-0.86	-6.65	-0.69	-4.68	-1.69	-2.24	-2.30	-1.67	6
181	1	K3	-1.37	-1.66	-2.62	-0.42	-1.31	-0.18	-0.36	-1.34	6
182	1	L19	-5.33	-5.33	-5.46	-4.52	-1.60	-1.78	-1.95	-1.34	6
183	1	M18	0.04	0.22	-0.12	-4.90	-1.79	-2.52	-2.56	-1.91	6
184	1	N7	-2.25	-1.32	-2.06	-1.78	-1.81	-1.46	-1.55	-1.89	6
185	1	O1	-1.01	-1.55	-1.15	-4.73	-1.95	-2.54	-2.73	-1.91	6
186	1	O18	-2.44	-2.71	-2.40	-3.09	-1.29	-0.38	-0.37	-1.56	6
187	1	P3	-0.70	-1.69	-1.65	-2.04	-1.48	-0.09	-0.22	-1.68	6
188	1	P6	1.01	-0.65	-1.28	-1.29	-1.97	-0.19	-0.55	-1.73	6
189	2	C14	1.14	1.01	0.90	-4.84	-0.85	-1.21	-1.58	-0.65	6
190	2	C4	-1.64	1.80	-0.01	-4.27	-1.29	-1.80	-2.06	-1.18	6
191	2	E9	-2.02	-2.45	-2.25	-1.33	-1.90	-1.68	-1.93	-1.66	6
192	2	G4	-1.32	-2.33	-1.39	-2.09	-1.22	-1.76	-2.00	-1.12	6
193	2	H20	-0.71	4.19	1.02	-4.21	-1.22	-1.02	-1.37	-0.83	6
194	2	H7	-1.21	-0.69	-1.38	-4.86	-1.77	-2.45	-2.72	-1.63	6
195	2	I22	-0.85	-1.13	-1.23	-0.60	-0.81	-1.19	-1.12	-0.97	6
196	2	I3	-3.05	0.61	-0.11	-4.57	-1.24	-1.44	-1.82	-1.00	6
197	2	J18	-8.66	2.84	0.23	-9.60	-3.41	-2.87	-3.53	-2.81	6
198	2	J22	0.01	1.45	0.15	-4.16	-1.35	-1.86	-2.16	-1.18	6

199	2	K2	-0.91	0.02	-0.62	-4.40	-1.39	-1.66	-1.96	-1.21	6
200	2	K4	-0.90	0.20	-0.68	-4.68	-1.45	-2.01	-2.30	-1.30	6
201	2	M2	-1.05	-0.65	-1.35	-3.24	-2.15	-2.53	-2.80	-1.98	6
202	2	M3	2.28	-0.66	-0.95	-3.65	-1.38	-1.58	-1.82	-1.28	6
203	2	M4	-1.52	-1.97	-1.74	-1.79	-1.43	-1.91	-2.07	-1.40	6
204	2	N10	-3.14	0.38	-1.43	-6.33	-3.06	-3.41	-3.85	-2.72	6
205	2	N2	-1.34	1.44	0.64	-1.98	-2.30	-0.96	-1.35	-2.07	6
206	2	N7	-4.89	-4.06	-4.19	-5.74	-3.06	-3.49	-3.93	-2.72	6
207	2	O19	-1.56	-1.16	-1.15	-1.38	-1.55	-1.68	-2.11	-1.20	6
208	2	O4	0.12	-2.16	0.11	-4.23	-1.25	-1.44	-1.75	-1.08	6
209	3	B22	0.16	1.66	0.29	2.47	-0.56	-1.02	-0.81	-0.78	6
210	3	C15	-1.82	0.37	-1.52	-4.59	-0.88	-1.49	-1.68	-0.83	6
211	3	C17	-1.57	1.49	-0.65	-4.04	-0.21	-0.26	-0.40	0.03	6
212	3	C20	-1.07	1.28	-1.05	-4.14	-0.55	-0.67	-0.75	-0.44	6
213	3	D22	-2.11	0.58	-0.94	-4.45	-0.99	-1.02	-1.10	-0.90	6
214	3	H22	0.84	0.59	0.60	-4.01	-0.61	-0.76	-0.86	-0.46	6
215	3	J1	0.25	2.55	1.41	-2.19	-1.47	-0.25	-0.35	-1.72	6
216	3	M17	3.91	1.57	0.99	-3.86	-1.12	-1.13	-1.22	-1.05	6
217	3	M20	1.14	-1.51	-0.74	-3.74	-0.37	-0.64	-0.75	-0.16	6
218	3	O17	-1.45	0.85	0.63	-1.81	-2.02	-1.08	-1.31	-1.99	6
219	3	O20	-0.70	1.46	-0.63	-4.08	-1.11	-1.05	-1.32	-0.77	6
220	4	B10	-4.98	2.76	-0.32	-4.05	-2.60	-2.21	-2.45	-2.52	6
221	4	D15	-0.52	-1.01	-0.50	-4.47	-0.96	-1.91	-1.96	-1.07	6
222	4	D16	-1.15	-1.53	-1.34	-4.31	-2.31	-3.03	-3.18	-2.32	6
223	4	H16	-0.15	-3.98	-0.08	-4.07	-1.51	-2.44	-2.51	-1.61	6
224	4	I22	0.70	0.27	0.69	0.35	0.13	-0.70	-0.38	-0.20	6
225	4	M11	-1.39	-4.73	-1.78	-4.50	-1.31	-2.17	-2.19	-1.44	6
226	4	M15	-0.45	0.28	-0.67	0.40	-1.68	-1.60	-1.84	-1.47	6
227	4	N12	-1.45	0.32	-0.53	-3.89	-1.14	-1.85	-1.91	-1.26	6
228	4	N16	0.40	1.81	0.57	-4.05	-1.66	-2.39	-2.49	-1.73	6
229	5	A1	-0.55	-0.97	-0.70	-1.10	-1.89	-0.76	-0.93	-1.43	6
230	5	F18	2.13	-1.88	-2.19	-3.44	-3.27	-0.42	-0.82	-2.25	6
231	5	I2	0.36	0.38	0.46	0.96	-0.34	-0.48	-0.49	-0.33	6
232	5	J15	-0.85	-1.06	-0.99	-3.27	-4.17	-1.72	-2.58	-2.44	6
233	5	O21	0.11	0.00	-0.46	-0.33	-2.01	-0.08	-0.52	-0.86	6
234	1	A1	-0.77	-0.70	-0.62	-1.49	0.21	0.59	0.49	0.31	n/a
235	1	A11	0.77	0.91	1.26	-0.21	1.09	1.42	1.30	1.25	n/a
236	1	A13	0.94	0.41	0.76	-0.28	0.67	0.98	0.97	0.66	n/a
237	1	A14	0.97	0.34	0.84	-0.82	0.72	0.99	1.00	0.69	n/a
238	1	A15	0.96	0.37	1.35	-0.04	1.01	1.22	1.19	1.10	n/a
239	1	A16	1.58	1.43	1.84	1.04	1.68	1.50	1.41	1.78	n/a
240	1	A17	-0.27	-0.17	0.03	-0.45	0.51	0.66	0.61	0.60	n/a
241	1	A18	-0.01	0.15	0.28	-0.69	0.79	0.87	0.88	0.78	n/a
242	1	A19	-0.32	-0.63	-0.41	-0.95	0.60	0.86	0.83	0.66	n/a
243	1	A2	0.25	0.10	0.33	-0.64	0.99	1.29	1.24	1.01	n/a
244	1	A20	0.66	0.32	0.72	-0.32	1.28	1.26	1.14	1.38	n/a
245	1	A21	0.07	-0.01	-0.07	-0.39	0.64	1.07	0.97	0.67	n/a
246	1	A22	-0.04	0.49	0.26	-0.12	0.57	0.95	0.75	0.79	n/a
247	1	A3	0.32	0.94	0.92	-0.24	0.55	0.92	0.79	0.65	n/a
248	1	A4	0.31	0.00	0.40	0.03	0.86	1.14	0.98	1.04	n/a
249	1	A5	-0.46	-0.30	-0.07	-0.80	0.84	0.80	0.75	0.91	n/a
250	1	A6	0.28	0.76	0.54	-0.37	0.95	1.28	1.14	1.06	n/a
251	1	A7	0.80	-0.05	0.39	-1.24	0.66	1.58	1.25	0.97	n/a
252	1	A8	0.88	0.34	0.79	-0.31	1.06	1.17	1.13	1.06	n/a
253	1	A9	-0.16	-0.11	-0.03	-1.12	0.59	1.24	1.04	0.75	n/a
254	1	B1	0.20	0.38	0.36	0.03	0.51	0.39	0.44	0.45	n/a
255	1	B10	0.20	0.15	0.45	0.10	1.23	0.67	0.90	1.05	n/a
256	1	B11	-0.22	-0.47	-0.17	-0.56	0.38	0.64	0.63	0.45	n/a

257	1	B12	-0.34	-0.13	0.21	-0.77	1.11	1.20	1.10	1.24	n/a
258	1	B13	0.73	0.91	1.35	0.05	0.84	0.93	0.95	0.83	n/a
259	1	B14	-0.02	-0.05	0.48	-0.19	0.95	0.99	0.98	0.92	n/a
260	1	B15	-0.32	0.12	0.14	-0.48	0.59	0.63	0.69	0.56	n/a
261	1	B16	0.29	0.38	0.60	-0.38	0.81	0.95	0.91	0.88	n/a
262	1	B17	0.47	0.02	0.82	-0.11	0.76	0.71	0.74	0.72	n/a
263	1	B18	0.08	0.50	0.52	-0.03	1.10	1.03	1.00	1.05	n/a
264	1	B19	-0.07	-0.83	-0.41	-0.42	0.45	0.53	0.49	0.48	n/a
265	1	B20	-0.12	-0.43	0.08	-0.62	0.98	1.00	0.99	0.92	n/a
266	1	B21	-0.61	-0.47	-0.19	-0.83	0.29	0.13	0.23	0.18	n/a
267	1	B22	-0.04	0.24	0.48	-0.74	0.68	0.74	0.65	0.77	n/a
268	1	B3	-0.36	-0.74	-0.32	-0.61	0.91	0.58	0.68	0.84	n/a
269	1	B4	1.63	0.78	1.85	0.35	1.46	0.83	1.23	0.93	n/a
270	1	B5	-0.25	-0.25	0.06	-0.75	1.10	1.11	1.04	1.19	n/a
271	1	B6	-0.05	-0.13	0.18	-0.72	0.99	0.93	1.06	0.84	n/a
272	1	B7	-0.11	-0.83	-0.17	-0.86	0.90	1.07	1.03	0.94	n/a
273	1	B8	0.14	0.23	0.01	0.07	0.86	0.91	0.84	0.96	n/a
274	1	B9	-0.10	-0.42	0.01	-0.80	0.99	1.17	1.09	1.11	n/a
275	1	C1	0.02	0.24	0.34	-0.29	0.36	0.02	0.11	0.30	n/a
276	1	C11	-0.51	-0.99	-0.64	-0.95	-0.08	-0.20	0.03	-0.33	n/a
277	1	C12	-0.18	-0.29	-0.03	-0.59	1.14	1.30	1.26	1.23	n/a
278	1	C13	-1.09	-0.75	-0.72	-0.81	0.30	0.14	0.34	0.03	n/a
279	1	C14	0.22	0.89	0.40	0.74	0.14	0.49	0.49	0.12	n/a
280	1	C15	0.18	0.17	0.40	-0.44	1.01	0.88	0.91	0.99	n/a
281	1	C16	0.38	-0.16	0.71	-0.51	0.54	0.27	0.40	0.40	n/a
282	1	C17	0.13	-0.27	-0.04	0.07	0.59	0.71	0.59	0.72	n/a
283	1	C18	0.69	0.37	0.64	-0.13	0.32	-0.03	0.17	0.12	n/a
284	1	C19	0.12	-0.26	-0.19	0.22	0.77	0.63	0.75	0.65	n/a
285	1	C2	-0.26	-0.42	-0.33	-0.50	0.35	0.63	0.57	0.40	n/a
286	1	C20	-0.79	-0.46	-0.79	-0.51	0.70	0.39	0.55	0.53	n/a
287	1	C21	0.02	-0.81	-0.04	-0.48	0.48	0.11	0.31	0.22	n/a
288	1	C22	-0.34	-0.88	-0.24	-0.79	0.53	0.40	0.47	0.46	n/a
289	1	C3	-0.14	-0.95	-0.31	-0.63	0.94	0.66	0.77	0.83	n/a
290	1	C4	-0.18	-0.04	-0.13	-0.36	0.85	0.78	0.89	0.76	n/a
291	1	C5	0.03	-0.28	0.11	-0.19	0.94	0.89	0.86	0.98	n/a
292	1	C7	-0.21	0.12	0.76	-0.34	1.05	1.11	1.03	1.14	n/a
293	1	C8	0.09	-0.50	-0.48	-0.14	0.61	0.51	0.55	0.57	n/a
294	1	C9	0.16	-0.19	0.21	-0.34	0.84	0.94	0.87	0.90	n/a
295	1	D1	-0.20	-0.33	-0.37	0.13	0.73	0.16	0.40	0.50	n/a
296	1	D10	-0.53	-1.23	-0.68	-0.68	0.01	-0.44	-0.13	-0.41	n/a
297	1	D11	-0.44	-0.15	-0.34	-0.36	0.46	0.11	0.26	0.26	n/a
298	1	D12	0.09	-0.89	-0.10	-0.65	0.65	0.43	0.56	0.60	n/a
299	1	D13	-1.81	-1.65	-1.57	-1.61	0.34	0.33	0.36	0.35	n/a
300	1	D14	0.66	0.35	0.51	-0.01	0.83	1.06	0.94	1.01	n/a
301	1	D15	-0.12	-0.07	-0.05	0.07	0.22	0.28	0.38	0.15	n/a
302	1	D16	-0.61	-0.24	-0.29	-0.86	0.63	0.59	0.64	0.63	n/a
303	1	D17	-0.29	-0.14	-0.35	-0.05	0.40	0.24	0.34	0.30	n/a
304	1	D18	-0.20	0.15	-0.09	-0.13	0.56	0.53	0.63	0.51	n/a
305	1	D19	-0.55	-1.03	-0.57	-0.60	-0.22	-0.77	-0.58	-0.43	n/a
306	1	D2	0.12	-0.27	0.03	-0.07	0.78	0.45	0.55	0.74	n/a
307	1	D20	-0.36	-0.54	-0.32	-0.13	0.08	-0.17	0.11	-0.20	n/a
308	1	D21	-0.65	-0.64	-0.76	-0.62	-0.01	0.27	0.28	-0.06	n/a
309	1	D22	-0.57	-0.72	-0.52	-0.08	0.36	0.09	0.27	0.09	n/a
310	1	D3	-0.60	-0.79	-0.49	-1.11	0.53	0.34	0.42	0.42	n/a
311	1	D4	-0.32	-0.47	-0.39	-0.71	0.45	0.14	0.32	0.26	n/a
312	1	D5	0.97	0.77	1.16	0.70	0.36	0.18	0.44	0.06	n/a
313	1	D6	0.02	0.18	0.30	0.12	0.38	0.60	0.53	0.47	n/a
314	1	D7	0.41	-0.26	0.00	0.12	0.87	0.82	0.78	0.97	n/a

315	1	D8	-0.38	-0.67	-0.04	-0.85	0.22	-0.18	0.03	-0.05	n/a
316	1	D9	0.01	-0.23	-0.18	-0.19	0.64	0.61	0.68	0.55	n/a
317	1	E1	-0.39	-0.29	-0.16	-0.45	0.35	-0.04	0.11	0.23	n/a
318	1	E10	0.31	0.41	0.47	0.16	0.35	0.36	0.45	0.26	n/a
319	1	E11	-0.84	-0.49	-1.03	-0.48	0.32	0.42	0.40	0.37	n/a
320	1	E12	0.06	-0.62	-0.05	-0.49	0.40	0.42	0.46	0.40	n/a
321	1	E14	-0.04	-0.34	0.11	-0.57	0.73	0.62	0.62	0.75	n/a
322	1	E15	-0.16	-0.55	-0.14	-0.84	0.74	0.63	0.81	0.57	n/a
323	1	E16	-0.61	-0.59	-0.57	0.03	0.14	-0.33	0.02	-0.20	n/a
324	1	E17	0.17	-0.05	-0.01	-0.72	0.55	0.49	0.51	0.59	n/a
325	1	E19	0.15	-0.25	-0.35	0.26	0.42	0.32	0.37	0.41	n/a
326	1	E2	-0.58	-0.22	-0.38	0.16	0.30	0.23	0.27	0.29	n/a
327	1	E21	0.21	0.32	0.75	-0.14	0.74	0.42	0.55	0.67	n/a
328	1	E22	1.13	-0.07	0.48	0.76	0.00	-0.01	0.10	-0.13	n/a
329	1	E3	-0.57	-0.72	-0.45	-0.97	0.23	-0.08	0.13	0.04	n/a
330	1	E4	0.48	-0.16	0.23	-0.14	0.40	0.02	0.23	0.20	n/a
331	1	E5	-0.15	-0.49	-0.19	-0.13	0.76	0.54	0.67	0.64	n/a
332	1	E6	0.82	-0.15	0.06	0.74	0.57	0.38	0.55	0.47	n/a
333	1	E7	0.04	0.30	0.31	0.47	0.84	0.70	0.78	0.73	n/a
334	1	E8	-0.02	-0.29	0.00	-0.78	0.41	0.39	0.53	0.23	n/a
335	1	E9	0.06	0.15	0.11	-0.13	0.64	0.56	0.55	0.61	n/a
336	1	F1	0.93	1.28	0.96	1.12	0.15	-0.12	0.03	-0.02	n/a
337	1	F11	-0.52	-1.02	-0.98	-0.86	-0.81	-1.46	-1.30	-1.08	n/a
338	1	F12	0.22	-0.35	0.26	-0.31	0.44	0.34	0.45	0.34	n/a
339	1	F13	-0.44	-0.47	-0.39	-0.31	0.28	0.36	0.41	0.25	n/a
340	1	F14	0.34	0.07	-0.03	0.44	0.45	0.49	0.57	0.42	n/a
341	1	F15	-0.79	-0.44	-0.70	-0.46	0.09	0.13	0.22	0.00	n/a
342	1	F16	-0.24	-0.30	-0.18	-0.06	0.43	0.01	0.12	0.31	n/a
343	1	F17	-0.36	-0.87	-0.62	0.24	-0.05	-0.64	-0.40	-0.26	n/a
344	1	F18	0.11	-0.04	-0.12	0.07	0.48	0.45	0.52	0.45	n/a
345	1	F2	0.03	-0.72	-0.52	-0.45	0.16	0.00	0.08	0.11	n/a
346	1	F20	-0.18	-0.77	-0.18	-0.74	0.19	-0.43	-0.07	-0.19	n/a
347	1	F21	0.97	0.34	0.90	0.60	0.33	0.31	0.43	0.13	n/a
348	1	F22	-0.36	-0.70	-0.66	-0.40	0.15	-0.24	-0.03	-0.04	n/a
349	1	F3	0.14	-0.69	-0.23	0.20	0.08	0.17	0.20	0.01	n/a
350	1	F4	-0.27	-0.61	-0.71	0.21	0.13	-0.30	-0.11	-0.01	n/a
351	1	F5	-0.21	0.09	0.06	-0.07	0.37	0.40	0.39	0.41	n/a
352	1	F6	-0.15	-0.85	-0.59	0.01	0.28	0.37	0.47	0.23	n/a
353	1	F7	-0.17	-0.47	-0.14	-0.50	0.44	0.56	0.62	0.44	n/a
354	1	F8	-0.16	-0.27	-0.27	0.08	0.44	0.50	0.43	0.50	n/a
355	1	F9	-0.75	-1.34	-1.15	-0.78	0.00	-0.83	-0.35	-0.45	n/a
356	1	G1	-0.04	-0.38	0.06	-0.31	-0.15	-0.51	-0.41	-0.24	n/a
357	1	G10	-0.49	-0.89	-0.90	-0.70	-0.06	-0.15	-0.02	-0.22	n/a
358	1	G11	-0.69	-0.58	-0.65	-0.50	0.18	-0.15	0.02	0.03	n/a
359	1	G12	-0.49	-0.51	-0.40	-0.48	0.42	0.73	0.64	0.59	n/a
360	1	G13	-0.26	-1.06	-0.45	-0.40	-0.20	-1.01	-0.54	-0.69	n/a
361	1	G14	-0.65	-0.38	-0.70	0.02	0.44	0.37	0.46	0.43	n/a
362	1	G15	-0.25	0.17	-0.38	0.45	0.45	0.12	0.25	0.34	n/a
363	1	G16	-0.40	-0.45	-0.27	-0.58	0.45	0.10	0.26	0.33	n/a
364	1	G17	-0.44	-0.97	-0.37	-0.90	0.41	-0.11	0.10	0.16	n/a
365	1	G18	-0.99	-0.80	-1.35	-0.72	-1.18	-1.85	-1.56	-1.57	n/a
366	1	G19	0.38	-0.01	0.54	-0.33	0.34	0.06	0.29	0.16	n/a
367	1	G2	-0.22	-1.36	-0.90	-1.06	-0.35	-0.48	-0.36	-0.48	n/a
368	1	G20	-0.26	-0.06	-0.33	0.09	-0.07	-0.13	-0.04	-0.22	n/a
369	1	G21	0.39	-0.50	0.26	-0.20	0.39	0.20	0.31	0.25	n/a
370	1	G22	-0.75	-0.63	-0.68	-0.70	0.02	-0.08	0.01	-0.10	n/a
371	1	G3	-1.02	-1.98	-1.95	-0.89	-0.98	-0.43	-0.23	-1.67	n/a
372	1	G6	-0.43	-0.19	-0.58	-0.27	0.56	0.66	0.69	0.48	n/a

373	1	G8	-0.14	-0.44	-0.14	-0.33	0.27	0.10	0.26	0.07	n/a
374	1	G9	-0.64	-0.12	-0.36	-0.40	-0.64	-0.71	-0.71	-0.67	n/a
375	1	H1	-0.16	-0.26	-0.08	0.28	0.05	-0.45	-0.26	-0.12	n/a
376	1	H10	-0.65	-1.08	-0.94	-0.42	-0.30	-0.98	-0.65	-0.67	n/a
377	1	H11	-0.11	-0.66	-0.62	-0.08	0.15	-0.01	0.15	0.00	n/a
378	1	H12	-0.03	-0.18	0.13	0.09	0.50	-0.06	0.11	0.40	n/a
379	1	H13	0.38	-0.30	0.08	0.32	-0.37	-0.65	-0.47	-0.57	n/a
380	1	H14	-0.72	-0.93	-0.64	-0.26	0.59	0.10	0.23	0.51	n/a
381	1	H15	-0.27	-0.96	-1.03	-0.30	0.16	-0.24	-0.02	-0.06	n/a
382	1	H16	-0.01	-0.27	-0.42	0.02	0.20	0.05	0.11	0.18	n/a
383	1	H17	-0.66	-0.82	-0.95	-0.04	-0.27	-0.74	-0.50	-0.52	n/a
384	1	H18	1.20	0.77	1.32	0.52	0.26	-0.47	-0.06	-0.15	n/a
385	1	H2	0.01	0.31	0.12	-0.17	0.22	0.38	0.25	0.40	n/a
386	1	H20	-0.66	-0.83	-0.84	-0.21	-0.05	-0.38	-0.27	-0.10	n/a
387	1	H22	-0.59	-0.45	-0.26	-0.09	-0.52	-0.85	-0.69	-0.70	n/a
388	1	H3	0.04	-0.10	-0.06	-0.17	0.28	-0.08	0.02	0.22	n/a
389	1	H4	-0.97	-0.91	-0.85	-0.59	0.07	-0.24	-0.02	-0.16	n/a
390	1	H5	-0.57	-0.21	-0.50	0.04	0.19	-0.01	0.22	-0.14	n/a
391	1	H6	-0.42	-0.34	-0.46	-0.30	0.35	0.21	0.41	0.15	n/a
392	1	H7	-0.59	-0.57	-0.51	-0.64	0.40	0.54	0.47	0.50	n/a
393	1	H8	-1.22	-0.88	-1.21	-0.23	-0.27	-0.97	-0.65	-0.61	n/a
394	1	H9	-0.47	-1.11	-0.85	-0.77	0.18	-0.33	-0.04	-0.15	n/a
395	1	I1	-0.68	-0.68	-0.85	-0.74	0.15	-0.43	-0.17	-0.09	n/a
396	1	I10	-0.49	-1.36	-0.79	-0.56	0.53	0.27	0.35	0.53	n/a
397	1	I11	-0.61	-0.66	-0.84	-0.06	0.22	-0.28	-0.07	0.03	n/a
398	1	I12	-0.46	-0.97	-0.89	-0.83	0.06	-0.30	-0.04	-0.18	n/a
399	1	I13	0.06	-0.54	-0.30	-0.55	0.39	-0.09	0.00	0.38	n/a
400	1	I14	-0.83	-0.85	-0.69	-0.32	0.43	0.05	0.20	0.32	n/a
401	1	I15	-0.60	-0.87	-0.46	-0.92	0.48	0.09	0.25	0.36	n/a
402	1	I16	0.43	0.27	0.64	0.33	0.52	0.14	0.33	0.35	n/a
403	1	I17	-0.19	-0.51	-0.21	-0.26	0.26	-0.40	-0.05	-0.09	n/a
404	1	I18	-0.75	-0.82	-0.83	-0.50	-0.47	-1.28	-0.76	-1.06	n/a
405	1	I19	0.29	0.06	-0.03	-0.58	0.22	0.05	0.08	0.25	n/a
406	1	I2	-0.06	-0.35	-0.32	-0.16	0.15	-0.02	0.20	-0.08	n/a
407	1	I20	-0.70	-0.50	-0.33	-0.38	0.71	0.64	0.71	0.71	n/a
408	1	I21	-0.51	-0.55	-0.80	-0.24	-0.39	-1.06	-0.76	-0.68	n/a
409	1	I22	-0.79	-0.63	-0.90	-0.27	-0.03	-0.43	-0.23	-0.24	n/a
410	1	I3	-0.31	-0.33	0.18	-0.82	0.39	0.17	0.22	0.34	n/a
411	1	I4	-0.02	-0.82	-0.89	0.17	0.06	-0.47	-0.13	-0.29	n/a
412	1	I5	0.18	-0.28	0.00	-0.14	0.50	0.38	0.54	0.37	n/a
413	1	I7	0.08	-0.31	-0.12	-0.42	0.53	0.22	0.38	0.39	n/a
414	1	I8	-0.01	-0.41	-0.07	-0.55	0.23	-0.18	0.03	0.03	n/a
415	1	I9	0.02	-0.68	-0.30	-0.41	0.51	0.07	0.25	0.40	n/a
416	1	J1	-0.37	0.01	-0.01	0.27	0.28	-0.26	-0.04	0.07	n/a
417	1	J10	-0.31	-0.76	-0.79	-0.07	0.33	-0.26	0.10	-0.01	n/a
418	1	J12	-0.25	-0.46	-0.04	-0.37	0.67	-0.11	0.19	0.40	n/a
419	1	J13	-0.69	-0.55	-0.68	-0.87	-0.47	-1.11	-0.93	-0.62	n/a
420	1	J14	-0.14	0.00	0.12	0.13	0.59	0.05	0.25	0.39	n/a
421	1	J15	0.24	-0.08	-0.13	-0.06	-0.16	-0.69	-0.31	-0.55	n/a
422	1	J16	-0.50	-0.56	-0.52	-0.10	0.56	-0.20	0.11	0.29	n/a
423	1	J17	-0.44	-0.42	-0.71	-0.01	0.36	0.08	0.18	0.32	n/a
424	1	J2	-0.02	0.39	0.12	0.03	0.34	0.18	0.23	0.29	n/a
425	1	J20	-0.11	-0.08	0.01	0.35	0.14	-0.59	-0.24	-0.20	n/a
426	1	J21	-0.18	0.03	-0.15	0.16	0.28	-0.16	0.05	0.08	n/a
427	1	J22	0.30	-0.17	-0.02	-0.12	-0.06	-0.28	-0.19	-0.10	n/a
428	1	J3	-0.10	-1.14	-0.54	-0.28	0.09	-0.03	0.05	0.02	n/a
429	1	J4	-0.32	-0.40	-0.47	-0.16	0.09	-0.14	-0.03	-0.07	n/a
430	1	J5	-0.28	-0.44	-0.46	0.02	-0.03	-0.09	0.06	-0.16	n/a

431	1	J6	0.42	0.25	0.53	0.00	0.32	0.27	0.38	0.25	n/a
432	1	J7	1.44	0.44	1.37	0.15	0.58	0.01	0.24	0.34	n/a
433	1	J8	-0.36	-0.85	-0.48	-0.39	-0.09	-1.00	-0.63	-0.48	n/a
434	1	J9	-0.52	-0.79	-0.60	-0.02	0.32	0.17	0.20	0.33	n/a
435	1	K1	-0.42	-0.61	-0.63	-0.13	-0.19	-0.58	-0.44	-0.33	n/a
436	1	K10	0.31	-0.34	0.28	-0.24	0.25	-0.25	-0.04	0.11	n/a
437	1	K11	0.03	-0.38	-0.19	-0.25	-0.14	-0.50	-0.34	-0.25	n/a
438	1	K13	-0.07	0.00	-0.06	0.18	0.03	-1.14	-0.50	-0.63	n/a
439	1	K14	0.45	0.20	0.25	0.59	0.53	0.31	0.42	0.43	n/a
440	1	K16	-0.06	-0.03	0.10	0.09	0.16	-0.35	-0.12	-0.02	n/a
441	1	K17	-0.85	-0.33	-0.48	-0.54	0.24	-0.38	-0.09	0.00	n/a
442	1	K19	-0.32	-0.11	-0.27	0.37	0.48	0.11	0.24	0.39	n/a
443	1	K2	-0.20	-0.76	-0.66	-0.37	0.22	-0.04	0.16	0.05	n/a
444	1	K20	-0.23	-0.33	-0.27	0.32	0.00	0.09	0.13	0.00	n/a
445	1	K21	-0.55	-0.70	-0.43	0.04	-0.55	-1.03	-0.92	-0.69	n/a
446	1	K22	-0.49	-0.53	-1.08	0.21	-0.63	-0.82	-0.72	-0.71	n/a
447	1	K4	0.55	0.24	0.44	0.32	0.41	-0.35	0.13	-0.09	n/a
448	1	K5	-0.42	-1.17	-0.77	-0.97	0.23	-0.36	-0.07	-0.05	n/a
449	1	K6	0.10	-0.19	0.33	-0.31	0.45	0.19	0.26	0.40	n/a
450	1	K7	0.45	0.34	0.27	0.40	0.25	0.47	0.46	0.26	n/a
451	1	K8	0.25	-0.53	0.17	-0.15	-0.10	-0.30	-0.23	-0.14	n/a
452	1	K9	0.15	-0.28	0.03	-0.66	0.26	0.14	0.25	0.21	n/a
453	1	L1	-0.28	-0.25	-0.47	0.16	-0.19	-0.26	-0.25	-0.16	n/a
454	1	L10	-0.20	-0.01	-0.55	-0.04	-0.56	-1.44	-1.04	-1.02	n/a
455	1	L11	-1.20	-0.65	-1.50	0.55	-0.86	-1.50	-1.43	-0.91	n/a
456	1	L12	0.68	0.62	0.63	0.85	0.53	-0.14	0.16	0.24	n/a
457	1	L13	-0.43	-0.58	-0.31	-0.55	0.00	-0.84	-0.46	-0.38	n/a
458	1	L14	0.93	0.43	0.52	0.43	0.37	-0.42	-0.01	0.01	n/a
459	1	L15	-0.06	0.50	0.02	0.83	-0.41	-0.83	-0.67	-0.55	n/a
460	1	L16	0.40	0.67	0.38	1.00	0.35	-0.16	0.01	0.22	n/a
461	1	L17	0.94	-0.07	0.75	0.83	0.09	-0.91	-0.45	-0.37	n/a
462	1	L18	0.22	-0.05	-0.34	0.58	-0.03	-0.74	-0.40	-0.36	n/a
463	1	L2	-0.65	-0.11	-0.58	-0.16	0.12	-0.14	0.02	-0.01	n/a
464	1	L20	-0.25	-0.40	-0.28	-0.18	-0.11	-0.77	-0.43	-0.44	n/a
465	1	L21	-0.33	-0.77	-0.58	0.13	0.06	-0.52	-0.14	-0.31	n/a
466	1	L22	-0.40	-0.21	-0.50	-0.16	0.18	0.09	0.16	0.13	n/a
467	1	L3	-0.36	0.01	-0.18	0.03	0.20	0.12	0.17	0.18	n/a
468	1	L4	0.21	-0.56	0.02	-0.11	-0.02	-0.45	-0.26	-0.19	n/a
469	1	L5	0.46	-0.31	-0.16	0.34	0.11	-0.33	-0.17	-0.07	n/a
470	1	L6	-0.01	-0.53	-0.12	0.11	0.35	-0.16	0.08	0.12	n/a
471	1	L7	-0.02	-0.46	-0.15	0.19	-0.13	-0.33	-0.32	-0.11	n/a
472	1	L8	0.44	0.23	0.02	0.51	0.22	0.03	0.13	0.22	n/a
473	1	L9	0.10	0.01	-0.02	0.41	-0.07	-0.80	-0.44	-0.38	n/a
474	1	M10	0.04	-0.38	-0.42	0.13	0.26	-0.01	0.13	0.15	n/a
475	1	M11	-0.53	-0.18	-0.52	-0.12	-0.04	-0.42	-0.20	-0.26	n/a
476	1	M12	0.36	0.01	0.43	-0.14	0.19	-0.24	-0.08	0.08	n/a
477	1	M13	0.43	-0.02	0.39	0.37	0.24	-0.26	-0.05	0.08	n/a
478	1	M14	0.44	0.57	0.28	0.08	0.35	0.12	0.20	0.32	n/a
479	1	M15	0.26	0.08	-0.01	0.10	0.47	0.02	0.23	0.26	n/a
480	1	M17	1.60	1.03	0.93	1.42	-0.03	-0.16	-0.04	-0.14	n/a
481	1	M19	0.17	0.16	-0.07	0.31	0.12	0.03	0.11	0.10	n/a
482	1	M2	-0.19	-0.44	-0.29	-0.77	0.00	-0.06	-0.06	-0.01	n/a
483	1	M20	0.10	-0.02	0.00	0.18	0.15	0.02	0.17	0.01	n/a
484	1	M21	-0.45	-0.88	-0.92	0.08	-0.80	-1.37	-1.24	-0.91	n/a
485	1	M22	0.90	0.49	0.69	0.55	0.20	-0.02	0.09	0.12	n/a
486	1	M3	0.01	-0.73	-0.34	0.11	0.20	-0.10	0.08	0.04	n/a
487	1	M4	-0.14	-0.46	-0.44	-0.79	-0.19	-0.55	-0.28	-0.46	n/a
488	1	M5	0.06	-0.40	-0.43	0.15	0.09	-0.07	-0.01	0.07	n/a

489	1	M6	-0.01	0.01	-0.05	0.10	0.11	0.06	0.08	0.12	n/a
490	1	M7	0.03	-0.68	-0.15	-0.60	0.26	0.06	0.12	0.21	n/a
491	1	M9	-0.05	-0.42	-0.13	-0.53	0.07	-0.33	-0.04	-0.28	n/a
492	1	N1	-0.67	-0.26	-0.42	-0.26	-0.18	-0.27	-0.23	-0.17	n/a
493	1	N10	-0.38	0.43	-0.24	0.78	-0.90	-1.69	-1.52	-1.13	n/a
494	1	N11	-0.07	-1.36	-0.46	-0.49	-0.47	-1.05	-0.79	-0.76	n/a
495	1	N12	-0.16	-0.45	-0.16	0.02	-0.09	-0.37	-0.25	-0.22	n/a
496	1	N14	-0.21	-0.18	-0.17	0.55	0.42	-0.16	-0.02	0.34	n/a
497	1	N16	-0.09	-0.39	0.09	0.21	0.27	-0.13	0.02	0.18	n/a
498	1	N17	0.14	-0.18	-0.20	0.59	-0.05	-0.51	-0.19	-0.34	n/a
499	1	N18	0.11	-0.61	-0.07	0.28	0.15	-0.50	-0.24	-0.04	n/a
500	1	N19	-0.23	-1.66	-0.21	-0.43	-0.54	-0.86	-0.93	-0.43	n/a
501	1	N2	-0.21	-0.34	-0.52	0.11	-0.10	-0.05	-0.02	-0.18	n/a
502	1	N20	-0.39	-0.72	-0.61	-0.31	-0.11	-0.75	-0.52	-0.33	n/a
503	1	N22	-0.44	-0.11	-0.30	0.15	0.02	-0.55	-0.23	-0.29	n/a
504	1	N3	-0.36	-1.05	-0.77	-0.61	-0.06	-0.35	-0.24	-0.17	n/a
505	1	N4	0.30	-0.15	0.18	0.37	-0.28	-0.33	-0.32	-0.24	n/a
506	1	N5	-0.05	-0.73	-0.62	-0.29	-0.19	-0.31	-0.24	-0.23	n/a
507	1	N6	0.17	-0.38	0.02	0.23	0.05	-0.05	0.08	-0.07	n/a
508	1	N8	1.29	0.33	0.34	1.19	-0.29	-0.52	-0.29	-0.48	n/a
509	1	N9	-0.74	-0.73	-0.99	0.19	-0.48	-1.02	-0.81	-0.70	n/a
510	1	O10	-0.56	-0.48	-0.53	-0.29	0.17	0.14	0.13	0.22	n/a
511	1	O11	-0.30	0.15	-0.55	0.41	-0.01	0.02	-0.01	0.04	n/a
512	1	O12	-0.68	-0.48	-0.65	-0.41	0.16	0.01	0.01	0.19	n/a
513	1	O13	0.31	0.09	0.20	0.34	-0.04	0.11	0.11	-0.03	n/a
514	1	O14	-0.54	-0.06	-0.25	-0.34	0.14	0.00	0.10	-0.02	n/a
515	1	O15	-0.11	-0.19	-0.30	0.49	0.00	-0.45	-0.22	-0.22	n/a
516	1	O16	0.04	-0.48	-0.24	-0.14	-0.16	-0.10	-0.06	-0.15	n/a
517	1	O17	1.34	0.90	1.32	0.77	0.54	0.40	0.43	0.60	n/a
518	1	O19	-0.43	-0.69	-0.65	-0.06	0.11	-0.11	0.09	-0.10	n/a
519	1	O2	-0.55	-0.61	-0.53	-0.03	-0.07	0.06	0.08	-0.10	n/a
520	1	O20	-0.58	0.32	-0.38	0.22	-0.11	0.02	-0.02	-0.03	n/a
521	1	O21	-0.49	-0.30	-0.45	-0.25	-0.13	-0.59	-0.41	-0.28	n/a
522	1	O22	-0.59	0.04	-0.46	0.66	-0.02	-0.32	-0.27	-0.05	n/a
523	1	O3	-0.20	-0.53	-0.51	-0.57	-0.37	-0.62	-0.58	-0.37	n/a
524	1	O4	0.28	-0.10	0.02	0.07	-0.04	-0.29	-0.11	-0.18	n/a
525	1	O5	-0.03	0.01	-0.13	0.24	-0.15	-0.24	-0.18	-0.17	n/a
526	1	O6	-0.11	-0.66	-0.37	-0.59	-0.32	-0.32	-0.33	-0.28	n/a
527	1	O7	0.43	0.43	0.67	0.42	0.43	0.31	0.45	0.31	n/a
528	1	O8	0.22	-0.84	-0.45	0.12	-0.64	-0.34	-0.49	-0.48	n/a
529	1	O9	0.09	-0.42	-0.03	-0.38	-0.31	0.11	0.12	-0.32	n/a
530	1	P1	-0.75	-0.57	-0.67	-0.14	-0.21	-0.12	-0.03	-0.31	n/a
531	1	P10	-0.05	-0.33	-0.68	-0.22	-0.94	-0.25	-0.47	-0.67	n/a
532	1	P11	0.16	0.13	-0.04	0.59	0.23	0.16	0.13	0.24	n/a
533	1	P12	-0.35	-0.37	-0.42	-0.31	0.10	0.17	0.16	0.15	n/a
534	1	P13	1.30	-0.02	0.64	0.13	0.30	0.00	0.26	0.09	n/a
535	1	P14	-0.85	-0.62	-0.84	-0.17	0.28	0.05	0.28	0.05	n/a
536	1	P15	0.36	-1.41	-0.10	-1.20	0.49	-0.45	0.08	-0.01	n/a
537	1	P16	-0.48	-0.42	-0.58	-0.14	0.13	0.12	0.08	0.23	n/a
538	1	P17	-0.34	-0.83	-0.60	-0.74	0.10	0.00	0.10	0.06	n/a
539	1	P18	-0.15	-0.39	-0.08	-0.24	0.22	0.06	0.17	0.14	n/a
540	1	P19	-0.52	-0.28	-0.47	0.07	0.24	-0.09	0.06	0.12	n/a
541	1	P20	-0.49	-0.20	-0.42	-0.09	-0.12	-0.29	-0.25	-0.11	n/a
542	1	P21	-0.73	-0.43	-0.57	-0.42	-0.36	-0.74	-0.49	-0.64	n/a
543	1	P5	-0.03	0.44	0.25	0.19	0.06	0.13	0.07	0.09	n/a
544	1	P7	-0.31	-0.42	-0.01	-0.24	0.02	0.05	0.05	0.04	n/a
545	1	P8	0.10	0.29	0.02	0.21	0.01	0.00	-0.07	0.10	n/a
546	1	P9	-0.18	-0.57	-0.42	-0.27	-0.08	0.02	-0.02	-0.05	n/a

547	2	A1	-0.91	-0.61	-0.48	-1.39	0.64	1.32	1.14	0.76	n/a
548	2	A12	-0.16	1.09	0.74	-0.58	0.83	1.38	1.24	0.98	n/a
549	2	A13	0.13	0.29	0.35	-0.61	0.73	1.23	1.08	0.85	n/a
550	2	A15	-0.62	0.11	0.09	-0.63	0.88	1.18	1.05	0.98	n/a
551	2	A18	0.31	0.87	0.87	0.25	0.84	1.24	1.08	0.98	n/a
552	2	A2	0.27	-0.16	0.65	-1.31	0.19	0.96	1.01	-0.12	n/a
553	2	A20	0.81	0.25	1.17	-1.38	1.09	1.11	1.21	0.94	n/a
554	2	A22	-0.33	-0.04	0.01	-0.71	0.67	0.98	0.89	0.77	n/a
555	2	A3	0.55	0.91	1.06	-0.60	0.99	1.72	1.55	1.21	n/a
556	2	A4	-0.05	0.31	0.17	-0.66	0.56	1.18	0.98	0.71	n/a
557	2	A6	-0.20	0.05	0.12	-0.60	0.65	0.92	0.92	0.54	n/a
558	2	A7	-0.27	0.13	0.25	-0.63	0.43	1.06	0.84	0.67	n/a
559	2	A9	0.11	0.71	0.68	0.13	0.88	1.48	1.35	1.01	n/a
560	2	B1	0.10	-0.23	0.15	-0.47	0.59	0.86	0.76	0.70	n/a
561	2	B10	-0.62	-0.35	-0.61	-0.54	0.30	0.81	0.73	0.34	n/a
562	2	B11	0.01	0.11	0.58	-0.04	0.84	1.36	1.14	1.01	n/a
563	2	B13	-0.26	-0.34	0.05	-0.44	0.65	1.08	0.96	0.74	n/a
564	2	B14	0.53	0.75	0.74	0.04	0.67	1.26	1.05	0.92	n/a
565	2	B15	-0.05	-0.06	0.29	-0.11	0.67	0.82	0.73	0.75	n/a
566	2	B16	1.27	-0.03	0.82	-0.03	-0.10	0.17	0.29	-0.38	n/a
567	2	B17	0.29	0.18	0.41	-0.49	0.74	1.19	1.07	0.76	n/a
568	2	B18	-1.03	-0.51	-0.78	-0.87	-0.19	0.26	0.15	-0.09	n/a
569	2	B19	-0.33	-0.60	-0.52	-0.46	0.05	0.33	0.28	0.00	n/a
570	2	B2	-0.44	0.12	-0.14	-0.33	0.57	1.21	1.05	0.72	n/a
571	2	B20	0.01	0.26	0.35	-0.59	0.76	1.08	1.02	0.83	n/a
572	2	B21	0.08	0.14	0.35	-0.11	0.75	0.91	0.85	0.79	n/a
573	2	B22	-0.75	-0.09	-0.54	0.00	0.30	0.33	0.35	0.24	n/a
574	2	B3	-0.70	-0.29	-0.57	-0.36	-0.26	-0.42	-0.25	-0.51	n/a
575	2	B4	0.25	0.34	0.45	-0.28	0.69	0.80	0.75	0.75	n/a
576	2	B5	0.14	0.60	1.07	-0.02	0.77	1.34	1.12	1.02	n/a
577	2	B6	-0.01	0.13	0.52	-0.12	1.02	1.29	1.21	1.07	n/a
578	2	B7	-0.47	-0.12	-0.57	-0.11	-0.46	0.04	-0.11	-0.29	n/a
579	2	B8	-0.52	0.04	-0.27	-0.53	-0.18	0.52	0.34	0.00	n/a
580	2	B9	-0.21	0.19	0.11	-0.37	0.96	1.19	1.08	1.11	n/a
581	2	C1	0.13	0.11	0.05	-0.25	0.69	0.64	0.63	0.71	n/a
582	2	C10	-0.81	-0.89	-0.79	-0.71	0.54	0.75	0.70	0.51	n/a
583	2	C11	-0.42	-0.25	-0.23	-0.62	0.34	0.70	0.60	0.39	n/a
584	2	C12	-0.27	-0.17	-0.05	-0.46	0.58	0.61	0.68	0.49	n/a
585	2	C13	-0.25	-0.38	0.12	-0.89	0.40	0.27	0.28	0.38	n/a
586	2	C15	-0.45	-0.29	-0.13	-0.94	-0.23	-0.31	-0.24	-0.38	n/a
587	2	C16	-0.51	0.17	-0.18	-0.21	0.25	0.76	0.64	0.35	n/a
588	2	C17	-0.88	-1.21	-1.16	-0.88	-0.23	-0.36	-0.23	-0.39	n/a
589	2	C18	0.10	0.34	0.26	0.29	0.59	0.75	0.73	0.65	n/a
590	2	C19	-0.38	-0.18	-0.22	-0.16	0.82	1.01	0.88	0.97	n/a
591	2	C2	-0.34	0.32	-0.04	-0.28	0.44	0.67	0.60	0.47	n/a
592	2	C20	-0.67	-0.55	-0.37	-0.25	0.72	0.70	0.72	0.65	n/a
593	2	C21	-0.63	-0.38	-0.38	-0.41	0.62	0.49	0.50	0.60	n/a
594	2	C22	-1.05	-0.09	-0.72	0.08	-0.68	-1.21	-1.18	-0.85	n/a
595	2	C3	-0.07	-0.15	0.37	-0.60	0.75	1.01	0.89	0.94	n/a
596	2	C5	-0.31	0.06	0.08	-0.47	0.63	0.78	0.73	0.65	n/a
597	2	C7	-0.90	-0.71	-0.91	-0.80	-0.12	0.20	0.19	-0.15	n/a
598	2	C8	-0.88	-0.42	-0.57	-1.58	-0.75	-0.88	-1.18	-0.53	n/a
599	2	C9	0.06	0.29	0.41	-0.58	0.81	1.13	0.96	1.01	n/a
600	2	D1	-0.10	0.53	0.22	0.28	0.44	0.89	0.72	0.65	n/a
601	2	D10	-0.40	-0.35	-0.65	-0.16	-0.39	-0.32	-0.22	-0.56	n/a
602	2	D11	-0.57	-0.68	-0.31	-0.40	0.34	0.67	0.53	0.50	n/a
603	2	D13	-0.23	-0.45	-0.29	-0.15	0.63	1.01	0.95	0.70	n/a
604	2	D15	-0.59	-0.61	-0.35	-0.67	-0.40	-0.75	-0.65	-0.55	n/a

605	2	D16	-0.70	-0.51	-0.34	-0.26	0.34	0.46	0.40	0.40	n/a
606	2	D17	0.02	-0.01	0.24	-0.12	0.34	0.40	0.31	0.50	n/a
607	2	D18	-0.54	-0.83	-0.51	-0.51	0.55	0.76	0.69	0.63	n/a
608	2	D19	-0.52	-0.55	-0.39	-0.18	-0.48	-0.83	-0.79	-0.63	n/a
609	2	D2	-0.45	-0.39	-0.50	-0.08	0.27	0.44	0.43	0.26	n/a
610	2	D20	-0.76	-0.33	-0.20	-0.54	0.57	0.59	0.59	0.58	n/a
611	2	D21	-0.31	-0.40	-0.29	-0.06	0.10	0.04	0.16	-0.04	n/a
612	2	D22	-0.37	-0.74	-0.53	-0.37	0.46	0.36	0.43	0.35	n/a
613	2	D4	-0.70	0.13	-0.39	-0.04	0.63	1.09	0.95	0.78	n/a
614	2	D5	-0.43	-0.31	0.05	-0.40	0.58	0.85	0.73	0.74	n/a
615	2	D6	-0.08	0.06	0.37	-0.53	1.14	1.10	1.09	1.13	n/a
616	2	D7	-1.68	-0.63	-1.21	-1.00	-0.94	-1.21	-1.19	-1.08	n/a
617	2	D8	-0.68	-0.91	-1.02	-0.20	-0.51	-0.51	-0.55	-0.46	n/a
618	2	E1	0.70	0.77	0.68	0.34	0.32	0.73	0.65	0.41	n/a
619	2	E10	-0.84	-0.49	-0.89	-0.33	0.16	0.26	0.29	0.10	n/a
620	2	E11	-0.67	-0.07	-0.34	-0.51	-0.79	-0.31	-0.50	-0.61	n/a
621	2	E12	-0.60	-0.74	-0.49	-0.65	0.65	0.61	0.64	0.65	n/a
622	2	E14	-0.57	-0.19	-0.22	-0.11	-0.64	-0.94	-1.09	-0.55	n/a
623	2	E15	-0.84	0.20	-0.22	-0.51	-0.83	-1.26	-1.50	-0.71	n/a
624	2	E16	-0.39	-0.28	-0.10	0.01	0.54	0.45	0.43	0.56	n/a
625	2	E17	-1.41	-1.12	-1.45	-0.41	-1.04	-1.65	-1.51	-1.28	n/a
626	2	E18	-0.68	-0.65	-1.21	-0.71	-1.26	-0.52	-0.95	-0.80	n/a
627	2	E19	1.58	1.39	1.46	0.84	0.53	0.55	0.55	0.49	n/a
628	2	E2	-0.39	-0.37	-0.52	-0.11	-0.13	0.11	-0.03	-0.02	n/a
629	2	E21	-0.21	-0.29	-0.11	-0.48	0.16	0.06	0.04	0.18	n/a
630	2	E22	-0.25	-0.36	-0.45	-0.61	-0.64	-0.92	-0.79	-0.85	n/a
631	2	E3	-0.71	-0.72	-0.81	-0.97	-0.71	-0.79	-0.84	-0.70	n/a
632	2	E5	-0.31	-0.46	-0.22	-0.78	0.08	0.09	0.15	-0.02	n/a
633	2	E6	0.25	0.31	0.62	-0.02	0.55	0.46	0.50	0.48	n/a
634	2	E7	-0.07	0.36	0.29	0.01	0.18	0.62	0.54	0.28	n/a
635	2	E8	-0.12	-0.63	-0.14	-0.70	0.21	0.17	0.16	0.19	n/a
636	2	F1	0.02	0.25	0.29	0.06	0.23	0.41	0.30	0.37	n/a
637	2	F11	-0.34	-0.63	-0.40	-0.28	0.06	0.14	0.10	0.10	n/a
638	2	F13	-0.19	-0.25	-0.14	0.05	0.29	0.35	0.28	0.27	n/a
639	2	F14	-0.56	-0.61	-0.34	-0.39	0.11	-0.16	0.00	-0.11	n/a
640	2	F15	-0.51	-1.10	-0.71	-0.57	-0.36	-0.84	-0.66	-0.60	n/a
641	2	F16	0.04	0.23	0.36	0.37	0.39	0.27	0.25	0.40	n/a
642	2	F18	-0.23	-0.42	-0.43	-0.07	0.29	0.29	0.29	0.30	n/a
643	2	F19	-0.88	-0.16	-0.79	-0.12	-1.30	-1.83	-1.82	-1.35	n/a
644	2	F2	-0.05	-0.05	-0.33	-0.37	-0.14	0.16	0.05	-0.07	n/a
645	2	F21	-0.37	-0.33	-0.44	0.09	0.38	0.13	0.22	0.33	n/a
646	2	F22	-1.01	-0.90	-0.88	-0.57	-0.43	-0.71	-0.67	-0.53	n/a
647	2	F4	0.54	0.64	0.74	0.21	0.14	0.63	0.51	0.23	n/a
648	2	F5	0.11	-0.03	0.04	0.27	0.31	0.44	0.36	0.39	n/a
649	2	F6	-0.27	-0.50	-0.15	-0.45	0.15	0.19	0.17	0.13	n/a
650	2	F7	1.36	-0.50	0.59	1.77	-0.93	-1.58	-1.82	-0.83	n/a
651	2	F8	-0.73	-0.55	-0.90	-0.03	-0.21	-0.20	-0.09	-0.36	n/a
652	2	F9	-0.76	-1.13	-0.77	-0.41	-0.81	-1.24	-1.04	-1.07	n/a
653	2	G1	-0.28	0.03	-0.14	0.37	0.01	0.06	0.11	-0.06	n/a
654	2	G11	-0.63	-0.76	-0.70	-0.35	0.04	0.05	-0.04	0.15	n/a
655	2	G14	-0.22	-0.41	0.00	-0.39	-0.58	-0.88	-1.06	-0.45	n/a
656	2	G18	-0.72	-0.91	-0.84	-0.21	-0.39	-0.27	-0.27	-0.45	n/a
657	2	G19	0.28	0.11	0.40	0.56	-0.32	-0.48	-0.57	-0.27	n/a
658	2	G2	-0.49	-0.39	-0.61	0.02	-0.17	-0.32	-0.29	-0.23	n/a
659	2	G20	-0.30	-0.58	-0.60	0.21	-0.28	-0.46	-0.28	-0.50	n/a
660	2	G21	-0.24	-0.39	-0.07	-0.27	0.19	0.16	0.12	0.21	n/a
661	2	G22	-0.66	-1.52	-1.08	-0.61	-1.22	-1.49	-1.41	-1.34	n/a
662	2	G3	-0.63	-1.19	-1.02	-0.84	-0.11	-0.33	-0.21	-0.29	n/a

663	2	G5	-0.96	-0.22	-1.26	0.05	-1.02	-0.47	-0.68	-0.80	n/a
664	2	G6	1.61	0.03	0.48	-0.26	-0.23	0.46	0.37	-0.19	n/a
665	2	G9	-0.39	-0.67	-0.62	-0.31	-0.21	-0.27	-0.31	-0.18	n/a
666	2	H1	-0.11	0.10	-0.16	0.20	0.01	-0.28	-0.13	-0.15	n/a
667	2	H10	-0.97	-1.65	-1.41	-1.17	-0.74	-1.04	-0.88	-0.98	n/a
668	2	H12	-0.18	-0.81	-0.43	-0.23	0.04	0.00	0.06	0.00	n/a
669	2	H13	-0.70	-0.88	-0.62	-0.46	-0.50	-0.49	-0.40	-0.61	n/a
670	2	H15	-0.76	-0.84	-1.08	-0.07	-1.04	-1.69	-1.68	-1.15	n/a
671	2	H17	-0.89	-0.80	-0.91	-0.03	-0.06	-0.57	-0.20	-0.46	n/a
672	2	H18	0.61	0.51	0.81	0.52	0.25	-0.18	-0.13	0.20	n/a
673	2	H19	-0.26	-0.23	-0.66	-0.31	-0.93	-1.55	-1.64	-0.95	n/a
674	2	H2	1.28	0.86	1.21	0.30	0.09	-0.07	-0.01	-0.01	n/a
675	2	H21	-0.37	-0.26	-0.48	0.20	-0.18	-0.25	-0.32	-0.14	n/a
676	2	H22	-0.17	-0.19	-0.19	-0.04	-0.04	-0.26	-0.23	-0.08	n/a
677	2	H4	-0.52	-1.20	-1.05	-0.70	-0.50	-0.71	-0.61	-0.69	n/a
678	2	H5	-0.66	-1.25	-1.07	-0.45	-1.19	-0.66	-0.97	-0.87	n/a
679	2	H6	-0.27	-0.38	-0.26	0.04	-0.09	-0.07	-0.10	-0.07	n/a
680	2	H8	-0.36	-0.39	-0.73	0.30	-0.77	-0.68	-0.76	-0.71	n/a
681	2	I1	-0.54	-0.16	-0.35	-0.71	-0.18	-0.12	-0.13	-0.21	n/a
682	2	I10	-1.01	-1.14	-1.48	-0.15	-1.13	-0.82	-1.00	-0.96	n/a
683	2	I11	0.28	-0.41	-0.59	-0.15	-0.07	-0.17	-0.10	-0.16	n/a
684	2	I12	-1.16	-0.43	-1.22	-0.54	-1.43	-1.34	-1.49	-1.32	n/a
685	2	I13	-0.51	-1.02	-0.88	-0.79	-0.21	-0.48	-0.43	-0.31	n/a
686	2	I14	-0.52	-0.72	-0.70	-0.58	-0.51	-1.00	-1.07	-0.48	n/a
687	2	I15	-5.09	-5.04	-4.84	-4.46	-1.10	-1.68	-2.02	-0.86	n/a
688	2	I16	-1.37	-0.62	-1.11	-0.65	-0.33	-0.03	-0.07	-0.27	n/a
689	2	I17	-0.32	-0.90	-0.80	-0.01	-0.77	-1.53	-1.36	-1.03	n/a
690	2	I18	-0.71	-0.45	-0.66	-0.21	-0.80	-0.82	-0.80	-0.83	n/a
691	2	I19	-0.52	-0.87	-0.46	-0.59	-0.53	-1.03	-1.01	-0.62	n/a
692	2	I2	-0.57	-0.13	-0.66	0.24	-1.03	-1.43	-1.56	-1.00	n/a
693	2	I20	-0.56	-0.66	-1.27	0.88	-0.85	-0.87	-0.86	-0.87	n/a
694	2	I21	-0.39	-0.18	-0.40	-0.17	-0.19	-0.13	-0.19	-0.16	n/a
695	2	I4	0.32	-1.74	-1.36	-1.82	-2.25	-2.53	-2.91	-2.00	n/a
696	2	I5	-0.58	-1.13	-0.47	-0.86	-0.38	-0.77	-0.71	-0.55	n/a
697	2	I7	-0.63	-0.59	-1.04	0.19	-1.22	-1.10	-1.08	-1.24	n/a
698	2	I8	-0.59	-1.11	-0.81	-0.43	-0.23	-0.62	-0.54	-0.38	n/a
699	2	I9	-1.05	-1.73	-1.61	-1.15	-0.39	-0.16	-0.22	-0.33	n/a
700	2	J1	-0.83	-0.01	-0.72	-0.24	-0.06	0.35	0.17	0.14	n/a
701	2	J10	-1.06	-1.43	-1.74	-0.87	-1.44	-1.15	-1.25	-1.35	n/a
702	2	J11	-0.70	-0.57	-0.81	-0.38	-0.22	-0.18	-0.07	-0.38	n/a
703	2	J12	-0.09	-0.32	-0.33	-0.24	0.27	0.13	0.22	0.18	n/a
704	2	J13	-0.55	-0.33	-0.67	0.33	-0.15	-0.22	-0.16	-0.24	n/a
705	2	J14	-0.28	-0.66	-0.45	-0.35	-0.15	-0.04	-0.08	-0.10	n/a
706	2	J15	0.12	-0.49	-0.51	0.10	-0.32	-0.57	-0.58	-0.31	n/a
707	2	J16	-0.66	-0.97	-1.09	-0.62	-0.97	-0.96	-0.90	-1.07	n/a
708	2	J17	-0.67	-0.35	-0.51	-0.23	-0.02	-0.15	-0.13	-0.06	n/a
709	2	J2	0.04	-0.39	-0.16	-0.28	0.09	0.40	0.24	0.28	n/a
710	2	J20	1.31	0.71	0.69	1.57	-0.05	-0.28	-0.11	-0.22	n/a
711	2	J21	-0.58	-0.85	-0.81	-0.07	-0.32	-0.40	-0.38	-0.35	n/a
712	2	J4	-0.35	-1.00	-0.77	-0.37	-0.30	-0.25	-0.29	-0.32	n/a
713	2	J5	-1.19	-0.89	-1.07	-0.84	-1.29	-0.91	-1.00	-1.28	n/a
714	2	J8	-1.00	-0.65	-1.30	-0.02	-0.58	-0.43	-0.41	-0.59	n/a
715	2	K10	0.48	-0.60	-0.12	1.09	-0.78	-0.72	-0.85	-0.63	n/a
716	2	K11	-0.10	-0.60	-0.50	-0.47	-0.21	-0.39	-0.22	-0.40	n/a
717	2	K12	0.26	-0.07	-0.32	0.14	0.23	0.38	0.36	0.27	n/a
718	2	K13	-0.32	-0.44	-0.36	-0.56	0.47	0.30	0.30	0.49	n/a
719	2	K14	-0.61	-1.07	-0.77	0.40	-0.79	-1.44	-1.60	-0.71	n/a
720	2	K15	-0.98	-1.19	-1.26	-0.24	-0.90	-1.44	-1.65	-0.75	n/a

721	2	K16	-0.31	0.07	-0.28	0.20	0.05	0.18	0.07	0.21	n/a
722	2	K17	-0.66	-0.83	-0.92	-0.73	-0.46	-0.59	-0.53	-0.50	n/a
723	2	K18	-1.18	-1.37	-0.92	-0.40	-0.58	-0.51	-0.71	-0.35	n/a
724	2	K19	-0.30	-0.31	-0.21	-0.11	0.51	0.45	0.44	0.55	n/a
725	2	K20	-0.95	-1.44	-1.18	-0.40	-0.38	-0.49	-0.50	-0.36	n/a
726	2	K21	-0.38	-0.21	-0.33	-0.02	0.45	0.12	0.22	0.36	n/a
727	2	K22	-1.04	0.11	-0.61	-1.72	-0.77	-0.91	-0.89	-0.76	n/a
728	2	K3	0.17	-0.57	-0.07	-0.29	-0.01	0.02	0.08	-0.10	n/a
729	2	K5	-1.18	-0.69	-1.20	-0.20	-0.93	-0.67	-0.79	-0.81	n/a
730	2	K6	-0.15	0.37	-0.16	0.14	0.08	0.40	0.27	0.24	n/a
731	2	K7	-0.14	-0.46	-0.30	0.27	-0.13	-0.22	-0.13	-0.26	n/a
732	2	K8	-0.42	-0.93	-0.68	-0.31	-0.53	-0.66	-0.74	-0.47	n/a
733	2	K9	-0.36	-0.96	-0.73	-0.18	-0.10	-0.31	-0.20	-0.21	n/a
734	2	L10	-1.84	-0.07	-1.74	-0.09	-1.54	-1.68	-1.78	-1.42	n/a
735	2	L11	-0.28	-0.51	-0.16	0.04	0.53	0.20	0.29	0.44	n/a
736	2	L12	-0.31	-0.01	-0.15	0.25	0.75	0.47	0.51	0.75	n/a
737	2	L13	0.13	0.40	0.08	0.42	-0.13	-0.10	-0.26	0.10	n/a
738	2	L14	0.00	-0.11	-0.07	0.51	-0.15	-0.38	-0.36	-0.15	n/a
739	2	L15	-0.47	-0.14	-0.78	0.35	-0.95	-1.55	-1.60	-1.00	n/a
740	2	L16	-0.97	-0.96	-0.82	-0.61	0.44	0.35	0.29	0.49	n/a
741	2	L17	-0.15	0.10	-0.10	0.54	0.47	0.24	0.25	0.49	n/a
742	2	L18	-0.11	-0.29	-0.28	-0.26	-0.29	-0.39	-0.41	-0.21	n/a
743	2	L2	-0.43	-0.15	-0.21	-0.13	0.36	0.90	0.71	0.55	n/a
744	2	L20	0.03	-0.25	0.03	-0.05	0.16	-0.18	-0.10	0.06	n/a
745	2	L21	-0.46	0.18	-0.33	0.08	0.40	0.13	0.25	0.27	n/a
746	2	L22	-0.43	-0.13	-0.18	0.11	0.17	0.10	0.10	0.12	n/a
747	2	L3	-1.40	1.34	-0.88	-0.90	-1.03	-0.83	-1.10	-0.68	n/a
748	2	L4	-0.40	-0.22	-0.98	-0.79	-1.15	-1.44	-1.75	-0.97	n/a
749	2	L5	-0.76	-0.70	-0.40	-0.38	0.02	0.20	0.19	0.00	n/a
750	2	L6	-0.13	-0.33	-0.11	-0.31	0.77	0.60	0.76	0.68	n/a
751	2	L8	-0.86	-0.94	-1.28	-1.49	-0.41	-0.49	-0.50	-0.37	n/a
752	2	L9	-0.10	0.15	0.07	-0.06	0.71	0.19	0.33	0.64	n/a
753	2	M10	-0.62	-0.41	-0.92	0.28	-0.25	-0.49	-0.45	-0.29	n/a
754	2	M11	-0.91	-1.16	-1.11	-0.99	-0.55	-0.67	-0.61	-0.61	n/a
755	2	M12	0.44	0.10	0.52	-0.36	-1.87	-1.37	-1.65	-1.64	n/a
756	2	M13	-0.42	-0.31	0.12	-0.37	0.60	0.42	0.38	0.65	n/a
757	2	M14	-1.15	1.02	-0.49	-0.73	-0.96	-1.56	-1.81	-0.79	n/a
758	2	M15	-0.40	-0.26	-0.31	-1.15	-0.99	-1.64	-1.80	-0.91	n/a
759	2	M16	0.03	-0.09	0.26	-0.26	0.58	0.36	0.42	0.52	n/a
760	2	M17	0.45	0.06	0.14	0.48	0.81	0.19	0.39	0.67	n/a
761	2	M18	-0.14	-0.21	-0.08	-0.22	0.68	0.41	0.48	0.61	n/a
762	2	M19	-0.34	-0.50	-0.42	-0.33	0.24	-0.11	0.02	0.16	n/a
763	2	M20	-0.31	-0.41	-0.17	-0.71	-0.08	-0.32	-0.31	-0.14	n/a
764	2	M21	0.17	-0.28	0.37	-0.23	0.52	0.50	0.46	0.57	n/a
765	2	M22	-1.12	-0.29	-0.96	1.52	-0.65	-0.52	-0.61	-0.56	n/a
766	2	M5	-1.18	-1.11	-1.42	-0.57	-0.65	-0.53	-0.53	-0.66	n/a
767	2	M6	-0.06	0.23	0.11	-0.27	0.87	1.22	1.05	1.03	n/a
768	2	M7	-1.06	-1.20	-1.05	-0.70	-0.96	-1.24	-1.10	-1.12	n/a
769	2	M8	-0.37	-0.90	-0.69	-0.67	-0.61	-0.85	-0.69	-0.76	n/a
770	2	M9	-0.31	-0.19	-0.41	-0.48	0.56	0.57	0.55	0.65	n/a
771	2	N1	-0.03	0.63	0.29	-0.55	-0.18	0.24	0.09	0.01	n/a
772	2	N11	-0.28	-0.17	-0.31	-0.10	0.33	0.31	0.38	0.29	n/a
773	2	N12	-0.06	-0.04	-0.06	-0.16	0.70	0.55	0.57	0.73	n/a
774	2	N13	-0.38	0.09	0.09	-0.04	0.18	-0.02	-0.01	0.24	n/a
775	2	N14	0.49	0.38	0.42	0.47	0.76	0.86	0.76	0.92	n/a
776	2	N15	-0.50	-0.53	-0.63	-0.02	-0.11	-0.33	-0.20	-0.22	n/a
777	2	N16	-0.47	-0.18	-0.10	-0.18	0.50	0.37	0.33	0.58	n/a
778	2	N17	0.12	0.22	-0.65	1.28	-0.48	-0.68	-0.77	-0.29	n/a

779	2	N18	0.12	0.10	0.35	0.03	-0.25	-0.21	-0.33	-0.11	n/a
780	2	N21	-0.19	0.14	-0.02	0.46	0.37	0.08	0.14	0.31	n/a
781	2	N22	0.08	0.14	0.24	0.14	0.37	0.31	0.32	0.40	n/a
782	2	N3	-1.97	-1.04	-1.71	-0.32	-1.10	-1.06	-1.22	-0.95	n/a
783	2	N5	-0.22	-0.35	-0.14	-0.13	0.76	0.61	0.63	0.72	n/a
784	2	N6	-0.95	-0.62	-0.68	-0.56	-0.97	-1.28	-1.45	-0.90	n/a
785	2	N8	0.11	0.73	0.27	0.37	0.02	0.02	-0.02	0.11	n/a
786	2	N9	0.01	-0.44	-0.18	-0.08	0.23	-0.33	-0.12	0.03	n/a
787	2	O1	-0.51	0.35	-0.33	-0.03	0.48	0.54	0.46	0.56	n/a
788	2	O10	0.90	1.12	1.30	-0.45	-0.29	-0.56	-0.55	-0.22	n/a
789	2	O11	-0.41	0.04	-0.43	0.70	-0.79	-0.79	-0.79	-0.78	n/a
790	2	O12	0.02	-0.68	0.02	-0.13	0.10	-0.21	-0.09	0.00	n/a
791	2	O13	-0.49	0.07	0.18	-0.91	0.66	0.53	0.52	0.73	n/a
792	2	O14	0.39	0.41	0.20	0.57	0.53	0.51	0.48	0.60	n/a
793	2	O16	-0.32	0.36	0.12	-0.30	0.15	-0.09	-0.01	0.08	n/a
794	2	O17	-0.99	-0.91	-1.12	-0.37	0.22	0.05	0.11	0.23	n/a
795	2	O18	-0.16	0.68	0.21	0.55	0.29	0.16	0.19	0.15	n/a
796	2	O2	-0.58	0.12	-0.28	-0.48	0.26	0.81	0.73	0.37	n/a
797	2	O20	-0.65	-0.69	-0.84	0.82	-1.22	-1.72	-1.90	-1.15	n/a
798	2	O22	-0.67	-0.02	-0.53	-0.37	0.36	0.48	0.41	0.45	n/a
799	2	O5	-0.30	-0.33	-0.41	-0.09	0.26	0.30	0.32	0.21	n/a
800	2	O6	-1.43	-0.12	-1.05	-1.20	-1.37	-1.49	-1.68	-1.32	n/a
801	2	O7	-1.56	-0.43	-1.07	-0.63	-0.95	-1.31	-1.11	-1.16	n/a
802	2	O8	0.39	0.72	0.24	0.61	0.32	0.84	0.67	0.49	n/a
803	2	O9	0.31	-0.02	-0.14	-0.11	0.18	0.01	0.07	0.15	n/a
804	2	P10	0.07	1.17	0.58	-1.38	-0.17	-0.22	-0.32	-0.01	n/a
805	2	P11	-0.59	-0.04	-0.23	-0.24	0.63	0.79	0.68	0.81	n/a
806	2	P12	-0.39	0.26	0.08	-0.26	0.53	0.90	0.74	0.69	n/a
807	2	P13	-0.08	0.20	0.06	0.05	-0.29	-0.38	-0.41	-0.24	n/a
808	2	P14	-0.34	0.58	0.24	0.13	0.66	0.60	0.51	0.81	n/a
809	2	P15	-0.12	0.19	0.28	-0.10	0.71	0.45	0.49	0.72	n/a
810	2	P16	-0.09	0.41	0.12	0.14	0.73	0.57	0.63	0.73	n/a
811	2	P17	-0.60	0.73	0.35	-0.08	0.52	0.49	0.47	0.53	n/a
812	2	P18	0.06	0.69	0.32	0.31	0.75	0.91	0.79	0.88	n/a
813	2	P19	0.05	0.22	0.40	0.31	0.85	0.58	0.64	0.79	n/a
814	2	P2	0.61	-0.48	-0.33	-1.11	-1.02	0.17	-0.11	-0.74	n/a
815	2	P20	0.43	0.45	0.29	0.69	0.55	0.81	0.64	0.76	n/a
816	2	P21	-0.15	-0.35	-0.10	-0.17	0.69	0.75	0.70	0.77	n/a
817	2	P3	-0.51	-0.91	-0.66	-0.59	-0.15	0.15	0.09	-0.08	n/a
818	2	P4	-0.80	0.43	0.01	-0.47	0.75	0.96	0.95	0.77	n/a
819	2	P5	0.05	0.86	0.66	-0.01	0.84	1.20	1.08	0.97	n/a
820	2	P6	0.02	0.66	0.25	0.31	0.32	0.73	0.59	0.45	n/a
821	2	P7	1.09	1.33	0.69	-1.29	-0.49	0.62	0.59	-0.61	n/a
822	2	P8	0.17	0.79	0.64	-0.13	0.61	0.97	0.84	0.75	n/a
823	2	P9	-0.25	0.12	0.56	-0.11	0.80	0.79	0.74	0.80	n/a
824	3	A1	0.13	-0.04	0.64	-1.48	0.61	0.38	0.46	0.49	n/a
825	3	A10	1.16	1.09	1.61	-0.01	0.69	0.63	0.72	0.57	n/a
826	3	A11	0.78	0.82	0.76	-0.31	0.24	0.65	0.60	0.28	n/a
827	3	A12	0.02	0.87	0.37	-0.31	0.68	0.66	0.72	0.64	n/a
828	3	A13	-0.68	-0.03	-0.15	-1.21	-0.04	-0.40	-0.32	-0.18	n/a
829	3	A14	0.16	0.51	0.44	0.21	0.68	0.83	0.83	0.68	n/a
830	3	A15	-0.21	0.39	0.24	-0.28	0.81	0.55	0.73	0.65	n/a
831	3	A16	-0.01	-0.08	-0.10	-0.11	0.60	0.57	0.58	0.61	n/a
832	3	A17	0.49	1.11	0.98	0.49	0.58	0.80	0.73	0.67	n/a
833	3	A18	0.17	0.49	0.36	0.08	0.38	0.59	0.47	0.51	n/a
834	3	A19	0.62	1.12	0.98	0.72	0.65	0.63	0.59	0.76	n/a
835	3	A2	-0.51	0.07	-0.30	-1.07	0.25	0.51	0.49	0.24	n/a
836	3	A20	-1.57	-0.30	-0.76	-1.80	-0.71	-0.95	-0.67	-1.07	n/a

837	3	A21	-0.17	0.46	0.23	0.48	0.36	0.58	0.47	0.51	n/a
838	3	A22	0.44	0.43	0.48	0.19	0.22	0.45	0.40	0.25	n/a
839	3	A4	0.11	1.71	0.74	-0.42	-0.22	0.05	-0.07	-0.14	n/a
840	3	A5	0.12	-1.48	-0.93	-1.45	-0.25	1.34	1.13	-0.26	n/a
841	3	A6	0.25	1.30	0.60	0.23	0.11	0.36	0.32	0.10	n/a
842	3	A7	0.74	0.57	0.42	-0.21	0.16	0.41	0.38	0.22	n/a
843	3	A8	0.39	0.59	0.75	-0.27	0.67	0.61	0.61	0.65	n/a
844	3	B1	0.42	0.55	0.72	0.44	0.60	0.58	0.58	0.60	n/a
845	3	B10	1.03	0.53	1.35	0.78	0.85	0.76	0.77	0.85	n/a
846	3	B11	-0.03	0.35	0.42	0.06	0.84	0.38	0.57	0.69	n/a
847	3	B12	-0.15	-0.60	-0.34	-0.15	0.45	0.30	0.47	0.26	n/a
848	3	B13	-0.40	-0.46	-0.47	-0.04	0.62	0.42	0.58	0.45	n/a
849	3	B14	-0.35	0.16	-0.03	-0.56	0.68	0.27	0.47	0.46	n/a
850	3	B15	0.20	0.05	0.33	-0.27	0.85	0.76	0.81	0.82	n/a
851	3	B16	0.21	0.80	0.59	-0.04	0.75	1.04	1.05	0.78	n/a
852	3	B17	0.18	0.13	0.13	-0.51	0.83	0.71	0.83	0.73	n/a
853	3	B18	-0.33	0.16	0.04	-0.10	0.46	0.34	0.39	0.38	n/a
854	3	B2	0.04	0.51	0.23	-0.11	0.65	0.63	0.64	0.57	n/a
855	3	B20	-0.13	-0.18	0.08	0.20	1.00	0.79	0.90	0.89	n/a
856	3	B21	-0.31	0.70	-0.55	1.28	-0.63	-1.19	-1.03	-0.75	n/a
857	3	B3	0.02	0.05	0.06	-0.03	0.75	0.52	0.58	0.62	n/a
858	3	B5	-0.04	-0.04	0.22	-0.56	0.87	0.69	0.76	0.74	n/a
859	3	B6	0.38	0.52	0.81	0.15	0.91	0.98	0.97	0.89	n/a
860	3	B7	0.47	-0.34	0.62	-0.04	0.97	0.70	0.81	0.84	n/a
861	3	B8	0.37	-0.50	0.83	-0.59	1.59	0.93	1.25	1.26	n/a
862	3	B9	0.30	0.05	0.33	0.25	-0.25	-1.06	-0.47	-1.05	n/a
863	3	C1	0.19	0.35	0.40	-0.04	0.47	0.36	0.35	0.46	n/a
864	3	C10	0.02	-1.03	-0.32	-0.67	0.85	0.40	0.61	0.64	n/a
865	3	C11	1.14	0.75	1.26	0.59	1.04	0.96	0.94	1.08	n/a
866	3	C12	-0.17	0.42	-0.08	-0.08	0.30	-0.33	-0.05	-0.04	n/a
867	3	C13	0.20	-0.06	0.35	-0.25	1.24	0.79	0.85	1.27	n/a
868	3	C14	1.34	0.41	1.57	-0.60	1.48	1.13	1.27	1.24	n/a
869	3	C16	-0.27	-0.62	-0.05	-0.59	0.95	0.54	0.72	0.75	n/a
870	3	C18	0.76	0.63	1.12	-0.33	1.41	1.14	1.15	1.40	n/a
871	3	C19	0.79	0.44	0.73	0.07	0.91	1.10	1.01	1.06	n/a
872	3	C2	-0.10	-0.35	-0.13	-0.21	0.10	-0.07	0.12	-0.14	n/a
873	3	C21	0.83	0.70	0.89	0.42	1.12	0.83	0.90	1.08	n/a
874	3	C22	0.76	0.96	0.99	0.44	0.94	0.74	0.83	0.87	n/a
875	3	C3	-0.27	-0.51	-0.36	-0.38	0.46	0.04	0.16	0.29	n/a
876	3	C4	0.03	0.16	-0.29	0.45	0.16	0.31	0.32	0.07	n/a
877	3	C5	0.13	0.10	0.43	-0.01	1.02	0.76	0.84	0.89	n/a
878	3	C7	0.24	0.11	0.71	-0.77	1.40	1.14	1.20	1.30	n/a
879	3	C8	0.18	0.51	-0.57	-2.00	-0.39	-0.16	-0.32	-0.24	n/a
880	3	C9	0.21	-0.28	0.37	-0.43	1.09	0.66	0.83	0.90	n/a
881	3	D1	0.56	0.34	0.46	-0.53	0.57	0.84	0.76	0.68	n/a
882	3	D10	-1.17	0.27	-0.56	-1.62	-0.38	-0.69	-0.77	-0.24	n/a
883	3	D11	0.99	0.48	1.24	0.11	1.62	0.88	1.14	1.33	n/a
884	3	D12	0.20	0.14	0.42	-0.40	0.94	0.43	0.48	0.85	n/a
885	3	D13	-0.11	-0.72	0.07	-0.55	1.21	0.75	0.89	1.11	n/a
886	3	D14	0.70	-0.16	0.82	-0.52	0.77	0.00	0.39	0.38	n/a
887	3	D15	0.41	0.09	0.56	-0.12	1.08	0.46	0.71	0.84	n/a
888	3	D16	0.50	0.48	0.58	-0.09	1.13	1.17	1.11	1.28	n/a
889	3	D17	0.61	-0.35	0.59	-0.10	0.91	0.79	0.89	0.82	n/a
890	3	D18	0.70	0.65	1.04	0.21	1.33	1.03	1.10	1.28	n/a
891	3	D19	0.33	0.26	0.74	-0.26	1.46	0.93	1.00	1.43	n/a
892	3	D2	-0.04	0.53	0.24	0.22	0.68	0.91	0.85	0.75	n/a
893	3	D20	0.15	0.42	0.64	0.34	1.31	0.98	1.03	1.24	n/a
894	3	D4	0.37	1.03	1.05	0.06	1.43	1.35	1.39	1.32	n/a

895	3	D5	0.78	1.08	1.31	-0.23	1.44	1.72	1.60	1.56	n/a
896	3	D6	0.60	0.50	1.03	-0.32	1.29	1.44	1.37	1.25	n/a
897	3	D7	0.26	0.61	0.56	0.34	1.17	0.84	0.86	1.19	n/a
898	3	D8	0.07	-0.10	0.41	-0.49	1.35	1.09	1.12	1.35	n/a
899	3	E1	0.47	0.74	0.78	-0.31	0.64	0.80	0.76	0.65	n/a
900	3	E10	0.29	-0.04	0.61	-0.07	1.38	0.84	0.97	1.30	n/a
901	3	E11	0.46	0.12	0.69	-0.24	1.35	1.01	1.00	1.45	n/a
902	3	E12	1.13	0.97	1.14	0.38	0.80	0.29	0.45	0.64	n/a
903	3	E13	0.46	0.01	0.61	-0.57	1.21	0.46	0.69	0.99	n/a
904	3	E14	0.59	0.47	0.64	0.32	1.23	0.73	0.88	1.06	n/a
905	3	E15	-0.19	-0.53	-0.06	-0.57	0.23	-0.43	-0.18	-0.04	n/a
906	3	E16	0.35	0.81	1.01	0.00	1.07	1.22	1.09	1.30	n/a
907	3	E17	0.67	0.73	1.23	-0.18	1.67	1.43	1.37	1.74	n/a
908	3	E18	0.16	0.66	0.52	0.10	1.47	1.09	1.07	1.57	n/a
909	3	E19	-0.33	-0.30	0.07	-0.53	1.09	1.03	1.07	1.07	n/a
910	3	E2	0.56	0.12	0.45	-0.23	1.03	1.24	1.13	1.15	n/a
911	3	E21	-0.16	0.32	0.30	-0.31	0.67	0.54	0.54	0.68	n/a
912	3	E22	0.52	0.03	0.86	-1.25	1.70	1.49	1.48	1.76	n/a
913	3	E3	-0.25	0.00	0.34	-0.70	0.90	0.58	0.75	0.63	n/a
914	3	E4	0.01	0.05	0.29	-0.01	1.01	1.25	1.13	1.09	n/a
915	3	E5	0.42	0.42	0.92	-0.28	1.54	1.31	1.24	1.62	n/a
916	3	E6	0.34	0.63	0.93	-0.49	1.49	1.41	1.34	1.66	n/a
917	3	E7	0.08	0.68	0.27	0.53	0.95	0.99	0.94	1.08	n/a
918	3	E8	-0.18	-0.15	-0.08	-0.90	0.81	1.12	1.06	0.88	n/a
919	3	E9	-0.48	-0.10	-0.03	-0.06	0.63	0.11	0.23	0.59	n/a
920	3	F1	1.24	1.05	1.38	0.56	0.94	0.71	0.89	0.76	n/a
921	3	F11	0.72	0.60	1.02	0.28	1.39	1.29	1.17	1.60	n/a
922	3	F12	-0.06	-0.02	0.09	-0.16	0.75	0.33	0.45	0.65	n/a
923	3	F13	0.90	0.15	0.80	-0.12	1.47	1.11	1.18	1.45	n/a
924	3	F14	0.65	0.09	0.46	0.33	0.63	0.42	0.52	0.58	n/a
925	3	F15	0.38	0.02	0.60	-0.39	1.28	0.69	0.74	1.31	n/a
926	3	F16	0.34	0.26	0.68	-0.26	1.43	0.99	1.07	1.40	n/a
927	3	F19	0.41	-0.24	0.47	-0.17	0.90	0.53	0.64	0.84	n/a
928	3	F2	0.29	0.19	-0.10	-0.01	0.68	0.68	0.72	0.64	n/a
929	3	F20	0.94	0.51	1.09	0.05	0.93	0.89	0.84	1.09	n/a
930	3	F21	-0.87	-0.78	-0.87	-0.80	-0.32	-0.38	-0.55	-0.10	n/a
931	3	F3	0.56	0.87	1.00	-0.18	1.21	1.49	1.36	1.34	n/a
932	3	F4	-0.11	0.27	0.47	-0.13	1.14	1.21	1.14	1.25	n/a
933	3	F5	0.98	1.29	1.52	0.72	1.15	1.22	1.09	1.25	n/a
934	3	F7	0.33	-0.42	0.26	-0.97	1.12	0.70	0.79	1.05	n/a
935	3	F8	1.24	0.74	1.17	0.17	1.18	0.93	0.93	1.27	n/a
936	3	F9	-0.73	-0.17	0.34	-0.01	-1.24	-1.61	-1.69	-1.15	n/a
937	3	G1	0.77	1.01	1.19	0.22	1.22	1.24	1.21	1.21	n/a
938	3	G10	1.22	1.25	1.62	0.52	1.41	1.31	1.21	1.57	n/a
939	3	G12	1.43	1.42	1.62	0.34	1.46	0.94	1.03	1.44	n/a
940	3	G14	1.06	0.62	0.99	0.30	1.14	0.95	0.93	1.21	n/a
941	3	G15	1.32	-1.09	1.29	-1.16	1.51	0.35	0.92	0.94	n/a
942	3	G16	0.87	0.30	0.83	-0.10	1.40	1.10	1.13	1.34	n/a
943	3	G18	1.67	1.47	1.81	0.26	1.19	1.03	0.99	1.36	n/a
944	3	G19	0.62	0.54	0.89	0.24	1.42	1.15	1.17	1.46	n/a
945	3	G2	0.37	0.26	0.60	-0.12	0.66	0.66	0.67	0.64	n/a
946	3	G21	0.04	-0.10	0.08	-0.49	1.02	1.24	1.17	1.12	n/a
947	3	G22	0.17	0.62	0.80	0.03	1.22	1.26	1.19	1.25	n/a
948	3	G4	-0.27	-0.26	-0.02	-0.51	0.90	0.98	0.90	1.04	n/a
949	3	G5	1.16	0.86	1.36	0.26	1.41	1.37	1.24	1.56	n/a
950	3	G6	1.43	1.48	1.76	0.56	1.59	1.34	1.30	1.62	n/a
951	3	G7	0.83	1.14	0.91	-0.28	1.26	1.28	1.18	1.39	n/a
952	3	G8	-1.18	-0.48	-0.91	-1.08	-0.18	-0.03	-0.27	0.11	n/a

953	3	G9	0.59	0.49	0.85	0.39	0.90	0.10	0.31	0.67	n/a
954	3	H1	0.06	0.92	0.29	0.28	0.63	0.40	0.46	0.54	n/a
955	3	H10	0.42	0.02	0.54	0.42	0.42	-0.31	-0.08	0.23	n/a
956	3	H11	0.91	0.43	1.13	-0.15	1.38	0.88	1.02	1.28	n/a
957	3	H12	0.59	0.43	0.77	0.00	0.54	0.18	0.26	0.53	n/a
958	3	H13	0.64	0.83	1.18	0.05	-0.87	-1.81	-1.52	-1.15	n/a
959	3	H15	0.54	0.37	0.51	-0.19	1.00	0.50	0.60	0.99	n/a
960	3	H16	0.76	0.58	1.51	0.01	1.34	0.67	0.77	1.31	n/a
961	3	H17	-0.20	0.45	0.09	0.47	0.27	-0.13	-0.13	0.37	n/a
962	3	H18	0.37	0.77	0.82	0.04	1.46	0.98	1.06	1.42	n/a
963	3	H19	1.12	0.90	1.25	0.56	1.48	0.92	1.03	1.44	n/a
964	3	H2	0.09	0.26	0.01	-1.52	0.21	0.49	0.43	0.25	n/a
965	3	H20	0.33	0.16	0.67	-0.40	1.45	0.83	1.00	1.29	n/a
966	3	H21	1.69	-0.62	1.75	-0.14	-0.30	-0.52	-0.66	-0.07	n/a
967	3	H4	1.07	0.80	1.04	-0.42	-0.36	0.14	0.17	-0.50	n/a
968	3	H5	1.11	1.57	1.73	0.92	1.35	1.28	1.26	1.37	n/a
969	3	H6	0.59	0.53	0.86	-0.14	1.26	1.04	1.11	1.17	n/a
970	3	H7	0.84	0.91	1.25	0.57	1.13	0.71	0.71	1.16	n/a
971	3	H8	1.01	1.07	1.36	0.27	0.84	0.53	0.64	0.74	n/a
972	3	H9	-0.64	-0.75	-0.66	-1.03	0.30	0.07	0.08	0.32	n/a
973	3	I1	0.19	0.61	0.51	0.03	0.85	0.57	0.72	0.71	n/a
974	3	I10	0.80	0.28	1.28	-0.43	1.44	1.03	0.97	1.57	n/a
975	3	I11	0.41	0.31	0.75	-0.27	1.11	0.94	0.86	1.22	n/a
976	3	I12	0.29	0.17	0.63	-0.22	1.26	0.75	0.79	1.22	n/a
977	3	I13	0.38	0.69	0.81	-0.07	1.17	0.84	0.87	1.23	n/a
978	3	I14	0.75	0.58	1.29	-0.30	1.47	1.31	1.29	1.50	n/a
979	3	I15	-0.44	-0.68	-0.28	-0.76	0.63	0.11	0.26	0.54	n/a
980	3	I17	-0.33	2.75	0.70	0.39	-0.27	-0.29	-0.49	0.01	n/a
981	3	I18	0.80	0.75	1.16	-0.26	1.34	0.92	0.98	1.30	n/a
982	3	I20	0.96	0.80	1.18	-2.15	-0.30	-0.08	-0.36	0.05	n/a
983	3	I21	-0.33	-0.57	-0.60	-0.58	0.17	-0.37	-0.12	-0.07	n/a
984	3	I22	0.47	0.09	0.62	-0.13	0.97	0.70	0.69	0.99	n/a
985	3	I3	0.36	0.48	0.40	0.23	0.74	0.38	0.52	0.55	n/a
986	3	I4	0.20	-0.88	-0.01	-0.91	0.84	0.78	0.83	0.78	n/a
987	3	I7	0.40	0.76	1.12	-0.23	0.88	0.59	0.61	0.87	n/a
988	3	I8	-0.17	-0.91	-0.95	-1.00	-0.14	-0.29	-0.42	0.03	n/a
989	3	I9	0.56	0.46	0.78	-0.13	1.01	0.64	0.79	0.91	n/a
990	3	J10	-0.66	-0.71	-0.59	-0.29	0.50	-0.11	0.12	0.30	n/a
991	3	J11	0.36	0.89	1.19	-0.07	1.18	0.95	0.98	1.22	n/a
992	3	J12	0.00	-0.30	0.02	-0.38	0.95	0.36	0.52	0.75	n/a
993	3	J13	0.51	-0.16	0.54	-0.70	1.31	0.92	0.98	1.22	n/a
994	3	J14	-0.13	0.09	0.17	-0.40	0.88	0.29	0.42	0.74	n/a
995	3	J15	0.71	0.02	0.85	-0.69	1.19	0.75	0.81	1.13	n/a
996	3	J17	1.00	0.08	0.89	0.49	-0.09	-0.18	-0.20	-0.08	n/a
997	3	J18	1.19	0.70	1.26	0.67	1.26	0.67	0.80	1.16	n/a
998	3	J19	0.66	0.12	0.52	-0.01	1.28	1.07	0.96	1.44	n/a
999	3	J20	0.74	0.77	1.02	0.03	0.92	0.72	0.69	0.96	n/a
1000	3	J21	0.37	-0.11	0.10	-0.13	0.44	0.21	0.16	0.51	n/a
1001	3	J22	1.15	0.20	1.04	0.06	-0.15	-0.25	-0.35	-0.01	n/a
1002	3	J3	0.88	0.12	1.20	-0.28	1.24	0.87	1.00	1.05	n/a
1003	3	J4	1.22	0.88	1.44	0.05	1.57	1.33	1.28	1.63	n/a
1004	3	J5	0.61	0.40	1.18	-0.28	1.34	0.73	0.90	1.17	n/a
1005	3	J6	-0.51	-0.55	-0.16	-0.58	1.28	0.78	0.86	1.23	n/a
1006	3	J7	0.90	1.03	1.32	0.11	1.51	1.32	1.30	1.59	n/a
1007	3	J8	1.01	0.38	1.34	-0.24	1.47	1.04	1.15	1.40	n/a
1008	3	K1	0.41	1.04	1.15	0.05	0.76	1.07	0.99	0.84	n/a
1009	3	K10	0.72	0.51	1.06	0.00	1.46	1.29	1.17	1.61	n/a
1010	3	K11	0.88	0.66	1.54	-0.23	1.35	1.24	1.22	1.41	n/a

1011	3	K12	0.75	1.05	1.18	-0.14	1.53	1.28	1.27	1.59	n/a
1012	3	K13	1.72	0.60	1.39	0.50	1.39	1.12	1.19	1.26	n/a
1013	3	K14	0.88	0.98	1.47	0.11	1.39	1.45	1.38	1.50	n/a
1014	3	K15	0.95	0.59	1.41	0.15	1.37	1.08	1.11	1.40	n/a
1015	3	K16	0.62	1.41	1.53	-0.18	1.58	1.32	1.33	1.66	n/a
1016	3	K18	1.18	1.04	1.72	0.55	1.57	1.22	1.20	1.65	n/a
1017	3	K19	1.08	1.05	1.42	0.31	1.24	1.17	1.05	1.39	n/a
1018	3	K2	-0.32	-0.27	-0.73	-0.62	-0.23	-0.09	-0.22	-0.02	n/a
1019	3	K20	0.77	1.55	0.94	-1.13	-0.33	-0.44	-0.56	-0.16	n/a
1020	3	K21	1.01	0.85	1.15	0.28	0.72	0.48	0.60	0.64	n/a
1021	3	K22	0.52	0.89	1.11	0.33	0.55	0.55	0.43	0.68	n/a
1022	3	K3	0.66	0.51	0.99	0.20	1.26	1.19	1.11	1.36	n/a
1023	3	K4	1.40	0.95	1.00	0.58	0.58	0.39	0.37	0.63	n/a
1024	3	K5	0.78	0.56	1.21	-0.56	1.10	0.89	0.99	1.02	n/a
1025	3	K6	1.01	0.45	1.37	-0.65	1.49	1.06	1.11	1.42	n/a
1026	3	K7	1.25	1.03	1.42	0.34	1.35	1.26	1.22	1.41	n/a
1027	3	K8	0.98	0.47	1.12	0.43	0.68	0.46	0.48	0.68	n/a
1028	3	K9	1.14	0.93	1.38	0.08	0.80	0.77	0.73	0.87	n/a
1029	3	L1	0.36	0.86	0.51	0.63	0.30	0.39	0.39	0.26	n/a
1030	3	L10	-0.21	0.65	0.16	-0.04	-0.97	-1.55	-1.46	-1.21	n/a
1031	3	L12	0.86	0.38	0.55	0.37	0.93	0.67	0.67	0.98	n/a
1032	3	L14	0.77	0.96	0.71	0.40	0.94	0.71	0.79	0.92	n/a
1033	3	L15	0.93	1.18	1.26	-0.03	0.54	0.60	0.57	0.58	n/a
1034	3	L16	1.58	1.11	1.41	0.52	1.32	1.17	1.16	1.36	n/a
1035	3	L18	1.36	1.26	1.64	0.85	1.39	1.04	1.08	1.40	n/a
1036	3	L2	0.77	1.24	1.09	0.63	0.62	0.72	0.66	0.66	n/a
1037	3	L20	1.47	1.15	1.43	0.82	1.40	1.12	1.12	1.44	n/a
1038	3	L21	1.04	0.37	0.93	1.47	0.06	-0.40	-0.46	0.18	n/a
1039	3	L3	1.60	1.12	1.84	0.75	1.20	1.17	1.13	1.19	n/a
1040	3	L5	1.15	1.05	1.61	0.50	1.45	1.12	1.08	1.51	n/a
1041	3	L9	1.32	0.82	1.28	0.56	1.01	0.53	0.70	0.88	n/a
1042	3	M15	1.27	1.15	1.40	0.44	1.27	1.04	1.06	1.26	n/a
1043	3	M16	1.46	1.29	1.52	0.78	1.47	1.32	1.31	1.49	n/a
1044	3	M19	0.98	0.84	1.11	0.58	0.97	0.65	0.64	1.07	n/a
1045	3	M2	-0.16	0.72	0.46	-0.89	-0.12	0.07	-0.15	0.11	n/a
1046	3	M21	1.27	0.65	1.05	0.53	0.85	0.38	0.56	0.69	n/a
1047	3	M3	0.33	-0.34	0.32	-0.11	-0.09	-0.42	-0.17	-0.45	n/a
1048	3	M4	1.74	0.75	1.74	0.27	1.21	0.96	1.12	1.02	n/a
1049	3	M5	0.73	0.75	0.63	0.60	-0.01	-0.22	-0.12	-0.08	n/a
1050	3	M6	1.35	1.65	1.86	0.65	1.61	1.41	1.35	1.70	n/a
1051	3	M7	1.59	1.89	1.60	1.06	0.77	0.59	0.68	0.69	n/a
1052	3	M9	1.28	0.86	1.14	-0.04	0.79	0.53	0.74	0.60	n/a
1053	3	N12	1.49	1.48	1.99	1.07	0.74	0.51	0.69	0.50	n/a
1054	3	N17	1.03	1.47	1.78	0.48	0.60	0.30	0.32	0.58	n/a
1055	3	N18	1.09	1.36	0.36	0.13	0.34	0.27	0.22	0.44	n/a
1056	3	N19	1.53	1.64	1.83	0.87	1.16	1.06	1.09	1.16	n/a
1057	3	N2	1.15	1.17	0.79	0.53	0.36	0.63	0.58	0.36	n/a
1058	3	N20	0.74	1.02	0.97	0.69	1.14	0.77	0.76	1.20	n/a
1059	3	N21	0.02	0.48	-0.04	0.77	0.35	0.12	0.22	0.21	n/a
1060	3	N3	0.61	0.48	0.64	0.07	0.66	0.45	0.57	0.58	n/a
1061	3	N4	1.68	1.50	1.98	0.19	1.10	1.18	1.12	1.13	n/a
1062	3	N9	1.52	1.00	1.21	0.19	0.94	0.73	0.87	0.76	n/a
1063	3	O1	0.92	1.25	1.27	0.93	1.01	1.08	1.03	1.12	n/a
1064	3	O12	0.46	0.72	0.74	0.41	0.56	0.70	0.70	0.62	n/a
1065	3	O14	0.21	1.28	0.79	-0.41	-0.10	1.05	0.83	0.13	n/a
1066	3	O15	0.72	0.42	0.93	-0.01	1.19	1.21	1.12	1.33	n/a
1067	3	O16	1.17	1.29	1.28	0.04	1.26	1.32	1.19	1.37	n/a
1068	3	O18	1.11	1.30	1.45	0.46	1.33	1.12	1.12	1.41	n/a

1069	3	O2	1.77	0.77	0.78	0.55	-0.19	0.25	-0.01	0.14	n/a
1070	3	O21	0.34	0.34	0.41	-0.30	0.79	0.96	0.90	0.87	n/a
1071	3	O22	-0.34	1.50	0.36	0.92	-0.67	-0.22	-0.41	-0.48	n/a
1072	3	O3	1.08	0.96	0.81	1.00	0.52	0.52	0.50	0.61	n/a
1073	3	O5	0.16	0.78	0.37	0.59	0.06	0.12	-0.03	0.27	n/a
1074	3	O6	1.09	0.88	1.36	0.02	1.11	1.35	1.26	1.24	n/a
1075	3	O7	0.88	1.37	1.18	0.93	0.95	1.25	1.08	1.11	n/a
1076	3	O8	1.26	0.40	1.29	0.16	0.83	0.77	0.82	0.70	n/a
1077	3	P1	0.71	0.63	0.90	-0.26	0.77	0.82	0.76	0.79	n/a
1078	3	P10	1.06	1.33	1.59	0.01	1.02	1.23	1.09	1.13	n/a
1079	3	P11	0.99	1.16	1.34	0.73	0.93	1.13	0.96	1.17	n/a
1080	3	P12	1.00	1.45	1.44	0.71	1.06	1.46	1.32	1.26	n/a
1081	3	P13	0.44	0.38	0.85	-0.39	1.11	1.15	1.02	1.26	n/a
1082	3	P14	1.17	1.35	1.00	0.82	0.49	1.20	1.04	0.60	n/a
1083	3	P15	0.39	1.03	0.77	0.13	1.01	1.00	0.97	1.05	n/a
1084	3	P16	0.79	1.12	1.37	-0.01	1.12	1.28	1.24	1.13	n/a
1085	3	P18	0.91	1.51	1.47	0.49	1.16	1.43	1.29	1.32	n/a
1086	3	P19	0.60	0.93	0.83	0.03	1.16	1.00	1.02	1.20	n/a
1087	3	P20	0.32	0.54	0.83	0.05	0.97	1.03	0.92	1.11	n/a
1088	3	P21	0.94	1.99	1.72	0.60	0.43	0.70	0.71	0.39	n/a
1089	3	P3	0.08	0.12	0.27	-0.17	0.90	0.91	0.88	0.99	n/a
1090	3	P6	0.52	-0.32	0.43	-0.83	0.75	0.72	0.85	0.62	n/a
1091	3	P9	0.02	0.55	0.73	-0.38	1.44	1.42	1.36	1.56	n/a
1092	4	A1	0.22	0.84	0.83	0.15	0.33	0.36	0.37	0.31	n/a
1093	4	A10	0.14	0.58	0.65	-0.59	0.87	0.92	0.91	0.86	n/a
1094	4	A11	0.32	0.66	1.01	0.02	1.31	1.34	1.31	1.36	n/a
1095	4	A13	0.36	0.22	0.18	-0.09	0.62	0.88	0.80	0.71	n/a
1096	4	A15	1.05	0.44	1.05	0.40	0.96	0.84	0.86	0.95	n/a
1097	4	A16	0.27	0.17	0.71	0.05	0.90	0.65	0.73	0.80	n/a
1098	4	A17	0.55	0.53	0.81	0.18	0.88	0.82	0.72	0.95	n/a
1099	4	A18	0.93	1.37	1.49	0.05	0.99	1.12	1.00	1.08	n/a
1100	4	A19	1.05	0.01	0.70	0.28	0.11	-0.23	-0.10	-0.08	n/a
1101	4	A2	0.12	0.95	0.63	0.11	0.45	0.65	0.61	0.54	n/a
1102	4	A20	1.27	0.99	1.66	0.87	0.99	1.01	0.96	1.01	n/a
1103	4	A21	0.71	0.85	1.03	0.17	0.75	0.74	0.76	0.73	n/a
1104	4	A22	1.28	1.23	1.37	0.93	0.88	0.68	0.76	0.75	n/a
1105	4	A3	0.77	0.82	1.36	-0.03	0.90	1.09	0.98	1.13	n/a
1106	4	A4	0.83	0.68	0.73	0.55	1.06	0.84	0.81	1.11	n/a
1107	4	A5	1.52	0.98	1.67	0.23	1.00	0.83	0.79	1.09	n/a
1108	4	A8	0.53	1.02	0.83	0.31	0.64	0.71	0.60	0.80	n/a
1109	4	A9	0.75	0.80	0.90	0.35	1.14	1.17	1.04	1.34	n/a
1110	4	B1	1.40	1.27	1.47	1.33	0.63	0.70	0.64	0.74	n/a
1111	4	B11	0.53	0.66	0.79	0.35	1.03	0.29	0.55	0.77	n/a
1112	4	B12	-1.24	-1.02	-1.03	0.13	-1.02	-1.67	-1.71	-1.08	n/a
1113	4	B13	0.17	-0.04	0.19	0.29	0.39	-0.33	-0.02	0.05	n/a
1114	4	B14	0.52	-0.06	0.66	0.74	-0.28	-1.08	-0.91	-0.55	n/a
1115	4	B15	-0.21	0.09	-0.01	0.00	-0.38	-1.16	-0.95	-0.67	n/a
1116	4	B17	-0.89	-0.53	-0.59	-0.62	-0.32	-1.16	-0.95	-0.61	n/a
1117	4	B18	0.06	0.00	0.81	-0.99	-0.43	-1.26	-0.99	-0.76	n/a
1118	4	B19	-1.02	-0.55	-0.98	-0.73	-0.04	-0.43	-0.25	-0.18	n/a
1119	4	B2	0.70	0.82	0.96	0.22	0.98	0.97	0.92	1.07	n/a
1120	4	B20	1.00	0.67	0.71	0.69	0.79	0.18	0.45	0.46	n/a
1121	4	B21	-0.10	-0.03	0.01	0.07	0.76	0.20	0.51	0.39	n/a
1122	4	B22	0.94	0.42	0.97	-0.10	0.80	0.28	0.45	0.64	n/a
1123	4	B3	-0.82	-0.83	-0.77	-0.21	-0.83	-1.52	-1.36	-1.03	n/a
1124	4	B4	0.66	0.08	0.89	-0.06	0.98	0.76	0.83	0.90	n/a
1125	4	B5	-0.53	0.04	-0.19	0.20	0.09	-0.87	-0.41	-0.42	n/a
1126	4	B6	-0.07	-0.36	0.04	-0.20	0.59	-0.21	0.23	0.14	n/a

1127	4	B7	0.65	0.34	0.60	0.53	0.11	0.06	0.10	0.06	n/a
1128	4	B8	1.14	0.82	1.75	0.03	0.89	0.15	0.45	0.63	n/a
1129	4	B9	0.26	0.02	0.54	-0.01	0.84	0.36	0.52	0.75	n/a
1130	4	C1	-0.06	-0.32	0.06	-0.31	0.90	0.61	0.71	0.84	n/a
1131	4	C10	-0.20	-0.26	0.26	-0.79	-0.15	-0.78	-0.58	-0.33	n/a
1132	4	C11	0.85	0.18	0.79	-1.05	-0.18	-1.73	-1.17	-1.00	n/a
1133	4	C12	-0.17	-0.39	-0.17	-0.59	-0.25	-1.25	-0.95	-0.67	n/a
1134	4	C13	-0.33	-0.62	-0.32	0.11	-0.30	-1.42	-1.04	-0.81	n/a
1135	4	C14	0.15	-0.29	-0.08	-0.21	0.34	-0.43	-0.13	0.03	n/a
1136	4	C15	-0.37	-0.46	0.06	-0.21	0.04	-0.87	-0.60	-0.31	n/a
1137	4	C16	0.12	-0.84	0.20	-0.64	-0.46	-1.53	-1.35	-0.77	n/a
1138	4	C18	0.41	-0.09	0.24	0.46	-0.04	-0.94	-0.55	-0.49	n/a
1139	4	C19	-0.28	-0.46	-0.20	-0.43	-0.34	-1.44	-1.13	-0.79	n/a
1140	4	C2	1.64	0.04	1.18	-0.46	0.58	0.69	0.72	0.55	n/a
1141	4	C20	-0.11	0.13	-0.19	0.28	-1.01	-1.74	-1.71	-1.18	n/a
1142	4	C21	0.40	0.80	1.03	0.32	0.65	0.24	0.24	0.67	n/a
1143	4	C22	-0.07	0.27	0.05	0.45	-0.59	-1.44	-1.24	-0.85	n/a
1144	4	C3	-0.40	-0.35	-0.16	-0.64	0.40	-0.28	0.07	0.00	n/a
1145	4	C4	0.27	0.65	0.35	0.76	0.92	0.68	0.72	0.89	n/a
1146	4	C5	-0.51	-0.46	-0.51	0.00	0.47	-0.09	0.07	0.31	n/a
1147	4	C7	0.37	-0.10	0.57	-0.05	0.92	0.26	0.49	0.69	n/a
1148	4	C8	-0.44	-0.23	-0.44	-0.24	0.32	-0.59	-0.12	-0.20	n/a
1149	4	C9	1.53	0.47	0.63	0.34	0.17	-0.07	0.00	0.15	n/a
1150	4	D1	0.68	0.72	0.71	0.63	0.58	0.34	0.31	0.62	n/a
1151	4	D10	-0.28	0.24	0.42	-0.33	-0.68	-1.35	-1.50	-0.61	n/a
1152	4	D11	0.62	0.14	0.71	0.24	0.20	-0.38	-0.07	-0.12	n/a
1153	4	D12	-0.40	-0.45	-0.49	-0.06	-0.73	-1.59	-1.46	-0.97	n/a
1154	4	D13	0.43	-0.36	0.18	0.66	-1.09	-1.76	-1.79	-1.15	n/a
1155	4	D14	-0.19	-0.91	-0.62	-0.31	-0.65	-1.25	-1.05	-0.90	n/a
1156	4	D17	-0.24	-0.38	-0.19	-0.07	0.24	-0.85	-0.45	-0.19	n/a
1157	4	D18	-0.46	-0.12	-0.58	0.02	-0.29	-1.34	-1.10	-0.64	n/a
1158	4	D2	0.08	0.14	0.14	0.08	0.65	0.59	0.62	0.63	n/a
1159	4	D20	0.06	-0.11	0.20	-0.09	0.08	-0.54	-0.29	-0.22	n/a
1160	4	D21	1.08	0.48	1.02	0.43	0.13	-0.29	-0.17	0.02	n/a
1161	4	D22	0.59	0.05	0.34	-0.06	-0.41	-1.18	-1.09	-0.64	n/a
1162	4	D3	-0.41	0.16	-0.46	0.36	-0.62	-1.11	-0.91	-0.86	n/a
1163	4	D4	-0.17	0.04	-0.01	0.19	0.35	0.03	0.12	0.30	n/a
1164	4	D6	-1.25	-0.90	-1.08	-0.46	0.07	-0.27	-0.14	-0.04	n/a
1165	4	D7	-0.36	0.34	0.16	0.26	-0.53	-1.08	-1.02	-0.63	n/a
1166	4	D8	-0.22	0.24	0.03	0.15	0.54	-0.17	-0.04	0.41	n/a
1167	4	D9	-0.16	-0.17	-0.06	0.55	0.05	-0.82	-0.50	-0.32	n/a
1168	4	E1	0.62	1.18	1.04	0.76	0.56	0.47	0.42	0.66	n/a
1169	4	E11	0.06	-0.42	-0.02	-0.44	-0.07	-0.87	-0.53	-0.43	n/a
1170	4	E12	-0.75	-0.40	-0.52	-0.66	-1.00	-1.65	-1.62	-1.09	n/a
1171	4	E13	0.15	-0.03	0.15	0.27	-0.72	-1.55	-1.52	-0.85	n/a
1172	4	E14	0.21	0.42	0.35	0.63	-0.03	-0.45	-0.38	-0.03	n/a
1173	4	E15	1.06	-0.10	0.91	1.08	-0.41	-1.17	-1.13	-0.53	n/a
1174	4	E17	0.88	0.92	0.72	1.47	-0.53	-1.61	-1.33	-0.93	n/a
1175	4	E18	-0.38	-0.57	-0.55	-0.95	-0.88	-1.30	-1.21	-0.94	n/a
1176	4	E2	0.47	0.48	0.12	0.66	-0.10	-0.19	-0.16	-0.13	n/a
1177	4	E21	0.33	0.50	0.53	0.83	0.47	0.07	0.25	0.32	n/a
1178	4	E22	0.33	0.96	0.57	1.02	-0.50	-1.46	-1.12	-0.90	n/a
1179	4	E3	0.10	-0.01	0.36	0.14	0.42	-0.01	0.10	0.33	n/a
1180	4	E4	1.11	0.86	1.07	0.79	0.79	0.53	0.60	0.75	n/a
1181	4	E5	0.25	0.06	0.13	0.00	0.53	-0.22	0.04	0.28	n/a
1182	4	E6	0.44	0.46	0.54	0.22	0.63	0.70	0.64	0.73	n/a
1183	4	E7	0.06	0.08	0.33	0.04	0.43	-0.21	0.00	0.23	n/a
1184	4	E8	0.28	-0.46	-0.04	-0.17	0.56	-0.15	0.27	0.17	n/a

1185	4	E9	0.19	0.29	0.43	0.40	0.35	-0.18	-0.02	0.17	n/a
1186	4	F1	-0.42	0.31	-0.23	0.28	0.19	0.08	0.09	0.21	n/a
1187	4	F11	0.04	0.03	-0.04	0.19	0.18	-0.60	-0.24	-0.20	n/a
1188	4	F12	-0.01	0.12	0.10	0.72	-0.74	-1.64	-1.68	-0.81	n/a
1189	4	F13	1.59	1.56	1.90	1.95	-0.30	-1.52	-0.99	-0.96	n/a
1190	4	F14	0.39	0.91	0.23	1.03	0.06	-0.07	-0.08	0.13	n/a
1191	4	F16	-0.32	-0.23	-0.36	0.00	-0.18	-1.15	-0.76	-0.66	n/a
1192	4	F17	-0.27	0.03	-0.04	-0.13	-0.73	-1.78	-1.31	-1.27	n/a
1193	4	F18	0.46	-0.28	-0.11	0.02	-0.56	-0.92	-0.77	-0.73	n/a
1194	4	F19	-0.18	0.38	0.03	0.31	0.31	-0.22	0.04	0.05	n/a
1195	4	F2	0.34	-0.03	0.38	-0.03	0.48	0.37	0.36	0.54	n/a
1196	4	F21	0.25	0.44	0.50	-0.43	-0.11	-0.53	-0.44	-0.22	n/a
1197	4	F22	-0.37	-0.94	-0.86	0.17	0.09	-0.87	-0.50	-0.30	n/a
1198	4	F3	-1.15	-1.33	-1.19	-0.34	-0.18	-0.64	-0.46	-0.41	n/a
1199	4	F4	-0.19	0.15	0.09	0.44	-0.21	-1.04	-0.74	-0.49	n/a
1200	4	F5	-0.63	-1.21	-0.52	-0.36	-0.68	-1.58	-1.57	-0.84	n/a
1201	4	F6	1.59	1.49	1.69	1.49	0.25	-0.44	-0.17	0.03	n/a
1202	4	F7	-0.16	-0.69	-0.48	0.31	-1.41	-1.80	-1.86	-1.35	n/a
1203	4	F8	-0.15	-0.41	-0.46	-0.42	0.15	-0.34	-0.10	-0.08	n/a
1204	4	F9	1.18	1.01	1.20	1.08	0.37	-0.64	-0.16	-0.17	n/a
1205	4	G1	0.30	0.65	0.57	0.59	0.56	0.37	0.42	0.57	n/a
1206	4	G11	0.20	-0.45	0.19	0.30	0.04	-0.59	-0.39	-0.17	n/a
1207	4	G12	0.12	-0.97	-0.16	-0.01	-0.76	-1.46	-1.24	-1.03	n/a
1208	4	G14	0.04	0.01	-0.14	-0.92	-0.40	-0.79	-0.76	-0.41	n/a
1209	4	G15	0.36	-0.04	0.13	0.35	-0.56	-1.37	-1.06	-0.94	n/a
1210	4	G16	-0.24	0.03	0.05	0.63	-0.60	-1.51	-1.44	-0.77	n/a
1211	4	G17	-0.25	-0.33	-0.28	0.61	-0.80	-1.73	-1.52	-1.09	n/a
1212	4	G19	-0.15	0.10	-0.03	0.32	0.86	-0.24	0.21	0.43	n/a
1213	4	G2	-0.21	0.50	0.19	0.48	0.60	0.45	0.47	0.62	n/a
1214	4	G20	0.80	0.40	0.98	0.70	0.32	-0.77	-0.14	-0.36	n/a
1215	4	G21	-0.27	0.20	0.06	0.52	-0.24	-1.16	-0.87	-0.58	n/a
1216	4	G3	0.08	-0.27	0.01	-0.10	-0.10	-0.78	-0.50	-0.42	n/a
1217	4	G4	0.79	0.80	0.59	0.69	0.54	0.38	0.47	0.46	n/a
1218	4	G5	-0.39	0.28	-0.06	0.25	0.40	-0.14	-0.01	0.31	n/a
1219	4	G6	0.28	0.55	0.22	-0.07	-0.57	-1.02	-1.04	-0.63	n/a
1220	4	G7	0.02	-0.18	0.02	0.26	0.01	-0.73	-0.45	-0.32	n/a
1221	4	G8	-0.52	-0.60	-0.65	-0.12	-0.96	-1.58	-1.45	-1.20	n/a
1222	4	G9	-0.06	0.30	-0.05	0.17	0.32	-0.31	-0.14	0.15	n/a
1223	4	H1	0.36	0.89	0.77	1.05	0.62	-0.16	0.17	0.31	n/a
1224	4	H10	0.36	0.22	0.34	0.93	-0.44	-1.31	-1.11	-0.68	n/a
1225	4	H11	-0.45	-0.35	-0.33	0.05	0.06	-0.51	-0.29	-0.17	n/a
1226	4	H12	-1.00	-1.18	-1.12	-0.68	-0.60	-1.47	-1.33	-0.83	n/a
1227	4	H13	-0.14	-0.31	-0.23	0.19	0.06	-0.63	-0.34	-0.24	n/a
1228	4	H14	-0.66	0.15	-0.41	0.03	-0.48	-0.93	-0.79	-0.65	n/a
1229	4	H17	0.08	-0.01	0.16	0.11	0.28	-0.70	-0.33	-0.14	n/a
1230	4	H18	-0.04	-0.17	-0.35	1.38	-1.07	-1.97	-1.83	-1.32	n/a
1231	4	H19	-0.09	0.33	0.21	0.28	0.43	-0.33	0.00	0.10	n/a
1232	4	H2	0.12	-0.15	0.27	0.07	0.48	0.06	0.20	0.37	n/a
1233	4	H20	0.34	0.25	0.58	0.18	0.13	-1.08	-0.60	-0.43	n/a
1234	4	H21	-0.05	0.20	0.22	0.32	0.31	-0.34	-0.13	0.09	n/a
1235	4	H22	-0.01	0.20	0.17	0.37	0.48	-0.43	-0.05	0.11	n/a
1236	4	H4	0.11	-0.03	-0.13	0.23	0.22	-0.33	-0.07	-0.04	n/a
1237	4	H5	-0.09	0.40	0.01	0.13	0.70	0.14	0.40	0.49	n/a
1238	4	H8	0.06	0.07	0.26	0.18	0.69	0.20	0.42	0.52	n/a
1239	4	H9	-0.25	-0.04	-0.04	0.15	0.29	-0.74	-0.31	-0.15	n/a
1240	4	I1	0.40	0.40	-0.09	1.11	0.21	0.00	0.09	0.15	n/a
1241	4	I10	0.30	0.11	0.10	0.24	0.01	-0.43	-0.19	-0.19	n/a
1242	4	I11	1.03	0.89	0.88	0.83	0.53	0.23	0.36	0.45	n/a

1243	4	I13	0.22	-0.30	-0.07	0.44	-0.02	-0.65	-0.35	-0.36	n/a
1244	4	I14	0.20	0.09	0.26	0.46	0.28	-0.28	-0.02	0.05	n/a
1245	4	I16	-0.12	0.89	-0.22	-0.05	-1.20	-2.05	-2.09	-1.30	n/a
1246	4	I18	-0.11	-0.02	0.10	-0.03	-1.31	-2.36	-2.23	-1.57	n/a
1247	4	I19	1.05	1.39	1.42	1.47	0.53	-0.14	0.08	0.35	n/a
1248	4	I2	0.64	0.64	0.46	0.97	0.65	0.17	0.35	0.53	n/a
1249	4	I20	0.65	0.23	0.47	0.48	0.48	-0.50	0.00	0.01	n/a
1250	4	I21	0.53	0.45	0.65	0.51	-0.09	-0.97	-0.57	-0.52	n/a
1251	4	I3	-1.01	1.03	-0.03	-1.63	-1.18	-1.91	-2.02	-1.21	n/a
1252	4	I4	1.33	0.85	1.13	0.67	0.47	-0.07	0.19	0.20	n/a
1253	4	I5	0.30	0.68	0.63	0.78	1.04	0.66	0.72	1.04	n/a
1254	4	I7	1.46	0.51	1.60	0.81	0.45	-0.03	0.16	0.28	n/a
1255	4	I8	-0.01	-0.21	-0.03	0.29	0.26	-0.53	-0.19	-0.05	n/a
1256	4	I9	-0.59	-0.22	-0.55	0.35	-0.26	-0.93	-0.67	-0.51	n/a
1257	4	J1	0.63	0.79	0.74	0.98	0.37	-0.23	0.02	0.12	n/a
1258	4	J10	0.80	0.14	0.61	0.63	-0.15	-0.77	-0.37	-0.54	n/a
1259	4	J11	0.66	1.21	0.64	1.17	-0.44	-1.09	-1.01	-0.59	n/a
1260	4	J13	0.83	0.98	1.02	0.99	0.17	-0.81	-0.28	-0.39	n/a
1261	4	J14	0.38	0.34	0.42	-0.13	-0.57	-1.68	-1.13	-1.25	n/a
1262	4	J15	0.34	1.14	0.48	1.69	-0.79	-1.91	-1.81	-1.08	n/a
1263	4	J16	0.45	0.84	0.49	0.27	-1.06	-1.96	-1.97	-1.20	n/a
1264	4	J17	1.24	0.88	1.09	0.79	0.89	-0.04	0.29	0.59	n/a
1265	4	J18	1.90	1.13	1.62	0.66	0.55	-0.22	0.07	0.30	n/a
1266	4	J2	1.31	0.42	0.93	0.40	-0.09	-0.22	-0.09	-0.22	n/a
1267	4	J20	1.12	1.25	1.23	1.49	0.34	-0.40	-0.18	0.15	n/a
1268	4	J21	1.52	1.30	1.45	1.38	0.40	-0.55	-0.16	0.06	n/a
1269	4	J22	1.72	1.12	1.74	1.08	0.16	-0.82	-0.51	-0.18	n/a
1270	4	J3	0.76	0.57	0.67	0.58	-0.82	-1.60	-1.41	-1.16	n/a
1271	4	J4	0.83	0.94	0.77	0.99	1.05	0.59	0.80	0.90	n/a
1272	4	J5	0.27	0.63	0.38	0.98	0.24	-0.36	-0.15	0.09	n/a
1273	4	J6	-0.03	-0.73	-0.16	0.29	-1.09	-1.73	-1.80	-1.13	n/a
1274	4	J7	0.82	0.74	0.88	0.55	0.57	-0.32	0.03	0.23	n/a
1275	4	K1	0.42	0.69	0.52	0.92	0.28	-0.11	0.06	0.12	n/a
1276	4	K11	1.26	0.36	0.92	1.09	0.65	0.02	0.31	0.43	n/a
1277	4	K13	0.87	-0.30	0.57	0.12	0.53	-0.38	0.07	0.07	n/a
1278	4	K14	1.37	1.56	1.68	1.42	0.77	0.09	0.33	0.57	n/a
1279	4	K17	0.75	0.00	1.03	0.18	-0.13	-0.75	-0.54	-0.33	n/a
1280	4	K18	0.58	-1.12	0.62	-0.48	0.02	-0.73	-0.42	-0.22	n/a
1281	4	K19	1.29	0.79	1.21	1.16	0.17	-0.45	-0.29	0.01	n/a
1282	4	K2	0.83	0.88	0.69	0.87	0.54	0.30	0.42	0.43	n/a
1283	4	K20	1.52	0.42	1.18	0.48	0.43	-0.35	0.15	-0.07	n/a
1284	4	K4	0.76	-0.22	0.63	0.45	0.58	0.03	0.26	0.37	n/a
1285	4	K5	1.45	0.71	0.63	0.03	0.05	-0.40	-0.22	-0.06	n/a
1286	4	K6	0.38	0.34	0.70	0.17	1.00	0.20	0.50	0.70	n/a
1287	4	K7	0.05	0.73	0.83	-0.09	0.32	-0.34	-0.13	0.19	n/a
1288	4	K8	-0.44	0.06	-0.06	-0.54	-1.06	-1.69	-1.86	-1.02	n/a
1289	4	L10	0.52	-0.22	0.48	0.66	0.02	-0.93	-0.51	-0.43	n/a
1290	4	L11	0.14	0.06	-0.08	0.62	-0.57	-0.78	-0.84	-0.44	n/a
1291	4	L14	0.77	0.83	0.66	0.89	-0.17	-1.18	-0.82	-0.58	n/a
1292	4	L15	0.38	-0.49	0.01	-0.08	-0.86	-1.34	-1.20	-1.00	n/a
1293	4	L17	1.53	0.72	1.64	0.91	0.46	-0.11	0.12	0.22	n/a
1294	4	L18	-0.57	-0.37	-0.27	-0.13	0.77	-0.03	0.12	0.69	n/a
1295	4	L20	1.45	1.10	1.62	1.46	0.87	0.11	0.47	0.55	n/a
1296	4	L21	0.69	0.13	0.85	0.51	0.17	-0.24	-0.23	0.25	n/a
1297	4	L22	0.27	0.52	0.67	0.02	-0.65	-1.40	-1.24	-0.91	n/a
1298	4	L3	1.52	1.69	1.52	-1.52	-0.97	-1.63	-1.77	-0.96	n/a
1299	4	L4	0.15	0.45	0.15	0.77	0.13	-0.25	-0.22	0.16	n/a
1300	4	L5	0.94	0.60	0.86	0.86	0.47	0.02	0.14	0.37	n/a

1301	4	L6	1.02	1.04	0.41	0.98	-0.60	-0.59	-0.60	-0.61	n/a
1302	4	L8	0.03	0.84	-0.21	0.97	-0.61	-1.05	-1.00	-0.61	n/a
1303	4	L9	-0.02	0.30	-0.22	1.19	-1.16	-1.92	-1.83	-1.36	n/a
1304	4	M10	-0.18	1.18	0.32	1.48	-0.96	-1.91	-1.78	-1.23	n/a
1305	4	M12	0.43	0.10	0.64	0.30	0.42	0.15	0.18	0.43	n/a
1306	4	M13	0.44	0.85	0.59	0.87	0.21	-0.40	-0.09	-0.10	n/a
1307	4	M14	0.56	0.85	0.78	0.37	0.85	0.66	0.69	0.88	n/a
1308	4	M16	-0.17	0.18	-0.07	-0.27	-0.79	-1.26	-1.31	-0.83	n/a
1309	4	M17	0.42	1.96	0.82	0.94	0.19	-0.32	-0.14	0.03	n/a
1310	4	M19	0.70	1.42	0.87	1.07	0.95	0.49	0.64	0.84	n/a
1311	4	M2	0.44	0.43	0.94	-0.06	0.98	0.57	0.75	0.76	n/a
1312	4	M20	-0.88	0.14	-0.74	0.34	-1.48	-1.80	-1.86	-1.52	n/a
1313	4	M3	1.21	0.19	-0.59	0.27	-0.07	-0.10	-0.12	-0.03	n/a
1314	4	M4	0.31	0.27	0.34	0.01	0.50	0.12	0.31	0.33	n/a
1315	4	M5	0.05	0.00	0.07	0.19	0.88	0.78	0.78	0.94	n/a
1316	4	M6	1.37	1.35	1.47	0.89	0.64	0.66	0.70	0.61	n/a
1317	4	M7	1.06	1.23	1.58	1.44	0.37	0.19	0.21	0.40	n/a
1318	4	M8	0.00	-0.19	-0.32	0.40	-1.17	-1.89	-1.74	-1.42	n/a
1319	4	M9	0.65	0.13	0.49	0.20	0.93	0.78	0.75	0.99	n/a
1320	4	N1	0.22	0.79	0.79	0.37	0.71	0.41	0.48	0.66	n/a
1321	4	N11	1.13	0.51	0.79	0.67	0.40	-0.04	0.15	0.26	n/a
1322	4	N13	-0.04	0.12	-0.50	-0.06	-1.44	-1.87	-1.67	-1.68	n/a
1323	4	N15	0.12	0.00	0.26	-0.01	-0.45	-1.37	-1.06	-0.84	n/a
1324	4	N17	0.08	0.01	-0.49	0.36	-0.71	-0.43	-0.52	-0.62	n/a
1325	4	N18	-0.53	0.25	-0.22	0.43	-0.20	-0.60	-0.48	-0.35	n/a
1326	4	N19	-0.52	-0.10	-0.38	0.07	-0.22	-0.54	-0.37	-0.40	n/a
1327	4	N2	0.50	0.88	0.68	0.81	0.57	0.28	0.33	0.52	n/a
1328	4	N20	1.31	1.30	1.48	1.10	0.65	0.27	0.38	0.56	n/a
1329	4	N21	-0.76	-1.82	-0.70	-1.21	-0.05	-0.46	-0.36	-0.12	n/a
1330	4	N22	0.48	0.58	0.63	0.45	0.51	0.09	0.31	0.32	n/a
1331	4	N3	-0.25	0.58	0.26	-0.08	-1.26	-1.91	-1.97	-1.34	n/a
1332	4	N4	0.53	0.20	0.28	0.37	0.40	0.24	0.44	0.17	n/a
1333	4	N5	-0.23	-0.65	-0.63	-0.10	0.48	0.55	0.63	0.38	n/a
1334	4	N6	-0.78	0.48	-0.94	-1.44	-1.18	-1.60	-1.53	-1.23	n/a
1335	4	N7	-0.31	-0.04	-0.08	-0.04	0.33	-0.62	-0.16	-0.11	n/a
1336	4	N8	0.52	-0.94	0.17	-0.29	-0.57	-1.22	-0.98	-0.79	n/a
1337	4	N9	-0.23	0.15	-0.22	0.39	-0.20	-0.62	-0.42	-0.39	n/a
1338	4	O1	0.38	0.41	0.68	0.82	0.47	0.24	0.31	0.43	n/a
1339	4	O10	-0.11	0.71	0.48	-0.09	0.07	-0.03	0.01	0.02	n/a
1340	4	O11	1.09	0.93	0.63	1.07	0.20	0.05	0.12	0.14	n/a
1341	4	O12	0.28	0.46	0.13	0.83	-0.18	0.03	-0.09	-0.01	n/a
1342	4	O13	1.50	1.65	1.34	1.76	0.60	0.83	0.73	0.75	n/a
1343	4	O14	1.11	1.14	0.86	0.99	0.50	0.70	0.63	0.64	n/a
1344	4	O15	-0.39	0.26	-0.15	0.49	-0.03	-0.18	-0.09	-0.11	n/a
1345	4	O16	0.45	0.33	0.21	0.43	-0.05	0.04	0.01	-0.04	n/a
1346	4	O17	1.52	0.97	0.41	0.48	-0.07	-0.21	-0.21	0.00	n/a
1347	4	O18	-0.36	0.23	-0.10	-0.08	-0.75	-1.03	-1.00	-0.86	n/a
1348	4	O19	1.53	1.89	1.67	1.67	0.60	0.45	0.63	0.44	n/a
1349	4	O2	0.59	0.54	0.82	0.54	0.75	0.57	0.64	0.71	n/a
1350	4	O20	0.43	0.78	0.47	0.78	0.68	0.46	0.53	0.63	n/a
1351	4	O21	-0.03	-0.12	-0.33	-0.80	0.13	-0.28	-0.01	-0.18	n/a
1352	4	O4	0.09	0.28	0.31	0.43	0.67	0.36	0.49	0.54	n/a
1353	4	O5	1.28	0.71	1.16	0.73	0.77	0.51	0.57	0.74	n/a
1354	4	O6	0.06	1.25	0.07	0.24	0.29	0.15	0.14	0.35	n/a
1355	4	O7	0.06	0.56	0.06	0.30	0.41	0.45	0.49	0.40	n/a
1356	4	O9	0.59	1.03	0.72	0.83	0.78	0.80	0.79	0.78	n/a
1357	4	P1	1.38	1.16	1.22	1.06	0.55	0.36	0.34	0.60	n/a
1358	4	P11	0.91	0.58	0.56	0.43	0.75	0.49	0.55	0.69	n/a

1359	4	P12	1.20	1.34	1.38	0.63	1.02	0.99	0.94	1.06	n/a
1360	4	P13	1.11	1.56	1.52	1.16	0.74	0.71	0.70	0.76	n/a
1361	4	P16	1.38	0.64	1.27	0.60	0.34	-0.04	0.06	0.22	n/a
1362	4	P17	0.87	0.73	0.95	0.60	0.76	0.91	0.86	0.84	n/a
1363	4	P18	0.34	0.73	0.59	0.32	0.77	0.46	0.55	0.69	n/a
1364	4	P2	0.39	0.26	0.49	-0.72	0.94	0.99	0.91	1.08	n/a
1365	4	P20	1.33	1.16	1.44	0.95	0.94	0.94	0.93	0.98	n/a
1366	4	P4	0.81	0.51	0.87	0.57	0.70	0.40	0.50	0.63	n/a
1367	4	P5	1.19	1.24	1.89	0.19	1.18	0.98	1.03	1.11	n/a
1368	4	P6	0.60	1.63	1.46	0.27	1.09	1.23	1.10	1.28	n/a
1369	4	P7	0.69	1.66	1.28	0.50	0.93	1.33	1.22	1.09	n/a
1370	4	P9	1.34	1.54	1.33	1.47	1.11	0.73	0.80	1.13	n/a
1371	5	A10	1.29	0.26	0.95	0.26	-0.22	0.10	0.01	-0.18	n/a
1372	5	A11	-0.84	-0.84	-0.12	-0.95	-0.82	-0.16	-0.29	-0.42	n/a
1373	5	A12	-0.60	-1.18	-0.86	-1.63	-1.42	-0.38	-0.49	-1.10	n/a
1374	5	A13	-1.18	-0.49	-0.84	-0.36	-0.52	-0.24	-0.39	-0.28	n/a
1375	5	A14	-0.86	-0.70	-0.72	-0.15	-1.00	-0.36	-0.55	-0.76	n/a
1376	5	A15	-0.89	-0.78	-0.90	-1.59	0.02	-0.16	-0.04	-0.33	n/a
1377	5	A16	-0.47	-0.98	-1.26	-1.18	-1.30	-0.32	-0.42	-1.00	n/a
1378	5	A17	-1.09	-0.62	-0.93	0.11	-1.00	-0.60	-0.77	-0.71	n/a
1379	5	A18	-0.16	-0.57	-0.03	-0.34	1.04	-0.04	0.14	0.44	n/a
1380	5	A19	-0.53	-0.19	-0.32	-0.31	-0.94	-0.66	-0.77	-0.81	n/a
1381	5	A2	0.65	0.12	0.41	0.41	-0.40	0.00	-0.11	-0.04	n/a
1382	5	A20	0.14	-0.57	-0.80	0.47	-1.42	-0.46	-0.70	-0.86	n/a
1383	5	A21	-0.01	-0.22	-0.61	-0.18	-1.06	-0.20	-0.47	-0.42	n/a
1384	5	A22	-0.63	-0.79	-1.45	-1.15	-1.00	-0.12	-0.19	-0.66	n/a
1385	5	A3	-0.91	0.06	-0.62	-1.83	-1.00	-0.44	-0.60	-0.71	n/a
1386	5	A5	0.19	0.47	0.39	-0.91	0.56	-0.76	-0.39	-0.86	n/a
1387	5	A6	0.88	-0.02	0.46	-1.70	-0.88	0.10	-0.16	-0.13	n/a
1388	5	A7	1.86	1.37	1.09	1.52	-0.64	0.93	0.73	0.35	n/a
1389	5	A8	0.75	0.28	0.28	0.93	0.92	0.35	0.57	0.44	n/a
1390	5	A9	-0.64	-0.36	-0.63	-1.39	-1.12	-0.10	-0.27	-0.61	n/a
1391	5	B1	-0.86	-0.68	-0.40	-0.79	-0.40	-0.10	-0.11	-0.23	n/a
1392	5	B10	-1.19	-0.93	-1.36	0.01	0.56	-0.18	0.19	-0.18	n/a
1393	5	B11	-1.46	-1.19	-1.19	-0.67	-0.70	-0.84	-0.85	-0.76	n/a
1394	5	B12	-0.38	-0.85	-0.69	-0.45	-0.46	-0.52	-0.44	-0.47	n/a
1395	5	B13	-1.37	-1.77	-1.46	-1.02	-0.64	-1.00	-0.93	-1.00	n/a
1396	5	B14	0.48	-0.38	-0.28	-0.38	-0.10	-0.08	-0.04	-0.23	n/a
1397	5	B16	-1.35	-0.70	-1.26	0.78	-1.18	-0.98	-0.95	-1.19	n/a
1398	5	B17	-0.90	-0.95	-1.11	-0.61	-0.58	-0.66	-0.62	-0.81	n/a
1399	5	B18	-1.08	-1.32	-1.37	-0.79	-1.24	-0.92	-1.03	-0.95	n/a
1400	5	B19	-1.50	-1.12	-1.18	-1.07	-0.28	-0.80	-0.70	-0.61	n/a
1401	5	B2	-0.46	-0.74	-0.63	-0.25	0.68	0.08	0.22	0.40	n/a
1402	5	B20	-1.11	-1.16	-0.92	-0.61	-0.46	-0.84	-0.65	-1.00	n/a
1403	5	B21	-0.78	-0.76	-0.79	-0.51	0.38	-0.56	-0.29	-0.47	n/a
1404	5	B22	-1.16	-0.82	-0.95	-0.56	-0.22	-0.74	-0.55	-0.81	n/a
1405	5	B3	0.48	-0.72	0.18	-0.51	-0.22	-0.34	-0.32	-0.37	n/a
1406	5	B4	-0.19	-0.21	-0.16	-0.09	0.32	-0.10	0.04	-0.13	n/a
1407	5	B5	-0.46	-0.97	-0.80	0.21	0.20	0.08	0.12	0.30	n/a
1408	5	B6	-0.70	-0.13	-0.05	-0.71	-0.76	-0.66	-0.75	-0.66	n/a
1409	5	B8	-0.46	-0.81	-0.88	-1.20	0.26	-0.12	-0.14	0.15	n/a
1410	5	B9	-1.12	-0.89	-1.14	0.03	-0.64	-0.76	-0.80	-0.66	n/a
1411	5	C10	-0.12	0.01	0.09	0.29	0.80	-0.30	-0.09	0.11	n/a
1412	5	C11	-0.36	-0.64	-0.27	-0.17	0.02	-0.40	-0.29	-0.37	n/a
1413	5	C12	1.00	0.02	0.76	0.68	0.50	-0.44	-0.16	-0.28	n/a
1414	5	C13	0.31	-0.27	0.27	-0.69	1.28	0.10	0.37	0.49	n/a
1415	5	C14	-0.59	-0.71	-0.29	-0.57	0.32	-0.24	-0.04	-0.09	n/a
1416	5	C15	0.39	-1.30	0.19	-0.92	0.02	-0.26	-0.24	-0.09	n/a

1417	5	C16	-0.82	-1.14	-0.55	-1.73	-0.04	-0.52	-0.42	-0.42	n/a
1418	5	C17	-0.69	-0.70	-0.69	-0.23	0.02	-0.88	-0.67	-0.61	n/a
1419	5	C18	-0.82	-0.67	-0.92	-0.82	-0.04	-0.50	-0.42	-0.52	n/a
1420	5	C19	-1.00	-0.50	-0.53	-0.88	-0.04	-0.54	-0.55	-0.28	n/a
1421	5	C2	-0.82	-1.66	-1.41	-1.48	-0.52	-0.88	-0.77	-0.90	n/a
1422	5	C20	-1.20	-0.74	-0.78	-0.50	-0.28	-0.56	-0.67	-0.28	n/a
1423	5	C21	-0.93	-0.70	-0.48	-0.48	0.44	-0.42	-0.32	-0.04	n/a
1424	5	C22	-0.91	-0.77	-0.85	-0.08	-0.10	-0.76	-0.65	-0.52	n/a
1425	5	C3	0.19	-0.44	0.16	-0.60	0.44	0.02	0.09	0.40	n/a
1426	5	C4	-0.67	-0.98	-0.63	-0.92	0.38	-0.54	-0.32	-0.28	n/a
1427	5	C5	0.31	-0.76	0.12	0.79	0.92	-0.82	-0.42	-0.28	n/a
1428	5	C7	-0.88	-1.20	-0.84	-0.84	-0.28	-0.78	-0.77	-0.52	n/a
1429	5	C8	0.53	-0.26	-0.06	0.08	-0.04	0.17	0.12	0.15	n/a
1430	5	C9	-0.13	-0.34	-0.19	-0.45	0.08	-0.20	-0.01	-0.33	n/a
1431	5	D1	0.27	-0.19	0.35	-0.53	0.62	0.00	0.07	0.25	n/a
1432	5	D10	0.13	-0.84	-0.33	-0.36	0.14	-0.46	-0.42	-0.18	n/a
1433	5	D11	0.66	-0.19	0.31	0.66	0.62	-0.44	-0.16	-0.18	n/a
1434	5	D12	-1.00	-1.62	-0.81	-0.48	-1.24	-1.18	-1.31	-1.00	n/a
1435	5	D13	-0.65	-1.48	-0.98	-0.62	-0.28	-0.76	-0.75	-0.52	n/a
1436	5	D14	0.08	-0.55	-0.07	-0.31	0.56	-0.36	-0.19	0.06	n/a
1437	5	D15	1.56	-0.26	0.86	0.13	0.14	-0.18	-0.04	-0.13	n/a
1438	5	D16	-1.38	-1.79	-1.41	-0.29	-1.42	-1.20	-1.41	-1.24	n/a
1439	5	D17	0.27	-0.55	0.26	0.52	0.14	-0.42	-0.37	-0.04	n/a
1440	5	D18	-0.04	-0.86	-0.11	-0.65	0.38	-0.40	-0.34	0.11	n/a
1441	5	D19	-0.87	-0.77	-0.86	-0.41	-1.42	-1.20	-1.44	-1.19	n/a
1442	5	D2	0.30	-0.14	-0.15	-0.11	0.32	-0.18	-0.16	0.20	n/a
1443	5	D20	-0.32	-0.59	-0.47	-0.06	0.62	-0.68	-0.42	-0.09	n/a
1444	5	D21	-0.75	-1.03	-0.61	-0.48	0.38	-0.74	-0.52	-0.33	n/a
1445	5	D22	-0.35	-1.48	-0.71	-0.59	-0.88	-0.64	-0.75	-0.61	n/a
1446	5	D3	-0.73	-0.86	-0.75	-0.49	0.62	-0.26	-0.16	0.20	n/a
1447	5	D4	-0.89	-1.89	-1.72	-0.61	-0.52	-0.78	-0.88	-0.47	n/a
1448	5	D5	-0.15	-0.41	0.09	0.07	0.80	-0.38	-0.19	0.15	n/a
1449	5	D6	-0.07	0.00	-0.03	-0.17	0.86	-0.18	0.01	0.40	n/a
1450	5	D7	-0.34	-1.03	-0.48	0.14	-0.22	-0.96	-0.95	-0.47	n/a
1451	5	D8	-0.71	-0.93	-0.81	-0.03	1.46	0.04	0.40	0.54	n/a
1452	5	D9	-0.23	-0.45	-0.21	0.06	0.86	-0.38	-0.24	0.30	n/a
1453	5	E1	0.41	0.11	0.55	-0.85	-0.34	0.00	0.01	-0.28	n/a
1454	5	E10	-0.38	-0.52	-0.18	-0.35	0.20	-0.22	-0.27	0.11	n/a
1455	5	E11	-0.03	0.06	0.26	0.31	0.38	-0.36	-0.34	0.15	n/a
1456	5	E12	-0.86	-0.70	-0.95	-0.46	0.14	-0.12	-0.24	0.44	n/a
1457	5	E13	0.12	-0.42	-0.06	0.03	-0.04	-0.80	-0.72	-0.52	n/a
1458	5	E14	0.33	-0.57	0.45	-0.49	0.92	-0.40	-0.14	0.15	n/a
1459	5	E15	-0.06	-1.05	-0.59	-1.01	0.14	-0.42	-0.32	-0.28	n/a
1460	5	E16	-0.93	-0.98	-0.82	-0.44	-0.22	-0.80	-0.75	-0.42	n/a
1461	5	E17	-0.90	-0.66	-0.80	0.45	-0.28	-0.78	-0.70	-0.57	n/a
1462	5	E18	-0.55	-0.54	-0.23	-0.82	-0.64	-0.88	-0.98	-0.66	n/a
1463	5	E19	-0.65	-0.67	-0.42	0.28	0.14	-0.82	-0.57	-0.57	n/a
1464	5	E2	0.02	-0.88	-0.27	-0.31	0.74	-0.10	0.04	0.25	n/a
1465	5	E21	0.32	-0.14	0.06	0.08	0.86	-0.12	0.07	0.25	n/a
1466	5	E22	-0.60	-0.84	-0.51	-0.76	0.08	-0.20	-0.14	-0.18	n/a
1467	5	E3	-0.25	-0.25	0.13	0.17	0.62	-0.20	-0.06	0.15	n/a
1468	5	E4	-0.40	-0.65	-0.66	-0.49	-0.82	-0.78	-0.85	-0.76	n/a
1469	5	E5	-0.58	-0.48	-0.29	-0.29	-0.82	-0.90	-1.05	-0.61	n/a
1470	5	E6	0.22	-0.11	0.20	0.50	0.50	-0.54	-0.39	-0.09	n/a
1471	5	E7	-0.39	-0.87	-0.79	-0.55	0.20	-0.84	-0.62	-0.52	n/a
1472	5	E8	0.48	-0.17	0.36	-0.02	-0.22	-0.64	-0.65	-0.37	n/a
1473	5	E9	-0.02	-0.35	-0.11	-0.49	0.14	-0.74	-0.57	-0.47	n/a
1474	5	F1	0.73	-0.30	-0.33	-0.87	0.14	0.49	0.47	0.25	n/a

1475	5	F11	0.67	0.34	1.12	0.46	1.34	-0.14	0.09	0.64	n/a
1476	5	F12	0.38	-0.76	-0.07	0.35	0.44	-0.56	-0.32	-0.13	n/a
1477	5	F13	0.11	-0.27	-0.10	0.60	-1.06	-1.04	-1.21	-0.76	n/a
1478	5	F14	0.53	-0.60	0.63	-0.11	0.38	-0.46	-0.42	0.20	n/a
1479	5	F15	0.51	-0.40	0.38	-0.22	0.38	-0.40	-0.34	0.20	n/a
1480	5	F17	0.02	-0.54	0.12	-0.41	0.56	-0.64	-0.42	-0.13	n/a
1481	5	F19	-0.83	-1.20	-0.80	-0.35	-1.36	-0.88	-1.18	-0.76	n/a
1482	5	F2	0.80	0.32	0.81	-1.15	0.68	-0.26	-0.19	0.35	n/a
1483	5	F20	0.36	-0.08	0.42	0.53	-0.28	-0.44	-0.62	0.01	n/a
1484	5	F21	-0.28	-0.83	-0.23	-0.40	0.26	-0.80	-0.52	-0.57	n/a
1485	5	F22	-0.56	-0.84	-0.39	-1.01	0.20	-0.44	-0.39	-0.18	n/a
1486	5	F3	-0.47	-0.45	-0.31	-0.10	0.92	-0.10	-0.06	0.59	n/a
1487	5	F4	1.14	0.15	1.14	0.41	0.62	-0.26	-0.16	0.25	n/a
1488	5	F5	0.42	-0.57	0.31	0.09	0.86	-0.48	-0.27	0.11	n/a
1489	5	F6	-0.05	-1.12	-0.20	-0.33	0.80	-0.44	-0.29	0.40	n/a
1490	5	F8	0.02	-1.08	-0.31	-0.18	0.80	-0.38	-0.21	0.35	n/a
1491	5	F9	-0.16	-0.79	-0.81	-0.11	-0.52	-0.52	-0.60	-0.42	n/a
1492	5	G1	1.19	0.30	1.32	1.09	0.44	-0.22	-0.19	0.15	n/a
1493	5	G10	0.69	-0.83	0.65	-0.84	0.68	-0.60	-0.34	-0.09	n/a
1494	5	G11	1.02	-0.63	0.55	-0.10	1.04	-0.48	-0.16	0.11	n/a
1495	5	G12	-0.52	-0.89	-0.55	-0.81	-0.16	-0.86	-0.85	-0.42	n/a
1496	5	G13	1.84	-0.26	1.46	-0.77	0.56	-0.18	-0.19	0.49	n/a
1497	5	G14	1.35	-0.39	1.05	-0.19	1.40	-0.32	-0.01	0.44	n/a
1498	5	G15	1.07	0.72	1.14	0.50	0.74	-0.12	-0.04	0.64	n/a
1499	5	G16	-0.20	-0.86	-0.15	-0.63	-0.76	-0.94	-1.16	-0.47	n/a
1500	5	G17	-0.59	-1.58	-0.98	-1.26	-1.48	-0.76	-1.10	-0.86	n/a
1501	5	G18	1.00	-0.74	0.45	-0.26	0.44	-0.68	-0.52	-0.13	n/a
1502	5	G19	0.22	-0.01	0.08	0.77	0.02	-0.70	-0.72	-0.13	n/a
1503	5	G2	-0.33	0.03	0.17	0.01	0.02	-0.30	-0.27	-0.09	n/a
1504	5	G20	1.06	0.45	1.21	-0.13	0.98	-0.42	-0.16	0.01	n/a
1505	5	G3	0.37	-0.55	0.42	-0.12	0.92	-0.20	-0.09	0.54	n/a
1506	5	G5	-0.72	-1.24	-0.85	-0.85	-1.18	-1.14	-1.28	-1.10	n/a
1507	5	G6	0.27	-1.01	-0.02	-0.34	0.02	-0.84	-0.75	-0.47	n/a
1508	5	G7	0.34	-0.47	0.07	0.38	-0.04	-0.86	-0.72	-0.52	n/a
1509	5	G8	0.15	-0.46	0.18	-0.32	0.50	-0.52	-0.44	0.06	n/a
1510	5	G9	1.02	-0.24	0.53	0.25	0.92	-0.10	-0.06	0.54	n/a
1511	5	H10	0.95	-1.06	0.39	-0.02	0.14	-0.80	-0.72	-0.28	n/a
1512	5	H11	1.08	-0.01	0.58	0.00	1.52	-0.30	0.01	0.49	n/a
1513	5	H12	0.96	0.12	0.84	0.35	0.26	-0.36	-0.29	0.01	n/a
1514	5	H13	0.52	0.00	0.66	-0.01	0.80	-0.54	-0.32	0.06	n/a
1515	5	H14	0.10	-0.94	-0.16	-0.30	-0.76	-0.96	-1.13	-0.61	n/a
1516	5	H15	1.05	-0.56	0.68	-0.48	0.62	-0.50	-0.34	0.11	n/a
1517	5	H16	-1.48	-1.04	-1.44	-0.77	-1.00	-0.92	-1.08	-0.81	n/a
1518	5	H17	0.29	-0.55	-0.14	0.46	0.02	-0.74	-0.70	-0.28	n/a
1519	5	H19	-1.12	-1.40	-0.88	-0.99	-1.65	-1.32	-1.64	-1.19	n/a
1520	5	H20	-0.04	-0.20	0.07	0.47	-0.76	-1.14	-1.23	-0.71	n/a
1521	5	H21	-0.52	-1.60	-0.20	-1.25	-0.76	-1.24	-1.26	-1.00	n/a
1522	5	H22	0.00	-0.61	0.00	0.18	0.14	-0.66	-0.57	-0.28	n/a
1523	5	H3	1.03	-0.71	0.44	-0.27	0.62	-0.36	-0.27	0.35	n/a
1524	5	H4	1.02	-0.47	0.46	-0.56	0.86	-0.44	-0.29	0.35	n/a
1525	5	H6	-0.74	-0.85	-0.79	-0.18	0.02	-0.80	-0.75	-0.33	n/a
1526	5	H8	-0.14	-0.72	0.20	0.01	0.98	-0.48	-0.29	0.30	n/a
1527	5	H9	1.96	0.83	1.57	1.43	-0.16	-0.66	-0.62	-0.47	n/a
1528	5	I1	0.73	0.40	0.66	-0.61	0.38	-0.16	0.04	-0.13	n/a
1529	5	I10	1.77	-0.04	1.09	0.84	0.26	-0.58	-0.44	-0.13	n/a
1530	5	I11	0.57	-0.92	0.22	0.59	-0.10	-0.92	-0.82	-0.61	n/a
1531	5	I12	0.28	-0.53	0.24	0.13	-0.28	-0.84	-0.80	-0.52	n/a
1532	5	I13	-0.15	-1.28	-0.17	-0.81	-1.36	-1.08	-1.44	-0.90	n/a

1533	5	I14	-0.32	0.06	0.23	0.19	-0.70	-0.64	-0.82	-0.42	n/a
1534	5	I15	-0.35	-0.83	-0.29	-0.35	0.20	-0.70	-0.60	-0.28	n/a
1535	5	I16	0.39	-0.11	0.52	0.24	0.44	-0.50	-0.44	0.06	n/a
1536	5	I17	-0.34	-0.34	-0.59	-0.45	-1.48	-1.00	-1.28	-0.81	n/a
1537	5	I18	0.52	0.33	0.35	0.76	-0.04	-0.46	-0.55	-0.04	n/a
1538	5	I19	0.02	0.15	0.13	0.86	-1.24	-0.72	-1.00	-0.66	n/a
1539	5	I20	-0.36	-0.06	-0.35	-3.79	-2.79	-1.22	-1.51	-2.39	n/a
1540	5	I21	0.01	0.00	-0.05	0.35	-1.42	-1.12	-1.33	-1.05	n/a
1541	5	I22	0.12	-0.20	0.30	0.34	-0.04	-0.48	-0.44	-0.23	n/a
1542	5	I3	0.51	0.10	0.70	-0.38	0.74	0.19	0.14	0.73	n/a
1543	5	I4	1.96	-0.30	1.54	-0.56	-0.34	-0.70	-0.93	-0.04	n/a
1544	5	I5	1.00	-0.52	0.54	0.26	-0.22	-0.92	-0.85	-0.52	n/a
1545	5	I7	1.24	-0.76	0.95	-0.18	0.56	-0.78	-0.52	-0.28	n/a
1546	5	I8	0.89	-0.37	0.64	0.55	0.26	-0.80	-0.65	-0.33	n/a
1547	5	I9	1.19	-0.77	0.65	-0.08	0.50	-0.60	-0.44	-0.13	n/a
1548	5	J1	0.08	-0.56	-0.06	-0.85	0.44	-0.10	-0.06	0.20	n/a
1549	5	J10	0.06	-0.70	0.12	0.19	-0.52	-1.10	-1.10	-0.81	n/a
1550	5	J11	0.55	-0.72	0.65	-0.23	1.10	-0.54	-0.24	0.06	n/a
1551	5	J12	-0.05	-0.73	-0.13	0.58	-0.58	-0.86	-0.90	-0.61	n/a
1552	5	J13	0.58	-1.01	0.41	-0.94	0.74	-0.40	-0.27	0.30	n/a
1553	5	J14	-0.27	-0.80	-0.10	-0.14	-0.16	-0.84	-0.77	-0.47	n/a
1554	5	J16	-0.71	-0.93	-0.83	-0.65	-1.30	-0.94	-1.28	-0.76	n/a
1555	5	J17	-0.36	-0.73	-0.40	-0.77	-0.16	-0.56	-0.55	-0.42	n/a
1556	5	J18	-0.89	-1.06	-1.14	-0.43	-1.00	-1.02	-1.16	-0.76	n/a
1557	5	J19	0.52	-0.31	0.61	0.25	0.14	-0.80	-0.70	-0.23	n/a
1558	5	J2	0.46	-0.08	0.18	-0.11	0.32	-0.30	-0.19	0.06	n/a
1559	5	J20	1.08	0.32	0.90	0.99	0.62	-0.86	-0.52	-0.42	n/a
1560	5	J21	-0.34	-0.75	-0.34	0.39	1.04	-0.48	-0.32	0.35	n/a
1561	5	J3	0.22	-1.01	-0.22	-0.79	0.14	-0.54	-0.47	-0.18	n/a
1562	5	J4	-0.02	-0.66	0.02	-0.40	0.14	-0.82	-0.60	-0.52	n/a
1563	5	J5	1.32	-0.42	1.21	0.78	0.32	-0.82	-0.70	-0.09	n/a
1564	5	J6	-0.41	-0.77	-0.61	0.51	0.08	-0.68	-0.65	-0.28	n/a
1565	5	J7	0.20	-0.75	-0.12	0.69	0.14	-0.78	-0.72	-0.28	n/a
1566	5	J8	0.66	-0.27	0.80	0.24	0.92	-0.44	-0.16	0.25	n/a
1567	5	J9	0.88	-0.05	0.66	0.69	1.04	-0.50	-0.27	0.15	n/a
1568	5	K1	0.65	-0.18	0.11	-0.07	-0.04	0.02	0.14	-0.18	n/a
1569	5	K10	-0.61	-0.57	-0.62	0.18	0.32	-0.80	-0.65	-0.37	n/a
1570	5	K11	-0.29	-0.37	-0.19	0.81	-0.88	-1.18	-1.26	-0.95	n/a
1571	5	K12	-0.69	-1.00	-0.83	-0.46	-0.46	-0.74	-0.88	-0.23	n/a
1572	5	K13	0.33	-0.93	0.03	-0.79	-0.28	-0.80	-0.77	-0.42	n/a
1573	5	K14	-0.15	-0.82	-0.30	-0.15	0.14	-0.64	-0.57	-0.13	n/a
1574	5	K15	-0.26	-0.83	-0.32	-0.22	-0.52	-0.72	-0.82	-0.37	n/a
1575	5	K16	-0.22	-0.76	-0.16	0.48	-0.82	-0.98	-1.08	-0.66	n/a
1576	5	K17	-0.64	-1.12	-0.64	1.04	-1.00	-1.14	-1.21	-1.00	n/a
1577	5	K18	0.45	-0.29	0.38	-0.43	1.04	-0.34	-0.11	0.30	n/a
1578	5	K19	0.16	-0.27	0.22	0.87	0.26	-0.72	-0.67	-0.09	n/a
1579	5	K2	0.48	1.11	1.10	0.26	1.22	0.23	0.50	0.54	n/a
1580	5	K20	-0.33	-0.99	-0.12	-0.17	0.26	-0.74	-0.65	-0.13	n/a
1581	5	K21	-0.02	-0.37	0.06	0.74	-0.40	-0.88	-0.90	-0.61	n/a
1582	5	K22	-0.18	-0.18	0.07	-0.45	-0.04	-0.16	-0.19	0.11	n/a
1583	5	K3	0.32	-0.85	-0.15	0.48	0.08	-0.56	-0.52	-0.23	n/a
1584	5	K4	-0.04	-0.46	0.17	-0.34	0.26	-0.66	-0.49	-0.13	n/a
1585	5	K5	0.02	-0.90	-0.31	0.31	-0.10	-0.84	-0.75	-0.37	n/a
1586	5	K6	0.25	-1.00	0.07	0.56	0.80	-0.70	-0.34	-0.18	n/a
1587	5	K7	-0.88	-1.18	-0.74	-0.64	-0.76	-1.12	-1.18	-0.81	n/a
1588	5	K8	0.01	-0.86	-0.32	0.28	-0.34	-1.02	-1.05	-0.52	n/a
1589	5	K9	0.38	-0.53	0.08	-0.43	0.20	-0.58	-0.39	-0.42	n/a
1590	5	L1	1.35	0.07	0.61	0.33	-0.22	0.08	0.07	-0.09	n/a

1591	5	L10	0.14	-0.03	-0.22	0.87	0.86	-0.32	-0.24	0.49	n/a
1592	5	L11	-0.59	-1.18	-0.74	0.41	-0.04	-1.04	-0.82	-0.71	n/a
1593	5	L12	-0.38	-1.10	-0.43	-0.51	-0.22	-1.06	-0.90	-0.81	n/a
1594	5	L13	-0.10	-0.91	-0.38	-0.17	0.44	-0.84	-0.57	-0.37	n/a
1595	5	L14	-0.13	-0.60	0.13	-0.10	0.50	-0.52	-0.44	0.20	n/a
1596	5	L15	-1.70	-1.49	-1.55	-0.78	-0.52	-0.94	-1.05	-0.66	n/a
1597	5	L16	-1.55	-1.07	-1.32	-0.74	-1.12	-1.22	-1.33	-1.14	n/a
1598	5	L17	-0.22	-0.59	-0.39	0.02	0.44	-0.54	-0.44	-0.09	n/a
1599	5	L18	-0.79	-1.02	-0.72	-0.34	-0.16	-0.82	-0.75	-0.42	n/a
1600	5	L19	-0.55	-1.29	-0.33	-0.27	0.26	-0.80	-0.57	-0.47	n/a
1601	5	L2	-0.09	-0.23	-0.34	-0.08	-0.28	-0.42	-0.37	-0.42	n/a
1602	5	L20	-0.80	-0.74	-0.74	0.11	-0.64	-1.14	-1.21	-0.81	n/a
1603	5	L21	-0.86	-1.36	-0.90	-0.09	-0.10	-0.88	-0.77	-0.61	n/a
1604	5	L22	-0.30	-0.52	-0.20	0.25	-1.30	-1.22	-1.41	-1.10	n/a
1605	5	L4	-0.72	-0.64	-0.81	-0.14	-0.58	-0.40	-0.62	-0.09	n/a
1606	5	L5	-0.56	-0.53	-0.11	0.17	0.26	-0.72	-0.60	-0.18	n/a
1607	5	L6	0.12	-0.21	0.46	0.22	0.74	-0.38	-0.24	0.20	n/a
1608	5	L7	-0.73	-0.80	-0.94	1.04	-1.06	-1.22	-1.31	-1.10	n/a
1609	5	L8	-0.33	-0.61	-0.51	-0.35	-0.22	-0.94	-0.82	-0.66	n/a
1610	5	L9	-0.35	-0.39	-0.34	1.14	0.38	-0.72	-0.52	-0.33	n/a
1611	5	M10	0.51	-0.56	0.30	-1.26	0.56	-0.14	0.01	0.06	n/a
1612	5	M11	0.09	0.02	0.62	-0.06	0.74	-0.48	-0.37	0.15	n/a
1613	5	M12	-0.98	-1.27	-0.90	-1.08	0.14	-0.36	-0.37	0.06	n/a
1614	5	M13	-0.62	-1.08	-0.68	0.23	-0.46	-0.98	-0.95	-0.81	n/a
1615	5	M14	0.04	-0.43	-0.07	-0.76	0.38	-0.56	-0.44	-0.18	n/a
1616	5	M15	-0.47	-0.91	-0.32	-0.56	-0.10	-0.78	-0.77	-0.37	n/a
1617	5	M16	-0.10	-0.09	0.35	-0.17	-0.58	-0.42	-0.52	-0.47	n/a
1618	5	M17	-0.28	-0.28	-0.24	0.00	0.44	-0.24	-0.19	0.20	n/a
1619	5	M18	0.72	-0.32	0.55	-0.36	0.68	-0.44	-0.29	-0.09	n/a
1620	5	M19	0.27	-0.80	-0.15	-0.06	0.98	-0.26	-0.14	0.54	n/a
1621	5	M2	-0.92	-0.44	-0.65	-0.38	0.26	-0.20	-0.14	0.01	n/a
1622	5	M20	0.36	0.45	0.58	-0.21	0.86	0.15	0.27	0.35	n/a
1623	5	M21	-0.87	-0.74	-0.54	-0.91	-0.04	-0.66	-0.62	-0.28	n/a
1624	5	M3	-0.25	-0.95	0.04	-0.73	-0.22	-0.62	-0.57	-0.47	n/a
1625	5	M4	-0.01	-0.35	0.25	-0.10	0.56	-0.28	-0.19	0.06	n/a
1626	5	M5	-0.23	-0.63	-0.11	-0.78	0.08	-0.36	-0.37	-0.04	n/a
1627	5	M6	-0.13	-0.71	-0.16	-0.83	0.26	-0.60	-0.52	-0.13	n/a
1628	5	M7	-0.04	-0.79	-0.13	-0.36	0.08	-0.36	-0.39	0.01	n/a
1629	5	M8	-0.59	-0.80	-0.30	0.04	-0.34	-0.80	-0.77	-0.42	n/a
1630	5	M9	-0.33	-1.26	-0.46	-1.12	-0.16	-0.80	-0.72	-0.57	n/a
1631	5	N1	-0.01	0.31	0.42	-0.58	0.20	0.35	0.29	0.30	n/a
1632	5	N10	0.11	-0.33	0.21	-0.30	0.98	0.10	0.27	0.59	n/a
1633	5	N11	-0.30	-0.40	-0.23	-0.38	-0.28	-0.42	-0.49	-0.18	n/a
1634	5	N12	-0.38	-0.51	-0.31	0.31	0.26	0.04	-0.01	0.64	n/a
1635	5	N13	1.90	1.17	1.69	1.30	0.92	0.10	0.19	0.64	n/a
1636	5	N14	-0.76	-0.18	-0.45	-0.40	-0.34	-0.30	-0.44	-0.04	n/a
1637	5	N15	0.14	0.25	0.43	-0.68	0.98	0.21	0.35	0.73	n/a
1638	5	N16	-1.18	0.11	-0.40	-0.89	-0.10	-0.12	-0.21	0.06	n/a
1639	5	N17	-0.21	-0.61	0.06	-0.42	0.50	-0.18	-0.16	0.30	n/a
1640	5	N18	-0.34	0.03	0.06	-0.48	0.08	0.15	-0.01	0.64	n/a
1641	5	N19	-0.43	-0.65	-0.40	-0.31	-0.16	-0.30	-0.21	-0.23	n/a
1642	5	N2	0.45	0.40	0.54	0.00	0.62	0.19	0.29	0.30	n/a
1643	5	N20	-0.69	-0.29	-0.18	0.15	0.68	-0.42	-0.14	0.01	n/a
1644	5	N21	-0.19	-0.09	-0.15	-0.68	-0.70	0.08	-0.11	-0.13	n/a
1645	5	N22	-0.19	-0.36	-0.17	-0.32	0.68	-0.18	-0.01	0.25	n/a
1646	5	N3	0.13	-0.57	0.15	-0.58	1.58	-0.08	0.24	0.59	n/a
1647	5	N4	1.64	0.87	0.97	0.80	0.32	-0.22	-0.14	0.15	n/a
1648	5	N5	0.18	-0.40	0.09	0.25	0.86	-0.40	-0.29	0.40	n/a

1649	5	N6	0.90	0.55	0.80	0.71	1.22	0.41	0.55	1.02	n/a
1650	5	N7	-1.02	-1.15	-0.87	-0.56	0.50	-0.66	-0.47	-0.04	n/a
1651	5	N8	-0.33	-0.79	-0.41	0.07	0.50	-0.34	-0.27	0.15	n/a
1652	5	N9	0.06	-0.59	0.08	0.27	1.28	-0.28	0.01	0.44	n/a
1653	5	O13	0.39	0.36	0.72	0.09	0.98	0.08	0.27	0.40	n/a
1654	5	O14	-0.16	-0.91	-0.06	-0.93	0.38	-0.10	-0.04	0.25	n/a
1655	5	O17	-0.97	-0.71	-1.04	-1.39	-1.06	-0.22	-0.29	-0.76	n/a
1656	5	O18	0.50	0.01	0.77	-1.50	1.40	0.39	0.68	0.64	n/a
1657	5	O19	-1.41	-1.17	-1.41	-0.94	-0.64	-0.42	-0.57	-0.52	n/a
1658	5	O2	1.58	0.76	1.89	-0.05	0.14	-0.04	0.07	-0.09	n/a
1659	5	O20	0.33	-0.09	0.81	0.04	0.98	0.14	0.27	0.44	n/a
1660	5	O22	-0.05	-0.34	-0.33	-1.07	0.08	-0.24	-0.16	-0.28	n/a
1661	5	O3	0.19	-0.55	-0.10	-0.48	1.04	0.17	0.35	0.68	n/a
1662	5	O5	0.23	-0.20	0.49	-1.07	0.86	0.08	0.22	0.44	n/a
1663	5	O9	-0.36	-0.27	-0.34	-0.34	0.26	-0.36	-0.29	0.06	n/a
1664	5	P1	1.62	1.71	1.74	-1.07	-0.46	0.89	0.68	0.25	n/a
1665	5	P10	-0.10	0.85	0.75	-0.42	0.80	0.97	0.98	0.78	n/a
1666	5	P11	1.34	1.13	1.63	0.36	0.86	0.81	0.85	0.83	n/a
1667	5	P12	1.15	1.19	1.46	-0.20	1.34	0.83	0.93	1.12	n/a
1668	5	P14	0.26	1.57	1.27	-0.53	0.80	1.19	1.24	0.88	n/a
1669	5	P16	0.44	0.81	0.50	-0.23	0.38	0.81	0.68	0.88	n/a
1670	5	P17	-0.41	0.90	0.46	-1.96	0.02	1.59	1.57	0.59	n/a
1671	5	P18	0.27	0.43	0.68	-0.82	0.80	1.15	1.06	1.21	n/a
1672	5	P19	0.27	0.34	0.42	-0.70	0.02	0.57	0.45	0.54	n/a
1673	5	P20	-0.40	0.29	0.28	-0.50	0.50	0.85	0.93	0.68	n/a
1674	5	P21	-0.21	0.18	0.66	-0.90	0.86	0.95	1.03	0.88	n/a
1675	5	P3	-0.07	0.53	0.40	-0.43	0.26	0.47	0.47	0.20	n/a
1676	5	P4	1.38	1.03	1.23	0.01	0.86	0.81	0.85	0.78	n/a
1677	5	P5	1.22	0.78	1.19	0.50	1.04	0.77	0.80	0.88	n/a
1678	5	P6	0.19	1.11	0.84	-0.97	1.34	1.03	1.18	0.44	n/a
1679	5	P7	1.08	-0.49	0.14	-0.20	0.26	0.25	0.37	0.01	n/a
1680	5	P9	1.54	1.26	1.39	0.06	1.52	1.07	1.16	1.40	n/a

Table F 3. Z-score measures of interest from Validation screening

#	Plate	Well	Ac-α-tub length z-score								
			S1	V2				V3				Reproducibility
				Rep1	Rep2	Rep3	Mean	Rep1	Rep2	Rep3	Mean	
1	1	B2	2.41	1.25	2.70	4.23	2.73	2.14	1.31	0.67	1.37	2
2	1	C10	2.19	1.24	2.95	3.03	2.41	0.33	2.21	1.23	1.26	2
3	1	G4	3.20	2.90	2.07	2.72	2.56	3.52	1.22	2.74	2.49	3
4	1	G5	2.82	2.60	7.62	3.92	4.71	3.69	4.50	4.26	4.15	3
5	1	K12	2.48	3.92	2.40	2.35	2.89	0.71	4.40	5.06	3.39	3
6	2	A14	1.61	2.77	4.48	6.01	4.42	3.88	3.45	3.74	3.69	2
7	3	A3	3.06	6.12	6.09	3.25	5.15	0.60	-0.26	0.61	0.32	2
8	3	F6	5.06	0.56	1.36	1.23	1.05	0.46	2.11	2.29	1.62	2
9	3	G17	2.99	0.97	2.00	2.77	1.91	2.01	2.67	1.73	2.14	2
10	3	L13	2.53	-0.05	0.90	0.84	0.56	0.22	2.18	3.19	1.86	2
11	3	N13	2.15	0.91	2.37	2.00	1.76	0.01	0.34	2.52	0.96	2
12	3	N16	2.48	-1.01	1.89	1.52	0.80	4.03	1.41	4.10	3.18	2
13	3	P7	2.55	1.13	2.40	1.14	1.56	2.04	0.15	2.14	1.44	2
14	4	A6	2.44	3.46	4.32	3.24	3.67	3.94	3.72	1.56	3.08	3
15	4	A7	2.57	3.47	3.61	3.48	3.52	4.36	2.90	6.88	4.71	3
16	4	K21	3.55	0.88	2.12	2.55	1.85	2.01	0.17	1.11	1.10	2
17	4	O22	2.06	2.61	1.56	3.83	2.67	1.22	1.25	4.57	2.35	2
18	4	O3	3.95	4.80	1.91	3.08	3.26	3.57	4.13	3.38	3.69	3
19	4	P21	4.09	1.57	4.16	0.80	2.18	2.19	1.55	2.04	1.93	2
20	4	P8	2.98	5.93	6.53	3.66	5.38	3.06	6.01	4.46	4.51	3
21	5	G22	1.84	2.12	3.23	1.73	2.36	2.83	2.82	2.21	2.62	2
22	5	O12	2.94	3.10	3.39	2.22	2.90	1.69	2.18	3.20	2.35	3
23	1	M16	3.04	-0.14	0.70	1.03	0.53	1.30	0.21	1.42	0.98	1
24	1	N21	2.76	0.29	1.80	1.37	1.15	0.79	1.19	1.95	1.31	1
25	2	A17	2.30	-0.36	1.80	0.68	0.70	1.53	1.77	1.48	1.59	1
26	2	F17	3.31	1.68	0.40	1.51	1.19	0.39	0.91	1.57	0.96	1
27	2	F20	2.37	0.86	2.92	1.40	1.72	0.22	3.79	0.72	1.58	1
28	2	K1	2.01	-0.19	1.89	1.36	1.02	-0.48	1.09	-0.45	0.06	1
29	2	N20	3.44	1.88	1.47	-0.03	1.11	-0.62	0.21	2.98	0.86	1
30	3	F17	3.16	1.48	2.76	-0.11	1.38	1.85	3.49	0.75	2.03	1
31	3	F18	4.19	0.12	1.81	1.36	1.10	1.89	1.67	1.16	1.57	1
32	3	G3	3.60	-0.25	0.62	1.18	0.51	-0.53	1.03	-0.27	0.08	1
33	3	H14	3.24	1.23	-0.13	1.02	0.71	1.22	-0.52	1.30	0.67	1
34	3	I6	2.79	0.53	-0.65	0.76	0.22	-1.17	-0.44	0.96	-0.21	1
35	3	L11	2.34	-0.72	0.54	-0.21	-0.13	-0.31	0.11	-1.39	-0.53	1
36	3	L19	1.89	-1.33	0.69	0.85	0.07	-0.22	1.85	-1.16	0.16	0
37	3	L4	2.04	0.10	1.80	2.26	1.39	-0.12	0.81	0.86	0.52	1
38	3	L6	2.59	-1.23	1.11	2.74	0.87	-1.30	0.46	0.11	-0.24	1
39	3	L7	2.42	0.70	0.18	1.75	0.88	-0.09	2.81	0.20	0.97	1
40	3	M10	2.00	-1.23	-0.54	-1.06	-0.94	-0.47	0.00	-1.69	-0.72	1
41	3	M11	1.97	-2.93	0.17	0.84	-0.64	-1.00	0.23	-0.18	-0.32	0
42	3	M13	1.92	0.38	0.84	1.02	0.75	-0.06	0.35	-0.63	-0.11	0
43	3	M14	2.57	0.59	1.54	1.24	1.12	-0.28	2.21	1.78	1.24	1
44	3	M18	1.98	0.15	0.36	-0.33	0.06	0.55	0.12	-0.25	0.14	0
45	3	N1	2.18	0.59	-0.18	0.57	0.33	1.30	-0.80	1.36	0.62	1
46	3	N10	3.97	1.69	2.52	1.41	1.87	0.71	1.28	0.59	0.86	1
47	3	N11	2.13	-0.15	-0.07	0.81	0.20	0.27	0.57	0.90	0.58	1
48	3	N14	2.21	1.40	1.37	0.63	1.13	-0.32	1.18	3.32	1.39	1
49	3	N15	3.17	0.98	1.75	2.49	1.74	-0.59	-0.19	2.18	0.46	1
50	3	N5	2.22	1.47	0.83	1.04	1.11	1.11	0.00	1.86	0.99	1
51	3	N6	2.59	0.13	2.78	0.84	1.25	-1.32	-0.47	0.27	-0.51	1
52	3	N7	2.30	0.46	0.34	0.10	0.30	-0.94	0.81	0.19	0.02	1
53	3	N8	2.54	-0.38	0.18	0.85	0.22	-1.17	0.24	0.42	-0.17	1
54	3	O11	1.78	0.07	1.03	-1.07	0.01	-0.15	0.04	0.61	0.17	0
55	3	O13	2.25	-1.41	0.56	-0.23	-0.36	-2.05	0.11	-0.25	-0.73	1
56	3	P17	1.83	0.86	0.91	1.17	0.98	0.73	-0.45	-0.38	-0.03	0
57	3	P4	2.17	0.29	1.67	1.36	1.11	-0.17	1.31	1.61	0.91	1
58	3	P5	1.55	-0.78	-0.56	-0.34	-0.56	-1.55	1.42	1.63	0.50	0
59	3	P8	1.66	0.28	-0.42	0.78	0.21	1.61	1.08	1.68	1.46	0
60	4	A12	1.38	1.89	2.21	0.67	1.59	1.27	1.90	2.99	2.05	0
61	4	P10	2.70	3.53	-0.03	0.51	1.33	2.26	-0.21	0.08	0.71	1
62	5	L3	2.16	1.25	-0.19	1.35	0.81	1.66	1.31	-0.46	0.84	1
63	5	P13	3.02	1.18	2.79	0.20	1.39	1.49	2.43	-0.84	1.03	1

Appendix G: Representative images from first pass screen

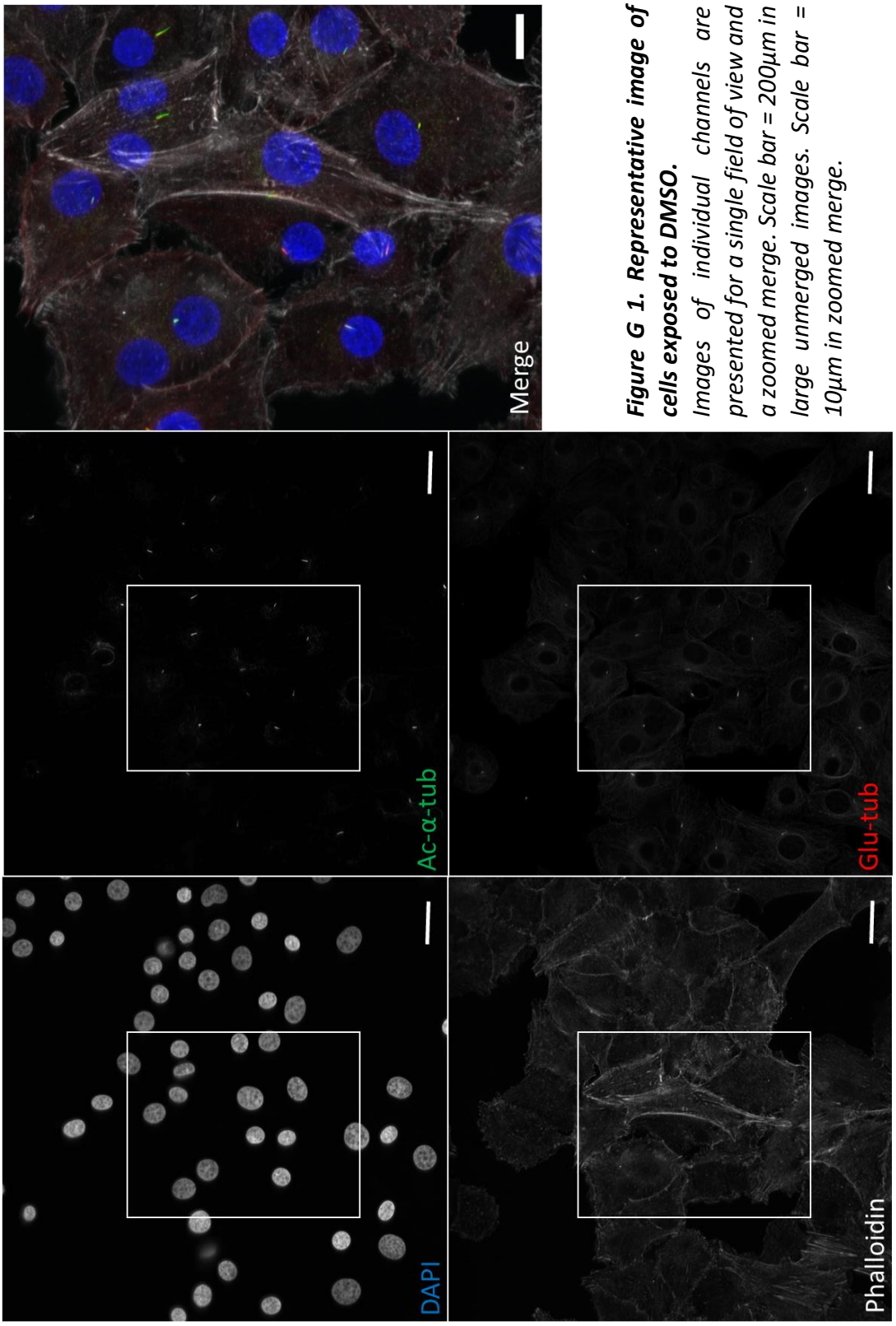

Figure G 1. Representative image of cells exposed to DMSO.
Images of individual channels are presented for a single field of view and a zoomed merge. Scale bar = 200µm in large unmerged images. Scale bar = 10µm in zoomed merge.

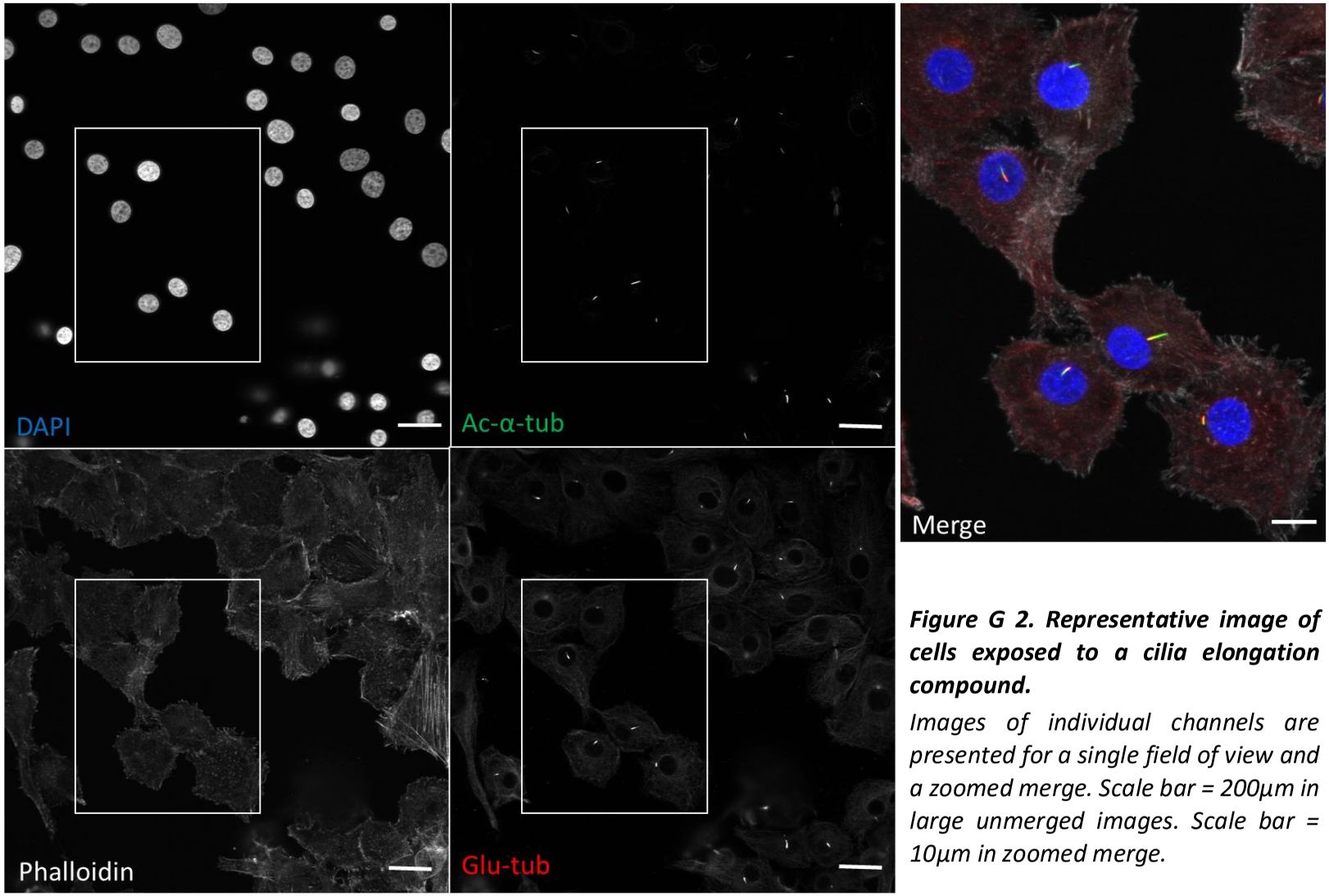

Figure G 2. Representative image of cells exposed to a cilia elongation compound.

Images of individual channels are presented for a single field of view and a zoomed merge. Scale bar = 200µm in large unmerged images. Scale bar = 10µm in zoomed merge.

8. Bibliography

AbouAlaiwi WA, Takahashi M, Mell BR, Jones TJ, Ratnam S, Kolb RJ, Nauli SM. 2009. Ciliary polycystin-2 is a mechanosensitive calcium channel involved in nitric oxide signaling cascades. Circulation research 104:860-869.

Anvarian Z, Mykytyn K, Mukhopadhyay S, Pedersen LB, Christensen ST. 2019. Cellular signalling by primary cilia in development, organ function and disease. Nature Reviews Nephrology 15:199-219.

Avasthi P, Maser RL, Tran PV. 2017. Primary cilia in cystic kidney disease. Kidney Development and Disease:281-321.

Aydelotte MB, Kuettner KE. 1988. Differences between sub-populations of cultured bovine articular chondrocytes. I. Morphology and cartilage matrix production. Connective tissue research 18:205-222.

Badano JL, Mitsuma N, Beales PL, Katsanis N. 2006. The ciliopathies: an emerging class of human genetic disorders. Annu. Rev. Genomics Hum. Genet. 7:125-148.

Bangs F, Anderson KV. 2017. Primary cilia and mammalian hedgehog signaling. Cold Spring Harbor perspectives in biology 9:a028175.

Benmerah A. 2013. The ciliary pocket. Current opinion in cell biology 25:78-84.

Berbari NF, O'Connor AK, Haycraft CJ, Yoder BK. 2009. The primary cilium as a complex signaling center. Current Biology 19:R526-R535.

Bertiaux E, Morga B, Blisnick T, Rotureau B, Bastin P. 2018. A grow-and-lock model for the control of flagellum length in trypanosomes. Current Biology 28:3802-3814. e3803.

Browning J, Saunders K, Urban J, Wilkins R. 2004. The influence and interactions of hydrostatic and osmotic pressures on the intracellular milieu of chondrocytes. Biorheology 41:299-308.

Calvert N, Grainger N, Hurworth M. 2013. Use of bovine carpal joints as a training model for cruciate ligament repair. ANZ journal of surgery 83:933-936.

Chang C-F, Ramaswamy G, Serra R. 2012. Depletion of primary cilia in articular chondrocytes results in reduced Gli3 repressor to activator ratio, increased Hedgehog signaling, and symptoms of early osteoarthritis. Osteoarthritis and cartilage 20:152-161.

Chowdhury T, Appleby R, Salter D, Bader D, Lee D. 2006. Integrin-mediated mechanotransduction in IL-1 β stimulated chondrocytes. Biomechanics and Modeling in Mechanobiology 5:192-201.

Chowdhury TT, Bader DL, Lee DA. 2001. Dynamic compression inhibits the synthesis of nitric oxide and PGE2 by IL-1β-stimulated chondrocytes cultured in agarose constructs. Biochemical and biophysical research communications 285:1168-1174.

Corrigan M, Ferradaes T, Riffault M, Hoey D. 2019. Ciliotherapy treatments to enhance biochemically-and biophysically-induced mesenchymal stem cell osteogenesis: a comparison study. Cellular and molecular bioengineering 12:53-67.

Degala S, Williams R, Zipfel W, Bonassar LJ. 2012. Calcium signaling in response to fluid flow by chondrocytes in 3D alginate culture. Journal of Orthopaedic Research 30:793-799.

Delaine-Smith RM, Sittichokechaiwut A, Reilly GC. 2014. Primary cilia respond to fluid shear stress and mediate flow-induced calcium deposition in osteoblasts. The FASEB Journal 28:430-439.

Dinsmore C, Reiter JF. 2016. Endothelial primary cilia inhibit atherosclerosis. EMBO reports 17:156-166.

Engel BD, Ludington WB, Marshall WF. 2009. Intraflagellar transport particle size scales inversely with flagellar length: revisiting the balance-point length control model. Journal of Cell Biology 187:81-89.

Farnum CE, Wilsman NJ. 2011. Orientation of primary cilia of articular chondrocytes in three-dimensional space. The Anatomical Record: Advances in Integrative Anatomy and Evolutionary Biology 294:533-549.

Fu S, Thompson C, Ali A, Wang W, Chapple J, Mitchison H, Beales P, Wann A, Knight M. 2019. Mechanical loading inhibits cartilage inflammatory signalling via an HDAC6 and IFT-dependent mechanism regulating primary cilia elongation. Osteoarthritis and cartilage 27:1064-1074.

Gambassi S, Geminiani M, Thorpe SD, Bernardini G, Millucci L, Braconi D, Orlandini M, Thompson CL, Petricci E, Manetti F. 2017. Smoothened-antagonists reverse homogentisic acid-induced alterations of Hedgehog signaling and primary cilium length in alkaptonuria. Journal of cellular physiology 232:3103-3111.

Gilula NB, Satir P. 1972. The ciliary necklace: a ciliary membrane specialization. The Journal of cell biology 53:494-509.

Goetz SC, Liem Jr KF, Anderson KV. 2012. The spinocerebellar ataxia-associated gene Tau tubulin kinase 2 controls the initiation of ciliogenesis. Cell 151:847-858.

Guilak F, Ratcliffe A, Mow VC. 1995. Chondrocyte deformation and local tissue strain in articular cartilage: a confocal microscopy study. Journal of Orthopaedic Research 13:410-421.

Hildebrandt F, Benzing T, Katsanis N. 2011. Ciliopathies. New England Journal of Medicine 364:1533-1543.

Hua K, Ferland RJ. 2017. Fixation methods can differentially affect ciliary protein immunolabeling. Cilia 6:1-17.

Huang B, Rifkin M, Luck D. 1977. Temperature-sensitive mutations affecting flagellar assembly and function in Chlamydomonas reinhardtii. Journal of Cell Biology 72:67-85.

Huang J, Ballou L, Hasty K. 2007. Cyclic equibiaxial tensile strain induces both anabolic and catabolic responses in articular chondrocytes. Gene 404:101-109.

Iomini C, Tejada K, Mo W, Vaananen H, Piperno G. 2004. Primary cilia of human endothelial cells disassemble under laminar shear stress. The Journal of cell biology 164:811-817.

Izawa I, Goto H, Kasahara K, Inagaki M. 2015. Current topics of functional links between primary cilia and cell cycle. Cilia 4:1-13.

Jacobs C, Spasic M. 2019. Regulation of gene expression by modulating primary cilia length. In: Google Patents.

Jensen C, Poole C, McGlashan S, Marko M, Issa Z, Vujcich K, Bowser S. 2004. Ultrastructural, tomographic and confocal imaging of the chondrocyte primary cilium in situ. Cell biology international 28:101-110.

Jensen CG, Davison EA, Bowser SS, Rieder CL. 1987. Primary cilia cycle in PtK1 cells: effects of colcemid and taxol on cilia formation and resorption. Cell motility and the cytoskeleton 7:187-197.

Kathem SH, Mohieldin AM, Abdul-Majeed S, Ismail SH, Altaei QH, Alshimmari IK, Alsaidi MM, Khammas H, Nauli AM, Joe B. 2014. Ciliotherapy: a novel intervention in polycystic kidney disease. Journal of geriatric cardiology: JGC 11:63.

Kaushik AP, Martin JA, Zhang Q, Sheffield VC, Morcuende JA. 2009. Cartilage abnormalities associated with defects of chondrocytic primary cilia in Bardet-Biedl syndrome mutant mice. Journal of Orthopaedic Research 27:1093-1099.

Kelly M. 2006. National Institute for Health and Clinical Excellence. Centre for Public Health Excellence. Public health programmes and interventions and NHS disinvestment.

Kim E, Guilak F, Haider MA. 2008. The dynamic mechanical environment of the chondrocyte: a biphasic finite element model of cell-matrix interactions under cyclic compressive loading. Journal of biomechanical engineering 130.

Kim J, Jo H, Hong H, Kim MH, Kim JM, Lee J-K, Do Heo W, Kim J. 2015. Actin remodelling factors control ciliogenesis by regulating YAP/TAZ activity and vesicle trafficking. Nature communications 6:1-13.

Kobayashi T, Dynlacht BD. 2011. Regulating the transition from centriole to basal body. Journal of Cell Biology 193:435-444.

Kozminski KG, Beech PL, Rosenbaum JL. 1995. The Chlamydomonas kinesin-like protein FLA10 is involved in motility associated with the flagellar membrane. The Journal of cell biology 131:1517-1527.

Kukic I, Rivera-Molina F, Toomre D. 2016. The IN/OUT assay: a new tool to study ciliogenesis. Cilia 5:1-14.

Labour M-N, Riffault M, Christensen ST, Hoey DA. 2016. TGFβ1–induced recruitment of human bone mesenchymal stem cells is mediated by the primary cilium in a SMAD3-dependent manner. Scientific reports 6:1-13.

Lehman JM, Michaud EJ, Schoeb TR, Aydin-Son Y, Miller M, Yoder BK. 2008. The Oak Ridge Polycystic Kidney mouse: modeling ciliopathies of mice and men. Developmental dynamics: an official publication of the American Association of Anatomists 237:1960-1971.

Liu H, Kiseleva AA, Golemis EA. 2018. Ciliary signalling in cancer. Nature Reviews Cancer 18:511-524.

Lu Q, Insinna C, Ott C, Stauffer J, Pintado PA, Rahajeng J, Baxa U, Walia V, Cuenca A, Hwang Y-S. 2015. Early steps in primary cilium assembly require EHD1/EHD3-dependent ciliary vesicle formation. Nature cell biology 17:228-240.

Luo N, Conwell MD, Chen X, Kettenhofen CI, Westlake CJ, Cantor LB, Wells CD, Weinreb RN, Corson TW, Spandau DF. 2014. Primary cilia signaling mediates

intraocular pressure sensation. Proceedings of the National Academy of Sciences 111:12871-12876.

Marshall WF. 2008. Basal bodies: platforms for building cilia. Current topics in developmental biology 85:1-22.

Marshall WF, Rosenbaum JL. 2001. Intraflagellar transport balances continuous turnover of outer doublet microtubules: implications for flagellar length control. The Journal of cell biology 155:405-414.

Mc Fie M, Koneva L, Collins I, Coveney CR, Clube AM, Chanalaris A, Vincent TL, Bezbradica JS, Sansom SN, Wann AK. 2020. Ciliary proteins specify the cell inflammatory response by tuning NFκB signalling, independently of primary cilia. Journal of cell science 133:jcs239871.

McEwen DP, Jenkins PM, Martens JR. 2008. Olfactory cilia: our direct neuronal connection to the external world. Current topics in developmental biology 85:333-370.

McGlashan S, Cluett E, Jensen C, Poole C. 2008. Primary cilia in osteoarthritic chondrocytes: from chondrons to clusters. Developmental dynamics: an official publication of the American Association of Anatomists 237:2013-2020.

McGlashan S, Haycraft C, Jensen C, Yoder B, Poole C. 2007. Articular cartilage and growth plate defects are associated with chondrocyte cytoskeletal abnormalities in Tg737orpk mice lacking the primary cilia protein polaris. Matrix biology 26:234-246.

McGlashan SR, Knight MM, Chowdhury TT, Joshi P, Jensen CG, Kennedy S, Poole CA. 2010. Mechanical loading modulates chondrocyte primary cilia incidence and length. Cell biology international 34:441-446.

Meier-Vismara E, Walker N, Vogel A. 1979. Single cilia in the articular cartilage of the cat. Pathobiology 47:161-171.

Millward-Sadler S, Wright M, Lee H-S, Caldwell H, Nuki G, Salter D. 2000. Altered electrophysiological responses to mechanical stimulation and abnormal signalling through α5β1 integrin in chondrocytes from osteoarthritic cartilage. Osteoarthritis and cartilage 8:272-278.

Miyoshi K, Kasahara K, Miyazaki I, Asanuma M. 2009. Lithium treatment elongates primary cilia in the mouse brain and in cultured cells. Biochemical and biophysical research communications 388:757-762.

Mizuno S. 2005. A novel method for assessing effects of hydrostatic fluid pressure on intracellular calcium: a study with bovine articular chondrocytes. American Journal of Physiology-Cell Physiology 288:C329-C337.

Moon H, Song J, Shin J-O, Lee H, Kim H-K, Eggenschwiller JT, Bok J, Ko HW. 2014. Intestinal cell kinase, a protein associated with endocrine-cerebro-osteodysplasia syndrome, is a key regulator of cilia length and Hedgehog signaling. Proceedings of the National Academy of Sciences 111:8541-8546.

Muhammad H, Rais Y, Miosge N, Ornan EM. 2012. The primary cilium as a dual sensor of mechanochemical signals in chondrocytes. Cellular and Molecular Life Sciences 69:2101-2107.

Nagai T, Mizuno K. 2017. Jasplakinolide induces primary cilium formation through cell rounding and YAP inactivation. PLoS One 12:e0183030.

Nguyen AM, Young Y-N, Jacobs CR. 2015. The primary cilium is a self-adaptable, integrating nexus for mechanical stimuli and cellular signaling. Biology open 4:1733-1738.

Nishida K, Yorimitsu M, Komiyama T, Kadota Y, Tetsunaga T, Yoshida A, Kubota S, Takigawa M, Ozaki T. 2008. Interleukin-4 downregulates the cyclic tensile stress-induced matrix metalloproteinases-13 and cathepsin B expression by rat normal chondrocytes. Acta Medica Okayama 62:119-126.

Novarino G, Akizu N, Gleeson JG. 2011. Modeling human disease in humans: the ciliopathies. Cell 147:70-79.

Ou Y, Zhang Y, Cheng M, Rattner JB, Dobrinski I, van der Hoorn FA. 2012. Targeting of CRMP-2 to the primary cilium is modulated by GSK-3β. PLoS One 7:e48773.

Pala R, Mohieldin AM, Sherpa RT, Kathem SH, Shamloo K, Luan Z, Zhou J, Zheng J-G, Ahsan A, Nauli SM. 2019. Ciliotherapy: remote control of primary cilia movement and function by magnetic nanoparticles. ACS nano 13:3555-3572.

Pazour GJ, Baker SA, Deane JA, Cole DG, Dickert BL, Rosenbaum JL, Witman GB, Besharse JC. 2002. The intraflagellar transport protein, IFT88, is essential for vertebrate photoreceptor assembly and maintenance. The Journal of cell biology 157:103-114.

Pazour GJ, Bloodgood RA. 2008. Targeting proteins to the ciliary membrane. Current topics in developmental biology 85:115-149.

Pazour GJ, Dickert BL, Vucica Y, Seeley ES, Rosenbaum JL, Witman GB, Cole DG. 2000. Chlamydomonas IFT 88 and its mouse homologue, polycystic kidney disease gene Tg 737, are required for assembly of cilia and flagella. The Journal of cell biology 151:709-718.

Pazour GJ, Witman GB. 2003. The vertebrate primary cilium is a sensory organelle. Current opinion in cell biology 15:105-110.

Pedersen LB, Rosenbaum JL. 2008. Chapter two intraflagellar transport (IFT): role in ciliary assembly, resorption and signalling. Current topics in developmental biology 85:23-61.

Phua SC, Chiba S, Suzuki M, Su E, Roberson EC, Pusapati GV, Schurmans S, Setou M, Rohatgi R, Reiter JF. 2019. Dynamic remodeling of membrane composition drives cell cycle through primary cilia excision. Cell 178:261.

Phua SC, Chiba S, Suzuki M, Su E, Roberson EC, Pusapati GV, Setou M, Rohatgi R, Reiter JF, Ikegami K. 2017. Dynamic remodeling of membrane composition drives cell cycle through primary cilia excision. Cell 168:264-279. e215.

Pingguan-Murphy B, El-Azzeh M, Bader D, Knight M. 2006. Cyclic compression of chondrocytes modulates a purinergic calcium signalling pathway in a strain rate-and frequency-dependent manner. Journal of cellular physiology 209:389-397.

Poole CA. 1997. Articular cartilage chondrons: form, function and failure. Journal of anatomy 191:1-13.

Poole CA, Flint MH, Beaumont BW. 1985. Analysis of the morphology and function of primary cilia in connective tissues: a cellular cybernetic probe? Cell motility 5:175-193.

Poole CA, Jensen CG, Snyder JA, Gray CG, Hermanutz VL, Wheatley DN. 1997. Confocal analysis of primary cilia structure and colocalization with the Golgi apparatus in chondrocytes and aortic smooth muscle cells. Cell biology international 21:483-494.

Poole CA, Zhang Z-j, Ross JM. 2001. The differential distribution of acetylated and detyrosinated alpha-tubulin in the microtubular cytoskeleton and primary cilia of hyaline cartilage chondrocytes. Journal of anatomy 199:393-405.

Praetorius H, Spring K. 2001. Bending the MDCK cell primary cilium increases intracellular calcium. The Journal of membrane biology 184:71-79.

Praetorius HA, Spring KR. 2003. The renal cell primary cilium functions as a flow sensor. Current opinion in nephrology and hypertension 12:517-520.

Rais Y, Reich A, Simsa-Maziel S, Moshe M, Idelevich A, Kfir T, Miosge N, Monsonego-Ornan E. 2015. The growth plate's response to load is partially mediated by mechano-sensing via the chondrocytic primary cilium. Cellular and Molecular Life Sciences 72:597-615.

Ran J, Yang Y, Li D, Liu M, Zhou J. 2015. Deacetylation of α-tubulin and cortactin is required for HDAC6 to trigger ciliary disassembly. Scientific reports 5:1-13.

Reed NA, Cai D, Blasius TL, Jih GT, Meyhofer E, Gaertig J, Verhey KJ. 2006. Microtubule acetylation promotes kinesin-1 binding and transport. Current Biology 16:2166-2172.

Rich D, Clark A. 2012. Chondrocyte primary cilia shorten in response to osmotic challenge and are sites for endocytosis. Osteoarthritis and cartilage 20:923-930.

Rieder CL, Jensen CG, Jensen LC. 1979. The resorption of primary cilia during mitosis in a vertebrate (PtK1) cell line. Journal of ultrastructure research 68:173-185.

Rix S, Calmont A, Scambler PJ, Beales PL. 2011. An Ift80 mouse model of short rib polydactyly syndromes shows defects in hedgehog signalling without loss or malformation of cilia. Human molecular genetics 20:1306-1314.

Rohatgi R, Scott MP. 2007. Patching the gaps in Hedgehog signalling. Nature cell biology 9:1005-1009.

Rosenbaum JL, Child F. 1967. Flagellar regeneration in protozoan flagellates. The Journal of cell biology 34:345-364.

Rowson D, Knight MM, Screen HR. 2016. Zonal variation in primary cilia elongation correlates with localized biomechanical degradation in stress deprived tendon. Journal of Orthopaedic Research® 34:2146-2153.

Rowson DT, Shelton JC, Screen HR, Knight MM. 2018. Mechanical loading induces primary cilia disassembly in tendon cells via TGFβ and HDAC6. Scientific reports 8:1-12.

Rydholm S, Zwartz G, Kowalewski JM, Kamali-Zare P, Frisk T, Brismar H. 2010. Mechanical properties of primary cilia regulate the response to fluid flow. American Journal of Physiology-Renal Physiology 298:F1096-F1102.

Scholey JM. 2003. Intraflagellar transport. Annual review of cell and developmental biology 19:423-443.

Schwartz EA, Leonard ML, Bizios R, Bowser SS. 1997. Analysis and modeling of the primary cilium bending response to fluid shear. American Journal of Physiology-Renal Physiology 272:F132-F138.

Sorokin S. 1962. Centrioles and the formation of rudimentary cilia by fibroblasts and smooth muscle cells. The Journal of cell biology 15:363-377.

Spasic M, Jacobs CR. 2017. Lengthening primary cilia enhances cellular mechanosensitivity. European cells & materials 33:158.

Sun S, Fisher RL, Bowser SS, Pentecost BT, Sui H. 2019. Three-dimensional architecture of epithelial primary cilia. Proceedings of the National Academy of Sciences 116:9370-9379.

Tanaka N, Ohno S, Honda K, Tanimoto K, Doi T, Ohno-Nakahara M, Tafolla E, Kapila S, Tanne K. 2005. Cyclic mechanical strain regulates the PTHrP expression in cultured chondrocytes via activation of the Ca2+ channel. Journal of dental research 84:64-68.

Taschner M, Lorentzen A, Mourao A, Collins T, Freke GM, Moulding D, Basquin J, Jenkins D, Lorentzen E. 2018. Crystal structure of intraflagellar transport protein 80 reveals a homo-dimer required for ciliogenesis. Elife 7:e33067.

Thompson C, Chapple J, Knight M. 2014. Primary cilia disassembly down-regulates mechanosensitive hedgehog signalling: a feedback mechanism controlling ADAMTS-5 expression in chondrocytes. Osteoarthritis and cartilage 22:490-498.

Thompson C, Plant J, Wann A, Bishop C, Novak P, Mitchison H, Beales P, Chapple J, Knight M. 2017. Chondrocyte expansion is associated with loss of primary cilia and disrupted hedgehog signalling. eCells and Materials Journal 34.

Thompson CL, Wiles A, Poole CA, Knight MM. 2016. Lithium chloride modulates chondrocyte primary cilia and inhibits Hedgehog signaling. The FASEB Journal 30:716-726.

Thorpe SD, Gambassi S, Thompson CL, Chandrakumar C, Santucci A, Knight MM. 2017. Reduced primary cilia length and altered Arl13b expression are associated with deregulated chondrocyte Hedgehog signaling in alkaptonuria. Journal of cellular physiology 232:2407-2417.

Urban J. 1994. The chondrocyte: a cell under pressure. Rheumatology 33:901-908.

Van der Heiden K, Hierck BP, Krams R, de Crom R, Cheng C, Baiker M, Pourquie MJ, Alkemade FE, DeRuiter MC, Gittenberger-de Groot AC. 2008. Endothelial primary cilia in areas of disturbed flow are at the base of atherosclerosis. Atherosclerosis 196:542-550.

Wann A, Knight M. 2012. Primary cilia elongation in response to interleukin-1 mediates the inflammatory response. Cellular and Molecular Life Sciences 69:2967-2977.

Wann AK, Thompson CL, Chapple JP, Knight MM. 2013. Interleukin-1β sequesters hypoxia inducible factor 2α to the primary cilium. Cilia 2:1-14.

Wann AK, Zuo N, Haycraft CJ, Jensen CG, Poole CA, McGlashan SR, Knight MM. 2012. Primary cilia mediate mechanotransduction through control of ATP-induced Ca2+ signaling in compressed chondrocytes. The FASEB Journal 26:1663-1671.

Ware SM, Aygun MG-, Hildebrandt F. 2011. Spectrum of clinical diseases caused by disorders of primary cilia. Proceedings of the American Thoracic Society 8:444-450.

Waters AM, Beales PL. 2011. Ciliopathies: an expanding disease spectrum. Pediatric nephrology 26:1039-1056.

Wheatley DN, Wang AM, Strugnell GE. 1996. Expression of primary cilia in mammalian cells. Cell biology international 20:73-81.

Wilsman NJ, Fletcher TF. 1978. Cilia of neonatal articular chondrocytes incidence and morphology. The Anatomical Record 190:871-889.

Wren KN, Craft JM, Tritschler D, Schauer A, Patel DK, Smith EF, Porter ME, Kner P, Lechtreck KF. 2013. A differential cargo-loading model of ciliary length regulation by IFT. Current Biology 23:2463-2471.

Yellowley CE, Jacobs CR, Li Z, Zhou Z, Donahue HJ. 1997. Effects of fluid flow on intracellular calcium in bovine articular chondrocytes. American Journal of Physiology-Cell Physiology 273:C30-C36.

Zhang C, Wei X, Chen C, Cao K, Li Y, Jiao Q, Ding J, Zhou J, Fleming BC, Chen Q. 2014. Indian hedgehog in synovial fluid is a novel marker for early cartilage lesions in human knee joint. International journal of molecular sciences 15:7250-7265.

Zhang J, Dalbay MT, Luo X, Vrij E, Barbieri D, Moroni L, de Bruijn JD, van Blitterswijk CA, Chapple JP, Knight MM. 2017. Topography of calcium phosphate ceramics regulates primary cilia length and TGF receptor recruitment associated with osteogenesis. Acta biomaterialia 57:487-497.